BERGISCHE UNIVERSITÄT WUPPERTAL

DISSERTATION

Successful Memory Formation in Paired-Associate Learning: Associative and Semantic Effects on Episodic Encoding

Submitted in accordance with the requirements for
the degree of **Doctor rerum naturalium (Dr. rer. nat.)**

in the

Faculty of Human and Social Sciences

Submitted by:

Carsten Klein

This dissertation was accepted by the University of Wuppertal in June 2026.

Acknowledgments

First and foremost, I would like to thank my doctoral supervisor, PD Dr. Markus Hofmann, for his indispensable advice and unwavering support over the past years. His profound knowledge and experience provided steady guidance and continual inspiration throughout my scientific journey.

I am also deeply grateful to Professor Dr. Ralph Radach for offering such a professional and supportive working environment. His confidence in my broad range of skills has had a lasting impact on my professional development, and I sincerely appreciate the opportunities that came with it.

Moreover, I would particularly like to acknowledge the invaluable contributions of Dr Patricia Pais-Roldán and Dr Andre Rölke-Wellmann. Their expertise in neuroimaging and data analysis was essential for the successful completion of this research. With their support, I developed skills that I had previously thought unattainable, and they were always available whenever I encountered difficulties.

My thanks also go to Nicole Franke, Dr. Anne Friede, Dr. Markus Jansen, Mareike Kleemann, Dr. Tobias Neukirchen, Dr. Laura Schwalm, Dr. Christian Vorstius, and Christoph Wigbels. They were far more than colleagues and helped make everyday work both enjoyable and meaningful.

Finally, I would like to express my deepest gratitude to my wife, Marie Stiebing, and my best friends, Christopher Hören, Alexander Pennekamp, and Tanja Ried, for their unwavering support. Their patience, encouragement and belief in me gave me the strength to complete this project, which would not have been possible without them.

Table of Contents

Summary V

Zusammenfassung VII

List of Figures IX

List of Tables X

List of Abbreviations XI

1. Theoretical Framework and Research Rationale 1

1.1 Mnestic Functions in Sub-Hippocampal Memory Systems 1
1.2 Word Co-occurrences as an Indicator of Associative and Semantic Relationship 8
1.3 Modeling Language and Cognition: Spreading Activation in Semantic Networks 12
1.4 Accessing Memory Formation via Cued Recall and Paired-Associate Learning 15
1.5 Present Neuroimaging Techniques Used to Study Memory Processes 17
1.6 Motivation for the Doctoral Thesis 25

2. Overview of the Empirical Studies 27

2.1 Introducing Study A 27
2.2 Introducing Study B 28
2.3 Introducing Study C 29

3. Study A: Associative and Semantic Priming in Paired-Associate Learning: Effects Under Short and Long Stimulus-Onset Asynchrony 30

3.1 Introduction 31
3.2 Methods 39
3.3 Results 44
3.4 Discussion 47
3.5 Conclusion 53

4. Study B: ERP Correlates of Associative Priming and Subsequent Memory Effects: Evidence from Sentence-Embedded Paired-Associate Learning 54

4.1 Introduction 55
4.2 Methods 61
4.3 Results 69
4.4 Discussion 76
4.5 Conclusion 82

5. Study C: The Impact of Associative vs. Semantic Long-Term Knowledge on Hippocampal Subfield Processing 83

5.1 Introduction 84
5.2 Experiment C1 (3T fMRI Pilot Study) 91
5.3 Experiment C2 (7T fMRI Main Study) 98
5.4 Discussion 112
5.5 Conclusion 120

6. General Discussion 121

6.1 Summary of the Key Findings 121
6.2 Integrative Synthesis and Limitations 123
6.3 Implications, Methodological Refinements, and Future Directions 128

7. Conclusion 142

8. References 143

9. Appendix 162

10. Declaration of Authorship 184

Summary

In paired-associate word learning, consolidation efficacy and subsequent recall depend not only on lexical features but also on associative and semantic long-term knowledge, as well as temporal dynamics during encoding. Manipulating these factors influences recall success, response times, and neural correlates that underlie the memory formation process. However, their specific contributions and the ways in which they interact have not yet been examined systematically. This doctoral thesis therefore presents three consecutive studies designed to disentangle associative and semantic priming effects in paired-associate learning from purely episodic encoding. Corpus-derived co-occurrence statistics were used to determine whether prime and target words were directly associated (based on association strength). Semantic feature overlap was quantified as the number of common associates shared by prime and target. This computational approach enabled a clear dissociation of associative relations from broader semantic similarity. Study A used a sentence-embedded paired-associate paradigm with short versus long stimulus-onset asynchrony manipulation between prime and target to show robust cued recall benefits for word pairs with a strong direct association and comparatively weaker effects for semantic feature overlap. This result pattern was evident across all three studies. The lack of an interaction between stimulus-onset asynchrony, direct association, and semantic feature overlap suggested that such encoding advantages arise primarily during lexical processing rather than from time-dependent integration mechanisms. Study B replicated the paradigm with a moderate stimulus-onset asynchrony and recorded electroencephalography to investigate neurophysiological correlates of encoding. Subsequent memory effects predicted trial-by-trial cued recall success regardless of the prime-target relation, thereby reflecting attentional engagement and general encoding depth rather than the presence of the associative-semantic manipulation. In contrast, parietal Late Positive Component amplitudes were increased when a strong direct association between prime and target supported an encoding state linked to later episodic recollection (i.e., retrieval of contextual details). Study C supplemented the previous findings with functional magnetic resonance imaging to map the effects of direct association, semantic feature overlap, and purely episodic encoding onto hippocampal subfield activity. In this study, the word pairs were presented side by side without

any sentence context. The dentate gyrus showed preferential engagement when novel episodic conjunctions had to be formed. Increased activity in CA3, on the other hand, was linked to high semantic feature overlap, which can be explained by its involvement in autoassociative (attractor-like) pattern completion processes. CA1 and subiculum activity further indicated an integrative comparator role in supporting the transfer to neocortical networks. In addition, cortical depth-resolved analyses (six equidistant depth surfaces sampled across the cortical ribbon) provided exploratory evidence consistent with condition-dependent recruitment in regions involved in semantic control. However, the effects did not vary with cortical depth. By integrating associative and semantic priming manipulations into a paired-associate learning paradigm and combining this with neuroimaging, this thesis tests predictions from Complementary Learning Systems (rapid hippocampal learning alongside gradual neocortical integration) and hippocampal attractor models (recurrent dynamics supporting pattern completion) in humans. These predictions were aligned with the functional organization of the hippocampal trisynaptic loop (dentate gyrus → CA3 → CA1 → subiculum). The findings support a hybrid account in which pre-existing lexical structure affects memory formation via pattern-completion-like processes in CA3 and parietal Late Positive Component amplitude dynamics. The dentate gyrus further mediates pattern separation to preserve the integrity of novel episodic traces. Overall, this work refines mechanistic models of encoding by disentangling distinct contributions to successful memory formation and providing measure-specific predictions that motivate targeted causal tests in future research.

Zusammenfassung

Beim Wortpaarlernen hängen die Konsolidierungseffizienz und der spätere Abruf nicht nur von lexikalischen Merkmalen ab, sondern auch von assoziativem und semantischem Langzeitwissen sowie von zeitlichen Dynamiken während der Enkodierung. Eine Manipulation dieser Faktoren beeinflusst die Abrufgenauigkeit, die Reaktionszeiten und neuronale Korrelate, die dem Gedächtnisbildungsprozess zugrunde liegen. Ihre spezifischen Einzelbeiträge sowie die Art und Weise, wie sie miteinander interagieren, sind jedoch bislang nicht systematisch untersucht worden. Diese Dissertation präsentiert daher drei aufeinander aufbauende Studien, die darauf abzielen, assoziative und semantische Priming-Effekte im Wortpaarlernen von rein episodischer Enkodierung abzugrenzen. Aus Textkorpora abgeleitete Kookkurrenzstatistiken wurden verwendet, um zu bestimmen, ob Prime- und Target-Wörter direkt miteinander assoziiert waren (basierend auf der Assoziationsstärke). Die semantische Merkmalsüberlappung wurde als Anzahl der gemeinsamen Assoziierten quantifiziert, die Prime und Target teilen. Dieser computationale Ansatz ermöglichte die klare Unterscheidung zwischen assoziativen Beziehungen und breiterer semantischer Ähnlichkeit. Studie A nutzte ein satzbasiertes Wortpaar-Paradigma mit einer Manipulation der Reizbeginn-Asynchronie (kurz vs. lang) zwischen Prime und Target, um robuste Vorteile im gestützten Abruf für stark direkt miteinander assoziierte Wortpaare und vergleichsweise schwächere Effekte für semantische Merkmalsüberlappung zu zeigen. Dieses Ergebnismuster zeigte sich über alle drei Studien hinweg. Die fehlende Interaktion zwischen Reizbeginn-Asynchronie, direkter Assoziation und semantischer Merkmalsüberlappung deutete darauf hin, dass solche Enkodierungsvorteile eher während der lexikalischen Wortverarbeitung entstehen als durch zeitabhängige Integrationsmechanismen. Studie B replizierte das Paradigma mit einer mittleren Reizbeginn-Asynchronie und zeichnete elektroenzephalographische Daten auf, um neurophysiologische Korrelate der Enkodierung zu untersuchen. Subsequent-Memory-Effekte sagten den Erfolg des durch Hinweisreize geleiteten Abrufs auf Trial-Ebene unabhängig von der Prime-Target-Beziehung vorher und spiegelten damit eher Aufmerksamkeitsengagement und allgemeine Enkodierungstiefe wider als das Vorhandensein der assoziativ-semantischen Manipulation. Im Gegensatz dazu waren die Amplituden der parietalen späten positiven Komponente erhöht, wenn eine starke direkte Assoziation zwischen Prime und Target einen Enkodierungszustand unterstützte, der mit späterer episodischer Erinnerung (d. h. Abruf von

Kontextdetails) verknüpft war. Studie C ergänzte die bisherigen Befunde durch funktionelle Magnetresonanztomografie, um die Effekte der direkten Assoziation, der semantischen Merkmalsüberlappung und der rein episodischen Enkodierung auf die Aktivität hippocampaler Subfelder abzubilden. In dieser Studie wurden die Wortpaare nebeneinander ohne Satzkontext präsentiert. Der Gyrus dentatus zeigte bevorzugte Rekrutierung, wenn neuartige episodische Verknüpfungen gebildet werden mussten. Erhöhte Aktivität in CA3 hingegen stand im Zusammenhang mit hoher semantischer Merkmalsüberlappung, was durch seine Beteiligung an autoassoziativen (attraktorähnlichen) Mustervervollständigungsprozessen erklärt werden kann. Aktivität in CA1 und dem Subiculum wies zudem auf eine integrative Vergleichsfunktion hin, die die Übertragung in neokortikale Netzwerke unterstützt. Zusätzlich lieferten kortikale Tiefenprofil-Analysen (sechs äquidistante Tiefenstufen entlang des kortikalen Bandes) explorative Evidenz, die mit einer bedingungsabhängigen Rekrutierung in an der semantischen Kontrolle beteiligten Regionen konsistent ist. Die Effekte variierten jedoch nicht mit der kortikalen Tiefe. Durch die Integration assoziativer und semantischer Priming-Manipulationen in ein Wortpaarlernparadigma und die Kombination dessen mit neuronaler Bildgebung testet diese Dissertation Vorhersagen von komplementären Lernsystemen (rasches hippocampales Lernen neben gradueller neokortikaler Integration) und hippocampalen Attraktormodellen (rekurrente Dynamiken, die Mustervervollständigung unterstützen) beim Menschen. Diese Vorhersagen standen im Einklang mit der funktionellen Organisation der trisynaptischen Hippocampus-Schleife (Gyrus dentatus → CA3 → CA1 → Subiculum). Die Befunde stützen einen hybriden Erklärungsansatz, nach dem bereits vorhandene lexikalische Strukturen die Bildung neuer Gedächtnisinhalte durch mustervervollständigungsähnliche Prozesse in CA3 und parietale Amplitudendynamiken der späten positiven Komponente beeinflussen. Der Gyrus dentatus vermittelt zudem Mustertrennung, um die Integrität neu gebildeter episodischer Spuren zu bewahren. Insgesamt verfeinert diese Arbeit mechanistische Modelle der Enkodierung, indem sie distinkte Beiträge zur erfolgreichen Gedächtnisbildung voneinander abgrenzt und messspezifische Vorhersagen liefert, die gezielte kausale Überprüfungen in der zukünftigen Forschung motivieren.

List of Figures

Figure 1. Simplified Multi-Store Model of Memory 1

Figure 2. Segmentation of Hippocampal Subfields (Study C, Experiment C2) 4

Figure 3. Neocortical Information Pathways and Hippocampal Connectivity 5

Figure 4. Hippocampal Trisynaptic Circuit and Associated Neuronal Pathways 8

Figure 5. Illustration of Direct Association and Semantic Feature Overlap 10

Figure 6. Semantic Word Processing in the Associative Read-Out Model …….....13

Figure 7. 64-Channel actiCAP EEG Setup Used in Study B 19

Figure 8. Blood Oxygen Level-Dependent (BOLD) Contrast Principle in fMRI 21

Figure 9. Schematic Illustration of Proton Spin Behavior During an MRI Scan 23

Figure 10. Experimental Sequence and Timing of a Trial: Study/Test Phase (Study A) 42

Figure 11. Mean Error Rates (Study A) 45

Figure 12. Model-Based Estimates of Response Times (Study A) …….....46

Figure 13. Experimental Sequence and Timing of a Trial: Study/Test Phase (Study B) 65

Figure 14. Mean Error Rates (Study B) 70

Figure 15. Model-Based Estimates of Response Times (Study B) 71

Figure 16. Late Positive Component (LPC) for Correctly Recalled Targets (Study B) 73

Figure 17. Subsequent Memory Effects During Target Encoding (Study B) 74

Figure 18. Exploratory Source Reconstructions of Encoding-Related ERP Effects 75

Figure 19. Functional Pathways Linking Cortex and Hippocampus (Schematic) 89

Figure 20. Experimental Sequence and Timing of a Trial: Study/Test Phase (Study C) 94

Figure 21. Mean Error Rates and Response Times (Study C; Exp. C1) 95

Figure 22. Mean β Estimates from Contrast-Defined Subfield Clusters (Study C; Exp. C1) ...97

Figure 23. 7T fMRI Preprocessing and Analysis Pipeline (Study C; Exp. C2) 102

Figure 24. Total Head Displacement Calculation (Study C; Exp. C2) 103

Figure 25. Mean Error Rates (Study C; Exp. C2) 107

Figure 26. Model-Based Estimates of Response Times (Study C; Exp. C2) …….108

Figure 27. Model-Based Estimates of Hippocampal Subfield Activity (Study C; Exp. C2) ..110

Figure 28. Cortical ROI Localization and Corresponding Activity Contrasts (Study C; Exp. C2) 112

List of Tables

Table 1. Example Stimulus Sentences by Experimental Condition (Study A) 40

Table 2. Means (*SD*s) and *F* Statistics for Controlled Variables (Study A) 41

Table 3. GLMM Estimates for Trial-Level Recall Success (Study A) 45

Table 4. LMM Estimates for Trial-Level Response Times (Study A) 47

Table 5. Example Stimulus Sentences by Experimental Condition (Study B) 63

Table 6. Means (*SD*s) and *F* Statistics for Controlled Variables (Study B) 63

Table 7. GLMM Estimates for Trial-Level Recall Success (Study B) 70

Table 8. LMM Estimates for Trial-Level Response Times (Study B) 72

Table 9. Mean Amplitudes for the Subsequent Memory Effect Analysis (Study B) 74

Table 10. Example Word Pairs by Experimental Condition (Study C) 92

Table 11. Means (*SD*s) and *F* Statistics for Controlled Variables (Study C) 92

Table 12. Functional Magnetic Resonance Imaging Results (Study C; Exp. C1) 97

Table 13. GLMM Estimates for Trial-Level Recall Success (Study C; Exp. C2) 108

Table 14. LMM Estimates for Trial-Level Response Times (Study C; Exp. C2) 109

Table 15. Means (± *SE*s) of Error Rates and Response Times (Klein, 2016) 135

Table 16. Model Comparison for Natural-Log-Transformed Response Times (Klein, 2016) ….....136

Table 17. Model Comparison for Lexical Decision Accuracy (Klein, 2016) ….....136

List of Abbreviations

AFNI	Analysis of Functional NeuroImages	LR	Likelihood Ratio
AIC(c)	(Corrected) Akaike Information Criterion	LRT(s)	Likelihood Ratio Test(s)
rmANOVA	Repeated-Measures Analysis of Variance	LS	Low Semantic Feature Overlap
AROM	Associative Read-Out Model	LSA	Latent Semantic Analysis
AS	Association Strength	MNI	Montreal Neurological Institute
BIC	Bayesian Information Criterion	MP(2)RAGE	Magnetization-Prepared (2) Rapid Acquisition Gradient Echo
BOLD	Blood-oxygen-level-dependent		
CA	Common Associates	MTG	Middle Temporal Gyrus
CA1	Cornu Ammonis Subfield 1	MTL	Medial Temporal Lobe
CA3	Cornu Ammonis Subfield 3	N400	N400 (ERP Component)
CLS	Complementary Learning Systems	NA	Non-associated
CI	Confidence Interval	OR	Odds Ratio
CSF	Cerebrospinal Fluid	OTG	Occipito-Temporal Gyrus
DA	Direct Association	P300	P300 (ERP Component)
DCM	Dynamic Causal Modeling	P600	P600 (ERP Component)
DG	Dentate Gyrus	PAL	Paired-Associate Learning
EC	Entorhinal Cortex	PCC	Posterior Cingulate Cortex
EEG	Electroencephalography	PHC	Parahippocampal Cortex
EMMs	Estimated Marginal Means	PP	Perforant Path
EPI	Echo-Planar Imaging	PPI	Psychophysiological Interaction
ER(s)	Error Rate(s)	PRC	Perirhinal Cortex
ERP	Event-Related Potential	RFP	Radio Frequency Pulse
(f)MRI	(Functional) Magnetic Resonance Imaging	ROI(s)	Region of Interest(s)
FreeSurfer	Neuroimaging Software	RSA	Representational Similarity Analysis
FreeView	Visualization Tool (FreeSurfer)	RT(s)	Response Time(s)
FSL	FMRIB Software Library	SA	Strong Association
GFP	Global Field Power	SEM	Semantic Feature Overlap
GLM	General Linear Model	SME(s)	Subsequent Memory Effect(s)
GLMM	Generalized Linear Mixed Model	SOA	Stimulus-onset Asynchrony
GM	Gray Matter	SPM	Statistical Parametric Mapping
HS	High Semantic Feature Overlap	STG	Superior Temporal Gyrus
IAM	Interactive Activation Model	STS	Superior Temporal Sulcus
ICA	Independent Component Analysis	SUB	Subiculum
IFG	Inferior Frontal Gyrus	T1/T2	T1/T2-Weighted (Scan)
ISI	Interstimulus Interval	TBI	Traumatic Brain Injury
LMM	Linear Mixed-Effects Model	TP	Temporal Pole
LPC	Late Positive Component	WM	White Matter

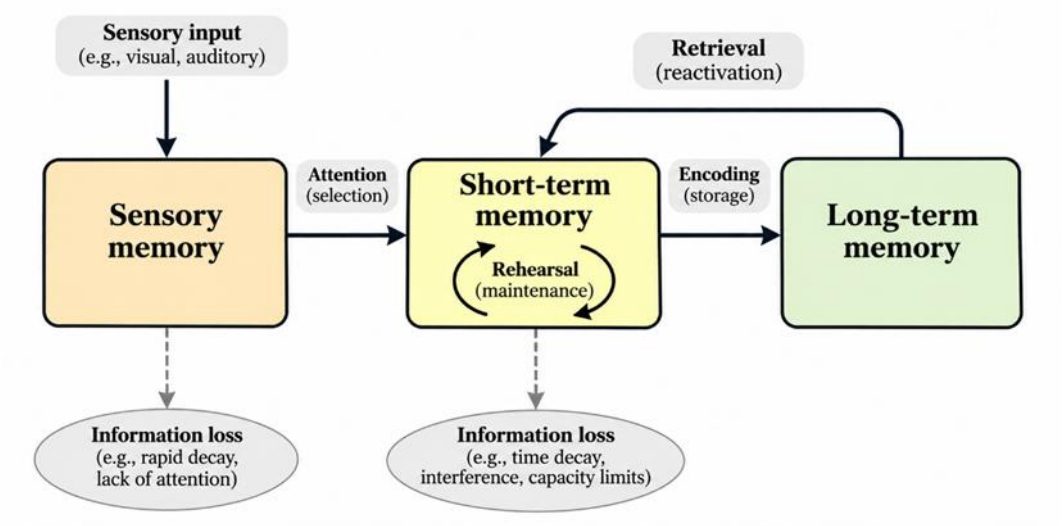
1. Theoretical Framework and Research Rationale

1.1 Mnestic Functions in Sub-Hippocampal Memory Systems

1.1.1 Information Storage in Memory Systems

Before considering the structure and functional organization of the main neural correlate of memory consolidation, it is important to contextualize the memory systems involved. The ability to consolidate, store, and retrieve abstract representations of sensory perceptions or cognitions in long-term memory is referred to as mnemonic function (Squire, 2004). Memory can be categorized into sensory, short-term, working, and long-term memory (Cowan, 2008). The functional organization of these memory systems and the information flow between them can be illustrated using a simplified version of the multi-store model proposed by Atkinson and Shiffrin (1968; Figure 1).

Figure 1
Simplified Multi-Store Model of Memory



Note. Schematic representation of information flow between sensory, short-term, and long-term memory, including attentional selection, rehearsal, encoding, retrieval, and potential information loss. Based on the multi-store model proposed by Atkinson and Shiffrin (1968).

Sensory memory acts as a relay station for specific sensory modalities and can be referred to, for example, as iconic memory in the context of visual perception (Baddeley, 2003). Short-term memory functions as a basic system for information processing, in which a limited capacity of information units is temporarily retained for further processing (Ma et al., 2014).

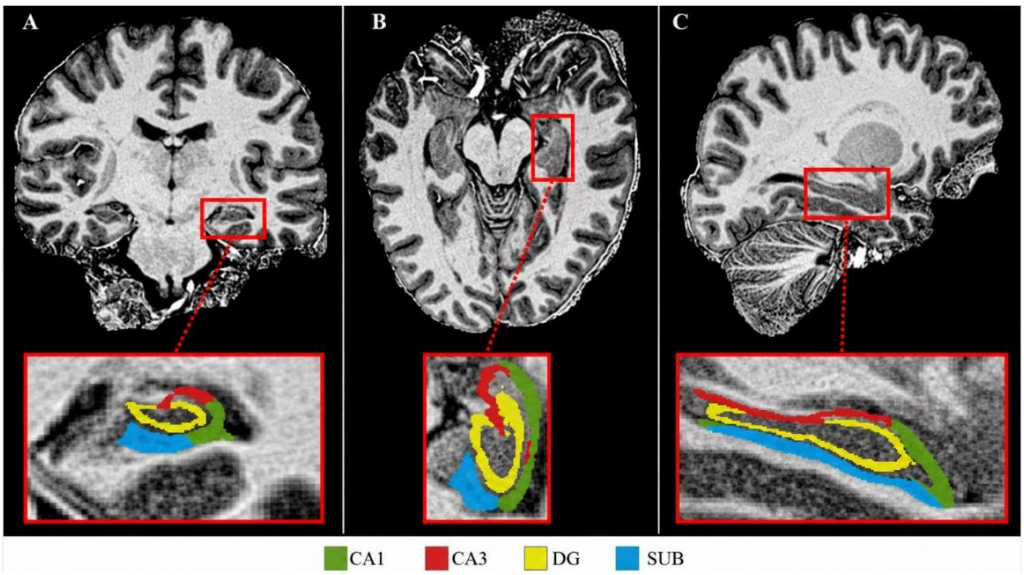
Above these two transient systems is working memory, which is used for activities such as reading, arithmetic, or reasoning (Baddeley, 2003). Working memory selectively transfers information to long-term memory. It can be divided into three components: the visuospatial sketchpad for visual information, the phonological loop for verbal information, and the central executive. The latter integrates both subsystems and acts as a modality-independent control unit that regulates attentional processes and transforms information between systems (Baddeley, 2012). In 2000, the episodic buffer was introduced as a multimodal integration system with limited capacity (Baddeley, 2000), simplifying the processing of relevant information units (Baddeley, 2012). This addition was crucial in explaining the phenomenon of chunking, which significantly improves memory performance for semantically related episodes (Baddeley, 2000).

Long-term memory is considered to be the persistent storage system of the cortex (Kandel et al., 2014). It is structurally divided into declarative and non-declarative memory systems. Non-declarative memory facilitates the automatic and largely unconscious expression of acquired information (Ullman, 2004), whereas declarative memory refers to consciously accessible knowledge that can be intentionally retrieved and is typically reportable explicitly (Squire & Dede, 2015; Squire & Wixted, 2011). Procedural memory, for example, is a prominent form of non-declarative memory that comprises learned skills and action sequences that can be executed efficiently without requiring conscious access to the underlying knowledge (Ullman, 2004). Declarative memory is further subdivided into semantic and episodic memory, which interact as subsystems. The neocortex and medial temporal lobe (MTL), particularly the hippocampus, serve as the associated neural correlates (Squire & Wixted, 2011). Episodic memory stores personal experiences and prospective content, such as remembering to perform a future action (Tulving, 2002). Semantic memory stores general knowledge about the world, including facts and language (Eichenbaum, 2017). This knowledge is organized into categories based on attributes (McRae & Jones, 2013). Accordingly, the focus of the present investigation aligns with the semantic subsystem of long-term memory.

1.1.2 Anatomical Structure of the Hippocampus

The cerebrum is divided into four lobes: the frontal lobe, the parietal lobe, the temporal lobe, and the occipital lobe. These structures envelop the limbic system, comprising subcortical areas such as the basal ganglia and thalamus. The cerebral cortex is characterized by the presence of sulci (grooves) or fissures (deeper grooves), which separate the brain gyri (ridges). The hippocampus, a component of the archicortex, functions as a central relay station within the limbic system and is present in a curved tubular form in each hemisphere (Amaral & Lavenex, 2007). The entorhinal cortex (EC) acts as a critical interface between the hippocampus and the cerebral cortex, facilitating bidirectional information transfer (Van Strien et al., 2009). Anatomically, the hippocampus extends along the anterior-posterior axis of the medial temporal lobe and is commonly differentiated into head, body, and tail, which show partially distinct connectivity profiles (Duvernoy, 2013). The hippocampal formation is further divided into three regions: the cornu ammonis, the dentate gyrus (DG) and the subiculum (SUB) (Amaral & Lavenex, 2007). The dentate fascia forms the granule cell layer of the DG and contains mossy fibers (mf), which are the axons of granule cells that extend into the cornu ammonis (Förster et al., 2006). In contrast, the SUB and cornu ammonis contain predominantly pyramidal cells, which are larger than granule cells and function as efferent neurons (Moser & Moser, 1998). The cornu ammonis is further subdivided into the subfields CA1, CA2, CA3, and CA4 (Duvernoy, 2013). Moreover, the fimbria (fim) is a key output pathway of the hippocampus and also carries commissural input from the contralateral hippocampus. In adult humans, high-resolution MRI-based subfield segmentations suggest that CA1 constitutes the largest proportion of hippocampal volume (35–40%), whereas DG and SUB each contribute roughly 20–25% and CA3 approximately 10–15%, with absolute volumes typically in the low cm^3 range per hemisphere (Iglesias et al., 2015). As part of the allocortex, the hippocampal formation is characterized by a comparatively simple laminar architecture (classically three-layered) relative to the six-layered neocortex (Duvernoy, 2013). Figure 2 shows the relevant hippocampal subfields for the present thesis.

Figure 2
Segmentation of Hippocampal Subfields (Study C, Experiment C2)



Note. The upper row shows a high-resolution 7T T1-weighted scan of a representative participant in (A) coronal, (B) axial, and (C) sagittal view. Red boxes mark the hippocampal region. The lower row shows corresponding magnified views with overlaid subfield labels (see legend for color coding). Visualization was performed using FreeView (Version 7.4.1; Fischl, 2012). CA1 = cornu ammonis field 1; CA3 = cornu ammonis field 3; DG = dentate gyrus; SUB = subiculum.

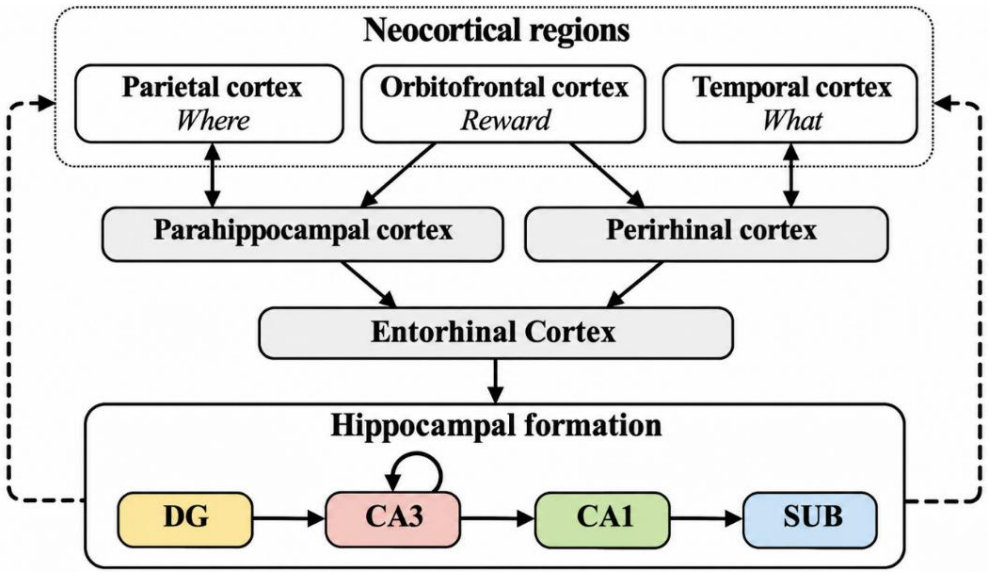
1.1.3 Hippocampal Subfield Connectivity

Each hippocampal structure has complex neural circuits, with recurrent excitatory connections between pyramidal neurons, that allow cells to self-activate through excitatory impulses from interneurons via axon collaterals (Brunel & Wang, 2001; Squire, 1992). The quality and latency of these mechanisms depend on the depth of the hippocampal subfield structure (Kumaran et al., 2016). Despite local recurrent connectivity within CA3, information transfer across subfields follows a predominantly unidirectional pathway, traversing densely packed cell layers from the DG to CA3 to CA1, with CA1 output typically relayed via the SUB before leaving the hippocampus (Duncan et al., 2012; Van Strien et al., 2009). This canonical feedforward sequence is commonly referred to as the hippocampal trisynaptic loop (Lee, GoodSmith, et al., 2020). The DG acts as an initial input station, receiving activation patterns from the EC via the perforant pathway (PP) (Duncan et al., 2012). Signals are transmitted from granule cells to pyramidal cells in CA3 (Förster et al., 2006). CA3 pyramidal neurons form extensive recurrent collateral connections within CA3 and project to CA1 via Schaffer collaterals (Squire, 1992). The CA1 region receives input from CA3 and sends output to both

the EC and the SUB (Duvernoy, 2013). The hippocampus integrates input from several regions, including the parahippocampal gyrus, perirhinal, prefrontal, and parietal cortices (Rolls & Treves, 2024). This connectivity allows the hippocampus to associate object representations with spatial information (Duvernoy, 2013). Input from the amygdala and orbitofrontal regions allows integration of reward-related information via connections to the nucleus accumbens (Rolls, 2007). In parallel, the PP bypasses the DG, allowing pre-existing information to flow directly from the EC to the CA3 region (Yassa & Stark, 2011). The EC consists of six layers, with neurons located just below the surface (Hafting et al., 2005). Output is generated by layers II and III, with layer II projecting primarily to the DG and CA3 and layer III projecting to the SUB and CA1 (Hafting et al., 2005). Incoming information reaches the EC via the perirhinal and parahippocampal cortices (Wiltgen et al., 2004), which in turn receive input from the neocortex (Takehara et al., 2003). Figure 3 provides a schematic overview of hippocampal connectivity and neocortical information pathways, drawing on the theoretical framework proposed by Rolls (2007). While this framework is primarily informed by findings from animal research, its applicability to human memory processing remains an empirical question.

Figure 3

Neocortical Information Pathways and Hippocampal Connectivity

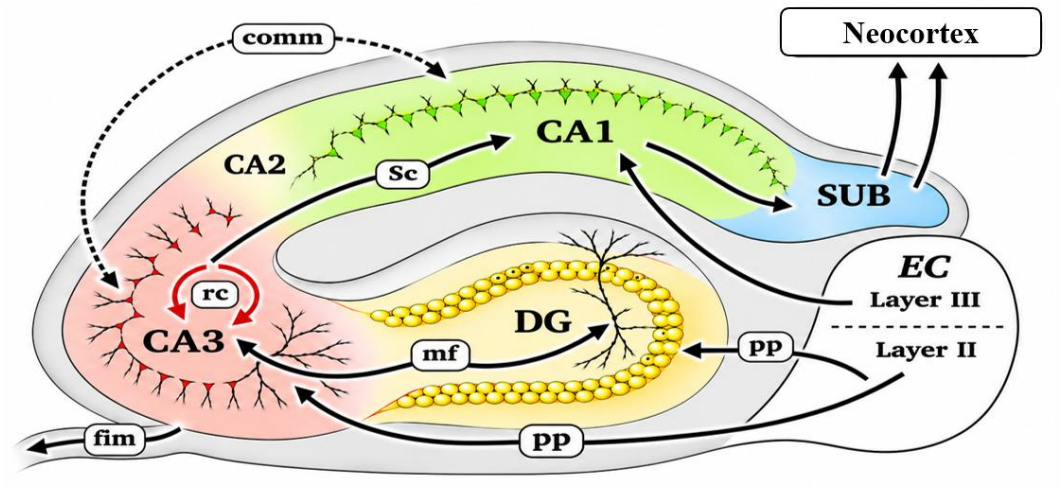


Note. Solid arrows indicate predominantly feedforward projections, whereas dashed arrows represent simplified feedback pathways. The recurrent loop illustrates CA3 autoassociative connectivity. Hippocampal connectivity and the functional dimensions of spatial (where), reward-related (reward), and object-related (what) information are based on Rolls (2007) and Rolls and Treves (2024). CA1 = cornu ammonis field 1; CA3 = cornu ammonis field 3; DG = dentate gyrus; SUB = subiculum.

Rolls' model of hippocampal connectivity is closely related to the Complementary Learning Systems (CLS) framework, which proposes that effective learning of novel memory content requires two complementary systems: one located in the neocortex and the other in the hippocampus (O'Reilly et al., 2014). The neocortical system is responsible for the acquisition of structured knowledge about the environment (McClelland et al., 1995), whereas the hippocampus facilitates rapid learning. Tse et al. (2007) showed that the consolidation of memory content in the neocortex is not always gradual but can also be extremely rapid if an associative *schema* that can accommodate new information has already been established. Using a hippocampus-dependent paired-associate task in rats, they found that memory for the original flavor-place associations became increasingly persistent over time as a putative neocortical schema gradually developed. Crucially, once this schema was in place, novel associations trained for only a single trial were rapidly assimilated and became independent of the hippocampus. Representations in the neocortex can therefore be considered parametric, as they encode a set of attributes rather than individual objects or features (Kumaran et al., 2016). The principle that the neocortex serves as a structured knowledge system has been derived from observations of multi-layer neural network models. These models learn to minimize misinterpretations of incoming information by adjusting the weights of the underlying concepts. This process can be explained by repeated, sustained excitation of the neural correlates of a concept, resulting in metabolic changes and increased network efficiency (Hebb, 1949). According to CLS theory, learning grouped attributes within a parametric system is relatively slow because each experience represents a unique environmental instance. Furthermore, optimizing connections among a subset of attributes necessarily alters the weighting of others, thereby increasing the risk of interference with previously acquired knowledge (Merhav et al., 2014). Accordingly, an additional learning system is required to mitigate these problems and store individual, unique learning experiences (McClelland & Goddard, 1996). The hippocampus, with other structures of the MTL, would be capable of representing this complementary, non-parametric learning system. In CLS theory, the DG and the CA3 region are the main components of this hippocampal system (Norman & O'Reilly, 2003). During an experience, the neocortex generates an activation pattern in the EC that represents a compressed form of information from different neocortical areas (O'Reilly et al.,

2014). The EC then transmits this information to the DG, CA1, and CA3 subfields of the hippocampus (Duvernoy, 2013). New patterns of activity in the EC activate a small group of neurons in the DG (via detonator synapses) and select a random subset of neurons in the CA3 region to represent the memory content (McClelland & Goddard, 1996). This activation pattern is made as distinct as possible from other memory content (Norman & O'Reilly, 2003). There is a stable correspondence between patterns in the EC and the CA1 region (Kumaran et al., 2016). In CA3, recurrent collateral connectivity can support autoassociative (attractor-like) dynamics (Rolls, 2007; Rolls & Treves, 2024), such that a partial input can reactivate a more complete stored representation. This mechanism has been discussed in cross-species reviews of the subfield-specific functional roles within the hippocampal circuit (Yassa & Stark, 2011) and is supported by human neuroimaging evidence implicating CA3 in completion-like retrieval under partial cueing (Grande et al., 2019). It is also consistent with the sharpening model of Wiggs and Martin (1998), which proposes that repeated stimulus presentation reduces neural responses because cortical representations become sparser and more selective. Neurons coding for relevant stimulus features maintain their responses, whereas responses associated with less relevant features are reduced, resulting in more efficient cortical representations. Within the framework of complementary learning systems (McClelland et al., 1995; McClelland & Goddard, 1996), this refers to the idea that the repeated reactivation of cortical activity patterns gradually reduces long-term dependence on the hippocampus while increasing the extent to which stored information is embedded in distributed cortical networks. The anatomical organization of the hippocampal circuit provides a framework for understanding these processes. Figure 4 schematically shows the canonical trisynaptic pathway and additional hippocampal connections, drawing on the anatomical and functional framework discussed by Yassa and Stark (2011). Neurons in Layer II of the EC project to the DG and CA3 via the perforant path, while DG granule cells project to CA3 via mossy fibers, contributing to the formation of distinct activity patterns. CA3 subsequently projects to CA1 via Schaffer collaterals, with information relayed to the SUB. The hippocampal trisynaptic pathway is predominantly feedforward, although recurrent collateral connections within CA3 provide substantial local feedback.

Figure 4
Hippocampal Trisynaptic Circuit and Associated Neuronal Pathways



Note. Schematic representation of the canonical hippocampal trisynaptic circuit (see Yassa & Stark, 2011), illustrating the major projections from the entorhinal cortex (EC) to the dentate gyrus (DG) and cornu ammonis field 3 (CA3) via the perforant path (pp), from the DG to CA3 via mossy fibers (mf), and from CA3 to cornu ammonis field 1 (CA1) via Schaffer collaterals (Sc). Additional connections include recurrent collaterals (rc) within CA3, direct entorhinal projections to CA1, projections from CA1 to the subiculum (SUB), commissural inputs (comm), and the fimbria (fim).

1.2 Word co-occurrences as an indicator of associative and semantic relationship

1.2.1 Applying computational methods to large text corpora

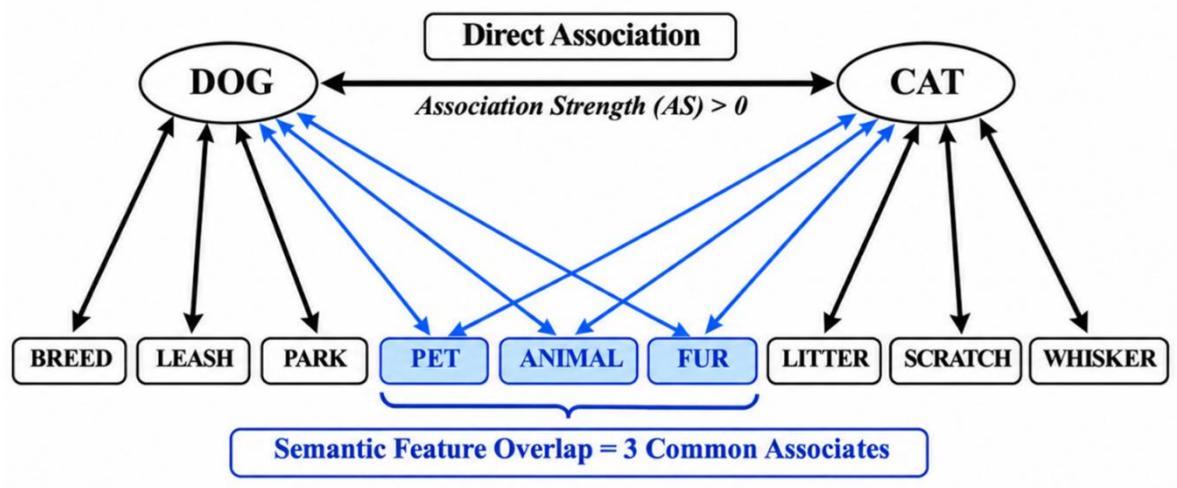
Research on language and cognition has made substantial progress due to advances in computational methods, particularly through the use of large-scale text corpora (McNamara, 2011). Sources including newspaper archives, online databases, and subtitles facilitate fine-grained, corpus-based analyses of language patterns (Evert, 2005; Goldhahn et al., 2012; Quasthoff et al., 2006) in various contexts, thereby offering implications for cognitive models of lexical-semantic representation and processing (Hofmann et al., 2011). Structured linguistic datasets are of great value to researchers, as they enable the quantification of word parameters such as frequency or co-occurrence. For instance, word frequency can be captured by simply counting the total number of occurrences in a text corpus (Quasthoff et al., 2006). Calculating the co-occurrence of two or more words within a given context (e.g., a sentence) provides a quantitative measure of their semantic similarity (Evert, 2005; Hofmann et al., 2011; Rapp & Samuel, 2002). Recent studies have further refined the understanding of word co-occurrence by identifying key semantic relations that drive this phenomenon (Zhao et al., 2023). It has

been shown that six semantic relations, such as ‘related to,’ ‘is a,’ ‘synonym,’ ‘has context,’ ‘antonym,’ and ‘manner of’ directly influence word co-occurrence patterns in natural language. Moreover, indirect co-occurrence can be explained through intermediate words and classified into broader relational categories such as ‘collocation and modification,’ ‘hyponymy,’ and ‘synonymy-antonymy,’ underscoring the structured nature of lexical association.

In the present thesis, word frequencies, sentence-level co-occurrences, and the total lexicon size were extracted from the German corpus of the Leipzig Wortschatz Project, comprising 70 million sentences (Goldhahn et al., 2012). The log-likelihood ratio for each word pair was computed based on these counts by testing the null hypothesis of independence, that the two words co-occur within sentences only at the rate that would be expected from their individual word frequencies (Dunning, 1993; Quasthoff et al., 2006). Associations were classified as positive when the observed co-occurrence exceeded this expectation and as negative when it fell below it. A direct association (DA) was only assumed for word pairs with observed co-occurrence above expectation. Positive log-likelihood ratio values that exceeded the χ^2 threshold corresponding to $p = .010$ were $\log_{10}$-transformed to quantify direct association strength (AS), whereas all other values received AS = 0 (Hofmann et al., 2011). Accordingly, DA was operationalized via corpus-derived AS, with word pairs treated as directly associated when AS > 0 and as non-associated otherwise (AS = 0). Semantic feature overlap was quantified by simply counting the number of common associates (CA) between two words (Rapp & Samuel, 2002). In line with the classification of syntagmatic relations by de Saussure (1959), a direct association is stronger for words that occur together more often than would be expected based on their overall frequency. Furthermore, paradigmatic relations reflect semantic similarity between two words (Rapp, 2002), which can be quantified by the overlap in their sets of associates. The number of common associates thus serves as a proxy for their shared semantic features (see Figure 5). Consequently, the greater the semantic feature overlap, the more reliably the words can be exchanged across many contexts without substantially changing the sentence meaning. Recent studies have extended these concepts by investigating how paradigmatic relations can be learned through contextual information. For instance, Smolek et al. (2023) suggest that temporal contiguity between morphologically related word forms enhances the learning of implicit relations through error-driven predictive learning. This

process relies on the increased salience of structural similarities and differences that occur when morphologically related forms are presented in close temporal proximity.

Figure 5
Illustration of Direct Association and Semantic Feature Overlap



Note. Hypothetical example of direct association and semantic feature overlap between "DOG" and "CAT". Bidirectional arrows represent direct associations, with blue arrows and labels identifying common associates whose number serves as a proxy for semantic feature overlap. Direct association is defined by positive association strength (AS > 0), reflecting significant, above-expected sentence-level co-occurrence quantified using the $\log_{10}$-transformed log-likelihood ratio.

1.2.2 Associative and semantic confound

The close relationship between direct association and semantic feature overlap poses a methodological challenge, as both systematically covary in natural language and therefore tend to co-occur in experimental stimulus materials (Hutchison, 2003; Lucas, 2000). This is particularly relevant when the goal is to attribute facilitation effects (e.g., in priming or word recognition) to a specific relational type rather than to general relatedness (Heyman et al., 2016; McNamara, 2005). Conventional approaches often employ free association norms, wherein participants are prompted to report the first word that comes to mind when presented with a cue (De Deyne et al., 2013). However, free association norms provide an aggregate behavioral index that often conflates direct associative relations with broader semantic similarity, making it difficult to identify word pairs that are strongly associated but not semantically related (Hutchison, 2003; Lucas, 2000; McNamara, 2005). As computational methods for analyzing large text corpora are becoming increasingly important for quantifying word relations (Evert,

2005; Hofmann et al., 2011; McNamara, 2011), the key question arises: To what extent are associative co-occurrence measures and semantic feature overlap confounded, especially when they serve as predictors for cognitive processes such as word recognition?

As outlined in Section 1.2.1, direct association is operationalized via corpus-derived sentence-level co-occurrence, whereas semantic feature overlap is quantified through the number of common associates shared by two words. Although these measures target relation types that are conceptually distinct (syntagmatic relatedness vs. paradigmatic similarity; Sahlgren, 2006), they rarely vary independently. According to Sahlgren (2006), syntagmatic relations describe the tendency of words to occur together in sequences or contexts (e.g., “doctor” and “hospital”), whereas paradigmatic relations capture similarity-based structure, that is, substitutability and shared neighborhood organization among words with related meanings (e.g., “doctor” and “physician”). In natural language, however, co-occurrence patterns blur the boundary between direct association and semantic feature overlap, because words that appear together often also share broader contextual similarity (Goldhahn et al., 2012). Crucially, the relationship is probabilistic rather than deterministic: some pairs can be strongly associated despite limited conceptual overlap (e.g., context-bound pairings), whereas other word pairs can be semantically similar while rarely co-occurring directly. It is precisely this partial dissociability that enables experimental tests to differentiate between direct association and semantic feature overlap, provided that the stimuli are constructed to minimize shared variance between these dimensions. Methodologically, this implies that stimulus selection cannot rely on related vs. unrelated contrasts alone, because such contrasts typically combine association strength and broader semantic similarity into a single composite factor (Hutchison, 2003; Lucas, 2000). Instead, the two dimensions should be manipulated in a way that matches overall distributions across experimental conditions and maximizes dissociation at the item level. This ensures that each predictor explains unique variance in behavioral or neural outcomes. Accordingly, the studies in this thesis employ a full-factorial stimulus set design approach that balances the overall number of associative and semantic relations across the stimulus set and reduces shared variance by orthogonally varying their magnitude at the item level (maximizing one dimension while minimizing the other; cf. Hofmann et al., 2018).

1.3 Modeling Language and Cognition: Spreading Activation in Semantic Networks

1.3.1 From Spreading Activations to the Associative Read-Out Model

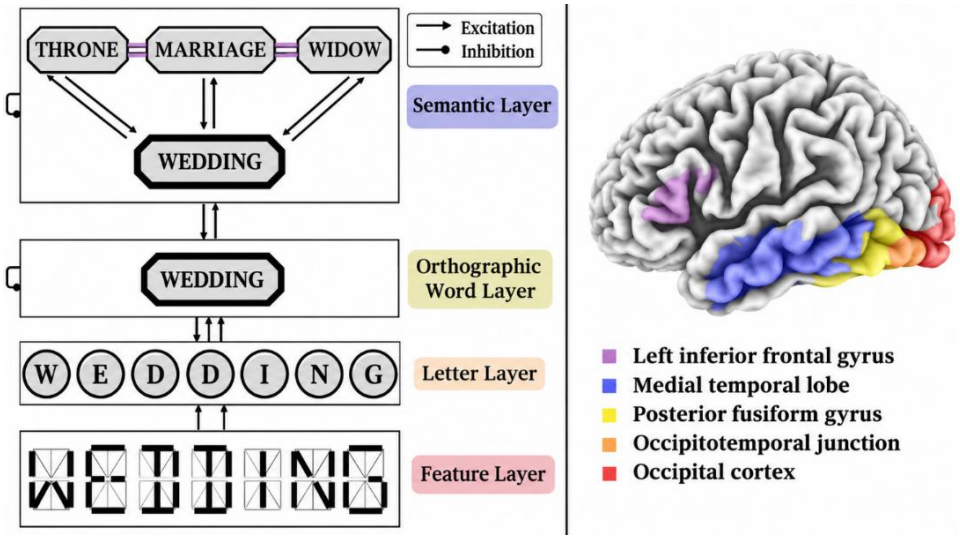
The spreading activation theory, initially introduced by Quillian (1967) as a theory of semantic memory search and subsequently elaborated by Collins and Loftus (1975), conceptualizes the cognitive representation of language as a network of interconnected nodes. Each node represents a word or concept, while the edges between them represent associative or semantic relationships. When external stimuli trigger activation, the resulting spread follows the connections of the network, with stronger activation for direct associations than for indirect ones. This theoretical framework provides a basis for understanding phenomena such as false memory (Roediger & McDermott, 1995) or associative and semantic priming (Hofmann et al., 2011; Meyer & Schvaneveldt, 1971), which is defined as facilitated processing of a target word attributable to prior activation of related lexical-semantic representations (Hutchison, 2003; Hutchison et al., 2013; McNamara, 2005). The use of text corpora as a fundamental resource in the computational modeling of this cognitive process facilitates the extraction of linguistic measures. Computational techniques, including word embeddings such as Word2Vec and GloVe, have been shown to enhance these analyses by mapping words into high-dimensional vector spaces (Mikolov et al., 2013; Pennington et al., 2014). These vectors capture both semantic and syntactic relations, thereby allowing for a more nuanced representation of language patterns. Based on the assumptions of the spreading activation theory, Hofmann et al. (2014) introduced the Associative Read-Out Model (AROM).

The AROM extends the original interactive activation model (IAM) of McClelland and Rumelhart (1981) by adding a semantic layer, using a symbolic language model in which long-term associations between words are defined by word co-occurrence statistics. Episodic links are reflected by an elevated resting-state activation of semantic word units for previously encountered items. This provides a retrieval baseline that can, for example, support old/new recognition by rendering the corresponding representations more active than those of novel items (Hofmann et al., 2011). As the original IAM only simulates orthographic processes in visual word recognition tasks, the AROM additionally considers associative and semantic relations between words. IAMs operate across multiple processing levels, including visual

features, letters, and words. In this localist architecture, units correspond to specific representational entities at each level, rather than information being encoded as a distributed pattern of activation across multiple units. Each level interacts bidirectionally, allowing activation to flow from lower levels (e.g., visual features of a letter) to higher levels (e.g., word recognition) and back, facilitating both bottom-up and top-down processing dynamics (McClelland & Rumelhart, 1981). The AROM added a semantic layer to simulate the dynamics of spreading activation within such a structured network. Figure 6 shows the architecture of the AROM alongside the proposed cortical representation.

Figure 6

Semantic Word Processing in the Associative Read-Out Model



Note. Left: Architecture of the Associative Read-Out Model, illustrating hierarchical interactions between feature, letter, orthographic word, and semantic processing layers. Excitatory and inhibitory conections are indicated by the respective arrow types. Right: proposed cortical representation of the model components. Adapted from Hofmann and Jacobs (2014).

By integrating neurobiological principles, the AROM provides insights into language processing at multiple levels, from letter recognition to semantic integration (Hofmann & Jacobs, 2014). It has been particularly effective in predicting behavior in primed lexical decision tasks (Rölke et al., 2018) or psychophysiological outcomes, such as left inferior frontal gyrus (IFG) activation, during semantic word processing (Rölke & Hofmann, 2020). The model was recently extended by a conjunctive layer (c-AROM; Rölke-Wellmann, 2021) to simulate the retrieval of learned versus forgotten words with high or low semantic feature overlap and by an explicit decision layer (AROM+; Sokolovič & Hofmann, 2024), which employs linear

leaky competing accumulators to model evidence accumulation based on activation from the episodic-semantic layer. The AROM+ integrates individual episodic memory traces and decision parameters, thereby enabling accurate prediction of accuracies and response times (RTs) in memory tasks.

1.3.2 Strengths and Limitations of Connectionist Models with Local Representations

Localist connectionist models, such as IAMs, play a central role in cognitive modeling. These models link individual nodes with specific concepts or features, making them particularly valuable for generating precise hypotheses about mental processes and their neural correlates. This discrete representation also enhances interpretability, providing clear visualizations of cognitive phenomena such as semantic priming, lexical decision-making, or word recognition (Grainger & Jacobs, 1996; Hofmann et al., 2011). Furthermore, recent extensions of localist models have been applied to neuropsychological conditions such as aphasia and semantic dementia by simulating the degradation of specific nodes and connections (Lambon Ralph et al., 2017). Despite their strengths, connectionist models with local representations face the challenge of learning novel associations and generalizing across unfamiliar stimuli. Furthermore, the biological plausibility of these models can be questioned, as they assume that a concept of knowledge is represented by a singular symbolic unit (Grainger & Jacobs, 1996; Hofmann & Jacobs, 2014; McClelland & Rumelhart, 1981). Neuroimaging studies suggest that a population of neurons is activated for each specific object, rather than a single unit representing knowledge (Plaut & McClelland, 2010; Quian Quiroga et al., 2008). The brain also does not operate deterministically, always producing identical results, but involves stochastic decision-making. An alternative is the approach of distributed representation of information, which uses hidden units to consider nonlinearity between inputs and outputs, as observed in learning processes (Rumelhart & McClelland, 1986).

However, distributed representations also face biologically implausible problems. For example, backpropagation, a common method that adjusts the weights of a neural network based on the error rates (ERs) from the previous epoch, transmits activation changes back to the input layer through the same connections. Neural synapses, in contrast, transmit

information only in a unidirectional manner. Parallel distributed processing models, which distribute information across multiple nodes, address some of these limitations through their dynamic and flexible learning capabilities. Emerging hybrid approaches seek to combine the interpretability of localist models with the adaptability of parallel distributed processing models. For example, integrating localist nodes into deep learning architectures has enabled more realistic simulations of cognitive processing and adaptive learning (Perconti & Plebe, 2020). Future research may enhance localist models by incorporating hierarchical processing layers that mirror cortical structures, improving their capacity to simulate complex phenomena like context-dependent meaning generation and multimodal integration (Kriegeskorte & Douglas, 2018). Recent breakthroughs in the field of artificial intelligence, particularly those pertaining to transformer-based architectures such as Bidirectional Encoder Representations from Transformers (Devlin et al., 2019) and the Generative Pre-trained Transformer architecture (Brown et al., 2020), have significantly expanded the potential of cognitive modeling. These models utilize attention mechanisms and bidirectional processing to capture complex semantic patterns and contextual dependencies (Vaswani et al., 2017). Their ability to generate nuanced semantic representations aligns closely with the principles of spreading activation theory (Collins & Loftus, 1975; Quillian, 1967). Incorporating such artificial intelligence systems would enable new ways of integrating cognitive theories with scalable computational frameworks to be explored.

1.4 Accessing Memory Formation via Cued Recall and Paired-Associate Learning

In cognitive psychology, cued recall tests have long served as a valuable method of probing memory accessibility under guided retrieval conditions (Adesope et al., 2017; Tulving & Pearlstone, 1966). Paired-associate learning tasks, in which participants study cue-target word pairs, are often employed beforehand to enable a systematic variation of cue diagnosticity, interference, and relational structure while holding item information constant (Kliegl & Bäuml, 2021; Wixted, 2004). Combined with subsequent cued recall, they provide an indirect index of encoding success, as they require the retrieval of previously acquired information in response to an associated cue (Roediger & Butler, 2011). Paired-associate

learning with subsequent cued recall operates on the premise that an appropriately linked cue activates a corresponding memory trace within a semantic network, in which concepts are linked on the basis of association strength and shared meaning. A key theoretical foundation for this is the concept of spreading activation (Anderson, 1983), which posits that the activation of a memory node propagates to related nodes within a semantic network. This propagation facilitates the retrieval process, particularly when the cue and the target share strong associative or semantic relations (Collins & Loftus, 1975; Hutchison, 2003). The power of retrieval cues was demonstrated very early on in a classic study by Tulving and Pearlstone (1966). In their experiment, participants were first presented with a list of words drawn from several categories, such as birds, furniture, or professions, without being informed of the underlying categorical structure. Later, one group was asked to freely recall the words, while another group was given the category names as retrieval cues. The cued recall group achieved a significantly higher recall rate (75%) compared to the free recall group (40%). This early experiment provided clear evidence that appropriately linked cues can facilitate access to stored information by activating related semantic networks. Roediger and Butler (2011) have provided further evidence that cued recall enhances recall accuracy and provides greater ecological validity compared to free recall. In everyday memory retrieval, context-related cues are typically present, making cued recall a closer approximation of real-world memory use. Ranganath and Ritchey (2012) further linked cued recall to coordinated activity in the medial temporal lobe (especially the hippocampus) and the frontoparietal control network. This aligns with the idea that successful recall relies on hippocampal pattern completion, which is supported by controlled, cue-guided retrieval. However, cue-guided retrieval is not without its challenges. If a cue is related to many potential target representations, the effectiveness of the retrieval process can diminish due to a phenomenon known as cue overload (Nairne, 2002; Watkins, 1976). Nairne's experiments demonstrated that an increase in the number of associations linked to a single cue results in lower recall accuracy, highlighting the balance between association strength and interference. Supporting evidence comes from Hintzman's (1984) work on the MINERVA model, which posits that retrieval is a function of the similarity between the cue and stored memory traces. His experiments revealed that cues with high distinctiveness lead to enhanced recall, whereas cues associated with multiple target representations lead to competitive interference. In a

comprehensive review, Wixted (2004) argued that the strength and clarity of the cue-target relationship are critical determinants of successful recall. In a series of experiments, robust memory traces coupled with precise cues led to higher recall probabilities, further underscoring the supportive role of memory trace distinctiveness. Besides, he emphasized that retrieval interference is a common cause of forgetting and that cue-overload manipulations (linking a single cue to multiple potential targets) provide a reliable way to induce response competition. In line with this, Kliegl and Bäuml (2021) conducted a review on proactive interference paradigms (including paired-associate learning) and discussed evidence that overlapping cue-target mappings (e.g., A-B, A-D) can induce response competition at retrieval, alongside list-differentiation accounts. Complementing these findings, Kahana (2020) used computational models to simulate memory retrieval processes. This work integrates both associative and semantic factors, showing that effective recall emerges from a complex interplay between the strength of individual memory traces and the broader structure of the semantic network. These models also shed light on the temporal dynamics of retrieval, helping to quantify interference effects that occur when multiple memory traces are activated simultaneously. Overall, paired-associate learning paradigms with subsequent cued recall tests provide a reasonable method for studying memory formation by integrating classic theories with contemporary empirical evidence. Despite their advantages, challenges such as cue overload and proactive interference continue to prompt refinements in experimental design, ensuring that these tests capture the complexities of long-term memory.

1.5 Present Neuroimaging Techniques Used to Study Memory Processes

1.5.1 Electroencephalography

Electroencephalography (EEG) is a non-invasive method used to record the electrical activity of the brain. By attaching electrodes to the scalp, EEG captures the synchronized electrical activity generated by neuronal populations in the cerebral cortex (Buzsáki et al., 2012; Olejniczak, 2006). These signals usually fall within the microvolt range, reflecting the postsynaptic potentials of pyramidal neurons (Buzsáki et al., 2012). EEG has become a standard tool in cognitive neuroscience, particularly in the study of processes such as memory

formation, attention, and perception (Buzsáki & Draguhn, 2004; Friedman & Johnson, 2000; Hauk & Pulvermüller, 2004; Rugg & Curran, 2007). EEG signals are primarily derived from the summation of excitatory and inhibitory postsynaptic potentials in cortical pyramidal neurons, whose apical dendrites are oriented perpendicularly to the cortical surface, allowing for the spatial summation of their electrical activity and its subsequent detection at the scalp (Buzsáki et al., 2012; Olejniczak, 2006). It is important to note that the EEG does not directly measure action potentials, which are too brief and localized to contribute significantly to the EEG signal. Instead, it is indicative of the collective activity of neuronal populations, particularly those undergoing synchronous activation within specific cortical areas (Buzsáki & Draguhn, 2004). The electrical potentials measured in EEG result from the flow of ions through the neuronal membranes (Buzsáki et al., 2012; Olejniczak, 2006), with sodium (Na^+), potassium (K^+), calcium (Ca^{2+}), and chloride (Cl^-) ions in particular generating localized electric fields. When these fields are synchronized across populations of neurons, they generate sufficient activity that can be measured at the scalp surface (Buzsáki et al., 2012). Thus, the EEG does not measure the activity of individual neurons, but rather the summed activity of large neuronal populations, typically firing synchronously within specific cortical areas. While action potentials are a direct signal transmission along axons, postsynaptic potentials (PSPs) are the primary source of the EEG signal (Olejniczak, 2006). PSPs are generated at the dendrites when signals arrive from other neurons. This causes a change in the neuron's membrane potential, resulting in electric fields that can build up (Olejniczak, 2006). The synchronous electric fields generated by neuronal activity in the cerebral cortex are therefore of particular importance. Furthermore, the recorded signal is affected by the conductivity properties of the brain, skull, and scalp. These act as volume conductors, effectively low-pass filtering the underlying neuronal activity, attenuating higher-frequency components (Buzsáki et al., 2012).

Recording an EEG involves the placement of electrodes at standardized locations on the scalp, often in accordance with the international 10–20 system (Jasper, 1958). Each electrode measures the voltage difference between two points, typically between an active recording site and a reference electrode, thereby providing information about the relative electrical potential in different regions of the brain (Keil et al., 2014; Picton et al., 2000). To

illustrate, in the 64-channel actiCAP electrode system (Brain Products GmbH, Gilching, Germany), electrodes are positioned over frontal, parietal, occipital, and temporal scalp regions (see Figure 7), thereby providing broad spatial coverage of electrical brain activity.

Figure 7
64-Channel actiCAP EEG Setup Used in Study B



Note. Left: participant wearing a 64-channel actiCAP (Brain Products GmbH) with active electrodes. Right: close-up view showing electrode distribution. Electrodes were positioned according to the extended international 10–20 system, covering frontal, temporal, parietal, and occipital regions. Images were de-identified by blurring facial features.

Modern EEG systems use electrodes embedded in caps to improve the accuracy and repeatability of electrode placement. Conductive gel is applied to ensure low impedance between the electrode and the scalp, which is necessary for high-quality signal detection (Kappenman & Luck, 2010; Picton et al., 2000). The signals are then amplified, as they are typically in the microvolt range and would otherwise be too weak to be processed by data acquisition systems (Picton et al., 2000). In an EEG system, amplification is followed by digitization, which converts the continuous analog signal into discrete values that can be processed by a computer. This is typically done at a sampling rate sufficient to capture the relevant frequency components of brain activity. For cognitive neuroscience, a sampling rate of at least 250 Hz is common, but higher rates may be used depending on the specific research needs (Keil et al., 2014; Picton et al., 2000).

One of the major challenges in EEG recording is the presence of noise and artifacts that can distort the signals and reduce the accuracy of data interpretation. Common sources of noise

include power line interference, muscle activity (e.g., from eye blinks or jaw movements), and electrode drift (Picton et al., 2000). These artifacts are particularly problematic in cognitive studies because they can mask the subtle brain responses of interest. Several techniques are used to mitigate these problems. Filtering is commonly used to attenuate high-frequency noise, low-frequency drifts, and power-line interference, depending on the applied filter characteristics (Keil et al., 2014; Picton et al., 2000). Ocular artifacts, such as blinks and eye movements, can be identified and corrected using independent component analysis (ICA) or regression-based methods (Delorme & Makeig, 2004). In addition, proper grounding and shielding of EEG equipment is essential to minimize external electromagnetic interference (Keil et al., 2014; Picton et al., 2000). Spontaneous EEG refers to the ongoing electrical activity of the brain that occurs in the absence of an explicit external stimulus or task. This type of brain activity is classified into distinct frequency bands: delta (0.5–4 Hz), theta (4–8 Hz), alpha (8–13 Hz), beta (13–30 Hz), and gamma (>30 Hz) (Buzsáki & Draguhn, 2004; Klimesch, 1999). These frequency bands are thought to reflect different states of consciousness and cognitive processes. However, event-related potentials (ERPs), the subject of Study B of the present doctoral thesis, provide insights into the temporal dynamics of cognitive processes such as memory formation (Rugg & Curran, 2007). ERPs are time-locked EEG responses elicited by specific sensory, cognitive, or motor events and are extracted by averaging the EEG signal over multiple trials in response to the same stimulus or task condition (Picton et al., 2000; Rugg & Curran, 2007). This improves the signal-to-noise ratio by canceling random fluctuations while preserving the brain's time-locked response to the event.

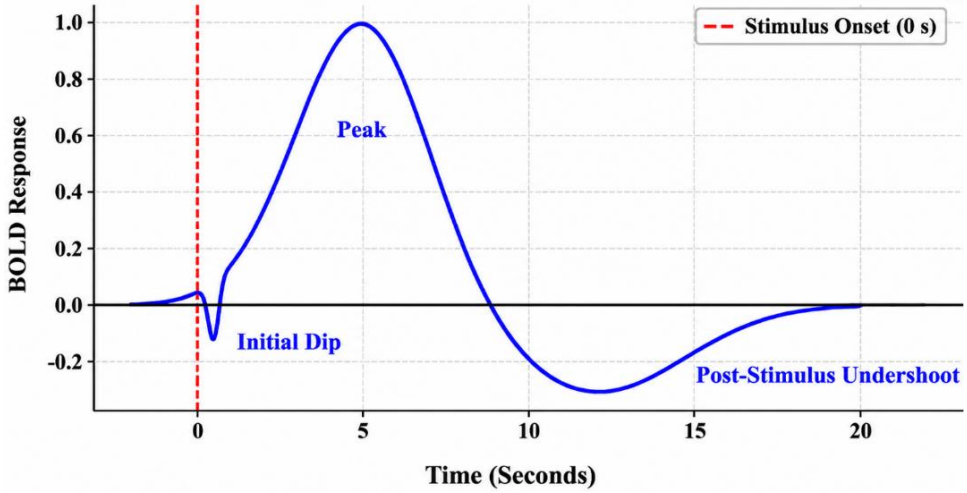
1.5.2 Functional magnetic resonance imaging

Functional magnetic resonance imaging (fMRI) is a suitable method for investigating deep brain structures during memory formation, such as those addressed in the present thesis. In this context, the blood oxygen level-dependent (BOLD) response is primarily used as a contrast mechanism for signal detection. The measuring principle can be summarized as follows: The magnetic properties of blood depend on the oxygenation state of hemoglobin. Deoxygenated hemoglobin is paramagnetic, whereas oxygenated hemoglobin is diamagnetic

(Ogawa et al., 1990). This results in differences in signal decay following a radiofrequency excitation pulse. In detail, fMRI relies on the hemodynamic response to local neural activity via neurovascular coupling (involving neurons, astrocytes, and vascular cells), such that cerebral blood flow in stimulated cortical tissue changes phasically (Lauritzen, 2005; Petzold & Murthy, 2011). Astrocytes support neuronal energy metabolism by taking up glucose from cerebral capillaries and supplying metabolic substrates to surrounding neurons (Magistretti & Allaman, 2015). The concentration of deoxygenated hemoglobin increases as neural activation initially raises oxygen extraction (Hillman, 2014; Lauritzen, 2005). Oxygen is released from oxyhemoglobin within red blood cells, thereby increasing the local concentration of deoxygenated hemoglobin in the stimulated brain area (Ances et al., 2008; Hillman, 2014). This increase is often referred to as the initial dip of the BOLD response (Figure 8) and typically emerges shortly after stimulus onset following cortical excitation (Hillman, 2014). Afterward, the relative concentration of oxygenated hemoglobin in the stimulated area increases as a compensatory response (Ogawa et al., 1990). The increase in oxygenated blood then leads to an excess in the corresponding area, which reaches its maximum after about four to six seconds, then decreases and returns toward baseline, often with a post-stimulus undershoot (Ances et al., 2008; Hillman, 2014).

Figure 8

Blood Oxygen Level-Dependent (BOLD) Contrast Principle in fMRI



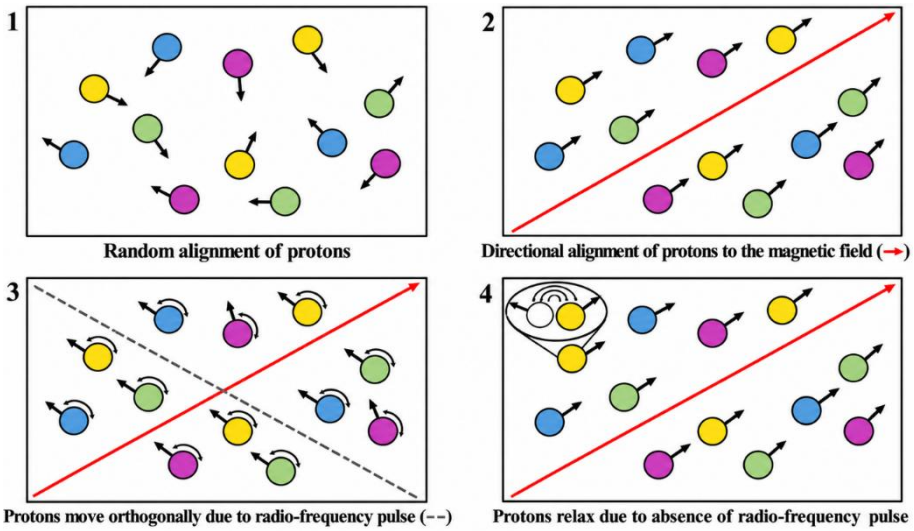
Note. Schematic illustration of the canonical hemodynamic response that underlies the blood oxygen level-dependent contrast in functional magnetic resonance imaging (fMRI).

In magnetic resonance imaging, the spin and precessional motion of the protons in the cortical hydrogen atoms are used (Pooley, 2005). An atomic nucleus consists of two distinguishable nucleons, the positively charged protons and the uncharged neutrons (Pykett et al., 1982). The atomic nucleus is characterized by an intrinsic angular momentum, whereby the accumulation of the individual rotations results in the total angular momentum (nuclear spin) around its own center of gravity (Pooley, 2005; Pykett et al., 1982). The scanner contains a magnetic coil that generates a constant magnetic field and aligns the spins horizontally in a north-south direction (Pooley, 2005). This ensures that the precession frequency of the protons can be calculated accurately (Bloch, 1946; Pykett et al., 1982). The direction of magnetization rotates around its own axis of rotation (Pooley, 2005). This molecular angular momentum, which rotates in the direction of an external magnetic field, is referred to as precessional motion (Bloch, 1946; Pooley, 2005). The clock rate of this precession is called the Larmor frequency and is calculated from the gyromagnetic ratio, the ratio between the spin of a particle and its magnetic property, and the strength of the applied magnetic field in Tesla (Bloch, 1946; Pykett et al., 1982).

In addition to the magnetic coil, the MRI scanner has a radio coil arranged perpendicular to the magnetic coil, which emits an electromagnetic radiofrequency pulse at a specific frequency to selective layers of the cortex (Pooley, 2005). When this radiofrequency pulse (RFP) has the same frequency as the precessional motion of the protons, energy is delivered to the protons and a resonance is generated (Bloch, 1946; Pooley, 2005). The protons move through this resonance, which allows parallel protons to align antiparallel (Bloch, 1946; Pooley, 2005). This leads to a phase-synchronous tilt of 90° (transverse magnetization). At the same time, and depending on the type of surrounding tissue, a certain percentage of the now transversely magnetized, phase-synchronous spins decay (Pooley, 2005; Pykett et al., 1982). It is measured when 63 percent of the signal has decayed, which is referred to as T2 relaxation (Pooley, 2005). This decay reflects the dephasing of the transverse magnetization caused by spin-spin interactions and the microscopic inhomogeneity of the magnetic field within tissue. Thereafter, when no more RFP is emitted from the radio coil, the in-phase precessing proton spins return to their original orientation (Pykett et al., 1982). This process is called longitudinal or T1 relaxation (Pooley, 2005; see Figure 9).

Figure 9

Schematic Illustration of Proton Spin Behavior During an MRI Scan



Note. The figure depicts nuclear spin alignment, radio-frequency excitation, and relaxation processes underlying magnetic resonance imaging (MRI) signal generation. The symbol positions are illustrative and not spatially meaningful.

The duration of longitudinal relaxation depends on the type of tissue, the viscosity, and the electronegativity of the nuclear environment, which is why differentiated tissue types can be easily distinguished and precise anatomical images and information can be generated using the time constant (Pooley, 2005; Pykett et al., 1982). The energy emitted by the spins to the surrounding tissue during T1 relaxation is measured by a receiving coil that is aligned in the direction of the transmitting coil (Pooley, 2005). The longitudinal relaxation lasts between 300 and 2,000 ms (Menon & Kim, 1999), and its duration determines how long to wait before applying another radiofrequency pulse. This time constant is referred to as the repetition time. In high- to medium-viscosity environments, the T1 time is significantly longer than the T2 time, which is relatively short at 100 ms per layer and depends on the amount of deoxygenated hemoglobin. The magnetic properties of the blood protein hemoglobin change depending on the absorption capacity of its up to four free oxygen bonds. This results in different signals: the T2 relaxation time is shorter for low-oxygen hemoglobin because its unpaired electrons cause local inhomogeneities in the magnetic field and thus faster dephasing of the hydrogen nuclear spins (Ogawa et al., 1990). To enable location determination, slice selection, phase encoding, and frequency encoding are used, each representing one of the three directional parameters (x, y, z).

The following overview is based on Huettel, Song, and McCarthy's *Functional Magnetic Resonance Imaging* (2014). It is deliberately concise and is intended to provide a brief introduction to temporal and spatial coding in fMRI. In most cognitive fMRI applications, images are acquired as T2-weighted time series (often using echo-planar imaging (EPI)) and functional contrasts are derived from the BOLD effects. However, because the hemodynamic response unfolds over several seconds, the temporal interpretation is constrained by both the repetition time and vascular dynamics, despite the fact that the underlying neural events are rapid. In the first dimension, a single slice is obtained at each time point following T1 and T2 (slice selection) through the excitation of a specific plane of the brain with a radio pulse transmitted through a gradient field parallel to the main magnetic field. This results in the scattering of the Larmor frequency in each layer parallel to the gradient field, as well as homogeneity within a layer. Each layer is characterized by a gradient strength, whereby the layer thickness is determined by the bandwidth of the time interval in the frequency spectrum of the pulse. Further gradient coils in the MRI scanner are responsible for the second and third dimensions, which mark two dimensions in space and change the frequency and movement of the protons accordingly. For the second dimension, the movements of the protons are excited to different degrees. Here, the precession frequency is responsible for the coding. It makes it possible to determine the current position of a spin on the precession cone. The phase is detected between the pulse and the reception of the signals at the receiving coil. In the third dimension, the resonance (i.e., the energy at which the protons align antiparallel) is attacked and causes a shift in the resonance phase. As a result, the spins each experience a magnetic field of different strength, which can be translated into a characteristic function of the position for the prevailing precession frequency. With the help of this information, it is possible to generate a three-dimensional topographical image that shows from which voxel the measured activity originates. In cognitive neuropsychology, a voxel is a three-dimensional volume element whose position is usually implicitly derived from other voxel clusters (Ashburner & Friston, 2000). The result is functional imaging of the activated brain areas with high spatial resolution.

1.6 Motivation for the Doctoral Thesis

The consolidation, storage, and retrieval of memories are fundamental to human cognition. Yet, the precise mechanisms underlying successful memory formation remain incompletely understood. Exploration of memory formation has frequently been framed around the interplay between episodic encoding and long-term knowledge (O'Reilly et al., 2014; Tulving, 2002). While episodic encoding is traditionally considered as a mechanism reliant on context-dependent and attentional factors (Paller & Wagner, 2002), associative and semantic long-term knowledge have been proposed to support or even compete with episodic processes during memory formation (Tulving, 2002). This doctoral thesis, which is titled *Successful memory formation in paired-associate learning: Associative and semantic effects on episodic encoding*, aims to disentangle these interactions through empirical findings and contribute to the theoretical understanding of how memory traces are formed, established and differentiated in the human brain. A hybrid experimental paradigm is employed that integrates two traditionally separate experimental families: priming (to manipulate pre-activation within lexical-semantic networks) and paired-associate learning (to test the formation of durable cue-target bindings). To reduce the often observed confound between associative relations and broader semantic similarity, both constructs are operationalized using corpus-derived statistics and probed in an orthogonal, full-factorial design.

Unraveling how associative and semantic long-term knowledge influences episodic encoding is not only crucial for advancing cognitive neuroscience but can also be used for practical applications such as optimizing learning conditions. Implicitly conditioned long-term relations may enhance memory retrieval, and exploiting these mechanisms could improve educational strategies, help people with learning difficulties, or facilitate foreign language acquisition. As a complementary perspective, the findings may also inform biologically plausible neural network models, further bridging the gap between cognitive and computational neuroscience. Furthermore, insights into the distinct roles of neurophysiological correlates such as hippocampal subfields may contribute to a more precise understanding of how specific lesions or inflammatory processes may affect memory formation.

The main goal of the present thesis is to contribute to the ongoing debate about the roles of episodic, associative, and semantic long-term relations in language-based learning. A more comprehensive understanding of how episodic encoding and implicitly conditioned associative-semantic relations interact will provide deeper insights into the distinct contributions of each memory system to successful learning and retention. To explore this dynamic relationship, three studies were conducted combining behavioral paradigms with EEG and fMRI. This multimethod approach enabled the investigation of the cognitive and neural mechanisms underlying episodic and long-term memory processes.

Study A examined how manipulating the stimulus-onset asynchrony (SOA) in a sentence-embedded paired-associate paradigm affects the formation of episodic, associative, and semantic long-term memories, with the aim of demonstrating that associative-semantic effects occur in addition to episodic effects and exploring whether there is an optimal timing for word presentation supporting the learning process. Given that electroencephalography provides unparalleled temporal resolution for probing neurophysiological correlates (Buzsáki et al., 2012), Study B focused on ERPs such as the Late Positive Component (LPC) and subsequent memory effects (SMEs) associated with deep language encoding (Mecklinger & Kamp, 2023; Paller & Wagner, 2002; Polich, 2007). Using the same paradigm but with a moderate SOA, the aim of this study was to map the temporal dynamics of successful memory encoding. Although EEG excels in temporal resolution, its ability to localize activity in subcortical structures is limited (Michel & Brunet, 2019). To address this, Study C employed fMRI to examine hippocampal subfield activity during paired-associate learning, providing insight into the spatial organization of the underlying memory processes. In doing so, theoretical assumptions from attractor-network models of rodents (Rolls & Treves, 2024) were placed within a human context and compared to empirically informed anatomical literature (Yassa & Stark, 2011). In addition, this study investigated associative and semantic effects in cortical regions linked to the semantic control network (Binder et al., 2009; Jackson, 2021).

2. Overview of the Empirical Studies

2.1 Introducing Study A

Study A was motivated by the long-standing debate about the existence of purely associative relations, as numerous studies have reported inconsistent findings (Hutchison, 2003; Lucas, 2000). For instance, Kumar et al. (2020) examined semantic priming using large-scale free-association networks. Their findings revealed that automatic activation and controlled expectancy effects interact dynamically, highlighting the fundamental challenge of disentangling purely associative and semantically mediated processes. To address this issue, Rölke et al. (2018) conducted a primed lexical decision paradigm with a full-factorial manipulation of direct association and semantic feature overlap, showing that these processes can be distinguished under different SOAs. Direct association effects only emerged at long SOAs, whereas high semantic feature overlap facilitated lexical decisions at short SOAs. Such result patterns demonstrate that associative activation requires time to propagate, as postulated by Collins and Loftus (1975), and that semantic priming effects tend to occur with short SOAs (Ferrand & New, 2003; Lucas, 2000), because semantic competition processes emerge when the SOA is too long (Neely, 1977; Plaut & Booth, 2000). Building on this, Study A aimed to examine how variations in the SOA affect the formation of episodic, associative, and semantic long-term memory. A sentence-embedded paired-associate paradigm (e.g., “the car has an engine”, with “car” as the prime and “engine” as the target) was implemented in a rapid serial visual presentation format (word-by-word) to enable precise temporal control over the prime-target interval in two SOA conditions (short vs. long). Direct association (strong vs. none) between prime and target was operationalized via corpus-derived association strength, computed from co-occurrence statistics using log-likelihood ratios (Hofmann et al., 2018). Semantic feature overlap (high vs. low) was computed by counting the number of common associates (Rölke et al., 2018; Rölke & Hofmann, 2020). The effects of this full-factorial manipulation were examined using a subsequent cued recall test, which measured trial-level recall success and response times. The goal was to determine whether prime-target timing modulates subsequent retrieval efficiency and to test whether Rölke et al.’s (2018) approach can be applied to a memory paradigm.

2.2 Introducing Study B

Study B builds on foundational work by Paller and Wagner (2002), who questioned the overlap between episodic encoding and implicitly conditioned associations. They proposed that episodic traces may either integrate with or operate independently of associative-semantic processes, a hypothesis that remains empirically underexplored. Previous studies (Rölke et al., 2018; Rölke & Hofmann, 2020) have demonstrated the logical and functional separability of associative and semantic priming effects in lexical processing but have not investigated their contribution to episodic encoding. This study employed a sentence-embedded paired-associate paradigm to examine these mechanisms, with rapid serial visual presentation (word-by-word) to display words under precise temporal control. Participants were instructed to learn sentences of the structure article, subject-prime, auxiliary verb, closed-class word, and target-object under full-factorial manipulation of direct association (strong vs. none) and semantic feature overlap (high vs. low) between prime and target. Corpus-derived co-occurrence statistics enabled a precise operationalization of associative and semantic relations, following the framework established by Hofmann et al. (2018). By measuring trial-level recall success and response times during delayed cued recall, this study aimed to determine whether associative and semantic priming facilitate memory formation independently or interactively. EEG data were collected to analyze ERP components during encoding, focusing on two key measures: the LPC, which is associated with deep, attentive encoding (Polich, 2007), and SMEs, which reflect neural markers of successful memory formation (Mecklinger & Kamp, 2023; Paller & Wagner, 2002). As both provide information about the temporal dynamics and success of memory formation (Kutas & Federmeier, 2011; Yonelinas, 2002), this study aimed to test the hypothesis that associative and semantic processes, although distinct, might modulate episodic encoding under certain conditions. The theoretical basis for this study derives from spreading activation models (Collins & Loftus, 1975) and interactive activation theories (McClelland & Rumelhart, 1981), which suggest that associative relations facilitate information integration over time. Semantic competition models (Plaut & Booth, 2000), on the other hand, argue that semantic overlap can delay processing due to feature competition, especially at longer SOAs. Study B addressed these conflicting predictions by presenting stimuli with controlled SOAs.

2.3 Introducing Study C

Study C addresses core concepts from CLS (O'Reilly et al., 2014) and attractor-network models (Rolls & Treves, 2024), testing them in a human context. It uses empirical reviews of pattern separation/completion (Yassa & Stark, 2011) as a reference point, which propose that the hippocampus integrates stored information with novel episodic input, thereby playing a dual role in reactivating long-term memory and generating new episodic conjunctions. The present study examined how associative and semantic long-term relations shape the formation of new episodic memory traces in hippocampal subfields using a paired-associate learning task during fMRI acquisition. Participants encoded word pairs under a full-factorial manipulation of direct association (strong vs. none) and semantic feature overlap (high vs. low). Direct association was operationalized using association strength, computed from co-occurrence statistics in a large text corpus (Dunning, 1993; Hofmann et al., 2018), while semantic feature overlap was computed by counting the number of common associates between word pairs (Rölke et al., 2018; Rölke & Hofmann, 2020). A subsequent cued recall test, in which trial-level recall success and response times were measured, was used to examine whether associative and semantic cueing facilitated the memory formation. FMRI data acquired at 3T and 7T enabled a detailed examination of hippocampal subfields, including the DG, CA1, CA3, and the SUB. The 3T dataset (Experiment C1) was originally acquired for the author's master's thesis (Klein, 2018) and was reanalyzed for the present thesis. The 7T main study (Experiment C2) built upon these findings by enabling more precise and sensitive subfield-level analyses at higher spatial resolution. The DG, which plays a key role in the formation of new, episodic associations (Yassa & Stark, 2011), is the first structure activated in the hippocampal trisynaptic loop. The CA3 region subsequently operates as a recurrent autoassociative (attractor-like) network, which supports pattern completion (Leutgeb et al., 2007; Rolls & Treves, 2024). CA1 and the SUB have been implicated in the top-down modulation of cortical activity, particularly when semantic similarities to existing memory traces are present (Eichenbaum, 2017; Rolls, 2007). Accordingly, Study C aimed to test the hypothesis that associative and semantic relations between two words modulate hippocampal activation patterns during encoding of novel stimulus material, with subfield-specific effects.

3. Study A: Associative and Semantic Priming in Paired-Associate Learning: Effects under Short and Long Stimulus-Onset Asynchrony

Abstract

This study examined how associative and semantic long-term knowledge support successful memory formation in a sentence-embedded paired-associate learning task and whether these effects are modulated by stimulus-onset asynchrony (SOA). Participants were instructed to learn sentences of the structure: article, subject-prime, auxiliary verb, closed-class word, and target-object (e.g., “the car has an engine”). In a subsequent test phase, they had to recall the target-object, given the preceding sentence context. The stimuli were presented using rapid serial visual presentation to enable precise temporal control of the prime-target SOA. Corpus-derived co-occurrence statistics were used to implement a full-factorial manipulation of direct association (strong vs. none) and semantic feature overlap (high vs. low) between the prime and the target word (cf. Hofmann et al., 2018). The SOA between prime and target was set to a short (300 ms) or long (1,450 ms) time interval. Both strong direct association and high semantic feature overlap led to more correct responses in the delayed cued recall test. Response times were selectively faster for strong direct association, but not for semantic feature overlap. No interactions were observed. SOA did not exert an influence on behavioral performance. The results demonstrate the influence of long-term knowledge on successful memory encoding, highlighting the impact of pre-existing associative and semantic relations on paired-associate learning. The selective response time benefit for strong direct association is consistent with the idea that broader semantic activation may induce cue overload and retrieval competition processes that limit response time benefits. The absence of SOA effects suggests that timing-dependent differences in associative activation spread and semantic integration during encoding did not translate into measurable differences at delayed cued recall. The logical separability of the different types of priming used in this study is discussed, as are constraints on the role of an optimal SOA for memory formation. Taken together, the findings show that associative-semantic priming effects established in lexical processing (Rölke et al., 2018) partially extend to paired-associate learning, but encoding-related SOA modulations do not provide an additional benefit under the present conditions.

Keywords: association, cued recall, paired-associate learning, semantics, stimulus-onset asynchrony

3.1 Introduction

One of the fundamental challenges in cognitive science and psycholinguistics is to understand the mechanisms through which verbal information is encoded and consolidated into long-term memory. Contemporary accounts distinguish episodic and semantic subsystems of long-term memory (Squire & Dede, 2015; Squire & Wixted, 2011). Episodic memory reflects contextually bound experiences and supports the binding of items to their spatiotemporal and linguistic context (Tulving, 2002), whereas semantic memory comprises decontextualized knowledge such as word meanings, category structure, and long-term lexical relations (Binder et al., 2009; McRae & Jones, 2013). Importantly, both systems interact during language comprehension and learning (Greenberg & Verfaellie, 2010). For instance, the use of semantic context and prior knowledge can facilitate episodic encoding by providing an interpretable relational structure which renders otherwise arbitrary pairings easier to bind and retain (Van Kesteren et al., 2012). Accordingly, the present study examines how pre-existing lexical-semantic relations, in particular associative relations and broader semantic similarity, shape the formation of stable cue-target mappings when word pairs are encoded in sentence contexts.

According to Anderson (1983), words with strong relational links are often processed more efficiently and are more likely to be integrated into pre-existing knowledge structures. This process is usually explained by models of spreading activation through lexical networks (Collins & Loftus, 1975), which propose that related words activate overlapping neural representations and therefore benefit from shared retrieval cues. Specifically, "[t]he longer a [prime] concept is continuously processed [...], the longer activation is released from the node of the concept" (Collins & Loftus, 1975, p. 411). This mechanism provides a straightforward account of associative and semantic effects during the encoding of word pairs. Processing one member of a word pair spreads activation to several related concepts, both associatively and semantically, thereby increasing the likelihood that the intended target representation is co-activated and linked with the preceding cue (Hutchison, 2003; Neely, 1991). Co-activation strengthens the functional link between the cue and the target, resulting in a more precise cue-target mapping during retrieval. At test, presenting the cue can then reinstate activation within the same lexical-semantic neighborhood, allowing for more efficient convergence on the target

via overlapping representations and multiple shared retrieval routes (Plaut & Booth, 2000). Importantly, this account predicts pronounced benefits for pairs with pre-existing associative relations, as the cue already has established pathways to the target in semantic memory (Hutchison, 2003). This effectively reduces search demands and increases the probability of target selection in situations of semantic competition (Neely, 1977; Plaut & Booth, 2000).

Cued recall paired-associate word learning paradigms are often used to investigate the impact of relational structures on successful memory formation (Meltzer & Constable, 2005; Okada et al., 2012; Rugg, Fletcher, et al., 1998). In this task format, participants are first presented with stimulus pairs, such as a prime and a target, embedded within a sentence. Subsequently, they are asked to recall the target when prompted by the prime (Wixted, 2004). The efficiency of this retrieval process is assumed to reflect the strength and accessibility of the underlying memory trace. Crucially, cued recall differs from recognition-based paradigms. Rather than relying on familiarity judgments (cf. Yonelinas, 2002), it requires generative retrieval processes. This puts more of a strain on the episodic component of memory formation. In paired-associate learning, this episodic demand additionally requires binding the prime-target relation to a specific linguistic context, thereby providing a direct test of how lexical long-term knowledge constrains the formation of item-specific episodic bindings. Several studies have demonstrated that recall performance is enhanced by semantic relations between the cue and the target (e.g., Mandera et al., 2017; Nelson et al., 2004). However, the relative contribution of associative and semantic relations, as well as the conditions under which one type dominates another in this task format, remain open empirical questions. Understanding this interaction is further relevant when considering how such relations are modulated by temporal dynamics during encoding, such as through the manipulation of SOA.

Distinguishing direct associative relations from broader semantic similarity is not only methodologically feasible but also crucial for understanding how lexical long-term knowledge shapes the formation of specific memory traces. Although both types of relations contribute to lexical processing, they reflect fundamentally different memory structures. Semantic similarity refers to the extent to which two words share meaning-related features (e.g., “doctor” and “nurse”), often captured by taxonomic or categorical structure. Associative relations, in contrast, reflect the likelihood that one word co-occurs with another word in a specific context

(e.g., “bread” and “butter”), irrespective of their conceptual similarity (Jones et al., 2015; Lucas, 2000). This distinction is particularly relevant in cued recall, where successful retrieval depends on a cue’s ability to reinstate a specific target rather than a broad semantic neighborhood. As associative relations provide more specific cue-target retrieval routes, semantic similarity may increase co-activation of competitors and thus raise selection demands (Hutchison, 2003; Lucas, 2000). Quantifying these relations has long posed a methodological challenge (see Hutchison, 2003; McNamara, 2005). Conventional approaches rely on free association responses, wherein participants report the first word that comes to mind when presented with a cue (De Deyne et al., 2013). However, free association norms provide an aggregate behavioral index of lexical relatedness that often conflates direct associative relations with feature-based similarity (see Hutchison, 2003; Lucas, 2000). This means that associatively related word pairs selected from free association norms are mostly semantically related as well, making it hard to attribute priming effects to associative relations alone. In practice, this is precisely the challenge McNamara (2005, p. 86) describes: to find two words that are highly associated but not semantically related in any plausible way.

Recent advances in corpus-based methods offer a more objective alternative. Word co-occurrence statistics, derived from large text corpora, have proven effective in capturing both types of relations. Direct associations can be computed using the log-likelihood values of word pairs that co-occur in sentences (Dunning, 1993; Hofmann et al., 2011; Mandera et al., 2017). Semantic similarity, on the other hand, can be estimated by counting the number of direct associations that two words have in common, based on the idea that semantically similar items tend to appear alongside other words with which they have a lot of overlap (Rölke et al., 2018; Rölke & Hofmann, 2020). It is important to note that, while association and semantic similarity are correlated in natural language, they are not interchangeable. The same word pair may be strongly associated yet semantically dissimilar (e.g., “devil” and “detail”) or semantically similar yet weakly associated (e.g., “cat” and “lion”). This independence makes it possible to experimentally isolate their respective contributions to memory and language processing. Within a memory paradigm, direct associations may strengthen the encoding of episodic bindings through predictive mechanisms, whereas semantic similarity may facilitate the integration of new information into pre-existing conceptual networks (McRae & Jones, 2013).

The distinction between associative and semantic effects in long-term memory has also been formalized in computational modeling, most notably in the development of spreading activation frameworks and connectionist models. McClelland and Rumelhart's Interactive Activation Model (IAM) (1981) originally described how orthographic information activates candidate word representations via excitatory and inhibitory connections. Nonetheless, the IAM did not fully account for the influence of semantics on word recognition and memory, particularly in tasks involving associative processing. To address this, Hofmann et al. (2011) proposed the Associative Read-Out Model (AROM). This model is an extension of the IAM that implements a semantic layer based on corpus-derived co-occurrence statistics. In the AROM model, lexical processing is conceptualized as a cascaded spread of activation across multiple layers, ranging from perceptual features and letters to orthographic representations and finally to semantic word units. Within the semantic layer, the spread of activation can be further distinguished between direct co-occurrence (associative relations) and broader semantic similarity (overlap in common associates). Associative relations model the rapid propagation of activation to units representing words that co-occur frequently, as captured by log-likelihood ratios. By contrast, semantic similarity aggregates activation across a broader set of features or shared associates, reflecting deeper category-level relations that can unfold more slowly, are more context-dependent, and may increase competition among candidate units (cf. Neely, 1977). By anchoring the model in corpus-based co-occurrence data, researchers can derive quantitative relational predictors that capture word processing and memory outcomes. For instance, Hofmann et al. (2011) demonstrated that a higher number of co-occurring associates within the stimulus set increases false “yes” responses to new items in an old/new recognition memory task. Building on this, Stuellein et al. (2016) showed that the number of associates within the stimulus set reliably modulates event-related potential (ERP) markers of recognition processing, with larger P200 amplitudes and reduced N400 amplitudes for highly associated words. Semantic similarity, in turn, modulates left inferior frontal gyrus functional connectivity during semantic priming (Rölke & Hofmann, 2020), and both associative relations and broader semantic similarity facilitate word processing in primed lexical decision (Rölke et al., 2018).

A key methodological tool for distinguishing associative from semantic processing is manipulating the time interval between the presentation of a prime and its corresponding target

word (Hutchison, 2003). This time interval, known as the SOA, determines the extent to which automatic versus controlled processes contribute to language comprehension and memory encoding (Lucas, 2000; McNamara, 2005). Short SOAs (≤ 300 ms) are assumed to activate automatic processes whereby items that are closely related, particularly those that are highly semantically similar, are facilitated due to residual activation from the prime. This mechanism typically results in semantic priming, whereby the target is processed more efficiently if it shares features with the prime. In contrast, longer SOAs (≥ 1,000 ms) allow controlled processes to be recruited, such as expectancy generation or strategic matching. These conditions favor associative priming, where the influence of direct pairwise associations is more pronounced (Hutchison, 2003; Lucas, 2000). A foundational study by Neely (1977) provided early evidence for the temporal dissociation between semantic and associative priming by systematically manipulating the SOA in a lexical decision task. This study demonstrated that short SOAs (≤ 250 ms) primarily facilitated targets that were semantically related to the prime. In contrast, longer SOAs enabled expectancy-based and associative priming effects to emerge. For example, facilitation for semantically expected targets remained consistent across SOAs, whereas facilitation or inhibition effects for less predictable targets varied systematically with timing. As the SOA increased, inhibitory effects due to expectancy violation became more pronounced, suggesting that strategic processes are recruited over time to modulate lexical access based on contextual cues. This temporal dissociation has since been confirmed and expanded upon in numerous subsequent studies (e.g., Ferrand & New, 2003; Lucas, 2000; McNamara, 2005), thereby supporting the idea that the time course of lexical activation varies depending on the type of relationship.

Building on this, Rölke et al. (2018) conducted a behavioral experiment in which they manipulated direct association and semantic feature overlap in a full-factorial design using co-occurrence-based measures from large corpora. By varying the direct association between prime-target pairs (strong vs. none) and the extent to which they shared common associates (high vs. low), the authors were able to clearly distinguish between the two relational types. SOA was included as a third factor, introducing a temporal dimension to this differentiation. The results revealed a double dissociation for lexical decisions in which priming at short SOAs (200 ms) was driven predominantly by semantic feature overlap, whereas at long SOAs (1,000

ms) priming effects were strongest for directly associated word pairs. This pattern highlights that associative and semantic priming reflect functionally distinct mechanisms in terms of their representational structure and temporal dynamics. Kumar et al. (2020) took a complementary empirical approach, examining three semantic network models that differed in their operationalization of *distance* (5,018-word directed and undirected step distance networks, and an association-correlation network) to predict lexical priming effects. Here, distance refers to how far two words are separated in the model's representational space. In the step-distance networks, the relationship between word pairs was quantified based on how many associative *steps* separate them in free association data. This was done by linking words via direct cue-response associations, whereby the prime-target relatedness was defined as the shortest path length between the two words in the resulting network (directed: cue → response; undirected: a relation, if an association exists in at least one direction; Nelson et al., 2004; Steyvers & Tenenbaum, 2005). Contrary to this, the association-correlation network did not rely on single cue-response associations. Instead, it connected words that showed similar overall association profiles (i.e., correlated response patterns across many cues), thereby capturing higher-order, indirect relations beyond direct associations (Kumar et al., 2020). In the first task, participants were asked to judge the semantic relatedness of word pairs with varying network path lengths. Response latencies exhibited a robustly quadratic relationship with distance. Longer paths slowed judgments down disproportionately before leveling off, replicating and extending prior work on associative network structures. In the second task, a progressive demasking paradigm with a short SOA (120 ms) was used, and a distinct linear escalation in target identification latencies was observed as the length of the network path increased. Significant differences emerged at path lengths of four steps and beyond, demonstrating that network-based distances can predict priming effects even under very brief SOAs. Furthermore, comparisons with two distributional models (Latent semantic analysis and Word2Vec) revealed that, while all models accurately predicted response latencies, they each captured different aspects of semantic relations. This suggests that distributional and network-based approaches provide complementary insights into the structure of semantic memory.

Although the influence of varying SOAs on lexical priming has been widely researched, the role of SOA in the formation of long-lasting memory traces remains unclear. Particularly in experimental designs that permit the dissociation of associative and semantic effects through partially independent but complementary mechanisms. As the timing of word presentation directly affects the consolidation window, it should alter the temporal dynamics of episodic binding during encoding. Therefore, memory formation quality may depend on the time interval between the prime and target. Neurophysiological data can provide important insights here to better understand the underlying mechanisms of this temporal modulation. For instance, Dambacher et al. (2012) used ERPs to examine the impact of different presentation rates (i.e., SOAs of 700 ms, 490 ms and 280 ms) on the dynamics of word frequency and predictability effects during sentence reading. Across three experiments, they found that the onset latency of early frequency effects decreased as the presentation rate increased and that a crucial early interaction between top-down (predictability) and bottom-up (frequency) processes only emerged at the near-natural SOA of 280 ms. Besides, they found that predictability effects were delayed and attenuated at the fastest presentation rate, and that the overall ERP morphology at the shortest SOA differed significantly from that at longer SOAs. Such results demonstrate how the temporal parameters typical of natural reading can influence core stages of lexical processing, implying that SOA plays a crucial role in shaping not only priming effects but also the time course of memory-relevant encoding processes in ecologically valid contexts. Shorter SOAs may therefore encourage the formation of fast, integrative representations, as in semantically coherent contexts, whereas longer SOAs might facilitate the formation of more deliberate, associative links that are stored independently. However, it remains unclear whether the SOA-dependent facilitation observed in priming generalizes to the formation of durable cue-target bindings that can be accessed after a delay. In subsequent cued recall, any timing effects may therefore be more likely to emerge as differences in retrieval efficiency, given that recall accuracy reflects multiple additional sources of variance beyond the transient activation dynamics induced during encoding.

The Present Study

This study addresses the long-standing debate concerning purely associative relations, an area in which prior research has yielded inconsistent findings (Hutchison, 2003; Lucas, 2000). Using a sentence-embedded paired-associate paradigm with varying SOA, the influence of different word relations on the formation of long-term memory traces was examined. To test for the independent contributions of associative, semantic, and episodic encoding processes, the experimental factors were defined as direct association (strong vs. none) and semantic feature overlap (high vs. low). The present study aimed to extend the applicability of Rölke et al.'s (2018) lexical decision approach to a memory paradigm, and to identify whether prime-target timing modulates subsequent retrieval efficiency in delayed cued recall (as reflected in response times on correctly recalled trials). During the study phase, participants learned sentences in which the prime-target relations were manipulated based on word co-occurrence statistics. SOAs between prime and target were set at either 300 ms (short) or 1,450 ms (long) through single-word presentation durations. In the subsequent cued recall test, participants were asked to recall the target object within the sentence context, with recall success (correct/ false) and response times being measured. Based on the theoretical background, three central hypotheses were derived: i) A higher level of recall success is expected for word pairs with strong direct association and for word pairs with high semantic feature overlap, reflecting facilitated encoding and more effective cue-based retrieval. ii) Faster response times are expected for word pairs with a strong direct association, as the retrieval cue enables more efficient access to the underlying memory trace. Effects of semantic feature overlap are expected to be smaller and potentially context-dependent, given broader semantic co-activation and possible competitor interference. iii) No significant main effect of SOA, nor any SOA-related interaction is expected regarding recall success, as SOA-dependent priming dynamics during encoding are presumed to be transient and unlikely to systematically influence the success of delayed recall performance. For response times, which provide an indirect index of memory-trace accessibility, SOA is expected to modulate the relative contribution of semantic feature overlap and direct association. Thus, short SOAs should enhance semantic effects that are relatively automatic, whereas long SOAs should amplify the effects of direct association.

3.2 Methods

Behavioral data were collected from a total of 82 healthy participants, comprising both students and non-students, recruited at Bergische Universität Wuppertal in Germany. Students eligible for course credit received it, whereas all other participants received no compensation. The target sample size was determined a priori using GLIMMPSE (Version 3.1.3; Glueck et al., 2025; Kreidler et al., 2013) for a mixed design with two between-subject groups (short versus long SOA) and four repeated-measures conditions corresponding to the 2 × 2 manipulation of direct association and semantic feature overlap. The calculation targeted the main effects, using $\alpha = .05$, a target power of $1 - \beta = .80$, and the Hotelling–Lawley trace. Expected cell means were derived from Rölke er al. (2018), as their study provided the closest available parameter estimates due to its use of the same orthogonal manipulation, included short and long SOAs, and used an overlapping subset of the prime–target materials. However, the task and outcome measures differed from those of the present study. The assumed standard deviation and within-subject correlation were specified as model inputs, yielding a required sample size of $N = 30$ (15 per SOA group). Fourteen participants were excluded from the analysis because their overall error rate, calculated across all experimental conditions in the test phase, exceeded the sample mean by more than 2 *SD*. Accordingly, the remaining sample size of $N = 68$ participants was deemed adequate. The mean age of these participants (39 women) was 30.54 years ($SD = 14.50$; range: 18–62 years). All participants were native German speakers, had normal or corrected-to-normal vision, and reported no history of psychiatric, neurological, or reading disorders.

The stimulus set comprised 184 unique German sentences, including 168 experimental items and 16 filler items, which served as primacy and recency trials. Four additional sentences were used in a practice run. The structure of each sentence was as follows: article, subject-prime, auxiliary verb, closed-class word, and target-object, with both the prime and the target being nouns. The length of the words in these sentences ranged from three to eight letters. Each word was presented individually in the center of the screen in the Courier New font. The auxiliary verbs employed included “to be”, “have”, and “become”, while closed-class words were either articles or prepositions. The direct association and semantic feature overlap

between the prime and target nouns were subjected to experimental manipulation. The strength of the direct association between the prime and target words was calculated as the $\log_{10}$-transformed log-likelihood ratio. This indicates that two words co-occur in sentences more frequently than would be predicted by their individual frequencies (Dunning, 1993; Hofmann et al., 2018). Pairs of prime and target words were classified as strongly associated (SA) if their association strength was at least 2, whereas non-associated (NA) pairs were assigned an association strength of zero, indicating that there was no significant co-occurrence within sentences. The degree of semantic feature overlap was determined by the number of direct associates shared between the two words, representing overlapping semantic features (e.g., Rölke et al., 2018). For each word, the 1000 words with the highest χ^2 values were identified as semantic features and the number of common associates was counted (Hofmann et al., 2018). Word pairs with a high semantic feature overlap (HS) had at least 10 common associates, while those with low overlap (LS) had none. The thresholds served as pragmatic selection criteria to obtain a sufficiently large and clearly differentiated stimulus set, rather than as universal or corpus-derived boundaries between weak and strong relations. No correlation between direct associations and common associates existed ($r < .3$). Table 1 shows an example sentence for each experimental condition. The full stimulus list is provided in Appendix A1 and can also be found in the open science repository (Appendix E).

Table 1
Example Stimulus Sentences by Experimental Condition (Study A)

Condition	German	English
SA-HS	Das Auto hat einen Motor.	The car has an engine.
SA-LS	Die Flasche ist aus Glas.	The bottle is made of glass.
NA-HS	Der Junge wird ein Student.	The boy becomes a student.
NA-LS	Der Abend ist eine Blamage.	The evening is a disgrace.

Note. German sentences are the original stimuli. HS = high semantic feature overlap; LS = low semantic feature overlap; NA = no direct association; SA = strong direct association.

The sentences belonging to the four experimental conditions were assigned to two lists (A and B), each containing half of the items per condition. Participants completed two study-test blocks, one per list, with list order (A→B vs. B→A) counterbalanced across participants. Both lists remained matched with respect to all controlled variables. Within each study and test

block, trial order was pseudorandomized for each participant, with no more than two sentences of the same experimental condition in sequence. Direct association strength and the number of common associates were computed using the German corpus of the Leipzig Wortschatz Project (Goldhahn et al., 2012), which is based on 800 million tokens and 43 million sentences extracted from online newspaper articles (1992–2006). The prime and target nouns, the auxiliary verb and the closed-class word were controlled for word frequency, word length and orthographic neighborhood in each condition (all *F*s < 1, see Table 2).

Table 2
Means (SDs) and F Statistics for Controlled Variables (Study A)

	SA-HS	SA-LS	NA-HS	NA-LS	*F* value
Clause length	26.52 (1.69)	26.45 (2.47)	27.02 (1.81)	26.69 (1.57)	0.74
AS $_{\text{prime-target}}$	3.29 (0.62)	3.27 (0.43)	0.00 (0.00)	0.00 (0.00)	0.02
CA $_{\text{prime-target}}$	23.74 (8.46)	0.00 (0.00)	23.71 (4.93)	0.00 (0.00)	0.00
			Prime		
Length	6.07 (1.07)	5.95 (1.38)	6.21 (1.24)	6.00 (0.99)	0.39
Frequency	10.29 (1.52)	10.07 (1.60)	10.45 (2.13)	10.43 (1.77)	0.41
OrthNeigh	0.74 (1.52)	0.90 (1.32)	0.74 (1.04)	0.60 (0.77)	0.47
			Target		
Length	6.38 (1.25)	6.31 (1.37)	6.62 (1.01)	6.50 (0.94)	0.58
Frequency	10.29 (1.78)	10.14 (1.66)	10.69 (2.18)	10.36 (1.69)	0.67
OrthNeigh	0.71 (1.45)	0.69 (1.02)	0.55 (0.94)	0.60 (0.77)	0.22
			Auxiliary verb (inflected)		
Length	3.17 (0.38)	3.12 (0.40)	3.24 (0.43)	3.14 (0.42)	0.67
Frequency	2.45 (0.50)	2.52 (0.51)	2.38 (0.49)	2.43 (0.50)	0.59
OrthNeigh	2.00 (0.00)	2.02 (0.15)	2.00 (0.00)	2.02 (0.15)	0.67
			Closed-class word (main clause)		
Length	2.90 (0.93)	3.07 (0.81)	2.95 (0.38)	3.05 (0.79)	0.45
Frequency	1.95 (1.08)	1.79 (0.75)	1.90 (0.88)	1.98 (1.07)	0.33
OrthNeigh	2.98 (1.60)	2.93 (1.40)	2.79 (1.18)	3.10 (1.34)	0.36

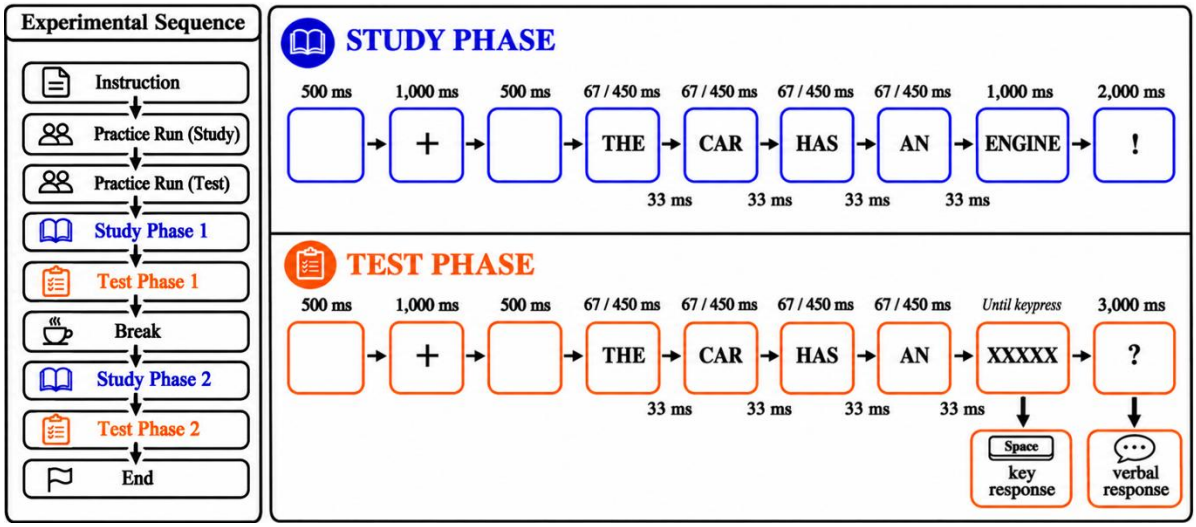
Note. F statistics for clause length and the lexical control variables were obtained from separate one-way between-item analyses of variance across the four experimental word pair conditions, $F(3, 164)$. For association strength (AS) and the number of common associates (CA), the *F* statistics compare SA-HS with SA-LS and SA-HS with NA-HS, respectively, $F(1, 82)$; values in the excluded conditions were fixed at zero by design. Clause length is reported in letters. AS and CA were calculated for each prime–target pair. HS = high semantic feature overlap; LS = low semantic feature overlap; NA = no direct association; OrthNeigh = number of orthographic neighbors; SA = strong direct association.

The target nouns had a word length of four to eight letters, a Leipzig word frequency class (Goldhahn et al., 2012) of six to seventeen, and a maximum of nine orthographic neighbors. The prime nouns had a word length of four to eight letters, a frequency of six to sixteen, and a maximum of seven orthographic neighbors.

Participants were given standardized instructions to familiarize themselves with the target-objects during the study phase in order to subsequently incorporate these target-objects into complete sentences during the test phase. To ensure task comprehension, the experiment began with four practice trials for the study phase and four practice trials for the test phase. The experiment consisted of two study-test blocks, each containing four primacy and four recency trials accounting for the 16 filler items described above. All filler trials were excluded from subsequent analyses. The stimuli were displayed centrally using the rapid serial visual presentation method (word-by-word) with PsychoPy (Version 2022.2.4; Peirce et al., 2019) on laptop computers operating at a a refresh rate of 60 Hz. The experiment was configured to run in full-screen mode, with a window size of 1,920 × 1,080 pixels. All laptop computers ran the 64-bit version of Windows 10. The experimental sequence and a detailed timeline of a trial in the study and test phases are illustrated in Figure 10.

Figure 10

Experimental Sequence and Timing of a Trial: Study/Test Phase (Study A)



Each trial began with the presentation of a blank screen (500 ms), followed by a centrally presented fixation cross (1,000 ms), and another blank screen (500 ms). Individual words were presented for either approximately 67 ms (four frames; nominally 70 ms) or 450

ms, depending on the SOA condition, except for the target-object, which was presented for 1,000 ms. The nominal duration of the blank intervals between the first four words was set to 30 ms in PsychoPy, corresponding to approximately 33 ms (two frames) at a refresh rate of 60 Hz. The resulting SOAs between the onset of the prime and the onset of the target-object were 300 ms (short SOA) and 1,450 ms (long SOA). During the study phase, each sentence concluded with an exclamation mark ("!") presented for 2,000 ms before the next trial began. Each study block was followed by a cued recall test phase. The trial sequence remained largely unchanged, except that the target-object from the previously studied sentences was replaced by five crosses ("xxxxx"). During their presentation, participants could indicate retrieval of the target word by pressing the space bar, with response times measured as the latency from the onset of the crosses to the keypress. Subsequently, a question mark ("?") appeared for 3,000 ms, during which participants were required to verbally report the recalled target word. An experimenter seated behind the participant monitored the verbal responses and coded them as correct or incorrect in real time. The next trial was initiated manually by pressing the space bar. Participants were instructed to respond as quickly and accurately as possible and were informed that feedback on their performance would be provided at the end. The task instructions and experimental scripts are available in the open science repository (Appendix E).

Statistical analyses were conducted in JMP® (Version 19.0.3; JMP Statistical Discovery LLC, 2025). Trial-level recall success (1 = correct, 0 = incorrect) was analyzed using a generalized linear mixed-effects model (GLMM) with a binomial distribution and logit link function. The fixed effects included direct association (DA; strong vs. none), semantic feature overlap (SEM; high vs. low), SOA (short vs. long), and all corresponding interaction terms. To account for the cross-classified structure of the data (trials nested within participants and items), random intercepts were included for subjects and items. The response times (RT) for correctly recalled trials were analyzed using a Gaussian linear mixed-effects model (LMM) on natural-log-transformed RTs, with the same fixed- and random-effects structure. The log-transformation was used to reduce positive skewness and improve adherence to the distributional assumptions of the model. For the Gaussian LMM, model assumptions were checked via Q–Q plots, residual-versus-fitted plots, and an Anderson–Darling test of residual normality (Appendix A2). As the diagnostics indicated deviations from residual normality, the

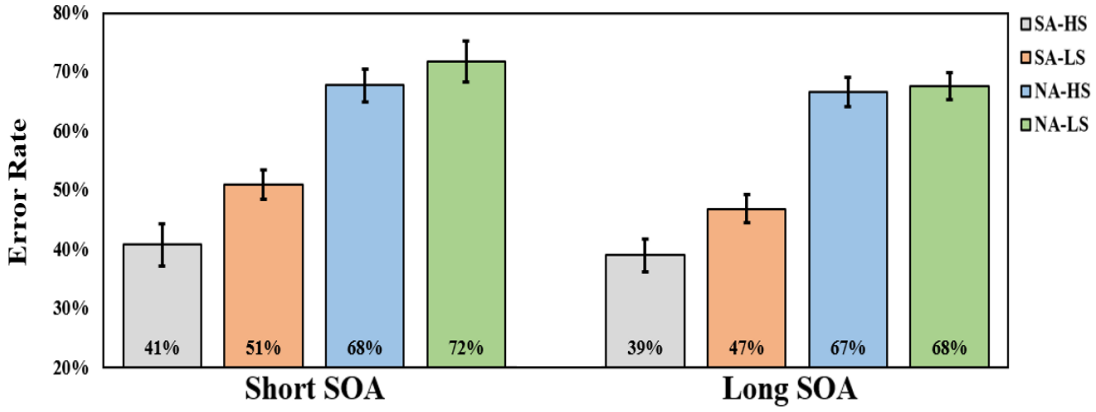
model was re-estimated after excluding trials whose residuals deviated from the participant-specific median by more than 2.5 scaled median absolute deviations (scaling factor = 1.4826). This criterion excluded 276 of the 4,790 correctly recalled trials (5.76%). Statistical inference used $\alpha = .05$. For both models, fixed effects were evaluated using Type III Wald *F*-tests with Kenward–Roger-approximated denominator degrees of freedom (Kenward & Roger, 1997). The complete test tables are provided in Appendix A3 (for the GLMM) and Appendix A4 (for the Gaussian LMM). In addition, coefficient-level tests (*t*/*z*) are reported alongside parameter estimates in the corresponding tables. Estimates are reported using effect coding (DA: none = -1, strong = +1; SEM: low = -1, high = +1; SOA: short = -1, long = +1), with the intercept representing the equally weighted mean across conditions on the model scale and the coefficients reflecting the corresponding effects. For the Gaussian LMM, model fit was assessed using R^2_m and R^2_c. For the GLMM, model fit is reported using the Akaike information criterion (AIC) and Bayesian information criterion (BIC; both based on the residual -2 log pseudo-likelihood) and Nakagawa's R^2_m / R^2_c on the latent logit scale (Nakagawa et al., 2017). Overdispersion was assessed using the generalized χ^2/df statistic.

3.3 Results

The binomial GLMM on trial-level recall success revealed a significant main effect of direct association, $F(1, 157) = 71.95$, $p < .001$, indicating higher recall success for word pairs with strong direct association compared to those with no direct association. Semantic feature overlap also showed a significant main effect, $F(1, 156) = 4.12$, $p = .044$, with higher recall success for word pairs with high compared to low semantic feature overlap. The main effect of SOA was not significant, $F(1, 65) = 2.14$, $p = .148$, and none of the interaction effects reached significance (all *p*s ≥ .147; see Appendix A3). The generalized χ^2 was 10,943 (df = 10,942), indicating no evidence of overdispersion ($\phi = 0.96$). Information criteria for the fitted model were AIC = 52,656, BIC = 52,729, $R^2_m = .009$ and $R^2_c = .343$, indicating that most explainable variance was attributable to subject- and item-level differences rather than the fixed experimental factors. Figure 11 shows the mean error rates for each experimental condition. Table 3 provides the coefficient-level parameter estimates (logit b), *SE*s, Wald *z*-test scores,

and odds ratios (OR) with 95% confidence intervals (CIs), as well as the random-intercept variance components for the fitted model.

Figure 11
Mean Error Rates (Study A)



Note. N = 68 participants. Error rate (%) = 100 × incorrect trials/total trials. Error bars represent 95% within-subject confidence intervals calculated from participant-level condition means using the Cousineau–Morey correction (Cousineau, 2005; Morey, 2008), with normalization performed separately for each SOA. HS = high semantic feature overlap; LS = low semantic feature overlap; NA = no direct association; SA = strong direct association; SOA = stimulus onset asynchrony. Short SOA = 300 ms; long SOA = 1,450 ms.

Table 3
GLMM Estimates for Trial-Level Recall Success (Study A)

Random effects	**σ^2**	***SE*(σ^2)**			
Subject intercept	0.443	0.083			
Item intercept	0.831	0.104			
Fixed effects	***b* (logit)**	***SE***	***z* value**	***p* value**	**OR [95% CI]**
(Intercept)	-0.364	0.109	-3.33	< .001	0.69 [0.56, 0.86]
DA	0.627	0.074	8.48	< .001	1.87 [1.62, 2.17]
SEM	0.150	0.074	2.03	.044	1.16 [1.00, 1.34]
SOA	0.122	0.084	1.46	.148	1.13 [0.96, 1.34]
DA × SEM	0.081	0.074	1.10	.274	1.08 [0.94, 1.25]
DA × SOA	-0.022	0.022	-1.01	.314	0.98 [0.94, 1.02]
SEM × SOA	-0.032	0.022	-1.44	.149	0.97 [0.93, 1.01]
DA × SEM × SOA	0.006	0.022	0.27	.784	1.01 [0.96, 1.05]

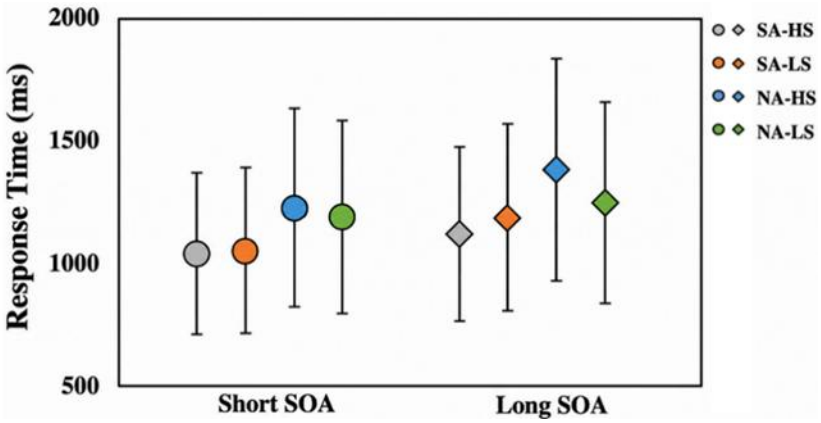
Note. Binomial generalized linear mixed-effects model (GLMM) with logit link, including random intercepts for participants and items (N = 68 participants; k = 168 items; n = 5,208 trials). Fixed-effect coefficients are reported on the log-odds scale using effect coding (-1/+1). DA = direct association (-1 = none; +1 = strong); SEM = semantic feature overlap (-1 = low; +1 = high); SOA = stimulus-onset asynchrony (-1 = short; +1 = long). Odds ratios (OR) represent exponentiated fixed-effect estimates; 95% confidence intervals (CI) are Wald intervals. p values are based on two-sided Wald z tests.

Although the DA × SEM interaction term was not significant, the descriptive pattern of error rates indicated a potentially stronger SEM difference under strong (vs. none) direct association. Exploratory pairwise comparisons of the DA × SEM LS-means revealed that the SEM effect was not significant when DA was absent (OR (high vs. low) = 1.15, 95% CI [0.76, 1.74], p = .511), but was significant when DA was strong (OR (high vs. low) = 1.59, 95% CI [1.05, 2.39], p = .028). However, these simple-effects contrasts should be treated as descriptive follow-up rather than as confirmatory evidence for a differential SEM effect across DA levels.

The Gaussian LMM on the natural-log-transformed RTs (correctly recalled trials only) revealed a significant main effect of direct association, $F(1, 160) = 11.02$, p = .001, reflecting shorter response times for strong directly associated compared to non-associated word pairs. No significant main effects were observed for semantic feature overlap, $F(1, 158) = 0.16$, p = .690, or SOA, $F(1, 66) = 0.23$, p = .631. None of the interactions reached significance (all ps ≥ .232; see Appendix A4). Model fit was R^2_m = .004 and R^2_c = .525, indicating that most explainable variance was attributable to subject- and item-level differences rather than the fixed factors. Figure 12 shows the model-estimated response times across SOAs and experimental conditions. Table 4 reports the coefficient-level parameter estimates (b), SEs, 95% CIs, and Kenward–Roger t-test scores, as well as random-intercept variance components for the model. A model comparison assessing the contribution of SOA terms is provided in Appendix A5.

Figure 12

Model-Based Estimates of Response Times (Study A)



Note. N = 68 participants. Response times (RTs) are presented as back-transformed estimated marginal means (geometric means) from the Gaussian linear mixed-effects model fitted to natural-log-transformed RTs for correctly recalled trials. Error bars represent 95% confidence intervals. HS = high semantic feature overlap; LS = low semantic feature overlap; NA = no direct association; SA = strong direct association; SOA = stimulus onset asynchrony. Short SOA = 300 ms; long SOA = 1,450 ms.

Table 4
LMM Estimates for Trial-Level Response Times (Study A)

Random effects	**σ^2**	***SE*(σ^2)**				
Subject intercept	0.606	0.104				
Item intercept	0.044	0.008				
Residual	0.619	0.013				
Fixed effects	***b***	***SE***	**[95% CI]**	***df***	***t* value**	***p* value**
(Intercept)	7.067	0.097	[6.87, 7.26]	71	72.97	< .001
DA	-0.070	0.021	[-0.11, -0.03]	160	-3.32	.001
SEM	0.008	0.021	[-0.03, 0.05]	158	0.40	.690
SOA	0.046	0.095	[-0.14, 0.23]	66	0.48	.631
DA × SEM	-0.025	0.021	[-0.07, 0.02]	158	-1.20	.232
DA × SOA	0.004	0.013	[-0.02, 0.03]	4,363	0.35	.729
SEM × SOA	0.004	0.012	[-0.02, 0.03]	4,361	0.30	.767
DA × SEM × SOA	-0.015	0.012	[-0.04, 0.01]	4,361	-1.18	.236

Note. Gaussian linear mixed-effects model (LMM) fitted to natural-log-transformed response times for correctly recalled trials, including random intercepts for participants and items (N = 68 participants; k = 168 items; n = 4,514 trials). Fixed-effect coefficients are reported on the natural-log scale using effect coding (-1/+1). DA = direct association (-1 = none; +1 = strong); SEM = semantic feature overlap (-1 = low; +1 = high); SOA = stimulus-onset asynchrony (-1 = short; +1 = long). Confidence intervals (CI) are 95% Wald intervals. *p* values are based on two-sided *t* tests with Kenward–Roger denominator degrees of freedom.

3.4 Discussion

The present study used a sentence-embedded paired-associate paradigm with varying SOAs to assess how episodic encoding is shaped by associative and semantic long-term knowledge, and how this influences subsequent cued recall. Behavioral analyses of trial-level recall success and response times revealed that memory performance is sensitive to the nature of prime-target relations, yet largely insensitive to SOA variations. With regard to the hypotheses outlined above (i–iii), the following patterns were observed:

(i) Associative and semantic relations led to greater recall success compared to unrelated word pairs, with direct associations providing the largest benefit. This advantage can be explained by the framework of spreading activation theory (Collins & Loftus, 1975), which states that words frequently co-occurring in natural language become closely linked in the mental lexicon. As a result, related concepts can be rapidly activated through established pathways, facilitating the binding of cue pre-activated target representations and enabling more

efficient encoding. Binding strength may increase further in sentences with integrative syntactic and semantic structures, as the target is reinforced within a predictive framework (Hutchison, 2003; Van Petten & Luka, 2012). In contrast, semantic feature overlap supports encoding processes through conceptual similarity and category-level integration (McRae & Jones, 2013). While this overlap facilitates elaborative encoding by linking new items to existing conceptual structures, it lacks the unidirectional, predictive strength that is typical of associative relations (Lucas, 2000; Nelson et al., 2004). Estes and Jones (2009) demonstrated that such direct associative relations provide privileged retrieval routes that reduce search demands and minimize interference, resulting in stronger and more accessible memory traces than relations based solely on shared semantic features. Furthermore, semantic primes tend to activate broader lexical networks (Hutchison, 2003), which can lead to cue overload and retrieval competition, especially in tasks requiring the recall of a specific target word (Nairne, 2002; Watkins, 1976). This type of semantic competition has been shown to reduce retrieval success in various memory tasks (Abdel Rahman & Melinger, 2009). Thus, although both types of relation enhance encoding, the consistently greater benefits of direct associations suggest that distributional associations exert a stronger and more reliable influence on memory formation than conceptual overlap. This aligns with neurocognitive models that propose distinct neural mechanisms for associative binding, which often depend on the hippocampus, and for semantic integration, which are more closely linked to neocortical regions such as the anterior temporal lobe (Binder et al., 2009; Ranganath & Ritchey, 2012). Crucially, the present study did not observe an interaction between associative and semantic relations in terms of recall success. The finding therefore corroborates Rölke et al.'s (2018) conclusion that the co-occurrence-based approach allows for the identification of pure associative and semantic priming effects. Applying their computational separation to a paired-associate paradigm, which was followed by a cued recall test, demonstrated that this dissociation also holds in a more ecologically valid context reflecting successful memory formation. Historically, distinguishing between these two types of relation has posed a central challenge for priming research, since associative and semantic influences on language processing frequently overlap and are difficult to disentangle using traditional stimulus norms (Lucas, 2000; McNamara, 2005).

(ii) Response times were faster for word pairs with a strong direct association, compared to those with no direct association. Semantic feature overlap did not reliably accelerate retrieval. This pattern suggests that associative cue-target relations activate more specific retrieval pathways due to their directional and unidimensional nature (Collins & Loftus, 1975), thereby acting as a retrieval shortcut even in delayed cued recall. In line with Estes and Jones (2009), predictability may leverage stronger cue-target contingencies to reduce cognitive effort and streamline target identification, facilitating faster recall under optimal conditions. This is consistent with previous research showing that higher association strength improves recall accuracy and reduces response latencies, particularly in tasks with minimal interference (Balota et al., 2004). By contrast, semantic primes activate broader lexical and conceptual networks (Hutchison, 2007), which may induce retrieval competition, thereby attenuating the potential facilitation effects on response time during recall (Abdel Rahman & Melinger, 2009; Nairne, 2002). Although semantic activation supports deeper encoding and has been shown to reinforce both new and existing memory traces via retroactive strengthening (Coutanche & Thompson-Schill, 2014), it may impede the retrieval process by increasing cognitive load when precise recall is required. Thus, semantic feature overlap can contribute to improved recall success without necessarily speeding target-specific access. Crucially, response time effects depend on the nature of the cued recall test. In this task format, accuracy took precedence over speed and sufficient time was available to retrieve the missing word. This may have reduced the sensitivity of response times to the underlying activation dynamics.

(iii) As expected, variations in the temporal spacing during episodic binding did not affect recall success. Processes such as activation propagation, contextual integration, and resolving semantic competition occur during initial encoding and are completed well before the delayed cued recall test. This pattern reinforces the interpretation of memory encoding as a temporally constrained process. As long as the prime-target relation has been successfully consolidated, variations in the temporal spacing of initial presentation have no impact on the recall performance. Contrary to expectations, SOA manipulations did not modulate response times, and no interaction between SOA and relation type was observed. One possible explanation is that any temporal effects arising from SOA during encoding may have become functionally irrelevant by the time memory was tested, due to the time interval between

encoding and retrieval. This aligns with prior research (Hutchison, 2007; Neely, 1991) showing that SOA effects are most pronounced in immediate priming paradigms, in which early activation dynamics directly influence response time patterns. By contrast, delayed cued recall relies on robust, consolidated memory traces that are less susceptible to transient variations in input timing (Loaiza & McCabe, 2012; Paller & Wagner, 2002). Additionally, the present paradigm may not have been sensitive enough to detect subtle temporal effects on recall latency, especially under conditions of high attentional control. The sentence-embedded, encoding context may have reduced the functional relevance of SOA differences even further. Sentence structures not only provide integrative semantic and syntactic support but also engage predictive mechanisms that can facilitate target processing when expectations are met, thereby reducing the relative impact of early activation dynamics on later retrieval (Kutas & Federmeier, 2011; Van Petten & Luka, 2012). As each word was presented individually and participants had sufficient time to integrate the prime-target relation successfully, even shorter SOAs enabled the processing of both semantic and associative relations to the same extent. Furthermore, the absence of time pressure during the recall test likely diminished any effect of subtle variations in encoding dynamics on response time. Instead, the strength and specificity of the encoded relation determined the response time, as reflected in the descriptive advantage for associatively related items. A central aim of this study was to evaluate whether varying SOAs could optimize semantic versus associative encoding processes in long-term memory. Overall, the findings suggest that, while theoretically relevant for early activation dynamics, SOA variations may not reliably influence recall latency in delayed memory tasks. Thus, the mechanisms supporting delayed cued recall in paired-associate learning appear to be partly dissociable from the activation dynamics typically captured in primed lexical decision.

Several limitations should be considered when drawing these conclusions. Although the SOA manipulation was theoretically designed to elicit associative and semantic priming effects (Lucas, 2000; McNamara, 2005), it only compared short (300 ms) and long (1,450 ms) intervals. This restricted the ability to detect intermediate or non-linear timing effects. Including multiple intermediate SOA levels (e.g., 200 ms, 500 ms, 800 ms, 1,200 ms) in future studies could help map the temporal trajectory of encoding and identify potential transitions between associative and semantic processing. The cued recall paradigm, while well suited for

assessing generative retrieval, makes it difficult to disentangle episodic from semantic contributions, as semantic relations can facilitate recall even when specific episodic bindings are weak (Greenberg & Verfaellie, 2010; Van Kesteren et al., 2012). Neurophysiological measures, such as ERP components that are sensitive to episodic encoding (e.g., Late Positive Component; Rugg & Curran, 2007), or to subsequent memory effects (Friedman & Johnson, 2000), could clarify whether SOA-sensitive mechanisms operate under higher cognitive load. Furthermore, they could provide insight into the interplay between associative activation spread, semantic network integration and episodic binding during recall. Finally, the extent to which the co-occurrence-based approach can be generalized to memory paradigms across typologically diverse languages and presentation modalities of verbal material (e.g., visual vs. auditory) cannot be determined from the present data.

Despite these limitations, the present study has several valuable implications for methodology and theory in cognitive psycholinguistics. Most notably, the co-occurrence-based approach was extended to research on explicit memory formation. The findings demonstrate its potential for generating objective stimulus sets in paired-associate cued recall tests and support its use as a reproducible, scalable alternative to subjective norms**.** This facilitates replication and cross-study comparability. The lack of an SOA effect implies that strictly time-centric models of encoding, which predict differential long-term outcomes as a direct function of millisecond-level timing during presentation, should be complemented by architectures that can distinguish between rapid distributional lexical activation and slower conjunctive episodic binding mechanisms. The AROM (Hofmann & Jacobs, 2014) provides a natural framework for this reconceptualization, as its semantic layer captures co-occurrence-driven activations and readily accounts for strong associative advantages. Extending the AROM with a conjunctive, hippocampal-like layer (c-AROM; Rölke-Wellmann, 2021) would explain how durable episodic bindings can be formed that are relatively insensitive to transient SOA differences once an engram is consolidated. Adding leaky/noisy evidence-accumulation dynamics during associative read-out further clarifies how strong associative cues generate rapid, focused decision trajectories while semantic feature overlap leads to broader, more competitive dynamics (Sokolovič & Hofmann, 2024). The results of the present study are consistent with this two-stage functional architecture in which (a) direct associations create rapid activation

pathways that affect encoding and retrieval probability, and (b) a conjunctive encoding process (e.g., pattern separation/completion in hippocampal circuits) consolidates item-pair bindings into stable traces whose later accessibility depends more on binding strength than on the precise millisecond timing of the original input.

From a modeling perspective, this suggests concrete refinements: First, connectionist simulations should treat SOA as a modulatory parameter that primarily affects the dynamics of early semantic activation (e.g., accumulation noise or decay rates) rather than the strength of the conjunctive update that produces stable memory engrams. Implementing a fast, semantic layer together with a slower, thresholded conjunctive update or short-term maintenance buffer would naturally reproduce SOA-sensitive immediate priming and SOA-insensitive delayed recall. Second, models should be fitted jointly to immediate measures (e.g., response time) and delayed measures (e.g., subsequent memory) so that AROM-style and c-AROM predictions can be empirically dissociated. AROM-style accounts predict an associative advantage for both immediate facilitation and later recall probability. In contrast, a c-AROM approach that implements hippocampal pattern separation predicts that semantic feature overlap will differentially tax conjunctive resources, thus interacting with encoding difficulty rather than with SOA per se.

Such model refinements would generate testable neural predictions. If distributional activation drives early facilitation, then manipulations that enhance direct association or semantic feature overlap should modulate early markers of semantic activation (e.g., N400) and functional connectivity among ventral-stream/temporal nodes. Conjunctive encoding, in contrast, should predict later subsequent memory signatures, such as the Late Positive Component or hippocampal-cortical coupling. Thus, an experimental approach that integrates modeling and neural data is needed to determine whether SOA primarily gates transient activation or modulates the strength of conjunctive updates.

3.5 Conclusion

To the best of the author's knowledge, the present study provides the first systematic examination of pure associative and semantic priming effects during memory encoding in a sentence-embedded paired-associate paradigm with varying SOAs. The results showed that both types of word relations led to robust cued recall benefits. The absence of SOA-related differences suggests that, once a prime-target memory engram has been successfully formed, the temporal spacing of cue presentation during encoding plays a negligible role in the subsequent retrieval. The superior recall performance for associatively related word pairs likely reflects the stronger impact of distributional regularities and the dynamics of spreading activation, which jointly facilitate more efficient encoding and retrieval. Although still beneficial, semantic relations may rely more on shared conceptual features that support the integration of information into existing semantic networks but offer comparatively weaker retrieval cues. Response times were selectively faster for associative relations, which may reflect reduced search demands due to already established retrieval pathways. In contrast, broader semantic activation may be more susceptible to interference from competing lexical or conceptual candidates, limiting response time benefits when target-specific access is required. Bridging the gap between short-term priming research and long-term memory models, this study further supports the functional dissociation between associative and semantic processes.

Declarations

Details on funding, data availability, and study-specific data collection sites are provided in Appendix F (Administrative Information).

4. Study B: ERP Correlates of Associative Priming and Subsequent Memory Effects: Evidence from Sentence-Embedded Paired-Associate Learning

Abstract

The aim of this study was to examine the fine-grained interplay of episodic and associative-semantic long-term knowledge in a sentence-embedded paired-associate paradigm and to probe separable contributions to encoding-related event-related potential (ERP) amplitudes. Participants were instructed to learn sentences of the structure: article, subject-prime, auxiliary verb, closed-class word, and target-object (e.g., "the car has an engine"). Later, they had to recall the target-object, given the preceding sentence context. Words were displayed using rapid serial visual presentation. Corpus-based co-occurrence statistics were used to orthogonally manipulate direct association (strong vs. none) and semantic feature overlap (high vs. low) between the prime and the target word (cf. Hofmann et al., 2018). Strong direct associations led to more correct responses, whereas semantic feature overlap showed no reliable main effect and no interaction was observed. However, descriptive trends suggested a potential supportive contribution in the presence of direct associations. This aligns with the largely additive pattern of associative and semantic influences reported for lexical processing (Rölke et al., 2018). Response times were faster for strong direct associations, with no effect for semantic feature overlap. ERPs were recorded during target-object encoding, with condition-related analyses restricted to correctly recalled trials. Further, ERPs were contrasted between subsequently correct vs. incorrect recall to quantify subsequent memory effects. Strong direct associations elicited a greater Late Positive Component (LPC; 460–800 ms) with an occipito-parietal scalp distribution, whereas semantic feature overlap showed no LPC modulation. Correctly recalled targets showed more positive-going ERP amplitudes, reflected in an attenuated N400 (250–500 ms) and an enhanced P600 (500–800 ms), both with a centro-parietal scalp distribution and regardless of associative-semantic priming manipulations. This study demonstrates that classic priming patterns from lexical processing (Rölke et al., 2018) can extend to paired-associate learning outcomes and further identifies dissociable ERP signatures during encoding that track associative priming effects (LPC).

Keywords: association, cued recall, episodic memory, late positive component, priming, semantics, subsequent memory effects.

4.1 Introduction

Episodic memory refers to the ability to consciously remember information from a specific learning event, together with the spatial, temporal, or other contextual information associated with it (Tulving, 2002; Yonelinas et al., 2019). Two central cognitive processes of episodic memory are encoding, during which information from an experience is integrated into a coherent, event-specific memory representation through the binding of item and contextual information (Mecklinger & Kamp, 2023; Yonelinas et al., 2019), and retrieval, during which this representation is accessed in response to an appropriate retrieval cue (Yonelinas et al., 2019). Because encoding success cannot be observed directly at the time of learning, encoding processes can be probed by relating neural activity during initial processing to performance on a later memory test (Mecklinger & Kamp, 2023; Paller & Wagner, 2002).

A seminal study by Paller, Kutas, and Mayes (1987) found that the amplitude of the Late Positive Component (LPC) at encoding can predict later successful episodic memory retrieval. They showed that the LPC is more positive for subsequently remembered than forgotten items, and later research has identified related positive-going subsequent memory effects (SMEs) across various materials, encoding tasks, and memory measures (Mecklinger & Kamp, 2023). These SMEs reflect successful episodic encoding. It is, however, questionable whether this episodic encoding can profit from long-term associations between words. Paller and Wagner (2002, p. 101) suggested the following important outstanding questions concerning SMEs: “How does encoding differ for episodes versus other types of information, such as […] implicitly conditioned associations? Do the neocortical encoding events that putatively support priming constitute a subset of those supporting episodic learning, or are they distinct?” The present study investigates whether episodic encoding effects are distinct from associative and semantic long-term knowledge usage, or whether episodic memory trace formation interacts with associative and semantic long-term processes. Implicitly “conditioned” associations between words can be addressed by word co-occurrence (e.g., Skinner, 1948; Steyvers & Tenenbaum, 2005). A large text corpus can be regarded as a sample of human experience (Hofmann, Remus et al., 2022), and when two words co-occur significantly more often in sentences than predicted by their individual word frequencies, they

are defined as directly associated (Dunning, 1993; Hofmann et al., 2011). The resulting log10-transformed χ^2 value can, for instance, reproducibly account for about 40% of the variance of the mean rated association between two words (Hofmann et al., 2018). Therefore, it can be conveniently used to define the long-term association strength between words. If the two words do not co-occur significantly often together, the association strength is defined as zero and the words are defined as "not associated". When counting the number of significant common associates, that two words share, this can be used to address semantic feature overlap by the number of common associates, for instance to define synonymy (Rapp & Samuel, 2002).

Rölke et al. (2018) used these definitions of implicitly acquired associative and semantic long-term relations (cf. Hutchison, 2003; Lucas, 2000) in a primed lexical decision task. While the classic semantic priming literature set the "challenge [to] find two highly associated words that are not semantically related in some plausible way" (McNamara, 2005, p. 86), this allowed for the first full-factorial manipulation of associative and semantic priming (see Savic et al., 2020, for a review). Rölke and colleagues (2018) found that associative priming effects occurred at both a short stimulus onset asynchrony (SOA; 200 ms) and a long SOA (1,000 ms), while semantic priming effects were constrained to a short SOA. This reflects the general result pattern of previous studies, in which semantic priming effects are primarily observed at a short SOA (Hutchison, 2003; Lucas, 2000), whereas they tend to diminish as SOA increases (Ferrand & New, 2003). Rölke and colleagues (2018) found no interaction effects between associative and semantic priming. Rather, pure associative and semantic effects behaved in a strictly additive fashion, suggesting that these two types of priming reflect separable processes, although their definitions are derived from the same principle of simple co-occurrence. Large-scale behavioral evidence shows that semantic priming is robust across a broad range of prime-target pairs while also demonstrating substantial variation in effect magnitude as a function of item characteristics, task, and prime-target timing (Heyman et al., 2016; Hutchison et al., 2013). Based on this evidence and the pattern observed by Rölke et al. (2018), we expected facilitated word processing through direct association and semantic feature overlap in the present cued-recall paradigm, resulting in higher recall success and shorter response times. Further evidence that semantic priming reflects a process distinct from associative priming comes from the functional magnetic resonance imaging study by Rölke

and Hofmann (2020). Blood-oxygen-level-dependent responses were exclusively sensitive to semantic, but not associative priming. The present study aims to replicate prior evidence for the logical separability of the associative and semantic long-term relations during priming. Moreover, it examines whether episodic encoding is logically distinct from these effects.

Such a simple additivity for episodic and associative-semantic processes can be derived from a simulation modeling study by Hofmann et al. (2011). They used an interactive activation model consisting of a visual feature, a letter, and an orthographic word layer (McClelland & Rumelhart, 1981) and extended it by an associative layer, in which the association strength is used to define long-term relations between words (Hofmann et al., 2011; Hofmann & Jacobs, 2014). To address episodic encoding, the studied old words simply obtained an increased resting-level activation in the associative layer than the non-studied new words (Glanzer et al., 1999; Yonelinas, 2002). To address associative relations to the other stimuli at retrieval, they counted the number of associated words in the stimulus set, in order to predict effects of veridical and false memories (Kimball et al., 2007; Roediger & McDermott, 1995). Although they found highly reliable old/new and association effects, importantly the episodic and associative factors did not interact, suggesting that episodic encoding is logically distinct from associative processes. The present study challenges this assumption by comparing correctly vs. falsely remembered words in a subsequent memory effects analysis.

Stuellein et al. (2016) basically used Hofmann et al.'s (2011) experimental design to show that associative relations to the other words in the stimulus set facilitate early top-down access to orthographic representations at the level of the P2 (Dambacher et al., 2006; Hauk & Pulvermüller, 2004). Moreover, they found semantic integration effects as reflected by the N400. The N400 is a negative-going amplitude deflection that peaks around 400 ms after stimulus onset, typically showing a centro-parietal maximum (Kutas & Federmeier, 2011). Its amplitude varies systematically with the accessibility of meaning-related information and is sensitive to contextual predictability, lexical characteristics, and semantic relatedness (Federmeier, 2022; Kutas & Federmeier, 2011). Semantic priming and increasing contextual predictability are generally associated with reduced negativity in the N400 time window, consistent with facilitated access to or processing of meaning-related information (Federmeier, 2022; Van Petten & Luka, 2012). The majority of studies not only show a reduction of the

N400 amplitude but also reduced reaction times and error rates (e.g., Alday & Kretzschmar, 2019; Lau et al., 2008). Stuellein et al. (2016) also found old/new main effects in the N400 time window, suggesting that item repetition (i.e., prior study-phase exposure) may account for the observed N400 effects. Importantly, the old/new effect did not interact with the associative manipulation (i.e., the number of associated items in the stimulus set), further supporting the idea that associative and episodic processes are partially distinct.

During memory retrieval, ERP effects before approximately 500 ms have traditionally been associated with familiarity-based old/new decisions, whereas later posterior positive effects have been linked to recollection (Rugg & Curran, 2007; Yu & Rugg, 2010). However, the functional interpretation and temporal characteristics of these effects remain debated. Recent evidence suggests that the recognition-related LPC may be more closely time-locked to the memory decision than to stimulus onset, such that its latency in stimulus-locked averages can be influenced by response timing (Sun et al., 2024). Nevertheless, late positive ERP effects have been observed across both recognition and recall paradigms and have commonly been associated with successful episodic retrieval (Yonelinas, 2002). Although early encoding-related effects have also been reported (Besson & Kutas, 1993; Fernández et al., 1998), ERP effects previous to 500 ms have more commonly been investigated in recognition-memory paradigms, including studies of old/new judgments (e.g., Rugg et al., 1998). At encoding, SMEs have been investigated since Sanquist et al. (1980) reported a larger late positive ERP response for subsequently remembered than forgotten items. A finding that has since been replicated in numerous studies (see Friedman & Johnson, 2000; Mecklinger & Kamp, 2023; Paller & Wagner, 2002, for reviews). Encoding-related SMEs are, however, not unitary but comprise multiple temporally and functionally distinguishable effects whose polarity, latency, and scalp distribution depend on the stimulus material, encoding task, and later memory measure (Mecklinger & Kamp, 2023). The LPC has often been considered a memory-related late positivity within the broader P3/P3b family, although the terminology and the degree of overlap between these components vary across paradigms (Friedman & Johnson, 2000; Leckey & Federmeier, 2020; Polich, 2007). While the P3b is generally associated with the processing of task-relevant information, attentional resource allocation, and context updating (Polich, 2007, 2020), the term LPC is commonly used in episodic-memory paradigms for a relatively

late posterior positivity associated with successful encoding or retrieval (Friedman & Johnson, 2000; Leckey & Federmeier, 2020). One possible account of late positive SMEs observed in previous studies of memory encoding is that fluctuations in arousal or attentional engagement influence the extent to which an item is processed during encoding, resulting in more positive amplitudes for subsequently remembered than forgotten items (Paller et al., 1987; Paller & Wagner, 2002). As an alternative explanation, Paller and colleagues (1987) proposed that these effects may be explained by differences in associative-semantic processing. These alternative theoretical accounts are tested in the present study.

To date, there is limited evidence on how SMEs relate to associative and semantic priming manipulations (but see Neville et al., 1986). There are some studies, however, that examine associative processes at encoding. For instance, Weyerts et al. (1997) presented word pairs at study. Participants either had to judge whether these words are semantically associated, or they had to make a non-associative judgment. They found an SME only in the associative encoding condition (see also Kamp et al., 2017; Kounios et al., 2001), a finding broadly consistent with the idea that LPC effects require contextual processes (Donchin & Coles, 1988). Höltje et al. (2019) took a closer look at the temporal dynamics of the processes by which activated schemata support the encoding of semantically congruent or incongruent information. Participants had to learn category exemplar words preceded by a category cue phrase. On the next day, recognition memory was tested. In addition to the expected behavioral effects of a reduced error rate for semantically related words, an SME was observed in the N400 time window. At frontal electrodes the SME did not differ between congruent and incongruent trials whereas the SME with a parietal distribution was specific for semantically congruent words. Therefore, the authors suggested that the activated schemata supported the encoding of item-specific details. Paller (1990) found an SME for later recalled words, but not for word stems that "primed" the completion of studied vs. non-studied items, suggesting an independence of subsequent memory and "priming" effects (see also Meng et al., 2014). Given similar evidence, Paller and Kutas (1992) argued that priming as a measure of implicit memory and recollection as a measure of explicit memory reflect distinct memory processes. Wagner et al. (2000) even found that repetition priming can hinder episodic encoding. Recently, Li et al. (2020) showed that conceptual priming influences the N400 and familiarity-based decisions, but not

recollection or the LPC. In sum, these findings are consistent with contemporary memory-systems accounts that distinguish episodic recollection from non-declarative expressions of prior experience such as priming (Squire & Dede, 2015).

The Present Study

The present study examines the effects of associative and semantic priming during memory encoding in a sentence-embedded paired-associate paradigm. To test the dissociable contributions of associative, semantic and episodic processes, the experimental factors were direct association (strong vs. none) and semantic feature overlap (high vs. low). Participants were instructed to learn the target-object of a presented sentence in every trial of the study phase. In the following test phase, they had to complete the previously learned sentences verbally with the missing target-object during cued recall. If the manipulated relations support memory encoding, facilitated word processing through direct association and semantic feature overlap should result in increased trial-level recall success and shorter response times during recall (Hofmann et al., 2018; Rölke et al., 2018). For the ERP data recorded during target encoding, top-down driven modulation from an associative level is expected (Hofmann & Jacobs, 2014). Semantic feature overlap may facilitate lexical access, but it may also induce semantic competition by co-activating multiple related features from which the intended representation must be selected. Since these processes could affect ERP amplitudes in opposing directions, we did not expect semantic feature overlap to produce a reliable effect. In this regard, the N400 could have been a plausible candidate for effects of semantic relatedness. However, as the present paradigm placed particular demands on the intentional encoding of the target-object and its integration with the prime and sentence context into a new episodic representation, our condition-related predictions were focused on a later positive ERP modulation. Specifically, we expected larger LPC amplitudes for target-objects that were directly associated with the preceding prime, reflecting expectancy-driven encoding even when semantic feature overlap was low. Regarding SMEs, it is assumed that target-words that are later recalled correctly elicit more positive waveforms during encoding than items that are recalled incorrectly. If the SMEs are driven by associative and semantic processes, interactions

between SMEs and associative as well as semantic priming are expected. Conversely, if the SMEs are independent of the priming effects, this would support the alternative explanation due to trial-to-trial variations in attention. Importantly, the predicted condition-related LPC modulation and the SME represent distinct experimental contrasts. The former was defined by the manipulated prime-target relations, whereas the latter was defined by subsequent recall success. Thus, despite potential temporal overlap, the LPC was not assumed to constitute a unitary index of both associative priming and successful episodic encoding in the present study.

4.2 Methods

4.2.1 Participants

Behavioral and electroencephalographic (EEG) data were collected from 35 right-handed participants at Bergische Universität Wuppertal in Germany, including both students and non-students. Those who were eligible received course credit, while all others took part without compensation. All participants were native German speakers, had normal or corrected-to-normal vision, and reported no history of psychiatric, neurological, or reading disorders. The target sample size was determined a priori using GLIMMPSE (Version 3.1.3; Glueck et al., 2025; Kreidler et al., 2013) for a one-group design with four repeated-measures conditions corresponding to the 2 × 2 manipulation of direct association and semantic feature overlap. The calculation targeted the main effects, using $\alpha = .05$, a target power of $1 - \beta = .80$, and the Hotelling–Lawley trace. Expected cell means were derived from Rölke and Hofmann (2020), which provided the closest available parameter source because it used the same orthogonal manipulation and an overlapping subset of the prime–target materials, although its task and outcome measures differed from those of the present study. Given the limited transferability of these estimates, the assumed covariance matrix was scaled by a factor of 1.25 to represent greater within-participant variability, yielding a required sample size of $N = 31$. This calculation used behavioral parameter estimates to inform participant-level sample size planning for the repeated-measures design. It was not a component-specific ERP power analysis. Four participants were excluded from the analysis, because their overall error rate,

calculated across all experimental conditions in the test phase, exceeded the sample mean by more than 2 *SD*. The mean age of the remaining 31 participants (21 women) was 24.12 years (*SD* = 7.04; range: 18–33).

4.2.2 Stimuli

The stimulus set comprised 184 unique German sentences, including 168 experimental items and 16 filler items, which served as primacy and recency trials. Four additional sentences were used in a practice run. The construction of the sentences followed the structure article, subject-prime, auxiliary verb, closed-class word, target-object, while both prime and target were nouns. The number of letters for each word type was three to eight units. The words were presented in the center of the screen in Courier New font. The auxiliary verbs were "to be", "have" or "become", whereas the closed-class words were either an article or a preposition. Direct association and semantic feature overlap between the prime and the target noun were experimentally manipulated. The direct association strength (first-order co-occurrence) of the prime and target words was computed by the $\log_{10}$-transformed log-likelihood that two words significantly occur more often together in sentences than is predicted by their single-word frequency (Dunning, 1993; Hofmann et al., 2011). Prime-target pairs with a strong direct association (SA) had an association strength of at least 2, whereas pairs with no direct association (NA) had an association strength of 0. This indicates that the words do not significantly co-occur together in the sentences. Semantic feature overlap (second-order co-occurrence) was defined by the number of common direct associates, which represent shared semantic features (cf. Rölke et al., 2018). Thus, the 1,000 words with the largest χ^2 values were used as the semantic features of each word, and the number of common associates was simply counted (Hofmann et al., 2018). Word pairs were defined to have a high semantic feature overlap (HS) when they had at least 10 common associates, and to have a low semantic feature overlap (LS) if they had 0 common associates. The thresholds were pragmatic selection criteria used to obtain a sufficiently large and clearly differentiated stimulus set. They were not intended to define universal or corpus-derived boundaries between weak and strong relations.

Table 5 provides some examples for the stimulus sentences. The full stimulus list is provided in Appendix A1 and can also be found in the open science repository (Appendix E).

Table 5
Example Stimulus Sentences by Experimental Condition (Study B)

Condition	German	English
SA-HS	Das Auto hat einen Motor.	The car has an engine.
SA-LS	Die Flasche ist aus Glas.	The bottle is made of glass.
NA-HS	Der Junge wird ein Student.	The boy becomes a student.
NA-LS	Der Abend ist eine Blamage.	The evening is a disgrace.

Note. German sentences are the original stimuli. HS = high semantic feature overlap; LS = low semantic feature overlap; NA = no direct association; SA = strong direct association.

The sentences of the four conditions (42 trials each) were further assigned to two lists (A and B), with each list containing half of the items from each condition. Participants completed two study-test blocks, one for each list, with the list order (A→B vs. B→A) counterbalanced across participants. It was ensured that both lists remained matched with respect to all controlled variables. Within each study and test block, the order of the trials was pseudorandomized for each participant, with no more than two sentences from the same condition appearing in sequence. Association strength and the number of common associates were computed from the German corpus of the Leipzig Wortschatz Project consisting of 70 million sentences (Goldhahn et al., 2012). The prime and target nouns, the auxiliary verb and the closed-class word were matched for word frequency, word length and orthographic neighborhood in each condition (all Fs < 1, see Table 6). The selected target nouns had a word length of four to eight letters, a Leipzig word frequency class of six to seventeen and a maximum of nine orthographic neighbors. The prime nouns had a word length of four to eight letters, a frequency of six to sixteen and a maximum of seven orthographic neighbors.

Table 6
Means (SDs) and F Statistics for Controlled Variables (Study B)

	SA-HS	SA-LS	NA-HS	NA-LS	*F* value
Clause length	26.52 (1.69)	26.45 (2.47)	27.02 (1.81)	26.69 (1.57)	0.74
AS $_{\text{prime-target}}$	3.29 (0.62)	3.27 (0.43)	0.00 (0.00)	0.00 (0.00)	0.02
CA $_{\text{prime-target}}$	23.74 (8.46)	0.00 (0.00)	23.71 (4.93)	0.00 (0.00)	0.00

			Prime		
Length	6.07 (1.07)	5.95 (1.38)	6.21 (1.24)	6.00 (0.99)	0.39
Frequency	10.29 (1.52)	10.07 (1.60)	10.45 (2.13)	10.43 (1.77)	0.41
OrthNeigh	0.74 (1.52)	0.90 (1.32)	0.74 (1.04)	0.60 (0.77)	0.47
			Target		
Length	6.38 (1.25)	6.31 (1.37)	6.62 (1.01)	6.50 (0.94)	0.58
Frequency	10.29 (1.78)	10.14 (1.66)	10.69 (2.18)	10.36 (1.69)	0.67
OrthNeigh	0.71 (1.45)	0.69 (1.02)	0.55 (0.94)	0.60 (0.77)	0.22
			Auxiliary verb (inflected)		
Length	3.17 (0.38)	3.12 (0.40)	3.24 (0.43)	3.14 (0.42)	0.67
Frequency	2.45 (0.50)	2.52 (0.51)	2.38 (0.49)	2.43 (0.50)	0.59
OrthNeigh	2.00 (0.00)	2.02 (0.15)	2.00 (0.00)	2.02 (0.15)	0.67
			Closed-class word (main clause)		
Length	2.90 (0.93)	3.07 (0.81)	2.95 (0.38)	3.05 (0.79)	0.45
Frequency	1.95 (1.08)	1.79 (0.75)	1.90 (0.88)	1.98 (1.07)	0.33
OrthNeigh	2.98 (1.60)	2.93 (1.40)	2.79 (1.18)	3.10 (1.34)	0.36

Note. *F* statistics for clause length and the lexical control variables were obtained from separate one-way between-item analyses of variance across the four experimental word pair conditions, $F(3, 164)$. For association strength (AS) and the number of common associates (CA), the *F* statistics compare SA-HS with SA-LS and SA-HS with NA-HS, respectively, $F(1, 82)$; values in the excluded conditions were fixed at zero by design. Clause length is reported in letters. AS and CA were calculated for each prime–target pair. HS = high semantic feature overlap; LS = low semantic feature overlap; NA = no direct association; OrthNeigh = number of orthographic neighbors; SA = strong direct association.

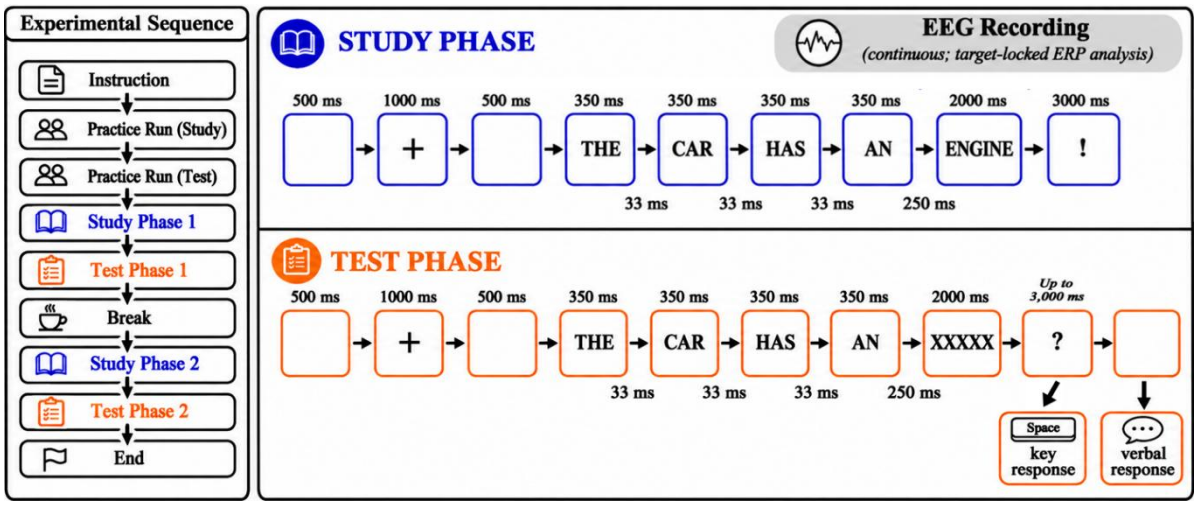
4.2.3 Experimental Procedure

Participants were instructed to learn target-objects during the study phase and were told that they have to complete each sentence with the corresponding target-object during the test phase. To familiarize the participants with the task, the experiment began with four practice trials for the study and test phase. The experiment subsequently comprised two study-test blocks. Each block included four primacy and four recency trials, corresponding to the 16 filler items described above. These trials were later excluded from all analyses. The stimuli were displayed centrally using the rapid serial visual presentation method (word-by-word) with PsychoPy (Version 1.9.0; Peirce et al., 2019) on a 24-inch Samsung B2430L monitor set to a resolution of 1,680 × 1,050 pixels and a refresh rate of 60 Hz. The experimental computer ran the 64-bit version of Windows 10 Pro, version 20H2. Before the experiment began, the viewing distance was measured and set to approximately 68 cm. The positions of the chair and monitor

then remained unchanged. Participants were instructed to keep their backs against the chair backrest and to avoid unnecessary head movements. At this distance, the width of a letter subtended approximately 1/3° of the visual angle. Figure 13 illustrates the overall experimental sequence and the trial timing in the study and test phases.

Figure 13

Experimental Sequence and Timing of a Trial: Study/Test Phase (Study B)



In the study phase, each trial started with a blank screen for 500 ms, a fixation cross in the middle of the screen for 1,000 ms and a subsequent blank screen for 500 ms. Each word was displayed for 350 ms, except for the target-object being displayed for 2,000 ms. The nominal blank-screen duration between the first four words was set to 30 ms in PsychoPy, corresponding to approximately 33.3 ms (two frames) at a refresh rate of 60 Hz. A blank screen was presented for 250 ms before the target to provide a sufficient baseline interval. In the study phase, the sentences ended with a "!", which was presented for 3,000 ms and led over to the next trial. After each block of the study phase there was a cued recall test phase. The experimental sequence was basically the same, but the target-object of the previously learned words from the study phase was now replaced by five crosses (xxxxx) and lasted 2,000 ms. This was immediately followed by a "?" which was presented for up to 3,000 ms. During this interval, participants indicated retrieval of the target word by pressing the space bar, with response times measured from the onset of the question mark to the keypress. This immediately initiated a blank screen, during which participants had to verbally name the recalled target word. If no keypress occurred, the blank screen appeared automatically after 3,000 ms, and the trial was coded as incorrect. An experimenter seated behind the participant listened to each

response and coded it online as correct or incorrect. The next trial was then started manually by pressing the space bar. Participants were asked to decide as quickly and accurately as possible and were told that they will receive feedback about the number of correct responses after the experiment. Instructions and experimental scripts are available in the open science repository (see Appendix E).

4.2.4 EEG Acquisition and Preprocessing

EEG was recorded during the encoding of the target-object in the study phase using a 64-channel active Ag/AgCl electrode system (actiCAP slim; Brain Products GmbH, Germany). The scalp electrode setup consisted of eight midline electrodes (AFz, Fz, FCz, Cz, CPz, Pz, POz, Oz) and 27 lateral electrode pairs (FP1/2, AF3/4, AF7/8, F1/2, F3/4, F5/6, FC1/2, FC3/4, FC5/6, FT7/8, T7/8, C5/6, C3/4, C1/2, TP7/8, TP9/10, CP5/6, CP3/4, CP1/2, P7/8, P5/6, P3/4, P1/2, PO7/8, PO3/4, PO9/10, O1/2). Two of the 64 recording channels, originally assigned to AF1 and AF2 in the cap configuration, were repurposed for electrooculographic recording and labeled HEOG and VEOG, respectively. All scalp electrodes were mounted in an elastic cap, with electrode positions arranged according to the extended international 10–20 system (see Appendix B4). VEOG and HEOG electrodes were placed above and at the outer canthus of the right eye to identify blink and eye movement artifacts. The electrodes were online-referenced to M2. A separate ground electrode was placed at Iz. Signals were recorded using a BrainAmp DC amplifier system (Brain Products GmbH, Germany) at a sampling rate of 500 Hz, with hardware high-pass and low-pass filter cutoff frequencies of 0.016 and 1,000 Hz, respectively. No additional software filters or notch filtering were applied during acquisition. All EEG recordings were performed in an electrically shielded room. Before recording, electrode impedances were checked and brought below 5 kΩ for the EEG electrodes and below 10 kΩ for the EOG electrodes by applying additional conductive gel where necessary.

For offline processing of the EEG data, BrainVision Analyzer (Version 2.2.2; Brain Products GmbH, 2021) was used. The continuous data were filtered using a zero-phase-shift Butterworth infinite impulse response filter operation comprising a 30 Hz low-pass component with a slope of 24 dB/octave and a 50 Hz notch component. Noisy channels, identified by

visual inspection based on flat-line signals or persistent noise contamination, were replaced by topographic spline interpolation with default settings for the order of splines (4), the maximum degree of Legendre polynomials (10), and default λ (1×10^{-5}). In total, 115 participant-specific channel instances were interpolated (M = 3.71, SD = 1.05; 5.8% of all channel instances). To ensure a satisfactory signal-to-noise ratio for each participant, continuous EEG data were automatically inspected using the following criteria: activity below 0.5 µV within a 100 ms time interval (M = 0.003%; range: 0.000–0.054%), amplitudes outside the range of -200 to +200 µV (M = 0.004%; range: 0.000–0.119%), voltage differences exceeding 100 µV within 100 ms (M = 0.289%; range: 0.000–0.922%), and voltage gradients exceeding 50 µV/ms (M = 0.001%; range: 0.000–0.004%). Data intervals that met these criteria were marked as bad and excluded from the subsequent analysis on an individual channel basis. The data were re-referenced to an average reference offline. Subsequently, an ocular correction independent component analysis was used to correct drift movements as well as blinks, using a limited Infomax algorithm. Stimulus-locked ERP waveforms were averaged from corrected, artifact-reduced trials. Each segment ranged from -200 to 800 ms and contained a baseline correction with a period of 200 ms pre-stimulus. As the LPC is usually largest at posterior parietal recording sites (Friedman & Johnson, 2000; Münte et al., 2000; Rugg & Curran, 2007) and data exploration (Figure 16) confirmed this assumption, the ERP analysis for the LPC was based on the following occipito-parietal electrode cluster: Pz, P1, P2, P3, P4, POz, PO3, PO4. The difference between subsequently remembered and forgotten stimuli is generally greatest over centro-parietal recording sites (Paller & Wagner, 2002; Wagner et al., 2000). In this regard, encoding conditions in which unitized item representations are formed are highly informative during word processing of associative and semantically related words and these are usually most pronounced at parietal recording sites (Kutas & Federmeier, 2011). The SME analysis was therefore based on the following centro-parietal electrode cluster: Cz, C1, C2, CPz, CP1, CP2, CP3, CP4. For each participant, experimental condition, and recall outcome, the mean amplitude within the respective LPC or SME time window was calculated separately at each electrode. These electrode-wise mean amplitudes were then averaged with equal weighting across the electrodes of the corresponding cluster, yielding a single cluster-level mean amplitude for statistical analysis. Across participants, seven interpolated channel

instances involved electrodes from the LPC cluster, and one involved an electrode from the SME cluster. The mean, standard deviation, and range of retained trial counts per condition in the final analysis were as follows: SA-HS correct, *M* = 29.45 (*SD* = 5.43), range = 18–36; SA-HS false, *M* = 12.75 (*SD* = 5.46), range = 8–24; SA-LS correct, *M* = 26.06 (*SD* = 6.62), range = 10–38; SA-LS false, *M* = 15.71 (SD = 6.53), range = 8–32; NA-HS correct, *M* = 18.68 (*SD* = 6.32), range = 10–31; NA-HS false, *M* = 23.19 (*SD* = 6.23), range = 11–32; NA-LS correct, *M* = 17.69 (*SD* = 7.94), range = 10–31; and NA-LS false, *M* = 24.48 (*SD* = 7.94), range = 11–35. To quantify the precision of the ERP estimates, analytical standardized measurement error (aSME; Luck et al., 2021) was calculated for each participant and experimental condition using virtual channels representing the predefined LPC and SME clusters (Appendix B6). Mean aSME values ranged from 0.71 to 1.02 µV for the LPC, from 0.52 to 0.93 µV for the early SME interval, and from 0.66 to 1.12 µV for the late SME interval.

4.2.5 Statistical analysis

Statistical analyses were conducted in JMP (Version 19.0.3; JMP Statistical Discovery LLC, 2025) and IBM SPSS Statistics for Windows (Version 27; IBM Corp., 2020). Behavioral data were analyzed using (i) a generalized linear mixed-effects model (GLMM; binomial distribution with logit link) for trial-level recall success (1 = correct, 0 = incorrect) and (ii) a Gaussian linear mixed-effects model (LMM) for natural-log-transformed response times (RTs), restricted to correctly recalled trials. The log-transformation was used to reduce positive skewness and improve adherence to the distributional assumptions of the model. For both models, the fixed-effects structure included direct association (strong vs. none), semantic feature overlap (high vs. low), and their interaction. To account for the crossed structure of the data (observations varying across both participants and items), random intercepts were specified for subjects and items in both models. For the Gaussian LMM, model adequacy was evaluated using Q–Q plots, residual-versus-fitted plots and an Anderson-Darling test of residual normality (Appendix B1). As the diagnostics indicated deviations from residual normality, the model was re-estimated after excluding trials whose residuals deviated from the participant-specific median by more than 2.5 scaled median absolute deviations (scaling factor

= 1.4826). This criterion excluded 171 of the 2,847 correctly recalled trials (6.01%). Statistical inference was based on $\alpha = .05$. Fixed effects were evaluated using Type III Wald *F*-tests, with denominator degrees of freedom approximated using the Kenward-Roger method. Full test tables are reported in Appendix B2 (GLMM) and Appendix B3 (LMM). Parameter estimates are supplemented by coefficient-level *t*/*z* tests in the respective tables. Estimates are reported using effect coding (direct association: none = -1, strong = +1; semantic feature overlap: low = -1, high = +1), with the intercept representing the equally weighted mean across conditions on the model scale and the coefficients reflecting the corresponding effects. For the Gaussian LMM, model fit is reported using marginal and conditional R^2 (R^2_m, R^2_c). For the GLMM, model fit is reported via Akaike information criterion (AIC) and Bayesian information criterion (BIC), based on the residual -2 log pseudo-likelihood, as well as Nakagawa's R^2_m and R^2_c on the latent logit scale (Nakagawa et al., 2017). Overdispersion was assessed using the generalized χ^2/df statistic. Whereas mixed-effects models are advantageous for trial-level data to account for hierarchical observations, ERP dependent variables (LPC, SME) were derived from single-subject averages and further reduced to cluster-level mean amplitudes. As no trial-level variance remained to be modeled and the data were structured on the participant × condition level, effects were probed using repeated-measures ANOVAs (rmANOVA). To examine LPC effects, mean amplitudes were analyzed using a 2 × 2 rmANOVA with the within-subject factors direct association (strong vs. none) and semantic feature overlap (high vs. low). For the SME, mean amplitudes were analyzed using a 2 × 2 × 2 rmANOVA with the within-subject factors direct association (strong vs. none), semantic feature overlap (high vs. low), and recall success (correct vs. incorrect). Effect sizes are reported as partial eta squared.

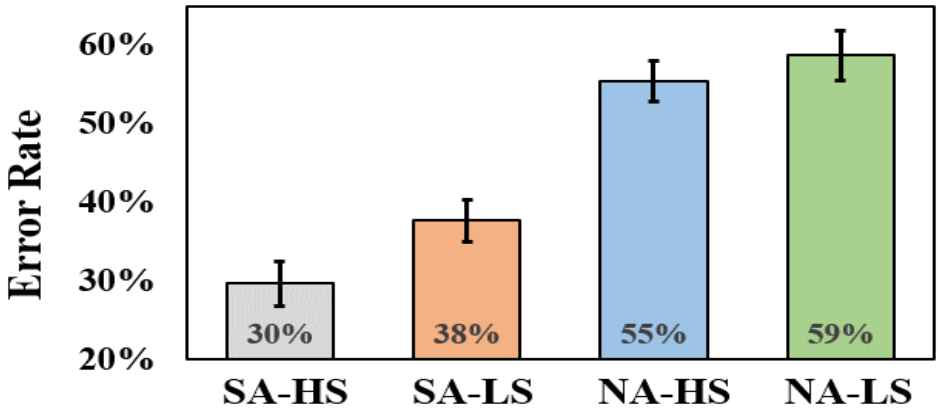
4.3 Results

4.3.1 Statistical Analysis of Behavioral Data

The binomial GLMM on trial-level recall success revealed a significant main effect of direct association, $F(1, 149) = 51.39$, $p < .001$, but no significant main effect was observed for semantic feature overlap, $F(1, 148) = 2.30$, $p = .131$, nor an interaction between the two factors,

$F(1, 148) = 0.48$, $p = .490$. Word pairs with strong direct association led to higher recall success compared to those with no direct association. The generalized χ^2 was 4,726 (df = 5,208), indicating no evidence of overdispersion ($\phi = 0.91$). Information criteria for the fitted model were AIC = 23,991, BIC = 24,030, Nakagawa's $R^2_m = .075$ and $R^2_c = .377$. Figure 14 shows the mean error rates for each experimental condition. Table 7 reports the coefficient-level parameter estimates (logit *b*), *SE*s, Wald *z*-test scores, odds ratios (ORs) with 95% confidence intervals (CIs), and the random-intercept variance components for the fitted model.

Figure 14
Mean Error Rates (Study B)



Note. N = 31 participants. Error rate (%) = 100 × incorrect trials/total trials. Error bars represent 95% within-subject confidence intervals calculated from participant-level condition means using the Cousineau–Morey correction (Cousineau, 2005; Morey, 2008). HS = high semantic feature overlap; LS = low semantic feature overlap; NA = no direct association; SA = strong direct association.

Table 7
GLMM Estimates for Trial-Level Recall Success (Study B)

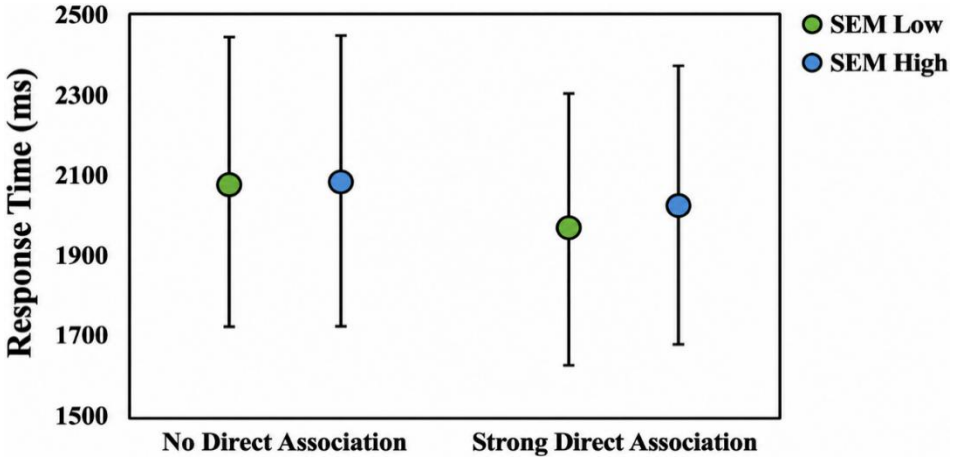
Random effects	**σ^2**	***SE*(σ^2)**			
Subject intercept	0.563	0.155			
Item intercept	1.034	0.141			
Fixed effects	***b* (logit)**	***SE***	***z* value**	***p***	**OR [95% CI]**
(Intercept)	0.262	0.159	1.64	.100	1.30 [0.94, 1.79]
DA	0.612	0.085	7.17	< .001	1.84 [1.56, 2.18]
SEM	0.129	0.085	1.52	.129	1.14 [0.96, 1.35]
DA × SEM	0.059	0.085	0.70	.487	1.06 [0.90, 1.26]

Note. Binomial generalized linear mixed-effects model (GLMM) with logit link, including random intercepts for participants and items (N = 31 participants; k = 168 items; n = 5,208 trials). Fixed-effect coefficients are reported on the log-odds scale using effect coding (-1/+1). DA = direct association (-1 = none; +1 = strong); SEM = semantic feature overlap (-1 = low; +1 = high). Odds ratios (OR) represent exponentiated fixed-effect estimates; 95% confidence intervals (CI) are Wald intervals. *p* values are based on two-sided Wald *z* tests.

Pairwise comparisons of the estimated marginal means for the interaction between direct association and semantic feature overlap indicated that the effect of semantic feature overlap was not significant when direct association was absent (OR [high vs. low] = 1.15, 95% CI [0.72, 1.85], p = .560), nor when direct association was strong (OR [high vs. low] = 1.46, 95% CI [0.90, 2.35], p = .122).

The Gaussian LMM on the natural-log-transformed RTs (correct trials only) revealed a significant main effect of direct association, $F(1, 162) = 6.29$, p = .013, but no significant main effect was observed for semantic feature overlap, $F(1, 160) = 0.86$, p = .356, nor an interaction between both factors, $F(1, 161) = 0.70$, p = .401. Word pairs with a strong direct association elicited faster response times than word pairs with no direct association. Figure 15 shows the model-estimated response times across experimental conditions.

Figure 15
Model-Based Estimates of Response Times (Study B)



Note. N = 31 participants. Response times (RTs) are presented as back-transformed estimated marginal means (geometric means) from the Gaussian linear mixed-effects model fitted to natural-log-transformed RTs for correctly recalled trials. Error bars represent 95% confidence intervals. SEM = semantic feature overlap.

Table 8 reports the coefficient-level parameter estimates (b), SEs, 95% CIs, Kenward–Roger t-test scores, as well as random-intercept variance components for the model. Model fit was R^2_m = .001 and R^2_c = .541, suggesting that most explainable variance was attributable to subject- and item-level differences.

Table 8
LMM Estimates for Trial-Level Response Times (Study B)

Random effects	**σ²**	***SE*(σ²)**				
Subject intercept	0.188	0.049				
Item intercept	0.001	0.001				
Residual	0.163	0.005				
Fixed effects	***b***	***SE***	**[95% CI]**	***df***	***t* value**	***p* value**
(Intercept)	7.619	0.078	[7.46, 7.78]	30	97.25	< .001
DA	-0.021	0.008	[-0.04, -0.01]	162	-2.51	.013
SEM	0.008	0.008	[-0.01, 0.03]	160	0.92	.357
DA × SEM	0.007	0.008	[-0.01, 0.02]	161	0.84	.404

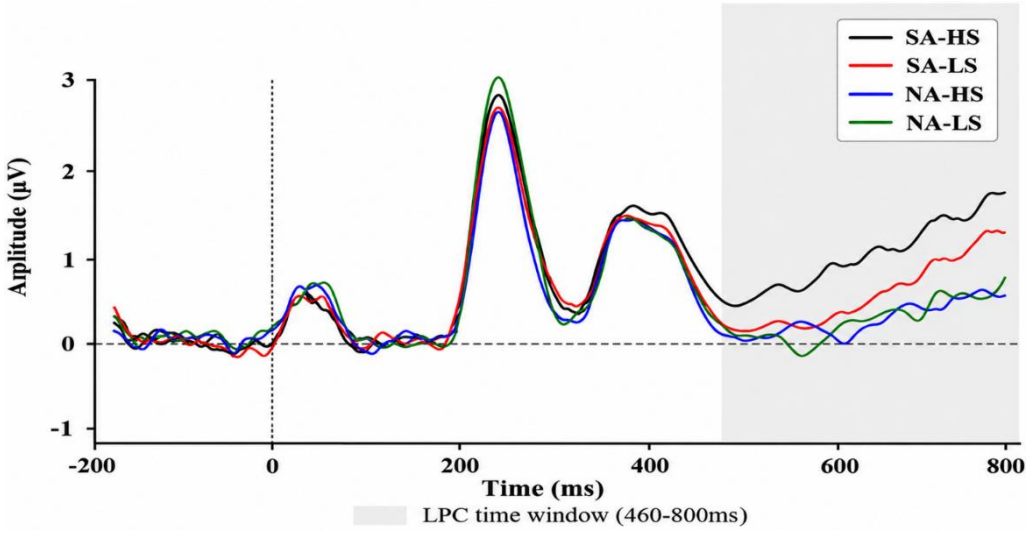
Note. Gaussian linear mixed-effects model (LMM) fitted to natural-log-transformed response times for correctly recalled trials, including random intercepts for participants and items (N = 31 participants; k = 168 items; n = 2,676 trials). Fixed-effect coefficients are reported on the natural-log scale using effect coding (-1/+1). DA = direct association (-1 = none; +1 = strong); SEM = semantic feature overlap (-1 = low; +1 = high). Confidence intervals (CI) are 95% Wald intervals. p values are based on two-sided t tests with Kenward–Roger denominator degrees of freedom.

4.3.2 Statistical Results of the ERP Data

Because the onset and duration of memory-related late positive ERP effects can vary with task demands and experimental paradigms (Friedman & Johnson, 2000; Mecklinger & Kamp, 2023), the LPC quantification window was not determined solely on the basis of predefined time windows used in previous studies. Instead, the effect was identified by jointly considering the temporal morphology of the Global Field Power (see Appendix B5), the expected latency, and its characteristic occipito-parietal scalp distribution. On this basis, the interval from 460 to 800 ms was selected for the LPC analysis. Given that one of the main aims of this study was to investigate the contributions of associative and semantic relations to successful memory formation, the initial analysis focused on subsequently correctly recalled words. The 2 × 2 rmANOVA on the LPC amplitude, with the factors direct association (strong vs. none) and semantic feature overlap (high vs. low), revealed a significant main effect of the factor direct association $F(1, 30) = 13.68$, $p < .001$, $\eta_p^2 = .32$, but no significant main effect of the factor semantic feature overlap, $F(1, 30) = 1.69$, $p = .204$, $\eta_p^2 = .06$, nor an interaction between both, $F(1, 30) = 0.88$, $p = .356$, $\eta_p^2 = .03$. Word pairs with a strong direct association

elicited more positive LPC amplitudes during target-object encoding than word pairs with no direct association (see Figure 16).

Figure 16
Late Positive Component (LPC) for Correctly Recalled Targets (Study B)



Note. N = 31 participants. Grand-average waveforms of the four experimental conditions, averaged with equal weighting across the eight electrodes included in the occipito-parietal electrode cluster. The shaded region indicates the time window used for statistical analysis. HS = high semantic feature overlap; LS = low semantic feature overlap; NA = no direct association; SA = strong direct association.

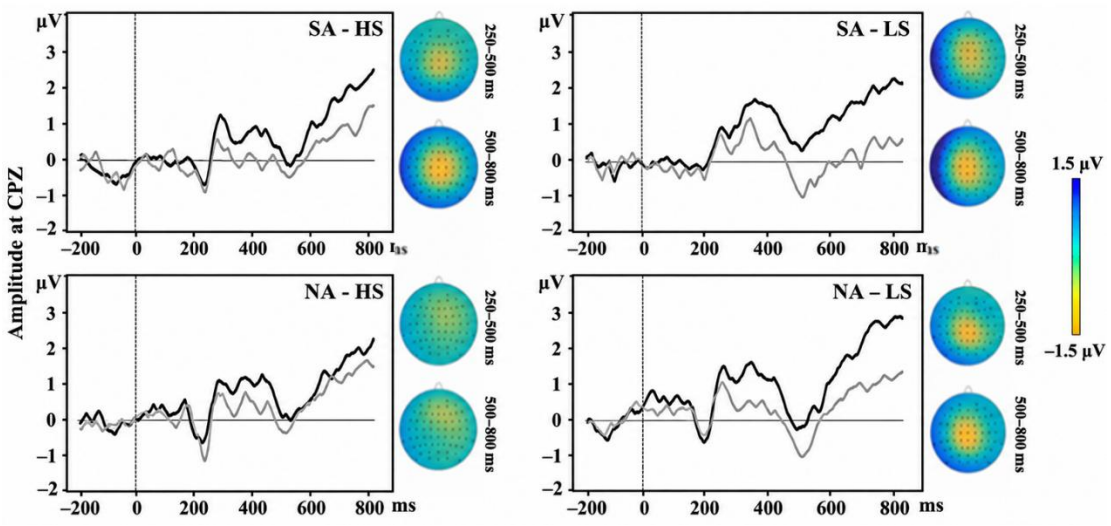
The mean LPC amplitudes (*SE*s) in the 460–800 ms window were as follows: 1.64 (0.22) µV for SA-HS, 1.23 (0.22) µV for SA-LS, 0.92 (0.21) µV for NA-HS, and 0.87 (0.22) µV for NA-LS. To examine whether these condition-related LPC effects differed as a function of subsequent recall success, an additional 2 × 2 × 2 rmANOVA was conducted including recall success as a third factor. This analysis revealed no significant interaction between recall success and direct association, $F(1, 30) = 2.09$, $p = .159$, $\eta_p^2 = .07$, no interaction between recall success and semantic feature overlap, $F(1, 30) = 1.47$, $p = .234$, $\eta_p^2 = .05$, and no three-way interaction, $F(1, 30) = 0.12$, $p = .728$, $\eta_p^2 = .004$. Thus, no reliable moderation of the condition-related LPC effects by subsequent recall success was observed.

When examining the differences between target-objects that subsequently elicited a correct or false recall, SMEs were found in the second negative deflection (N400; 250–500 ms) and the late positive deflection (P600; 500–800 ms) in a centro-parietal area (Figure 17). The 2 × 2 × 2 rmANOVA for the SME with the factors direct association (strong vs. none), semantic feature overlap (high vs. low) and recall success (correct vs. false) in the early N400 time

window revealed a significant main effect of the factor recall success $F(1, 30) = 10.69$, $p = .003$, $\eta_p^2 = .26$, but no significant main effect of the experimental factors or interaction (Fs < 3.32, ps > .05; see Appendix B7). The 2 × 2 × 2 rmANOVA in the late P600 time window also revealed a significant main effect of the factor recall success $F(1, 30) = 35.08$, $p < .001$, $\eta_p^2 = .54$, but again no significant main effect of the experimental factors or interaction (Fs < 3.36, ps > .05; Appendix B8). Later correctly recalled words elicited larger positive amplitudes during target encoding than did forgotten or falsely remembered words in centro-parietal areas, independent of the experimental condition (Table 9).

Figure 17

Subsequent Memory Effects During Target Encoding (Study B)



Note. N = 31 participants. Topographic scalp plots illustrate the differences between experimental conditions. Black represents correct recall; gray represents false recall. HS = high semantic feature overlap; LS = low semantic feature overlap; NA = no direct association; SA = strong direct association.

Table 9

Mean Amplitudes for the Subsequent Memory Effect Analysis (Study B)

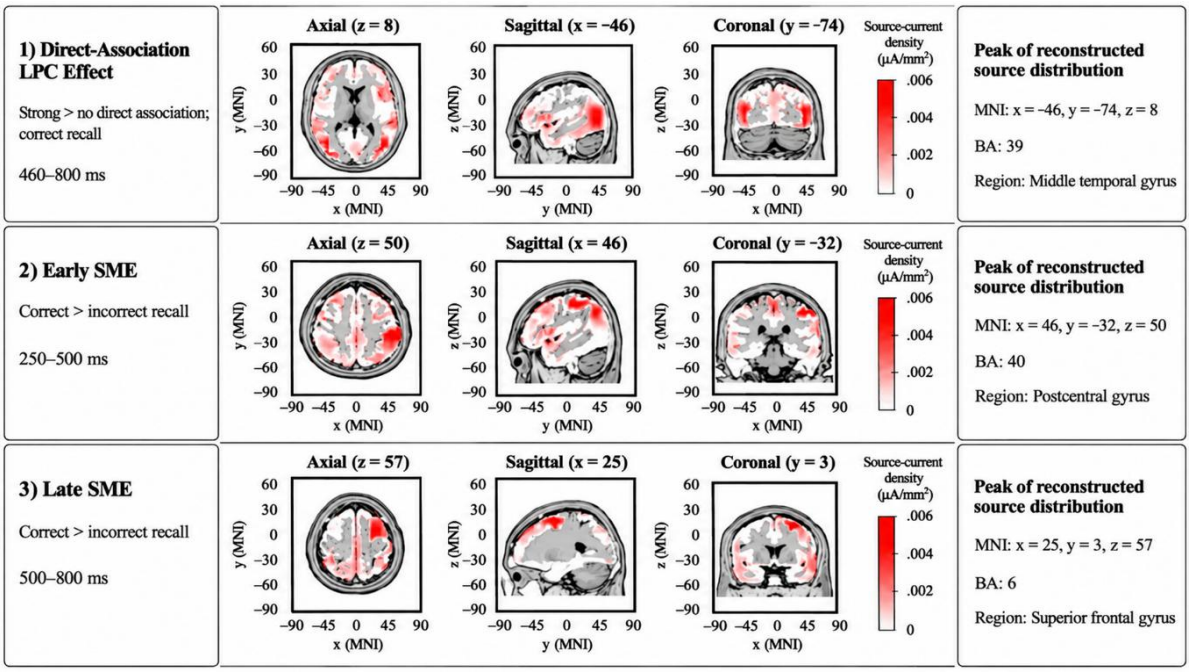
	N400 (250–500 ms)		P600 (500–800 ms)	
	Correct	False	Correct	False
	M (*SE*)	*M* (*SE*)	*M* (*SE*)	*M* (*SE*)
SA-HS	0.54 (0.12)	0.05 (0.18)	1.34 (0.16)	0.57 (0.24)
SA-LS	0.32 (0.13)	0.23 (0.19)	1.07 (0.19)	0.45 (1.14)
NA-HS	0.44 (0.16)	0.30 (0.17)	0.90 (0.23)	0.83 (0.22)
NA-LS	0.54 (0.17)	0.12 (0.13)	1.10 (0.27)	0.29 (0.19)

Note. N = 31 participants. Amplitudes are reported in microvolts (μV). HS = high semantic feature overlap; LS = low semantic feature overlap; NA = no direct association; SA = strong direct association.

To provide an exploratory spatial characterization of the observed ERP effects, source reconstruction was performed using Transient LORETA in BrainVision Analyzer (Version 2.2.2; Brain Products GmbH, 2021). The reconstructions were based on grand-average difference waves and the standard Montreal Neurological Institute (MNI)-Colin-T2 head model implemented in the software. Source-current density (μA/mm²) was averaged across the respective ERP time windows. The reconstructed maxima showed different spatial distributions across the direct-association LPC effect and the early and late SMEs. The corresponding MNI coordinates, Brodmann areas, and anatomical labels are reported in Figure 18. Because the reconstructions were not subjected to participant-level inferential testing, they should be interpreted as a descriptive supplement.

Figure 18

Exploratory Source Reconstructions of Encoding-Related ERP Effects



Note. Source reconstructions were calculated from grand-average difference waves using Transient Low-Resolution Electromagnetic Tomography (LORETA) in BrainVision Analyzer (Version 2.2.2; Brain Products GmbH, 2021) and the standard Montreal Neurological Institute (MNI)-Colin-T2 head model implemented in the software. Source-current density (μA/mm²) was averaged across the respective event-related potential (ERP) time windows. MNI coordinates, Brodmann areas (BA), and anatomical labels are provided for the reconstructed maximum of each effect. LPC = late positive component; SME = subsequent memory effect.

4.4 Discussion

The present study investigated whether direct association (strong vs. none) and semantic feature overlap (high vs. low) between prime and target elicit dissociable effects during episodic encoding. Moreover, the separability of these long-term knowledge effects from episodic encoding was assessed using subsequent memory effects. The behavioral results revealed that strong directly associated word pairs improved recall success, whereas semantic feature overlap did not lead to a robust main effect. The descriptive pattern suggested a potential supportive contribution when a strong direct association was present, but no interaction between the factors was observed. The dissociability of these two relations is further supported by the response time analysis, in which only direct associations accelerated recall. A similar picture was provided by LPC analysis in an occipito-parietal electrode cluster for correct responses, in which exclusively direct associations increased the positivity of the LPC. Neither associative nor semantic effects were found in the subsequent memory analysis in the N400 or P600 time window in a centro-parietal electrode cluster. Instead, these analyses showed only an increased positivity for correctly recalled compared to falsely recalled target words, which further supports a dissociation between episodic encoding success and the two long-term knowledge relations investigated. When the prime was directly associated with the recalled target, participants showed markedly lower error rates than in the non-associated conditions. Crucially, associative and semantic influences did not interact, consistent with Rölke et al.'s (2018) conclusion that the word co-occurrence-based approach enables the identification of pure associative and semantic priming components and suggesting that this dissociation extends to episodic paired-associate learning outcomes. In the classic priming literature, there was a long-standing theoretical difficulty of separating these two processes (Hutchison, 2003; Lucas, 2000; McNamara, 2005). While Rölke et al. (2018) demonstrated that these types of relations reflect distinct processes during primed lexical decision, this study shows that this distinction also applies to episodic memory formation during sentence reading.

Associative and semantic relations can be derived from a theoretically parsimonious approach of word co-occurrence (Rölke et al., 2018; Unger et al., 2020). Further evidence for the logical separability of these two types of priming comes from the sensitivities of different

neurocognitive methods that are either sensitive to associative or semantic priming. While Rölke and Hofmann (2020) found that the blood-oxygen-level-dependent (BOLD) response is only sensitive to semantic feature overlap, the present study shows that the ERP is exclusively sensitive to direct association, probably suggesting that associative and semantic processes may act at different timescales. When associative activation spreads from the prime to the target across multiple common associates, converging activation may accumulate over time (Collins & Loftus, 1975; Sokolovič et al., 2026). Therefore, a method that is relatively insensitive to the temporal dynamics of spreading activation might be more sensitive in this case (Rölke & Hofmann, 2020). The effect of a direct associative relation between the prime and the target, in contrast, might depend more strongly on the temporal dynamics of spreading activation (Hofmann et al., 2011; Radach & Hofmann, 2016). Such rapidly developing effects may therefore be more readily captured by ERPs.

When examining target words that were subsequently recalled correctly, a main effect of associative priming, but not semantic priming, was observed in the LPC. Targets with a strong direct association to the prime elicited a more positive LPC response than non-associated targets. At retrieval, the LPC has been associated with recollection (e.g., Rugg & Curran, 2007). The present results indicate that associative long-term knowledge affects a similar time window during encoding. Accordingly, successful episodic encoding due to long-term associations seems to exhibit basically the same temporal dynamics as recollection (Yonelinas, 2002). Rölke et al. (2018) found that associative priming effects are apparent at a short SOA, but that they become stronger at a long SOA. This could be explained by the associative spreading activation theory, which proposes that "[t]he longer a [prime] concept is continuously processed [...], the longer activation is released from the node of the concept" (Collins & Loftus, 1975, p. 411). The late effect can also be explained in terms of interactive activation models of semantic processes (Hofmann & Jacobs, 2014; McClelland & Rumelhart, 1981). Assuming that the prime word unit is held active by a recurrent process (Kumaran & McClelland, 2012; Rölke & Hofmann, 2020; Rölke-Wellmann, 2021, chapter 4.5), the prime and the target units may continuously increase their activation by associative excitation, which explains the greater sensitivity of late time windows for the associative priming effect. The present ERP data primarily revealed condition-related effects driven by direct associative

relations, whereas Rölke and Hofmann's (2020) functional magnetic resonance imaging results were selectively sensitive to semantic feature overlap. This cross-method dissociation suggests that the null finding of semantic priming effects in the LPC time window may partly reflect modality-specific sensitivity to different temporal dynamics of lexical-semantic activation. Specifically, BOLD responses may be better suited to capture slowly accumulating, feature-based semantic activation, whereas ERPs may be more sensitive to fast, transient associative excitation. The long SOA may offer an alternative account for the absent semantic effect. Rölke et al. (2018) reported no semantic priming effects at an SOA of 1,000 ms, and in the present design 1,360 ms elapsed between prime and target onset. Thus, the missing semantic priming effect might simply reflect the long SOA, in which semantic priming effects are typically diminished (Ferrand & New, 2003). The reason for this may lie in two opposing processes that are apparent at a long SOA (Plaut & Booth, 2000): On the one hand, facilitation can be observed when activation spreads from the prime to the common semantic features with the target (Hofmann et al., 2011). On the other hand, words can receive a strong activation that are not associated with the target (Rölke et al., 2018). Such semantic competition could have reduced the likelihood of observing facilitatory semantic priming effects. This possibility seems particularly relevant to the present sentence-embedded paradigm, in which an auxiliary verb and a closed-class word intervened between prime and target. Processing these words may have introduced additional lexical and contextual activation during the relatively long prime–target interval, thereby reducing the persistence or selectivity of prime-induced semantic activation at target onset. Direct associations and semantic similarity may both contribute to priming in standard paradigms, as recently formalized and simulated by Sokolovič et al. (2026) in their Sequential Read-Out Model (see Fig. 4). However, priming based on shared semantic features appears to be more sensitive to temporal and contextual factors (Rölke et al., 2018; Rölke-Wellmann, 2021), potentially rendering it more susceptible to interference.

In the SME analyses, neither main effects of associative or semantic priming nor interactions involving SMEs were observed, although significant SMEs emerged in an early N400 and late P600 time window with a centro-parietal distribution. The late P600 SME was quite expected (e.g., Paller et al., 1987; Sanquist et al., 1980). The early N400 SME, however, was more unexpected as this finding would be more typical on frontal electrodes (Mecklinger

& Müller, 1996; Otten & Rugg, 2001; Packard et al., 2017). Höltje et al. (2019) suggested that processes reflected by frontal SMEs contribute in a highly similar fashion to the formation of memory traces as parietal SMEs do. They also found that this effect occurs irrespective of semantic congruency. In the present study, no frontal SME could be detected. There are some cues to the functional locus of these earlier SMEs in the previous literature. For instance, Neville et al. (1986) presented context sentences and a target word, in which the semantic context was either congruent with the target (A type of bird. Robin), or not (A type of weapon. Sheep). They demonstrated early SMEs starting around 250 ms for congruent contexts, while the effects for incongruent contexts were constrained to the LPC. These results support the assumption that early effects require semantically congruent contexts, while late effects would be more sensitive to associative manipulations. Crucially, the functional difference between early and late SMEs has not yet been theoretically framed. As a solution to this problem, Neville et al. (1986) suggested that early effects may reflect the initial encoding, while late effects may go beyond this processing stage. Schott et al. (2002) found late effects when the words had been remembered, while they found early effects when a word stem was completed with the primed (i.e., the learned) word, in absence of successful remembering. Together, these findings suggest that early and late SMEs may index partially distinct encoding processes. Consistent with this proposed distinction, the exploratory source reconstruction yielded spatially distinct reconstructed maxima for the early and late SMEs, located in the right postcentral and right superior frontal gyri, respectively. However, neither the present design nor the descriptive source reconstruction permits a more specific functional interpretation of these effects. Future studies combining encoding-related EEG measures with separate assessments of different memory outcomes (e.g., item recognition and source memory) may help clarify whether the two time windows differentially predict specific aspects of subsequent memory performance.

Beyond this potential functional distinction, it remains unclear whether early and late SMEs are differentially affected by associative and semantic long-term knowledge. Fernández et al. (1998) examined this possibility indirectly by assuming that high-frequency words have more meanings and are associatively related to a greater number of other words. They presented words in blocked lists containing only high-frequency words, thereby maximizing associative

opportunities within a block. A block consisting of high- and low-frequency words was intended to reflect an interim level of associative opportunities, while a block consisting only of low-frequency words was assumed to provide comparatively few associative opportunities. Rather than inferring associative or semantic relatedness from proxy manipulations, the present study orthogonally manipulated direct association (via corpus-derived association strength) and semantic feature overlap (via common associates), thereby disentangling their respective effects. At the behavioral level of recall rates, Fernández et al.'s predictions were confirmed. A block that exclusively consisted of high-frequency words elicited the best recall rates, followed by mixed blocks in which there was no difference between high- and low-frequency words. The worst recall performance was obtained in blocks consisting of low-frequency words only. Although they found SMEs starting around 200 ms for high-frequency and around 350 ms for low-frequency words, there were no differential word frequency effects for the different blocking conditions. These findings provide some indirect evidence that associative and/or semantic processes do not affect SMEs. In the present study, word frequency was controlled and associative-semantic effects were examined separately. This approach more clearly supports the conclusion that associative and semantic relations did not modulate the SMEs. The results suggest that SMEs are not driven by pure associative and semantic processes. Rather, trial-to-trial variations in attention remain one possible explanation. When words have been attentively studied in a language context, they are recalled, while failure to recall the items can be explained by low attention (Paller & Wagner, 2002; Polich, 2007). The absence of SME modulations by associative or semantic long-term knowledge, as well as the absence of corresponding interactions, thus seems to give an empirical answer to Paller and Wagner's (2002, p. 101) question, whether "implicitly conditioned associations" are distinct from episodic encoding. Though associative LPC effects were apparent when focusing on correctly recalled words in occipito-parietal sites, these cannot be observed when further including incorrectly recalled words in the SME analysis. Moreover, the reconstructed maximum of the direct-association LPC effect in the left middle temporal gyrus was spatially distinct from the reconstructed maxima of the early and late SMEs. Although this descriptive pattern cannot establish distinct neural generators, it is consistent with partially separable neurofunctional contributions to associative processing and successful episodic encoding. Future research using

simultaneous EEG and functional magnetic resonance imaging (fMRI) recordings could examine these putative distinctions more directly by incorporating single-trial ERP amplitudes as regressors in the fMRI analysis. Such a multimodal approach could identify brain regions whose hemodynamic activity covaries with electrophysiological variation related to associative processing, semantic feature overlap, and episodic encoding, thereby characterizing the temporal and neuroanatomical dynamics of these processes more comprehensively. It may also help clarify whether differing patterns observed across EEG and fMRI studies reflect differences in temporal resolution, spatial sensitivity, or the neurophysiological signals captured by the two methods.

Although the final sample size was broadly consistent with those commonly used in ERP research and matched the a priori target, sensitivity to comparatively subtle effects remained constrained. This is especially relevant to the absence of reliable effects of semantic feature overlap. The relatively long prime–target interval and the intervening sentence material may further have attenuated the magnitude or consistency of these effects, given the possibility that facilitation and semantic competition operated in opposing directions. Accordingly, the non-significant semantic findings may partly reflect the specific temporal and contextual conditions of the present paradigm and should not be interpreted as evidence against feature-based semantic involvement in general. Future studies with larger samples and systematic variation of these design-related factors may provide more precise estimates of semantic contributions. Two additional methodological limitations concern the ERP analyses. First, the LPC quantification window was informed by the morphology of the present dataset. Although the selected time window was additionally guided by established LPC characteristics, it was not defined independently of the data subsequently used for statistical analysis. Some degree of selection bias therefore cannot be ruled out. Future studies could reduce this risk by using an independent collapsed-localizer procedure (Luck & Gaspelin, 2017) or by quantifying component timing more objectively using fractional-area latency measures (Kiesel et al., 2008). Second, the number of retained trials was unequal across conditions and comparatively small in some participant-level cells, particularly for false-recall trials in the directly associated conditions. Because some corresponding ERP estimates showed comparatively high aSME values, interactions involving recall success should be interpreted cautiously.

4.5 Conclusion

This study provides a systematic investigation of pure associative and semantic priming during memory encoding, using a sentence-embedded paired-associate paradigm that combines behavioral measures with EEG data. The results revealed that associative long-term knowledge facilitated cued recall success and accelerated response times. Semantic feature overlap did not demonstrate such effects but exhibited a descriptive, non-significant trend that was consistent with a potential supportive contribution for cued recall success. Pure associative relations were associated with occipito-parietal LPC effects, whereby the late window might be explained by dynamics of spreading activation: the longer a prime concept is continuously processed, the larger its activation becomes. Thus, later time windows may be more sensitive to associative processes. Neither semantic main nor interaction effects were observed for recall success, response time or LPC data. This corroborates Rölke et al.'s (2018) conclusion that associative and semantic priming reflect distinct processes. Furthermore, centro-parietal electrodes revealed early N400 and late P600 SMEs of episodic encoding, which were not affected by associative or semantic relations. This supports the idea that SMEs reflect trial-to-trial variations in attention. In sum, these findings suggest that the effects of successful vs. unsuccessful episodic encoding are distinct from long-term memory-driven effects in successful encoding.

Declarations and Publication Note

Details on funding, data availability, and study-specific data collection sites are provided in Appendix F (Administrative Information). Following the submission and defense of this dissertation, Study B was published in the following peer-reviewed journal article. The present chapter largely reproduces the published version, with minor editorial and formatting adjustments and modifications to the presentation of the statistical results:

Klein, C., & Hofmann, M. J. (2026). ERP correlates of associative priming and subsequent memory effects: Evidence from sentence-embedded paired-associate learning. *International Journal of Psychophysiology, 228,* Article 113458. https://doi.org/10.1016/j.ijpsycho.2026.113458

5. Study C: The Impact of Associative and Semantic Long-Term Knowledge on Hippocampal Subfield Processing

Abstract

This study investigated how associative and semantic long-term relations influence episodic encoding processes within hippocampal subfields during paired-associate learning. Corpus-derived co-occurrence statistics were used to orthogonally manipulate the direct association (strong vs. none) and semantic feature overlap (high vs. low) between word pairs (cf. Hofmann et al., 2018). Two fMRI experiments were conducted: a 3T pilot study and a 7T main study. In both, participants learned word pairs during scanning and subsequently completed a cued recall test. Behavioral results showed that both strong direct associations and high semantic feature overlap improved recall success, whereas response times were only facilitated by direct associations. Neuroimaging results showed that pairs without a pre-existing associative relation elicited greater activation in the left dentate gyrus (DG), indicating a heightened demand for conjunctive encoding in response to novelty. Meanwhile, high semantic feature overlap elicited increased CA3 activation, in line with feature-based completion processes. The activation patterns observed in CA1 and the subiculum (SUB) were consistent with proposals that these regions support comparator/output-interface functions linking hippocampal encoding to cortical long-term representations. Finally, complementary exploratory cortical depth-resolved ROI analyses in regions associated with semantic control indicated condition-dependent recruitment, but no evidence for depth-specific modulation. Together, these findings suggest that pre-existing associative and semantic relations modulate hippocampal encoding in a subfield-sensitive manner, offering a mechanistic account of how episodic traces interact with associative-semantic long-term knowledge. This aligns with animal attractor models of hippocampal function (Rolls & Treves, 2024) and convergent work on hippocampal pattern separation/completion (Yassa & Stark, 2011).

Keywords: association, episodic encoding, hippocampal subfields, language modeling, paired-associate learning, semantics

5.1 Introduction

The human brain has an enormous capacity to acquire knowledge from long-term experience. To approximate this accumulated experience in a measurable form, computational approaches from artificial intelligence and natural language processing can be used to derive long-term associative relations between words (Hofmann et al., 2018). Typically, large text corpora are used to approximate aspects of human experience by calculating the co-occurrence of words in natural language. These co-occurrence statistics serve as a proxy for the content of consolidated long-term memory, which is modeled using probabilistic algorithms. Direct word associations can be computed using the logarithmic probability that two words co-occur in the sentences of a large text corpus more frequently than would be expected based on their individual frequencies (Dunning, 1993; Hofmann et al., 2011). The resulting log-transformed χ^2 value has been shown to reliably account for approximately 40% of the variance in mean-rated word associations (Hofmann et al., 2018). This makes it a useful measure for defining the long-term association strength between words. If two words do not co-occur significantly more often than by chance, their association strength is set to zero, and they are considered “not associated”. Semantic feature overlap, in turn, can be quantified by counting the number of common associates between two words.

This methodological distinction has proven valuable for disentangling associative from semantic priming effects. For instance, Rölke et al. (2018) showed that associative priming occurs at both short (200 ms) and long (1,000 ms) stimulus-onset asynchronies (SOAs), whereas semantic priming was restricted to short SOAs. Notably, they found no interaction between associative and semantic priming. The effects were found to be strictly additive, indicating that both types of priming rely on different underlying mechanisms, although both are based on co-occurrence principles. This additivity may result from the distinct temporal dynamics with which associative and semantic information are processed within the brain, with associative relations being retrieved more flexibly across varying task demands. This is consistent with accounts of spreading activation (Collins & Loftus, 1975), which assume that activation preferentially propagates along already established links, such that direct associations lead to comparatively faster and stronger activation spread than indirect relations.

Nevertheless, indirect relations can still support performance because the two concepts converge on shared semantic features. This shifts processing toward feature-based integration when associative activation spread is reduced. Accordingly, word processing facilitated by both direct association and semantic feature overlap should result in reduced error rates and faster response times during cued recall.

The Complementary Learning System (CLS) framework (Marr, 1970; McClelland et al., 1995) provides a compelling theoretical account of how rapid episodic encoding and stable semantic knowledge formation are organized by distinct but interacting neural systems. In this framework, neural network models instantiate two components: a fast-learning, highly plastic system typically attributed to the hippocampus, which is capable of one-shot learning but prone to rapid decay; and a slow-learning, robust system, reflecting the neocortex, that integrates across multiple episodes to form stable semantic representations. Within the hippocampus, subfield specialization supports this neural separation, and recent research highlights the importance of functional differentiation along the longitudinal (anterior/posterior) axis. Poppenk et al. (2013) proposed that the anterior hippocampus is biased toward global representations and pattern completion, whereas the posterior hippocampus supports fine-grained, local representations and pattern separation. Findings by Schapiro et al. (2017) further support the CLS model by combining fMRI with representational similarity analysis. Participants viewed sequences where certain object pairs consistently co-occurred. In the hippocampus, associated objects elicited more distinct neural patterns, indicating episodic separation, whereas cortical regions such as the entorhinal cortex showed greater pattern similarity, reflecting statistical integration. This functional organization may arise from differences in subfield composition and entorhinal grid cell inputs. Dalton et al. (2022) demonstrated distinct patterns of anatomical connectivity along the longitudinal axis using track-density imaging, revealing that specific cortical regions preferentially project to distinct hippocampal segments.

Evidence from high-resolution fMRI data illustrates the specific involvement of hippocampal subfields in different memory processes. In an early study, Eldridge et al. (2005) used event-related fMRI at 3T with manually delineated region of interest (ROIs) for DG, CA2/3, CA1, and SUB to dissociate encoding and retrieval processes in the human

hippocampus. During encoding, participants studied word-picture pairs while maintaining central fixation. Retrieval involved "remember/know" judgments, classifying items as recollected, familiar, or forgotten. DG and CA2/3 activation were significantly greater during encoding of subsequently recollected items compared to forgotten ones, suggesting a key role in forming distinct episodic traces. In contrast, SUB activation peaked during "remember" responses but not for familiarity-based decisions, underscoring its function in contextual reinstatement during retrieval. Building on this, Bakker et al. (2008) employed a repetition lure discrimination task during incidental encoding to probe pattern separation in DG/CA3. Participants viewed a randomized sequence of first presentations, repetitions, and visually similar "lures" of everyday objects while performing an orthogonal indoor/outdoor judgment task designed to suppress intentional memory strategies. Within DG/CA3, BOLD responses to lures were elevated relative to both repetitions and novel items, demonstrating a bias toward orthogonalizing overlapping inputs, a neural signature of pattern separation. In contrast, CA1 and SUB exhibited reduced activity for lures, paralleling their response to repetitions and reflecting pattern completion processes. More recently, Suthana et al. (2011) used ultra-high-field 7T fMRI and cortical unfolding to analyze hippocampal subfields during associative learning. Participants encoded and retrieved unrelated pairs across six blocks, revealing that anterior subfields such as CA2 and CA3 were selectively engaged during encoding, whereas CA1 and the posterior SUB were more active during retrieval. A neural model in which the DG performs pattern separation to reduce memory interference (Aimone et al., 2011; Sahay et al., 2011; Yassa & Stark, 2011), while CA3 implements pattern completion and reactivates complete memory traces via recurrent connectivity is most likely (Grande et al., 2019; Rolls & Treves, 2024).

Neurogenesis in the adult human hippocampus, particularly in the DG, suggests that novel neurons are integrated into existing circuits on a daily basis (Eriksson et al., 1998), although this remains controversial (Snyder, 2019). These new neurons exhibit heightened excitability as well as plasticity and have been proposed to support pattern separation and interference reduction in the dentate gyrus, thereby improving discrimination of overlapping representations during encoding (Aimone et al., 2011; Sahay et al., 2011). Empirical support for this mechanism comes from optogenetic studies in rodents. In the seminal experiment by

Ramirez et al. (2013), rodents were first exposed to a neutral environment (Context A) in which DG neurons were labeled with channelrhodopsin-2 (ChR2). In a separate context (Context B), the same neurons were optogenetically stimulated during fear conditioning. When the rodents were later re-exposed to Context A, which had never been associated with aversive learning, they showed robust freezing behavior, suggesting that a novel, artificial association had formed between the two contexts via shared hippocampal activation. Such findings highlight the role of the DG, not only in binding disparate elements into coherent memory representations but also in enabling the integration of new experiences into existing memory frameworks. As noted by Hainmüller and Bartos (2020), some mature granule cells appear to exhibit stable place fields across different contexts or temporal instances, suggesting an integrative role that complements the discriminative function of younger granule cells (Aimone et al., 2011; Sahay et al., 2011).

This functional duality may allow the hippocampus to both separate and link experiences depending on behavioral demands. High semantic feature overlap should facilitate pattern completion, whereby activation of one item partially reactivates its pair. Yassa and Stark (2011) associate this function primarily with the CA3 subfield, while recurrent collateral connectivity in the hippocampal attractor model (Rolls, 2007; Rolls & Treves, 2024) provides a computational implementation. When applied to the human domain, both perspectives are complementary. Recent research by Lee et al. (2015) refined this model by showing that pattern completion is not a uniform function across CA3, but rather varies along its transverse axis. Distal CA3, which is characterized by stronger recurrent collaterals and denser entorhinal input, shows robust coherence in spatial representations even when confronted with conflicting environmental cues. This stability can be considered a key feature of pattern completion. Proximal CA3, which is closer to the DG and receives less entorhinal input, shows pattern separation by remapping under similar conditions. Therefore, high semantic feature overlap should increase CA3 activation, reflecting holistic memory reconstruction based on overlapping semantic features.

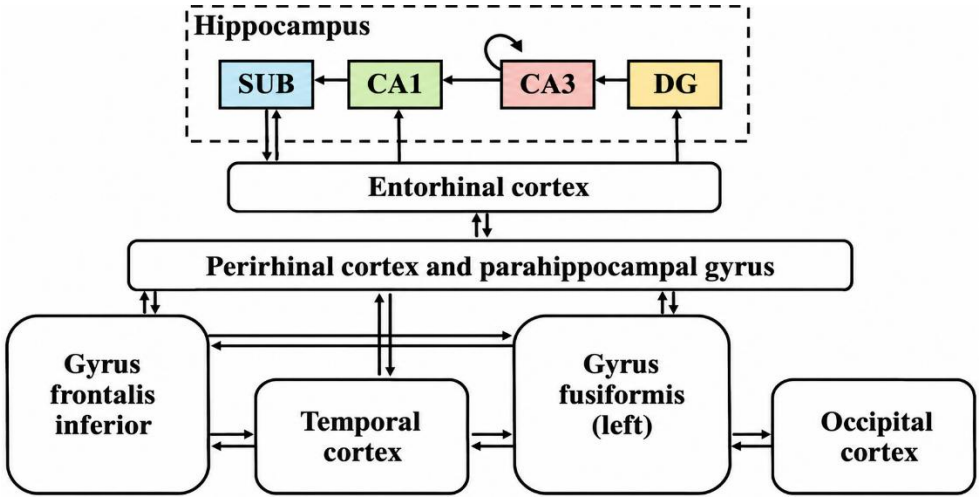
In addition to analyzing hippocampal subfields alone, it seems logical to examine cortical areas that are functionally linked to the hippocampal memory system. Recent meta-analyses emphasize that semantic processing involves a distributed, left-lateralized network

comprising regions such as the inferior frontal gyrus, middle temporal gyrus, and posterior inferior parietal lobe (Binder et al., 2009). In line with this distributed account, an event-related fMRI study by Wible et al. (2006) found that activity in bilateral posterior superior and middle temporal regions was modulated by semantic relatedness during a primed lexical decision task, with stronger priming associated with reduced activation for highly related word pairs. Notably, the left IFG shows heightened activation during tasks requiring controlled semantic retrieval, suggesting a crucial role in modulating hippocampal engagement during memory encoding (Binder et al., 2009). This aligns with findings from Rölke and Hofmann (2020), who investigated the functional connectivity of the left IFG during semantic priming using a full-factorial experimental design that manipulated direct association and broad semantic similarity. Participants completed a lexical decision task on noun-noun word pairs while undergoing fMRI acquisition, and psychophysiological interaction (PPI) analyses were performed with the left IFG as the seed region. Results revealed that under conditions of low semantic similarity, functional connectivity between the left IFG and regions such as the fusiform gyrus, anterior cingulate cortex, orbitofrontal cortex, and critically, the hippocampus, was significantly increased. Direct associations alone did not modulate connectivity patterns. These findings support the idea that semantic processing and memory systems are tightly integrated (Binder et al., 2009) and that the left IFG dynamically coordinates with memory-related structures during semantic conflict resolution. A direct interplay between semantic control mechanisms and hippocampal memory processes during implicit word processing can therefore be assumed.

According to Rolls and Treves (2024), cortical input reaches the hippocampus via a hierarchical pathway. First through the parahippocampal and perirhinal cortices, followed by the entorhinal cortex, the main cortical gateway to hippocampal structures (Eichenbaum et al., 2007; Yonelinas et al., 2024). As demonstrated by Price and Devlin (2011), information flow along this pathway is bidirectional (i.e., full interactivity) as far as the entorhinal cortex, thereby allowing dynamic exchange between cortical and hippocampal representations. The hippocampal system is assumed to have a unidirectional flow of information with top-down excitation mediated via CA1 and the subiculum (Rolls & Treves, 2024; Yassa & Stark, 2011). From there, information typically enters the DG for pattern separation. Figure 19 provides an overview of this cortico-hippocampal input pathway and its directionality.

Figure 19

Functional Pathways Linking Cortex and Hippocampus (Schematic)



Note. Arrows indicate the direction of information flow between regions; double-headed arrows denote bidirectional connectivity. CA1 = cornu ammonis field 1; CA3 = cornu ammonis field 3; DG = dentate gyrus; SUB = subiculum.

Recent ultra-high-resolution imaging studies have provided detailed insights into the laminar organization of the hippocampal/entorhinal circuitry during encoding. Maass et al. (2014) demonstrated that novelty detection primarily activates the superficial layers of the entorhinal cortex and DG/CA3 regions, while successful subsequent memory encoding is predominantly associated with activity in the deep layers of the EC and the pyramidal cell layer of CA1. These laminar-specific activation patterns suggest a functional division between initial sensory integration (superficial layers) and the establishment of durable mnemonic traces (deep layers), providing a precise mechanism for memory consolidation at the microcircuit level. The authors suggested that successful recollection is critically dependent on coordinated activity between deep entorhinal layers and CA1 pyramidal neurons, enabling the translation of pattern-separated hippocampal codes into neocortically accessible memory representations. Complementing these findings, Libby et al. (2012) used resting-state fMRI to examine the intrinsic functional connectivity profiles of the perirhinal cortex (PRC) and parahippocampal cortex (PHC) with hippocampal subfields. In two experiments, they demonstrated that the PRC showed preferential connectivity with the anterior subfields of the hippocampus, whereas the PHC was more strongly connected to the posterior hippocampus. Whole-brain analyses showed that the PRC was functionally linked with anterior temporal and frontal regions, while the PHC

was connected to posterior medial temporal, parietal, and occipital brain regions. These results highlight a functional division along the hippocampal longitudinal axis, suggesting that distinct neocortical inputs are routed through separate hippocampal subfields, thereby supporting different aspects of memory processing. However, shortcut pathways, sometimes referred to as perforant pathways, can bypass the DG and project directly to CA3, facilitating rapid associative matching via pattern completion (Yassa & Stark, 2011). This mechanism supports efficient pattern completion processes that are essential for memory retrieval. Top-down reactivation of distributed cortical memory traces is thought to be mediated by CA1 and the SUB, which function as major output nodes projecting back to neocortical areas (Rolls & Treves, 2024). Taken together, these findings highlight the bidirectional and interactive architecture of episodic and semantic memory systems, emphasizing the complementary roles of feedforward encoding and feedback-driven retrieval processes.

The Present Study

This study aims to deepen the understanding of the interplay between pre-existing associative and semantic long-term knowledge and novel, purely episodic associations during memory encoding, with a particular focus on specific hippocampal subfields. During fMRI acquisition, participants were instructed to learn word pairs presented on each trial of the study phase. In the subsequent test phase, they completed a behavioral cued recall test. Accounting for the independent contributions of associative, semantic, and episodic processes, the experimental conditions were either direct association (strong vs. none) or semantic feature overlap (high vs. low). To enhance spatial resolution of the results within hippocampal subfields, two fMRI studies with identical experimental designs were conducted: a 3T pilot study (Experiment C1), using a dataset originally acquired for the author's master's thesis (Klein, 2018), and a 7T main study (Experiment C2), which comprised additional cortical depth-resolved ROI analyses (layer-inspired; six equidistant depth surfaces sampled across the cortical ribbon). Based on the theoretical framework, the following hypotheses were derived: (i) At the behavioral level, faster response times and lower error rates are expected for word pairs with strong direct association and high semantic feature overlap during cued recall. High

semantic feature overlap may also interfere with memory encoding, as numerous related features have to be filtered before the most relevant semantic unit can be selected. (ii) At the neural level, greater activation in the DG is expected for unrelated word pairs, reflecting the formation of novel episodic conjunctions. CA1/SUB activation is expected to be greater for semantically related but non-associated word pairs, reflecting increased integration demands when semantic feature overlap must be bound without direct associative support. Modulation of CA3 activity by semantic processing demands is further assumed. This effect may be stronger for semantically related yet not directly associated word pairs, as reduced associative activation spread may increase reliance on CA3-mediated pattern completion. (iii) The cortical depth-resolved ROI analyses follow a theory-informed but exploratory approach. For regions implicated in semantic control, greater activity is expected under conditions of reduced cue support and increased semantic processing demands (e.g., non-associated word pairs with low or ambiguous semantic feature overlap). (iv) Regarding cortical depth, novelty-related processing is expected to preferentially engage superficial depth surfaces, whereas strong cue support should be associated with greater activity in deeper depth surfaces.

5.2 Experiment C1 (3T fMRI Pilot Study)

5.2.1 Methods

Participants

The 3T fMRI pilot study included N = 20 participants (9 women), comprising both students and non-students recruited at Freie Universität Berlin, Germany, with a mean age of M = 31.60 years (SD = 10.06, range: 21–58 years). Inclusion criteria were right-handedness, German as a first language, and normal or corrected-to-normal vision. Exclusion criteria were a confirmed diagnosis of dyslexia and an elevated error rate during the test phase (recall success rate < 20% across all experimental conditions). At the trial level, responses with reaction times deviating by more than two *SD*s from the participant's mean were excluded from the analysis (n = 86 trials). Response times were analyzed conditional on correct recall.

Stimuli

A total of 160 German word pairs were presented in a 2 × 2 full-factorial design crossing direct association (strong direct association, SA; no direct association, NA) and semantic feature overlap (high, HS; low, LS). Each of the four resulting experimental conditions (SA-HS, SA-LS, NA-HS and NA-LS) contained 40 stimuli. Table 10 presents example stimuli for each condition. The full stimulus list is provided in Appendix C1 and can also be found in the open science repository (Appendix E).

Table 10
Example Word Pairs by Experimental Condition (Study C)

	Semantic feature overlap:	
	High	Low
Direct Association:		
Strong	*driver → car*	*devil → detail*
No	*frame → scale*	*date → moose*

Direct association and semantic feature overlap were obtained through the computation of log-likelihood tests using a corpus of 43 million sentences from the German language, as part of the Leipzig Wortschatz project (Bordag, 2007; Dunning, 1993; Quasthoff et al., 2006). The text corpus is primarily composed of online newspapers from the period between 1992 and 2006, consisting of 800 million tokens and 43 million sentences. No synonyms were included, and the word candidates with the most pronounced co-occurrence value were consistently selected. The number of letters in each word type ranged from three to eight. All stimuli were presented in a centered, side-by-side format. The font was Times New Roman, with capital letters, and a size of 40. The stimulus material was statistically controlled for word frequency, word length, and orthographic neighbors (Fs(3,156) ≤ 1, ps > .05; see Table 11).

Table 11
Means (SDs) and F Statistics for Controlled Variables (Study C)

	Prime				
	SA-HS	**SA-LS**	**NA-HS**	**NA-LS**	***F* value**
Length	5.38 (1.46)	5.48 (1.47)	5.26 (1.40)	5.58 (1.36)	0.44
Frequency	11.25 (2.06)	11.83 (2.02)	11.43 (1.93)	11.20 (2.31)	0.59
OrthNeigh	1.78 (1.80)	1.60 (1.88)	1.73 (1.84)	1.70 (1.71)	0.07

	Target				
	SA-HS	**SA-LS**	**NA-HS**	**NA-LS**	***F* value**
Length	5.60 (1.50)	5.43 (1.28)	5.85 (1.39)	5.75 (1.37)	0.71
Frequency	10.95 (2.10)	10.58 (2.06)	10.88 (2.23)	11.13 (2.23)	0.45
OrthNeigh	1.80 (1.87)	1.50 (1.52)	1.63 (1.61)	1.93 (1.80)	0.48

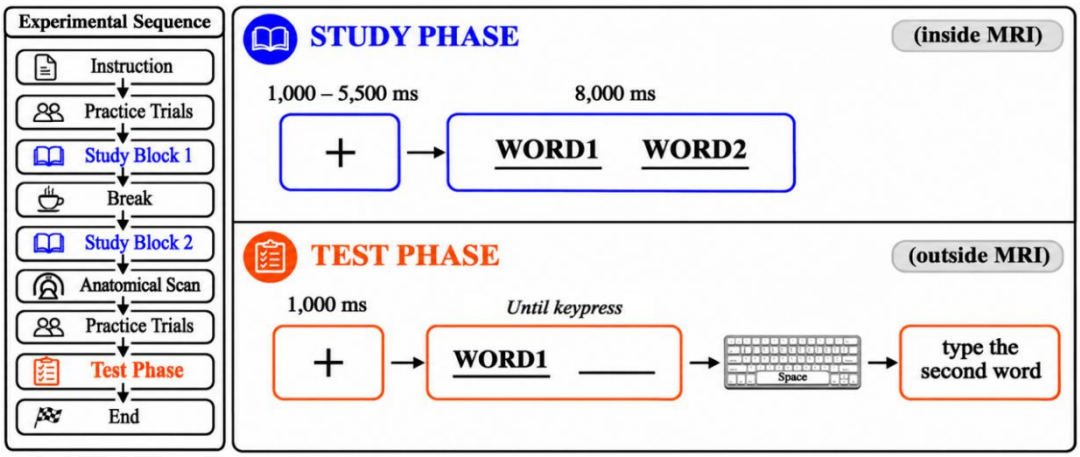
Note. F statistics for the lexical control variables were obtained from separate one-way between-item analyses of variance across the four experimental word pair conditions, $F(3, 156)$. Analyses were conducted separately for primes and targets. Length is reported in letters. HS = high semantic feature overlap; LS = low semantic feature overlap; NA = no direct association; OrthNeigh = number of orthographic neighbors; SA = strong direct association.

Procedure

Participants received standardized instructions indicating that they would be presented with word pairs and should silently form a sentence that contained both words. They were then positioned in the MRI scanner and completed five practice trials before the study phase began. Practice stimuli were neither associatively nor semantically related to the subsequent study stimuli. After 80 trials, participants were given a short break. All participants received the same word pairs in each block, presented in a fully randomized order for each participant. During the study phase, each trial began with a fixation cross presented for a jittered duration of 1,000–5,500 ms to reduce temporal predictability and minimize anticipatory responses, followed by the simultaneous presentation of both words side by side for 8,000 ms. An anatomical scan was then acquired, followed by a test phase outside the MRI scanner. During the test phase, each trial began with a fixation cross presented for a fixed duration of 1,000 ms, followed by the presentation of the first word of each pair on the left side of the screen. The word remained visible until participants pressed the space bar to indicate retrieval of the associated word. Participants were then prompted to type the corresponding second word using the keyboard. The test phase also began with five practice trials. As in the study phase, stimulus pairs were presented in a fully randomized order. Figure 20 illustrates the temporal structure of a trial in both the study and test phases. Stimulus presentation was implemented in Presentation (Version 18.1; Neurobehavioral Systems, 2015) for the study phase and in PsychoPy (Version 1.83.04; Peirce et al., 2019) for the test phase. The task instructions and experimental scripts are available in the open science repository (see Appendix E).

Figure 20

Experimental Sequence and Timing of a Trial: Study/Test Phase (Study C)



MRI data were acquired using a 3T magnetic resonance tomograph (SIEMENS MAGNETOM TrioTim syngo MR B17), at the Center for Cognitive Neuroscience of the Freie Universität Berlin. The resolution of the anatomical scans was 1.0 mm^3, while the resolution of the functional scans was 1.8 mm^3. Anatomical scans were acquired with a repetition time of 1,900 ms, an echo time of 2.52 ms, a flip angle of 9°, and a detector bandwidth of 170 Hz/pixel. Functional runs had a repetition time of 800 ms, an echo time of 30 ms, a flip angle of 60°, and a detector bandwidth of 2,144 Hz/pixel. For the sake of measurement sensitivity, whole-brain coverage was omitted to allow faster interval measurements. Instead, seven slices were acquired diagonally from the parieto-occipital junction to the anterior part of the temporal lobe, covering the hippocampus and surrounding brain areas. The processing of the fMRI data was carried out using the SPM12 plugin of MATLAB (Version 2017b; The MathWorks, 2017). Starting with the slice time correction, the acquisition slices were referenced to the middle slice. The anatomical slices were aligned in ascending order and the functional slices were interleaved (i.e., first the odd and then the even slices). This was followed by an automatic B-spline interpolation for realignment and manual inspection of each participant for gross motion artifacts. Next, co-registration of the functional and anatomical scans was performed. After preprocessing, the onset times and durations were used to specify a 2 × 2 design matrix at the single-subject level. Six realignment parameters (three rotations and three translations along the *x*, *y*, and *z* axes) were included as nuisance regressors. To account for inter-individual variability in response latency, each condition regressor was modeled using the canonical hemodynamic response function augmented with its first temporal derivative (capturing

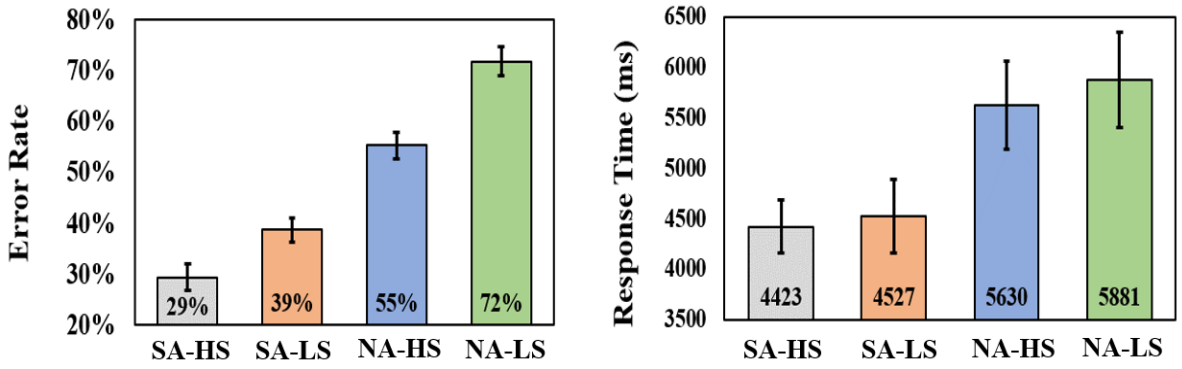
latency/onset shifts), while no dispersion derivative was included. Finally, a general linear model (GLM) was implemented with the stimulation paradigms as essential regressors to estimate condition-specific beta maps. Group-level effects were evaluated using a 2 × 2 rmANOVA on the cluster-averaged β estimates for each regressor. Only correctly recalled trials were analyzed. Statistical inference was family-wise error corrected ($\alpha < .05$), with a minimum cluster extent threshold of $k \geq 20$ voxels.

5.2.2 Results

Behavioral Results

Error rates were computed across all cued recall trials, whereas response times were analyzed only for correctly recalled trials. The descriptive statistics for both error rate and response times per word pair condition of the 3T fMRI pilot study are shown in Figure 21.

Figure 21
Mean Error Rates and Response Times (Study C; Exp. C1)



Note. $N = 20$ participants. Error rate (%) = 100 × incorrect trials/total trials. Response times are based on correctly recalled trials only. Error bars represent 95% within-subject confidence intervals calculated from participant-level condition means using the Cousineau–Morey correction (Cousineau, 2005; Morey, 2008). HS = high semantic feature overlap; LS = low semantic feature overlap; NA = no direct association; SA = strong direct association.

The 2 × 2 rmANOVA on the response time revealed a significant main effect of direct association, $F(1, 19) = 50.58$, $p < .001$, $\eta_p^2 = .73$, but no significant main effect of semantic feature overlap, $F(1, 19) = 0.78$, $p = .388$, nor an interaction between both factors, $F(1, 19) = 0.17$, $p = .685$. The 2 × 2 rmANOVA on the error rate revealed significant main effects for direct association, $F(1, 19) = 904.85$, $p < .001$, $\eta_p^2 = .98$, and semantic feature overlap, $F(1, 19)$

= 85.20, $p < .001$, $\eta_p^2 = .82$, as well as an interaction effect between both factors, $F(1, 19) = 8.62$, $p = .008$, $\eta_p^2 = .31$. To resolve the significant interaction, simple effects of semantic feature overlap were examined separately within each level of direct association using paired-samples *t*-tests, with *p* values Holm-adjusted for the two tests (Holm, 1979). High semantic feature overlap reduced error rates both for word pairs with no direct association, $t(19) = 8.92$, $p_{Holm} < .001$, and for word pairs with strong direct association, $t(19) = 5.64$, $p_{Holm} < .001$. The interaction was further examined by comparing the HS-LS difference scores between these two simple effects, which was significant $t(19) = 2.86$, $p = .010$. Consistent with the descriptive pattern, the error rate reduction from low to high semantic feature overlap was larger for word pairs with no direct association ($\Delta = 17.4$ percentage points) than for word pairs with strong direct association ($\Delta = 9.8$ percentage points).

fMRI Results

Probabilistic cytoarchitectonic mapping (maximum probability maps) implemented in the SPM Anatomy Toolbox 3.0 (Eickhoff et al., 2005) was used to localize the effects at the level of hippocampal subfields. The results revealed that word pairs that were not directly associated elicited greater activation than word pairs with a strong direct association in a region most likely located in the DG of the hippocampus (probability = .80). Furthermore, the presentation of non-associated word pairs resulted in a CA1 effect. The CA3 subfield of the hippocampus was identified as the most probable site of the semantic feature overlap effect, with high semantic feature overlap resulting in greater activation (probability = .86). Finally, a significant interaction was found between direct association and semantic feature overlap, which was most likely located in the DG (localization probability = .60). Pairwise comparisons revealed that, for word pairs without a direct association, high semantic feature overlap elicited greater activation compared to low semantic feature overlap, $t(1420) = 4.17$, $p < .001$. In contrast, for word pairs with a strong direct association, semantic feature overlap had no significant effect on activation, $t(1420) = -0.77$, $p = .440$. This suggests that the DG may also be sensitive to semantic feature overlap for word pairs without a direct association. The

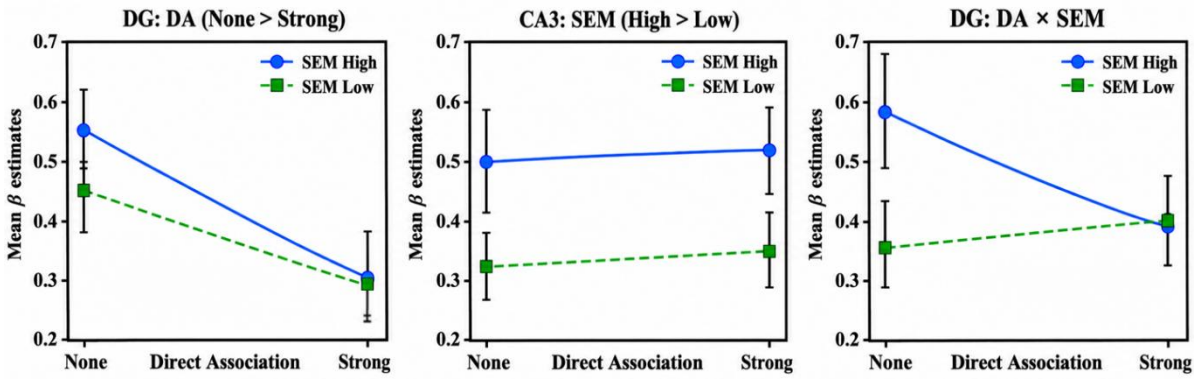
significant fMRI results are summarized in Table 12. The corresponding mean β estimates are provided in Figure 22.

Table 12
Functional Magnetic Resonance Imaging Results (Study C; Exp. C1)

Region (top probabilities)	Cluster Size in Voxels	Hemisphere	MNI Coordinates *x* / *y* / *z*	*F* value
DA (No > Strong):		Left	-44 /-20 /-22	24.52
CA1 (.60)	28			
DG (.80)	38			
SEM (High > Low):		Left	-38 /-7 /-34	16.52
CA3 (.86)	27			
DG (.74)	42			
DA × SEM:		Left	-38 /-31 /-3	11.72
CA1 (.50)	28			
DG (.60)	41			

Note. N = 20 participants. MNI coordinates refer to the peak voxel of each contrast-defined cluster. Results are family-wise error corrected ($\alpha < .05$), with a cluster extent threshold of $k \geq 20$ voxels. Effect localization is based on probabilistic cytoarchitectonic mapping using the SPM Anatomy Toolbox 3.0 (Eickhoff et al., 2005). CA1 = cornu ammonis field 1; CA3 = cornu ammonis field 3; DA = direct association; DG = dentate gyrus; MNI = Montreal Neurological Institute; SEM = semantic feature overlap.

Figure 22
Mean β Estimates from Contrast-Defined Subfield Clusters (Study C; Exp. C1)



Note. N = 20 participants. Points show condition-wise general linear model parameter estimates extracted from the peak voxel of each contrast-defined cluster. Error bars represent ± 1 standard error of the mean across participants. Cytoarchitectonic localization was based on probabilistic maps from the Statistical Parametric Mapping (SPM) Anatomy Toolbox 3.0. Peak-voxel maximum probabilities were .80 for DG (DA), .86 for CA3 (SEM), and .80 for DG (DA × SEM). CA3 = cornu ammonis field 3; DA = direct association; DG = dentate gyrus; SEM = semantic feature overlap.

5.3 Experiment C2 (7T fMRI Main Study)

5.3.1 Introducing Experiment C2

As accurate delineation of hippocampal subfields is crucial for understanding their distinct contributions to memory encoding, the following main study aims to extend and replicate the previous findings by employing ultra-high-field (7T) functional MRI. In contrast to conventional 3T imaging, 7T MRI provides substantially higher spatial resolution and enhanced signal-to-noise ratios, thereby enabling a more refined examination of the fine-grained neural activity within medial temporal lobe structures. These enhancements are particularly valuable in experimental paradigms involving the encoding of multiple stimuli, such as word pairs, where subtle variations in processing depth or associative strategies can elicit distinct activation patterns within the subfields of the hippocampus. Recent methodological advances have demonstrated the feasibility of consistently resolving hippocampal substructures at ultra-high field strengths. For instance, Prudent et al. (2010) demonstrated that 7T MRI, in combination with optimized sequences and advanced head coil techniques, can achieve spatial resolutions down to 100 micrometers in young adults, allowing reliable identification of subfields such as the DG and CA3. While these regions are known to play differential roles in mnemonic computations, they remain difficult to separate functionally at lower field strengths. Using the enhanced spatial specificity of 7T imaging, the main study aims to examine whether hippocampal activation during encoding more robustly predicts subsequent memory performance, thereby offering deeper insights into the neural underpinnings of episodic, associative and semantic memory formation. Furthermore, the use of the identical experiment enables a direct comparison with the prior 3T findings. This allows for an assessment of the added value of ultra-high-field imaging.

5.3.2 Methods

Participants

Data were collected from 31 healthy participants, comprising both students and non-students, recruited at Bergische Universität Wuppertal and Forschungszentrum Jülich,

Germany. Participants who were students received course credit, while the others were compensated with €30. All participants were native German speakers, had normal or corrected-to-normal vision, met the safety requirements for high-field MRI, and reported no history of neurological or psychiatric disorders. The target sample size was determined a priori using GLIMMPSE (Version 3.1.3; Glueck et al., 2025; Kreidler et al., 2013) for a one-group design with four repeated-measures conditions corresponding to the 2 × 2 manipulation of direct association and semantic feature overlap. The calculation targeted the main effects, using $\alpha = .05$, a target power of $1 - \beta = .80$, and the Hotelling–Lawley trace. Expected cell means were derived from Rölke and Hofmann (2020), whose study provided the closest available parameter estimates because it employed the same orthogonal manipulation and an overlapping subset of the prime–target materials. However, the task and outcome measures differed from those of the present study. Given the limited transferability of these estimates, the assumed covariance matrix was scaled by a factor of 1.25 to represent greater within-participant variability, yielding a required sample size of $N = 31$. Five participants were excluded from the data analysis due to an elevated error rate in the cued recall test (recall success rate < 20% across all experimental conditions). Of these five participants, one additionally met the fMRI exclusion criterion for excessive head motion. The mean age of the remaining 26 participants was $M = 24.35$ years ($SD = 6.21$; range: 19–49, 19 women). As exclusions reduced the final sample below the initial target, statistical power may be lower than planned. 7T MRI studies typically provide greater statistical power, and a study employing a comparable methodology involved a comparable sample size (Grande et al., 2019). Thus, the final sample was considered adequate for the planned analyses. Nevertheless, results for smaller effects should be interpreted with caution.

Stimuli and Experimental Procedure

The stimulus material was identical to that used in the 3T fMRI pilot study. Prior to the MRI acquisition, a 7T MR-safety screening was conducted, and informed written consent regarding the specific risks was obtained from all participants. The experimental methods were approved by the local institutional review board (EK 318/19, RWTH Aachen University, Germany). The experimental procedure was basically the same, but the anatomical scan was

performed immediately after positioning in the scanner. In addition, a resting state fMRI scan was performed in which the participants were asked to remain still, awake, with their eyes closed, and without thinking about anything in particular. Moreover, a pneumatic belt was positioned around the participant's chest, and a pulse oximeter was placed on the second, third, or fourth finger of the left hand to measure respiration and cardiac function, to control for potential interference of the physiological signals on the fMRI responses (Glover et al., 2000).

MRI Data Acquisition

MRI data were acquired on a Siemens Magnetom Terra 7 T scanner equipped with a Nova Medical 1-channel transmitter (Tx) and 32-channel receiver (Rx) head coil at Forschungszentrum Jülich. A high-resolution anatomical volume was acquired with an MP2RAGE sequence (repetition time = 4,300 ms; echo time = 2 ms; matrix = 256 × 376 × 400; 0.60 × 0.60 × 0.60 mm^3). Functional MRI data were acquired using a GE-EPIK sequence [50, 56–58, 61, 62] with the following parameters: repetition time = 1,900; echo time = 22 ms; flip angle = 85°; partial Fourier = 5/8; 3-fold in-plane/3-fold inter-plane (multi-band) acceleration; bandwidth = 875 Hz/pixel; αPC/αMain = 9°/90°. A more detailed description of the sequence is available in Yun and Shah (2017, 2020) and Yun et al. (2019, 2022). B0 shimming was performed using the manufacturer's standard protocol. For the fMRI acquisition, the matrix size was 336 × 336 × 72 slices, with a voxel size of 0.63 × 0.63 × 0.63 mm^3. The number of acquired fMRI volumes varied due to the randomized stimulation (range: 452–765 volumes; *M* = 488.4, *Mdn* = 482). Magnitude and phase images were reconstructed for each fMRI scan.

Software and Versions for MRI (Pre-)Processing

Structural and functional MRI (pre-)processing and ROI segmentation were performed using AFNI (Analysis of Functional NeuroImages, Version 23.3.07; Cox, 1996), ANTs (Advanced Normalization Tools, Version 1.0; Klein et al., 2009), FreeSurfer (Version 7.4.1; Fischl, 2012), LayNii (Version 2.5.0; Huber, Poser, et al., 2021), and MATLAB (R2022b; The MathWorks, 2022). Unless stated otherwise, subsequent tool calls refer to these versions.

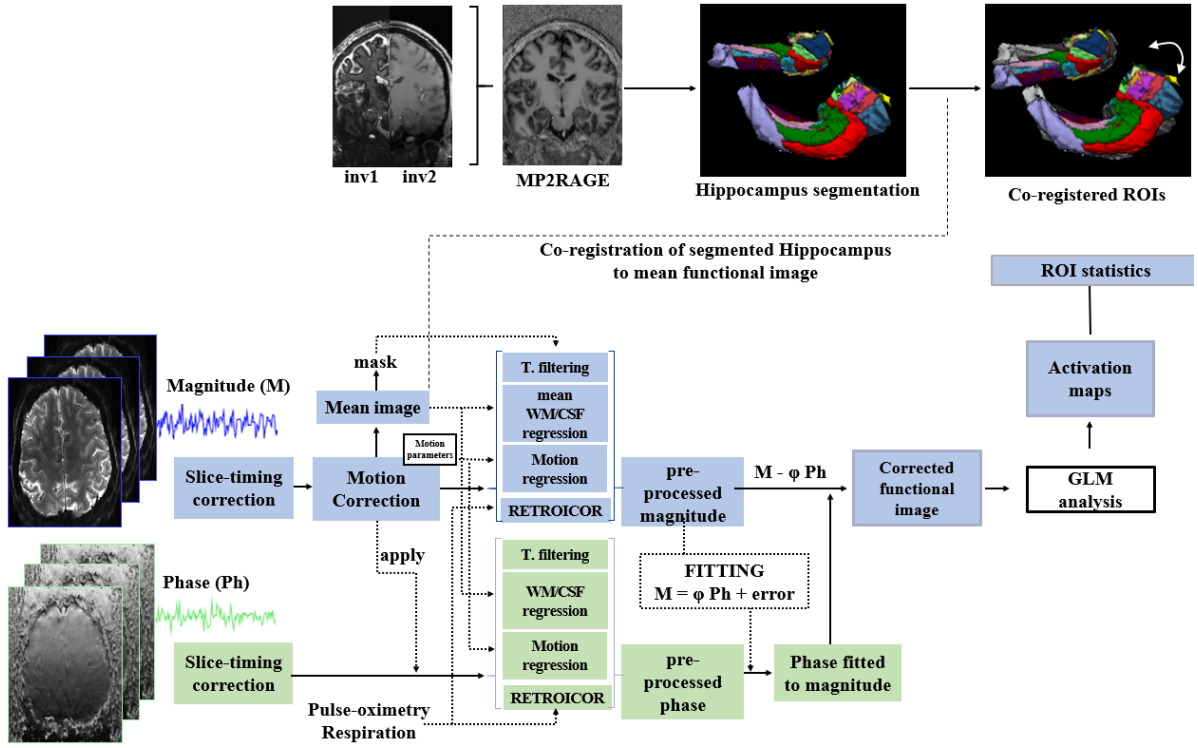
Structural MRI Preprocessing, Segmentation, and ROI Delineation

The two inversion images from the MP2RAGE acquisition and the corresponding uniform T1-weighted image were denoised with `LN_MP2RAGE_DNOISE` (LayNii) to reduce background noise and generate an MPRAGE-like T1-weighted volume. This brain image was then fed into `recon-all` (FreeSurfer), which yielded a brain mask, a series of segmentations and registration files for potential spatial normalizations. To obtain a detailed segmentation of the regions of interest, `segment_HA_T1.sh` (FreeSurfer) was executed after `recon-all` (FreeSurfer). This resulted in 28 ROIs per hemisphere, which covered hippocampal subregions and amygdala nuclei (Appendix C6). From these, the four ROIs relevant to the present study were defined by aggregating head and body for CA1, CA3, DG, and SUB. The segmentation of the hippocampal subfields and the resulting ROI masks are illustrated in Figure 2. While the use of the SPM Anatomy Toolbox 3.0 (Eickhoff et al., 2005) was straightforward in the 3T pilot study for volume-based probabilistic cytoarchitectonic localization (maximum probability maps), the main study used a novel 7T sequence (Yun et al., 2019, 2022) with superior spatial resolution that enabled subject-specific surface reconstruction and sampling of functional effects across the cortical ribbon. As the Julich Brain Atlas (Amunts et al., 2020) does not provide a surface-based parcellation that resolves cortical depth, the Destrieux Atlas (Destrieux et al., 2010) was used as a surface-based macroanatomical labeling scheme (gyral/sulcal labels) to define cortical ROIs consistently across participants and to facilitate anatomical assignment of depth-sampled effects. The analyses presented in the results section included cortical depth (six depth surfaces) as an additional factor. However, since no main or interaction effects of cortical depth were observed, this factor was omitted to enhance readability. Automatic co-registration of structural and functional images was performed using ANTs, and visual quality control indicated good alignment for all participants (see Appendix C5). When necessary, hippocampal co-registration was enhanced with FreeView's manual co-registration tool by applying rigid-body transformations. To reduce co-registration errors, the ROIs were eroded by two voxels using `3dmask_tool` (AFNI).

fMRI Preprocessing and First-Level GLM Analysis for Hippocampal Data

The analysis pipeline of the functional MRI data is summarized in Figure 23.

Figure 23
7T fMRI Preprocessing and Analysis Pipeline (Study C; Exp. C2)



Note. GLM = general linear model; inv1/inv2 = first and second inversion images; MP2RAGE = magnetization-prepared 2 rapid acquisition gradient echoes; RETROICOR = retrospective correction of physiological noise using cardiac and respiratory traces; ROI(s) = region(s) of interest; T. Filtering = temporal band-pass filtering; WM/CSF regression = regression of white matter and cerebrospinal fluid nuisance signals.

The magnitude and phase images reconstructed from each fMRI scan were subjected to a series of preprocessing steps and combined to generate a clean magnitude fMRI image. First, both sets of images were slice-timing corrected using the SPM 12 plugin of MATLAB. To correct for motion, the magnitude images (which carry anatomical information) were initially realigned to the first volume using `3dvolreg` (AFNI). The resulting matrix was then applied to the phase images using `3dAllineate` (AFNI). The fMRI data from one participant were excluded from the analysis due to head displacement of 90 mm accumulated over the functional scan (500 TRs / 950 s). The total head displacement was calculated as shown in Figure 24.

Figure 24

Total Head Displacement Calculation (Study C; Exp. C2)

$$\sqrt{\left(diff(M_{r1})\right)^2 + \left(diff(M_{r2})\right)^2 + \left(diff(M_{r3})\right)^2 + \left(diff(M_{t1})\right)^2 + \left(diff(M_{t2})\right)^2 + \left(diff(M_{t3})\right)^2}$$

Note. Rotational parameters (Mr1..3, in degrees) and translational parameters (Mt1..3, in mm) were obtained from the realignment step. diff(·) denotes the frame-to-frame difference between consecutive volumes. Rotations were converted to millimeters using an arc-length approximation ($\Delta s \approx r \cdot \Delta\theta$, with $\Delta\theta$ expressed in radians) assuming a head radius of r = 60 mm. The displacement time course was padded with zero for the first volume to match scan length.

Magnitude and phase images were then subjected to a regression step to remove the influence of motion, respiration/cardiac function, and partial volume effects. The mean of the realigned magnitude image was obtained using `3dTstat` (AFNI) and used to segment the brain into cerebrospinal fluid (CSF), gray matter (GM), and white matter (WM) tissue, with fast in FSL (FMRIB Software Library, Oxford, UK). The mean time course of the CSF and the WM was extracted from the generated masks in magnitude and phase images using `3dmaskave` (AFNI). This was then used as a regressor of no interest. In parallel, when available, the pulse and respiration traces obtained during the scan session were synchronized with the fMRI data and utilized to generate 36 physiological regressors (a combination of sine and cosine Fourier series). In 7 of the 31 participants, the physiological traces could not be included in the preprocessing pipeline due to the presence of noise or errors in the recorded data. These issues were typically the result of incorrect positioning of the pulse oximeter or movement of the participant's fingers during the scan. Moreover, a band-pass filter was applied to all voxel time courses, to preserve only the frequencies between 0.005 and 0.12 Hz (presumably reflecting neuronal signals recorded with fMRI; Pais-Roldán et al., 2022; Yuen et al., 2019). After individual preprocessing of the magnitude and the phase images, the phase time courses were fitted using `3dTfitter` (AFNI) and subsequently subtracted from the magnitude time courses using `3dcalc` (AFNI). This was done to correct for bias related to ascending veins or those running over the pial surface, which can carry BOLD signal downstream from the activation site. It is assumed that the signal in the magnitude time course that can be explained by its phase component is related to field inhomogeneities, which are likely to result from venous interference (Curtis et al., 2014; Menon, 2002; Pais-Roldán et al., 2022). The resulting images were considered to be clean after the steps above. Afterwards, the clean fMRI images were

baseline-normalized to a mean of 100 and then subjected to a GLM analysis using `3dDeconvolve` (AFNI). Four stimulation vectors were provided ("SA+HS", "SA+LS", "NA+HS" and "NA+LS"). The resulting beta maps, together with the segmented hippocampus, were then used as input data for `mri_segstats` (FreeSurfer), which computed mean β estimates for each ROI separately for each participant and hemisphere.

fMRI Preprocessing and First-Level GLM Analysis for Cortical Depth-Resolved ROI Analyses

A high-resolution MP2RAGE structural image was used to identify and segment the cortical ribbon and to derive depth-resolved sampling across cortical thickness. Following the execution of FreeSurfer's `recon-all`, the white matter and pial surfaces were obtained. Thereafter, six equidistant depth sampling surfaces (1–6) were created, spanning the cortical ribbon from the white matter/gray matter boundary (0% depth) to the pial surface (gray-matter/cerebrospinal fluid boundary; 100% depth). This was achieved by employing `mris_smooth` and `mris_expand` in FreeSurfer. For each participant, the mean functional image was overlaid with the cortical ribbon to visually inspect anatomical-functional alignment. Voxels showing clear misregistration were excluded using a participant-specific exclusion mask. First-level modeling was performed using `3dDeconvolve` (AFNI), with the same condition regressors (SA+HS, SA+LS, NA+HS, NA+LS) as in the hippocampal ROI analysis. The resulting beta maps were then projected (sampled) onto each depth surface with `mri_vol2surf` (FreeSurfer). The six cortical depth surfaces were aggregated into three depth bins: 1. superficial (surfaces 5–6; closest to pial), 2. middle (surfaces 3–4), and 3. deep (surfaces 1–2; closest to WM). Depth-resolved values were summarized within nine cortical regions per hemisphere defined by the Destrieux atlas (FreeSurfer aparc.a2009s; Destrieux et al., 2010), which was read in Matlab using `read_annotation`. The following regions were included in the cortical depth-resolved ROI analyses: 1. inferior frontal gyrus (IFG); 2. middle temporal gyrus (MTG); 3. posterior cingulate cortex (PCC); 4. occipito-temporal gyrus (OTG); 5. superior temporal gyrus (STG); 6. temporal pole (TP); 7. superior temporal sulcus (STS); 8. entorhinal cortex (EC); 9. perirhinal cortex (PRC). Mean β estimates per ROI and depth bin were then computed for each participant and hemisphere using `mri_segstats` (FreeSurfer).

Statistical Inference (ROI Analyses)

For all ROI analyses, β estimates were derived from correctly recalled trials only, to index successful encoding. The mean and range of trial numbers per condition in the final analyses were as follows: *M* = 29, range 15–39 (SA-HS); *M* = 26, range 15–36 (SA-LS); *M* = 20, range 8–35 (NA-HS); *M* = 13, range 2–29 (NA-LS). Group-level effects were tested on mean β estimates (*z*-standardized within participants to ensure comparability across ROIs) using linear mixed-effects models (LMM) implemented in JMP® (Version 19.0.3; JMP Statistical Discovery LLC, 2025) with Kenward–Roger-approximated denominator degrees of freedom (Kenward & Roger, 1997). Hippocampal subfield effects were evaluated using an LMM with direct association (strong vs. none), semantic feature overlap (high vs. low), hemisphere (left vs. right), and subfield (DG, CA1, CA3, SUB) as fixed effects, and random intercepts for participant and subfield within participant to account for repeated measures across subfields. Hypothesis-driven effects were evaluated via planned, subfield-specific simple-effect contrasts. Exploratory cortical effects were examined in a single LMM, with ROI and hemisphere included as fixed effects (and their interactions with direct association and semantic feature overlap). The model additionally included cortical depth bin (deep, middle, superficial) and all depth-related interaction terms. To test whether cortical depth improved model fit, a full and a reduced model (with vs. without depth terms) were compared using model selection criteria. Follow-up simple-effects tests were only conducted to resolve significant planned contrasts in the hippocampal analysis or for significant interactions with the experimental factors in the exploratory cortical depth-resolved analyses. The Holm procedure was used to correct the *p* values for family-wise error across each ROI-specific family of follow-up contrasts. Model assumptions were assessed using standard residual diagnostics (Q–Q plots and residuals-versus-fitted plots). Following the identification of deviations from residual normality, β estimates were screened for outliers to reduce potential scaling or ROI-extraction artifacts. Estimates deviating from the ROI-specific median by more than 2.5 scaled median absolute deviations (scaling factor = 1.4826) were excluded. The LMMs were subsequently re-estimated. The number of excluded observations per ROI is provided in Appendices C7 and C9. The main text highlights significant results relevant to the hypotheses, whereas complete model outputs are provided in Appendices C8 and C10.

Analysis of Behavioral Data

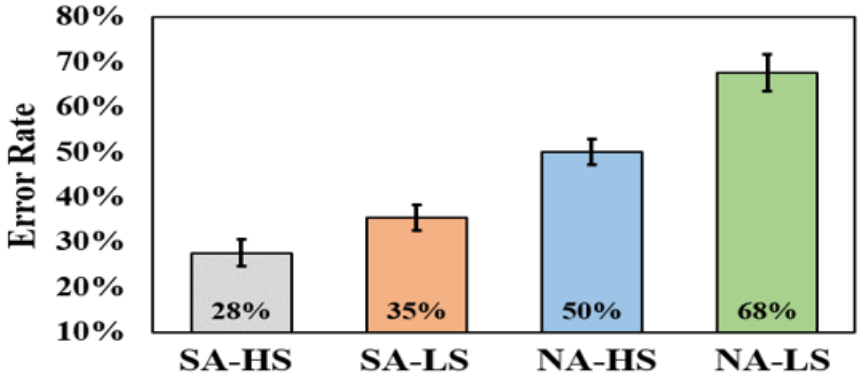
Statistical analyses were conducted in JMP® (Version 19.0.3; JMP Statistical Discovery LLC, 2025). To ensure comparability across studies, the behavioral analyses followed the same analysis pipeline as in Study B. For trial-level recall success (1 = correct, 0 = incorrect), a generalized linear mixed-effects model (GLMM; binomial distribution with logit link) was fitted. For natural-log-transformed response times (RTs), restricted to correctly recalled trials, a Gaussian linear mixed-effects model (LMM) was fitted. The log-transformation was used to reduce positive skewness and improve adherence to the distributional assumptions of the model. In both models, the fixed-effects structure included direct association (DA; strong vs. none), semantic feature overlap (SEM; high vs. low), and their interaction term. To account for the crossed structure of the data, random intercepts were specified for subjects and items. For the Gaussian LMM, model assumptions were evaluated using Q–Q plots, residual-versus-fitted plots, and an Anderson-Darling test of residual normality (see Appendix C2). As the diagnostics indicated deviations from residual normality, the model was re-estimated after excluding trials whose residuals deviated from the participant-specific median by more than 2.5 scaled median absolute deviations (scaling factor = 1.4826). This criterion excluded 142 of the 2,271 correctly recalled trials (6.25%). Statistical inference was based on $\alpha = .05$. Fixed effects were evaluated using Type III Wald *F*-tests with Kenward–Roger-approximated denominator degrees of freedom (Kenward & Roger, 1997). Full test tables are reported in Appendix C3 (GLMM) and Appendix C4 (LMM). Parameter estimates are supplemented by coefficient-level *t*/*z* tests in the respective tables. Estimates are reported using effect coding (direct association: none = -1, strong = +1; semantic feature overlap: low = -1, high = +1), with the intercept representing the equally weighted mean across conditions on the model scale and the coefficients reflecting the corresponding effects. For the Gaussian LMM, model fit is summarized using R^2_m and R^2_c. For the GLMM, model fit is reported using the Akaike information criterion (AIC), Bayesian information criterion (BIC; both based on the residual -2 log pseudo-likelihood), and Nakagawa's R^2_m / R^2_c on the latent logit scale (Nakagawa et al., 2017). Overdispersion was assessed using the generalized χ^2/df statistic.

5.3.3 Results

Behavioral Results

The binomial GLMM on trial-level recall success revealed a significant main effect of DA, $F(1, 138) = 52.65$, $p < .001$, indicating that word pairs with a strong direct association led to higher recall success compared to those with no direct association. Further, a significant main effect of SEM was observed, $F(1, 136) = 11.81$, $p < .001$, suggesting that word pairs with high semantic feature overlap improved recall success compared to those with low semantic feature overlap. There was no interaction between both factors, $F(1, 136) = 1.16$, $p = .283$. The generalized χ^2 was 3,594 (df = 4,160), indicating no evidence of overdispersion ($\phi = 0.86$). Information criteria for the fitted model were AIC = 19,795, BIC = 19,833, Nakagawa's R^2_m = .114 and R^2_c = .483. Figure 25 shows the mean error rates for each experimental condition. Table 13 reports the coefficient-level parameter estimates (logit b), SEs, Wald z-test scores, odds ratios (ORs) with 95% confidence intervals (CIs), as well as the random-intercept variance components for the fitted model.

Figure 25
Mean Error Rates (Study C; Exp. C2)



Note. N = 26 participants. Error rate (%) = 100 × incorrect trials/total trials. Error bars represent 95% within-subject confidence intervals calculated from participant-level condition means using the Cousineau–Morey correction (Cousineau, 2005; Morey, 2008). HS = high semantic feature overlap; LS = low semantic feature overlap; NA = no direct association; SA = strong direct association.

Pairwise comparisons of the DA × SEM estimated marginal means (EMMs) indicated that the SEM effect was significant when DA was absent (OR [high vs. low] = 2.56, 95% CI [1.43, 4.59], p = .002), but not significant when DA was strong (OR [high vs. low] = 1.65, 95% CI [0.91, 2.96], p = .096). This pattern should be interpreted with caution, as the DA × SEM

interaction term in the GLMM was not significant, indicating insufficient evidence that the SEM effect differs reliably between DA levels.

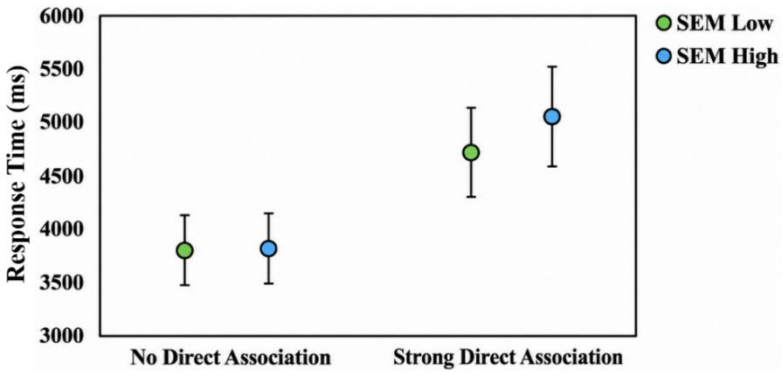
Table 13
GLMM Estimates for Trial-Level Recall Success (Study C; Exp. C2)

Random effects	**σ²**	***SE*(σ²)**			
Subject intercept	0.854	0.255			
Item intercept	1.495	0.212			
Fixed effects	***b* (logit)**	***SE***	***z* value**	***p***	**OR [95% CI]**
(Intercept)	0.277	0.209	1.33	.185	1.32 [0.86, 2.02]
DA	0.762	0.105	7.26	< .001	1.14 [1.74, 2.64]
SEM	0.360	0.105	3.44	< .001	1.43 [1.17, 1.76]
DA × SEM	-0.111	0.105	-1.06	.291	0.90 [0.73, 1.10]

Note. Binomial generalized linear mixed-effects model (GLMM) with logit link, including random intercepts for participants and items (N = 26 participants; k = 160 items; n = 4,160 trials). Fixed-effect coefficients are reported on the log-odds scale using effect coding (-1/+1). DA = direct association (-1 = none; +1 = strong); SEM = semantic feature overlap (-1 = low; +1 = high). Odds ratios (OR) represent exponentiated fixed-effect estimates; 95% confidence intervals (CI) are Wald intervals. p values are based on two-sided Wald z tests.

The Gaussian LMM on the natural-log-transformed RTs (only correct trials) revealed a significant main effect of DA, $F(1, 154) = 53.48$, $p < .001$, suggesting faster response times for word pairs with a strong direct association compared to those with no direct association. No significant main effect was observed for SEM, $F(1, 153) = 0.84$, $p = .361$, nor an interaction between both factors, $F(1, 153) = 1.12$, $p = .292$. Model fit was $R^2_m = .052$ and $R^2_c = .341$. Figure 26 shows the model-estimated response times across experimental conditions.

Figure 26
Model-Based Estimates of Response Times (Study C; Exp. C2)



Note. N = 26 participants. Response times (RTs) are presented as back-transformed estimated marginal means (geometric means) from the Gaussian linear mixed-effects model fitted to natural-log-transformed RTs for correctly recalled trials. Error bars represent 95% confidence intervals. SEM = Semantic feature overlap.

Table 14 reports the coefficient-level parameter estimates (b), *SE*s, 95% CIs, Kenward–Roger *t*-test scores, and random-intercept variance components for the fitted model.

Table 14
LMM Estimates for Trial-Level Response Times (Study C; Exp. C2)

Random effects	**σ^2**	***SE*(σ^2)**				
Subject intercept	0.018	0.006				
Item intercept	0.026	0.004				
Residual	0.125	0.004				
Fixed effects	***b***	***SE***	**[95% CI]**	***df***	***t* value**	***p* value**
(Intercept)	8.339	0.031	[8.28, 8.40]	39	269.96	< .001
DA	-0.115	0.016	[-0.15, -0.08]	154	-7.31	< .001
SEM	-0.014	0.016	[-0.05, 0.02]	153	-0.92	.360
DA × SEM	0.017	0.016	[-0.01, 0.05]	153	1.06	.292

Note. Gaussian linear mixed-effects model (LMM) fitted to natural-log-transformed response times for correctly recalled trials, including random intercepts for participants and items (N = 26 participants; k = 160 items; n = 2,129 trials). Fixed-effect coefficients are reported on the natural-log scale using effect coding (-1/+1). DA = direct association (-1 = none; +1 = strong); SEM = semantic feature overlap (-1 = low; +1 = high). Confidence intervals (CI) are 95% Wald intervals. p values are based on two-sided t tests with Kenward–Roger denominator degrees of freedom.

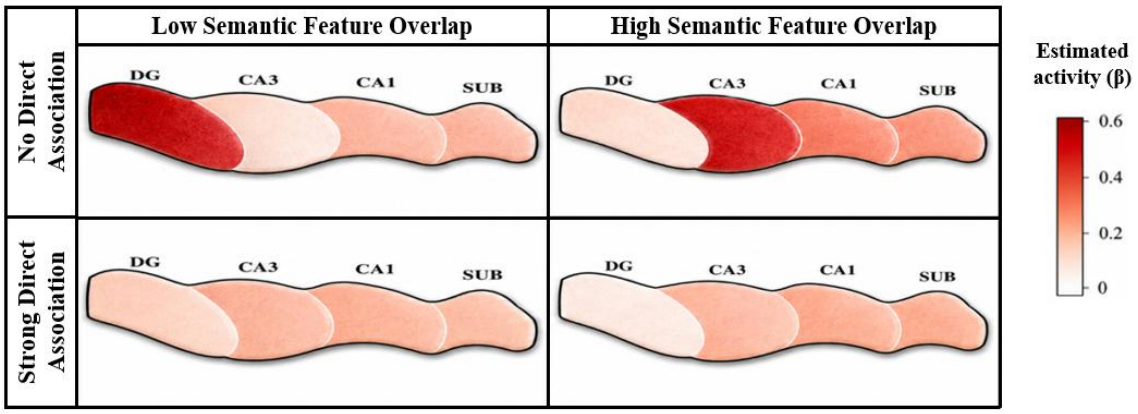
fMRI Results for the Hippocampal Subfield Analysis

Hippocampal subfield activity was analyzed using an LMM including DA (strong vs. none), SEM (high vs. low), hemisphere (left vs. right), and subfield (DG, CA1, CA3, SUB) as fixed effects, with random intercepts for participant and subfield within participant. Type III Wald F-tests did not reveal significant main effects or interactions involving the experimental factors (all ps > .05; full model output is provided in Appendix C8). Model fit was R^2_m = .042 and R^2_c = .105. In line with the a priori hypotheses, subfield-specific contrasts of averaged EMMs were conducted with effects reported as differences in estimated marginal means (Δ_{EMM}). To test the novelty-related episodic binding hypothesis, activity for unrelated word pairs (no direct association and low semantic feature overlap) was compared with the averaged DG activity across all remaining conditions that provided at least one source of associative or semantic cue support. This contrast indicated greater DG activity for unrelated word pairs (Δ_{EMM} = 0.24, SE = 0.11, t(660) = 2.18, p_{Holm} = .028). In exploratory simple-effect tests, the DA contrast remained significant under low SEM (Δ_{EMM} = 0.20, SE = 0.10, t(658) = 2.00, p_{Holm} = .041), but not under high SEM (Δ_{EMM} = 0.04, SE = 0.10, t(656) = 0.40, p_{Holm} = .691). To

assess whether semantic processing demands modulate CA3 activity as a function of associative cue support, the SEM effect was compared between DA levels (DA × SEM contrast within CA3). This planned comparison was significant ($\Delta_{contrast}$ = 0.25, *SE* = 0.11, *t*(647) = 2.27, p_{Holm} = .024). Follow-up simple effects indicated a significant SEM effect when DA was absent (Δ_{EMM} = 0.30, *SE* = 0.13, *t*(651) = 2.31, p_{Holm} = .021) whereas the SEM effect was not significant when DA was strong (Δ_{EMM} = 0.05, *SE* = 0.13, *t(645)* = 0.38, p_{Holm} = .704). To test the semantic integration account, activity was compared between high and low SEM under conditions without DA. The planned SEM contrast within CA1 was not significant (Δ_{EMM} = 0.12, *SE* = 0.11, *t*(652) = 1.09, p_{Holm} = .276). The analogous comparison within the SUB showed a small descriptive trend in the expected direction, but this effect was also not significant (Δ_{EMM} = 0.13, *SE* = 0.10, *t*(666) = 1.30, p_{Holm} = .194). Figure 27 illustrates the model-estimated activity of hippocampal subfields across experimental conditions.

Figure 27

Model-Based Estimates of Hippocampal Subfield Activity (Study C; Exp. C2)



Note. *N* = 26 participants. Two-dimensional unfolded hippocampal flatmaps display estimated marginal means averaged across hemispheres for each combination of direct association (none vs. strong) and semantic feature overlap (low vs. high). Color intensity represents estimated activity (β), with warmer colors indicating higher values. CA1 = cornu ammonis field 1; CA3 = cornu ammonis field 3; DG = dentate gyrus; SUB = subiculum.

fMRI Results for the Cortical Depth-Resolved ROI Analysis

An LMM was fitted to the cell-averaged β estimates to assess the effects of DA (strong vs. none) and SEM (high vs. low), as well as their interaction, with cortical ROI (nine regions) as a fixed factor. Hemisphere (left vs. right) was also included to account for lateralization but was not specified as a moderator of DA or SEM. The model included random intercepts for the

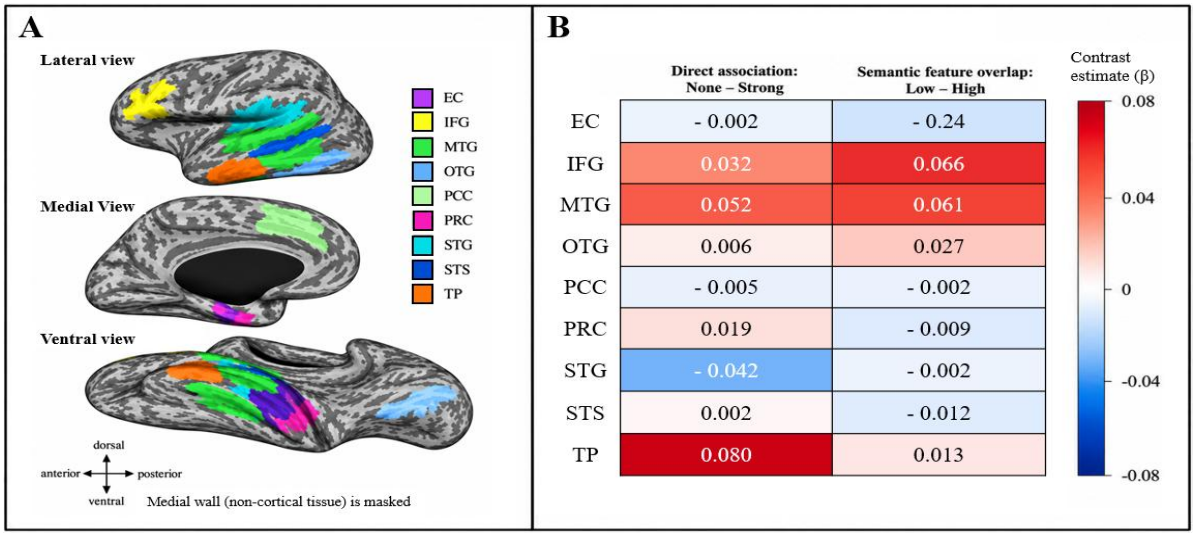
participant and for the ROI within participant combination. To assess whether cortical depth (deep vs. middle vs. superficial) provided incremental explanatory value, a full model including depth and all depth-related interaction terms was compared against a reduced model excluding all depth terms while retaining the corresponding non-depth predictors. Model comparison was performed under maximum likelihood estimation. Information criteria favored the reduced model (AICc = -5070, BIC = -4763) over the full model (AICc = -5026, BIC = -4562; ΔAICc = 44.15, ΔBIC = 200.38), providing no support for cortical depth (see Appendix C12). Cortical depth was therefore omitted and inference is reported for the reduced model.

Significant main effects were observed for DA, SEM, ROI, and hemisphere (DA: $F(1, 5131) = 14.93$, $p < .001$; SEM: $F(1, 5131) = 10.15$, $p = .002$; ROI: $F(8, 5131) = 26.71$, $p < .001$; hemisphere: $F(1, 5131) = 24.76$, $p < .001$). As expected, the effects of DA and SEM varied by ROI, reflected in significant DA × ROI and SEM × ROI interactions (DA × ROI: $F(8, 5131) = 7.71$, $p < .001$; SEM × ROI: $F(8, 5131) = 6.86$, $p < .001$). However, the DA × SEM interaction was not significant ($F(1, 5131) = 0.03$, $p = .868$), and there was no evidence for a DA × SEM × ROI interaction ($F(8, 5131) = 1.54$, $p = .139$). Hemisphere differences also varied by ROI (ROI × hemisphere: $F(8, 5131) = 8.44$, $p < .001$), but as hemisphere served only as a control factor to account for lateralization, follow-up contrasts for DA and SEM were computed from EMMs averaged across hemisphere and the other experimental factor. To resolve the DA × ROI interaction, ROI-specific EMM contrasts were tested for DA (none - strong). Significant DA effects were observed in IFG, MTG, STG, and TP (ps $\leq .008$). The effects were positive in the IFG, MTG, and TP (none > strong) and negative in the STG (strong > none): IFG, $t(5134) = 2.66$, $p = .008$; MTG, $t(5134) = 4.31$, $p < .001$; STG, $t(5134) = -3.48$, $p = .001$; TP, $t(5134) = 5.69$, $p < .001$. No DA effects were observed in the EC, OTG, PCC, PRC, or STS (ps $\geq .126$). To resolve the SEM × ROI interaction, ROI-specific EMM contrasts were tested for SEM (low - high). Significant SEM effects were observed in the MTG and the IFG (both low > high): MTG, $t(5130) = 5.46$, $p < .001$; and IFG, $t(5130) = 4.95$, $p < .001$. SEM contrasts in the EC and OTG did not survive Holm correction and no SEM effects were observed in the PCC, PRC, STG, STS, or TP (ps $\geq .313$). Model fit for the reduced model was $R^2_m = .077$ and $R^2_c = .121$. The full set of contrast statistics is provided in Appendix C11. Figure

28 illustrates the anatomical distribution of the nine cortical ROIs and their corresponding model-based contrasts across the two experimental factors.

Figure 28

Cortical ROI Localization and Corresponding Activity Contrasts (Study C; Exp. C2)



Note. (A) Anatomical localization of the nine ROIs on an inflated cortical surface of the left hemisphere. (B) ROI-wise estimated marginal mean contrasts from the reduced linear mixed-effects model (N = 26), averaged across hemispheres and levels of the other experimental factor. Values show contrast estimates (β), with red indicating positive differences, blue indicating negative differences, and color reflecting their magnitude. EC = entorhinal cortex; IFG = inferior frontal gyrus; MTG = middle temporal gyrus; OTG = occipitotemporal gyrus; PCC = posterior cingulate cortex; PRC = perirhinal cortex; ROI = region of interest; STG = superior temporal gyrus; STS = superior temporal sulcus; TP = temporal pole.

5.4 Discussion

The present study investigated how episodic encoding and associative-semantic long-term relations contribute to successful memory formation. Analyses were conducted at the behavioral level, within hippocampal subfields and associated neocortical regions. The results addressed hypotheses (i–v) as follows: (i) The behavioral data of Experiments C1 and C2 both demonstrated that strong effects on error rates can be predicted from associative and semantic long-term knowledge. Word pairs with a strong direct association were recalled more successfully than those without such relations. Word pairs with high semantic feature overlap further improved recall success, especially when direct association was absent. However, response times exhibited a more selective pattern. Word pairs with a strong direct association yielded faster responses than those with no direct association, whereas semantic feature overlap did not affect response speed in the cued recall test. This pattern suggests that associative

relations facilitate faster access to the target representation, consistent with the spreading-activation account (Collins & Loftus, 1975), whereas semantic feature overlap primarily supports recall success without measurably accelerating retrieval in the present paradigm. Thus, given the selective response time pattern, the co-occurrence-based approach used to distinguish between direct associations and semantic feature overlap in lexical processing (Rölke et al., 2018; Rölke & Hofmann, 2020) can only be partially transferred to the present paired-associate learning paradigm. As the response time analyses were restricted to target words that were subsequently recalled correctly, encoding-related priming processes were already completed by the time of recall. Therefore, response times do not offer direct insights into the cognitive effort involved in word processing. The observed differences are most likely due to the characteristics of the experimental paradigm itself. Further, the finding that only associative relations affected recall success, whereas semantic relations did not, suggests that associative processing may involve temporally extended patterns of neural activation. Semantic feature overlap may be more sensitive to short temporal windows and thus less likely to be effectively captured in a cued recall paradigm such as the one used in this study.

(ii) At the neural level, the high-resolution fMRI data suggested a clearer dissociation within the hippocampal subfields. Novel, non-associated word pairs led to increased DG activation, which is consistent with the superior role of the DG in pattern separation and the formation of new conjunctive units (Aimone et al., 2011; Leutgeb et al., 2007; Sahay et al., 2011; Yassa & Stark, 2011). In line with this novelty-related account, DG activity was greater for unrelated word pairs relative to conditions providing associative or semantic cue support. By contrast, CA3 activity increased with semantic feature overlap, particularly when no direct association was present, consistent with autoassociative (attractor-like) matching and pattern completion dynamics that operate on overlapping feature conjunctions (Bakker et al., 2008; Rolls & Treves, 2024; Yassa & Stark, 2011). Besides DG and CA3 recruitment, the effects observed in CA1/SUB were less robust and did not provide clear evidence of semantic integration processes, particularly in CA1. However, SUB showed some descriptive sensitivity to semantic feature overlap when direct association was absent. This pattern is broadly compatible with the hierarchical flow of information in the hippocampus, with CA1 acting as a comparator between cortical input and CA3/SUB output serving as a major output node that

relays consolidated representations to neocortical areas (Vinogradova, 2001). Further, recent anatomical evidence suggests the presence of non-canonical, reciprocal projections from SUB back to CA1, involving both excitatory and inhibitory elements (Amaral & Lavenex, 2007). These back-projections suggest a more dynamic and modulatory interaction within the hippocampal circuit, potentially supporting integrative processes necessary for processing associative information that fits existing schemas, as well as the transmission of such information to cortical regions involved in semantic memory. Word pairs with high semantic feature overlap showed increased CA3 activation, particularly in the absence of a direct association. This likely reflects representational interference between semantic units, which places greater computational demands on CA3 processes that arbitrate between pattern separation and completion. Although omnibus tests from the full subfield model did not reveal significant main effects or interactions, planned subfield-specific comparisons provided evidence that the SEM effect in CA3 depended on associative cue support. Semantic feature overlap increased CA3 activity when direct association was absent, whereas the SEM effect was not reliable when direct association was strong. This suggests that word pairs with a strong direct association may engage mnemonic retrieval processes that bias CA3 toward autoassociative pattern completion (Norman & O'Reilly, 2003; Yassa & Stark, 2011). In line with this, Kumaran and McClelland (2012) used a computational model called REMERGE to show that recurrent collaterals in CA3 amplify common features across overlapping inputs to support autoassociative pattern completion, thereby resolving competition. This mechanism enables CA3 to dynamically balance the trade-off between pattern separation and completion depending on task demands. These findings are consistent with the seminal rodent electrophysiology study by Leutgeb et al. (2007), which showed that CA3 neuronal ensembles develop distinct population codes in response to overlapping but behaviorally relevant input patterns, suggesting that recurrent collaterals may be the key to disambiguating similar memory traces. This dynamic modulation indicates that the hippocampal circuit can flexibly shift between integrating and discriminating memory representations, thereby minimizing interference while preserving generalisation when new information overlaps with existing knowledge (Yassa & Stark, 2011).

(iii) In addition to the hippocampal analysis, the engagement of cortical structures

associated with semantic processing and control was observed during the encoding of non-associated or low semantic feature overlap word pairs. The TP was selectively sensitive to associative relatedness, with greater activation when direct associations were absent and there was no robust modulation by semantic feature overlap. By contrast, IFG and MTG responses increased both when associations were absent and when semantic feature overlap was low, consistent with heightened demands on controlled semantic access and selection during encoding when long-term knowledge provides less facilitation. This aligns with meta-analytic accounts of controlled semantic retrieval (Binder et al., 2009) and with PPI evidence that the IFG dynamically interacts with hippocampal structures during semantic conflict resolution (Rölke & Hofmann, 2020). In a large-scale meta-analysis of 121 fMRI studies on semantic control, Jackson (2021) demonstrated the involvement of a semantic control network, comprising the IFG, posterior MTG, inferior temporal gyrus and the dorsomedial prefrontal cortex. These regions were consistently activated in studies requiring the retrieval or selection of semantic information under high control demands, such as resolving ambiguity, inhibiting dominant but irrelevant meanings and retrieving weak associations. This pattern is consistent with the present findings, suggesting that increased engagement of the IFG and MTG during the encoding of word pairs with no direct association and low semantic feature overlap may reflect increased demands on controlled semantic access and selection, thereby guiding memory encoding via controlled access to long-term conceptual representations. Frank and Willems (2017) provided converging evidence by showing that both word predictability and semantic similarity modulate language processing via distinct neural pathways. Using a combination of EEG and fMRI, the authors demonstrated that, although both dimensions elicited similar N400 effects, they were spatially distinct at the cortical level. Predictability was primarily linked to activity in the left inferior temporal sulcus and posterior fusiform gyrus (often referred to as the visual word form area), whereas semantic similarity recruited cortical regions associated with the broader semantic control network, such as the left TP or MTG. Although predictability was not manipulated in the present design, this dissociation provides a useful conceptual framework. Low semantic feature overlap was associated with increased engagement of temporal semantic processing regions, particularly the MTG, which may reflect more effortful feature-based retrieval and integration. Moreover, the STG showed higher

activation for strong directly associated (vs. non-associated) word pairs, consistent with more automatic integration when associative cues are available. This aligns with prior work implicating the STG in effortless integration of familiar associations (Preston & Eichenbaum, 2013; Suthana et al., 2011). Thus, the present results support partially dissociable contributions of associative relatedness and semantic feature overlap to encoding-related cortical engagement. The findings align with the CLS framework, which posits that rapid, hippocampally mediated episodic encoding coexists with slower, neocortically mediated semantic integration (McClelland et al., 1995). Within this model, the DG/CA3 circuitry balances pattern separation and completion. The DG orthogonalizes novel input, while CA3 supports reactivation of existing semantic templates. Results from both experiments show that semantic feature overlap can both facilitate (via CA3 completion) and challenge (via DG separation) episodic encoding, depending on the associative context. The bidirectional pathway through EC and PRC to hippocampal subfields (Rolls & Treves, 2024) does not seem to play a significant role during the time interval of encoding but may support the dynamic interplay between cortical semantic control and hippocampal episodic processes at later stages.

(iv) Although the 7T acquisition enabled depth-resolved analyses of cortical ROIs, model comparison provided no evidence that cortical depth improved model fit, and no reliable depth effects were observed. This null finding suggests that associative and semantic encoding did not differentially engage cortical depth surfaces in a way detectable with the protocol used. Prior work has shown layer-dependent activity during memory processing (Finn et al., 2019; Lawrence et al., 2018), but several factors may explain the absence of effects here. For example, the total partial volume, signal-to-noise ratio variability between different slices, and residual motion or physiological noise could obscure the depth-dependent signals (Polimeni et al., 2010). Moreover, the cognitive demands of the paired-associate task may have favored distributed network-level engagement over depth-specific effects. Finally, transient depth-dependent dynamics may not be adequately captured by the BOLD signal at the temporal resolution of the present acquisition.

Ultra-high-field fMRI provides unparalleled access to detailed neural representations, particularly within hippocampal subfields. However, achieving this level of precision requires methodological compromises that must be considered. One of the most significant challenges

is striking a balance between spatial resolution, whole-brain coverage, and acquisition time. Although high-resolution 7T protocols such as EPIK, which were used in Experiment C2, can resolve submillimeter anatomical features, they often require extended scan durations or a reduced field of view, which can limit the capture of distributed neural activity. Recent advances in MRI hardware and pulse sequence design are beginning to overcome these limitations. For instance, Feinberg et al. (2023) demonstrated that a next-generation 7T scanner employing parallel transmission and optimized multi-echo echo-planar imaging can achieve an isotropic resolution of 0.56 mm across the whole brain. This suggests that high-resolution and broad coverage are not fundamentally incompatible. In Experiment C2, these technological advances were considered strategically, with resolution prioritized over global coverage and a focused field of view targeting hippocampal subfields. This approach enabled high spatial specificity in a region of theoretical interest while maintaining acceptable scan efficiency. Gains in spatial detail are often accompanied by increased sensitivity to signal distortions. At higher field strengths, susceptibility artifacts, particularly in the medial temporal regions, can degrade signal quality. Physiological noise sources, such as cardiac and respiratory fluctuations, also contribute disproportionately to the BOLD signal. These effects can be particularly problematic in the anterior hippocampus. To address this, the acquisition protocol emphasized physiological monitoring and advanced reconstruction. For instance, Vu et al. (2017) demonstrated that combining multi-echo acquisitions with dynamic correction for physiological cycles can significantly enhance the signal-to-noise ratio of hippocampal voxels. Therefore, Experiment C2 implemented comparable measures, such as slice-specific field mapping and the collection of physiological regressors. These measures effectively mitigated noise-related distortions and improved signal fidelity in hippocampal subfields. Beyond these technical limitations, the challenge of achieving generalizability through a sufficient sample size remains. Ultra-high-field imaging is often accompanied by strict exclusion criteria, and the significant resources required to conduct the research limit the number of participants, raising concerns about statistical power and replicability. Although the sample size was consistent with standard practices in high-resolution imaging, the modest size of the sample may lead to skepticism about its reliability. However, evidence from recent large-scale 7T studies supports the reliability of subcortical measures even in small samples. For example,

Groot et al. (2024) analyzed resting-state data from 56 healthy adults acquired at 7T with 1.5 mm isotropic resolution and physiological noise correction. They demonstrated highly reproducible connectivity patterns in deep brain structures including the hippocampus. Similarly, Kreitz et al. (2023) used high-resolution 7T fMRI (0.9 mm^3 voxels) to track memory consolidation following a motor sequence task in 18 participants. They observed robust subfield-specific activity during the offline replay phase. Importantly, convergent patterns were observed across both experiments (C1 and C2), with the 7T data offering improved spatial precision. This convergence across imaging modalities suggests that the observed effects likely reflect stable cognitive-neural mechanisms, rather than being artifacts of sampling constraints or scanner-specific resolution. Although the limitations of ultra-high-field imaging cannot be entirely eliminated, the current methodological approach, based on design optimization and recent empirical validation, substantially mitigates their potential impact.

The present findings offer novel insights into both applied and theoretical domains. In practical terms, processes involving semantic binding in the hippocampus appear well suited for use in cognitive training or rehabilitation. For instance, associative learning tasks that pair novel stimuli with existing semantic anchors may enhance the efficiency with which information is encoded. This might be particularly true for clinical populations with memory impairments. Subtle deficits in semantic memory, for example, are often overlooked in patients with traumatic brain injury (TBI), as emphasized by McCurdy and Duff (2025). In their study, participants with moderate TBI and matched controls completed a series of narrative and semantic fluency tasks, alongside a word association paradigm designed to assess relational integration in long-term memory. Although overall cognitive performance remained intact, the TBI group experienced specific difficulty in retrieving and linking semantically related concepts. This indicates a disruption to the hippocampus-mediated binding mechanisms. Such findings suggest that targeting hippocampal subfield differentiation using structured semantic-associative paradigms could lead to more precise diagnostics and enable interventions aimed at restoring encoding processes. Another differentiation approach provided by Poppenk and Moscovitch (2011) could also motivate future research in this context. They demonstrated that the size of posterior versus anterior hippocampal segments predicts memory differences between healthy young adults. In their study, the hippocampus was segmented relative to the

uncal apex, dividing it into anterior and posterior segments. Recollection performance was then assessed using standardized episodic memory tasks. The results showed that better memory was associated with proportionally larger posterior segments and smaller anterior segments, while total hippocampal volume did not predict memory performance. Further work should therefore examine how individual variability in posterior hippocampal structures relates to the balance of pattern separation and completion during memory encoding. Furthermore, detailed mapping of hippocampal dynamics shows promise for neuromodulatory interventions. Techniques such as transcranial alternating current stimulation, when aligned with theta-gamma oscillatory cycles, may enhance associative binding by synchronizing with underlying hippocampal rhythms. These approaches align with broader initiatives to develop personalized cognitive training protocols that incorporate structural and functional specificity, particularly for aging or neurologically vulnerable populations. From a theoretical perspective, the present findings contribute to a more nuanced understanding of hippocampal function, for example, within the CLS framework. In this model, the hippocampus rapidly encodes novel associations, while the neocortex gradually extracts generalized knowledge. The subfield-specific activation patterns observed during semantic encoding extend the scope of CLS beyond episodic memory, highlighting its significance in structured semantic integration. Recent computational research supports this view. Sun et al. (2023), for instance, introduced a refined CLS model that integrates cortical replay with hippocampal subfield dynamics, demonstrating how CA1/CA3 interactions enable flexible generalization across overlapping semantic domains. The differentiation of hippocampal subfields according to the depth and novelty of associations is consistent with such frameworks. Rather than reflecting incidental involvement, the contributions of the hippocampus to semantic memory appear to reflect a core organizational mechanism involved in the integration and restructuring of episodic, associative and semantic knowledge. Rolls and Treves (2024) proposed a hierarchical hippocampal model in which cortical inputs reach the DG to support pattern separation, then proceed to CA3 for pattern completion, and finally propagate via CA1 and SUB back to the neocortex. The present results are broadly consistent with key aspects of this sequence. Specifically, the DG supports the formation of novel conjunctions, CA3 contributes to both associative and semantic processing, and CA1/SUB activity patterns align with a role in integrating hippocampal representations.

5.5 Conclusion

This study used a paired-associate paradigm combining behavioral measures with 3T and 7T fMRI data to provide a systematic examination of pure associative and semantic priming during memory encoding. The results show that long-term associative and semantic memory traces play a significant role in shaping episodic encoding processes in the human hippocampus. Strong direct associations and high semantic feature overlap both improved recall success, demonstrating the practical value of utilizing existing memory networks for learning. Response time was exclusively facilitated by direct association, indicating that associative relations are superior for accessing memory once the encoding process has been completed. At a neural level, enhanced DG activation for non-associated word pairs suggests that the DG plays a crucial role in forming novel episodic conjunctions in the absence of pre-existing links. CA3 showed enhanced activation for semantically overlapping but non-associated word pairs, highlighting its role in autoassociative (attractor-like) pattern completion driven by semantic similarity. These findings are consistent with the hippocampal attractor model in rodents proposed by Rolls (2007), whereby cortical inputs traverse the DG for pattern separation and engage the CA3 region for pattern completion, before being broadcast to the neocortex via the CA1/SUB region. The cortical depth-resolved ROI analyses revealed that hippocampal engagement is embedded within a broader network of semantic regions showing similar activation patterns. This indicates the existence of a coordinated interplay between hippocampal subfields and cortical regions during associative and semantic priming. In sum, this study advances theoretical accounts of hippocampal function. It provides evidence that associative and semantic relations interact to optimize memory encoding and emphasizes the importance of considering long-term semantic structure and episodic novelty in human memory models.

Declarations

Details on funding, data availability, study-specific data collection sites, ethics approval, and preregistration are provided in Appendix F (Administrative Information).

6. General Discussion

6.1 Summary of the Key Findings

This doctoral thesis examined how pre-existing long-term knowledge, operationalized through direct association and semantic feature overlap derived from word co-occurrence statistics, interacts with episodic encoding. It introduces a hybrid methodological paradigm that embeds two dissociable priming manipulations within a paired-associate learning framework, thereby linking transient pre-activation effects to the formation of durable cue-target bindings. Using evidence from behavioral, electrophysiological, and neuroimaging data, the present work pursued three aims: (Study A) to determine whether lexical relations modulate memory encoding through shared or distinct mechanisms within a specific temporal window; (Study B) to examine the sensitivity of ERP markers (LPC; SMEs) to these encoding dynamics; and (Study C) to delineate how hippocampal subfield activation represents associative and semantic effects differently during the formation of episodic memory traces.

In Study A (behavioral), participants encoded target words embedded in sentence contexts during paired-associate learning. Later, cued recall success and response times were assessed. Three factors were orthogonally manipulated: direct association (strong vs. none), semantic feature overlap (high vs. low), and SOA (300 ms vs. 1,450 ms). Strong direct association between prime and target led to a robust recall benefit, consistent with cue-driven spreading activation accounts (Collins & Loftus, 1975) that facilitate access to the target representation. Semantic feature overlap also enhanced recall success, albeit to a smaller extent. This was likely because feature-based activation promotes broader co-activation (Hutchison, 2003; McNamara, 2005) and can recruit competing target representations that first must be excluded (Nairne, 2002; Watkins, 1976). In line with this, response times were faster for word pairs with a strong direct association, while semantic feature overlap showed no corresponding effect. Varying the SOA between prime and target had no effect on the recall performance, suggesting that the facilitatory influences of associative-semantic relations do not depend on the temporal dynamics manipulated here. The findings indicate that associative relations provide a privileged retrieval route that reduces search demands in delayed cued recall, whereas semantic feature overlap supports encoding in a more context-dependent manner.

In Study B, the experimental paradigm was replicated, but this time with a fixed SOA between the prime and the target words. The manipulation of direct association and semantic feature overlap was maintained, and EEG was recorded for ERP analysis focusing on the occipito-parietal LPC (460–800 ms) and centro-parietal SMEs (correctly vs. falsely recalled trials) within the N400 (250–500 ms) and P600 (500–800 ms) latency ranges. While the behavioral results roughly resembled those of Study A, the neurophysiological data were of particular interest here. Target words that had a strong direct association with the preceding prime elicited a more positive LPC amplitude compared to those that were unrelated. However, semantic feature overlap showed no modulation of the LPC amplitude. SMEs, observed in some studies as a semantic-linked modulation in the N400 time window (Höltje et al., 2019) or as a later positive deflection overlapping the LPC (Rugg & Curran, 2007), predicted trial-by-trial memory success but did not interact with the associative or semantic manipulations. This double dissociation suggests that effects of direct association engage an encoding pathway whose temporal and topographical characteristics are similar to recollection-related parietal activity (LPC). By contrast, the SMEs likely reflect partially orthogonal processes (e.g., attentional engagement, item-level elaboration, or processing depth; Mecklinger & Kamp, 2023; Paller & Wagner, 2002), which predict later memory performance independently of the priming condition. These findings align with prior ERP studies showing separable parietal and frontal SMEs and the conditions under which each SME emerges (Kamp et al., 2017).

In Study C, a high-resolution 7T fMRI study was conducted to investigate the specific contributions of hippocampal subfields (DG, CA3, CA1, and SUB) using the same factorial manipulations. The experimental procedure once again employed a paired-associate learning task. However, in contrast to the preceding studies, the two words were presented in isolation rather than within the context of a sentence. This enabled the spatial evaluation of associative and semantic encoding effects independent of syntactic or contextual influences. The behavioral results were largely similar to those observed in the previous studies: strong direct associations led to the greatest improvements in recall success. High semantic feature overlap also enhanced recall performance, particularly in the absence of associative relations. Further, response time facilitation was observed for words with strong direct association, suggesting that direct associations can accelerate access to stored information once encoding has taken

place, provided there is not too much interference. At the neural level, non-associated word pairs elicited greater activation in the DG than did strongly associated pairs. This aligns with the assumption that the DG supports the formation of novel conjunctive traces, likely via pattern separation (Aimone et al., 2011; Bakker et al., 2008; Sahay et al., 2011). Conversely, CA3 exhibited selectively greater activation for word pairs with high semantic feature overlap, consistent with the assumption that this subfield contributes to associative binding via pattern completion (Grande et al., 2019; Yassa & Stark, 2011). Cortical depth-resolved ROI analyses further revealed that hippocampal subfield engagement is embedded within a broader semantic-control network (Binder et al., 2009; Jackson, 2021; Preston & Eichenbaum, 2013), where increased activation in the IFG and MTG was evident under high-demand conditions (e.g., when words lacked direct associations), and strongly associated words preferentially recruited the PCC and STG, consistent with the idea of effortless integration of familiar associations.

6.2 Integrative Synthesis and Limitations

This subchapter integrates the experimental strands of the doctoral thesis into a coherent account of how pre-existing associative and semantic knowledge shapes the formation of lasting memory traces and how they interact with rapid episodic encoding. Each study served as a complementary methodological anchor to demonstrate how (a) direct association and semantic feature overlap differentially bias the encoding process, (b) these influences manifest in temporally precise electrophysiological correlates and subfield-specific BOLD profiles, and (c) their convergence delineates a multilevel, CLS-consistent framework of memory formation that provides a foundation for subsequent computational and empirical follow-up research. Study A provided behavioral evidence that corpus-derived direct association and semantic feature overlap can reliably bias the success of subsequent cued recall regardless of a specific SOA and that priming effects are not just limited to lexical decision tasks. This finding was further explored in Study B, which investigated the temporal dynamics of encoding to show that strong direct associations and successful memory encoding map onto LPC/SME dynamics, which covary with later recall. Study C further provided anatomical resolution at the hippocampal subfield level to offer a comprehensive picture and showed differential

recruitment of CA3 activity depending on semantic feature overlap as much as DG activity driven by novelty demands, which reflects pure episodic encoding. It is important to note that the different empirical levels examined in this thesis should not be considered in isolation, as conclusions about the underlying mechanism must be drawn from convergent rather than method-specific evidence. The use of a multilevel experimental design structure, comprising behavioral, EEG, and fMRI approaches, therefore enabled the separation and characterization of associative and semantic influences on encoding across complementary levels of analysis, as well as the evaluation of contemporary mechanistic accounts (e.g., CLS; Norman & O'Reilly, 2003; hippocampal attractor models; Rolls, 2007). In light of these guiding principles, the results show that the behavioral effects closely correspond to the electrophysiological correlates, and both converge with the subfield-specific fMRI findings. The data suggest that direct association and semantic feature overlap are not simply two aspects of the same facilitation process but rather involve partly distinct mechanisms. Associative relations tend to evoke recollection-like, cue-specific facilitation that speeds up retrieval, whereas semantic feature overlap supports integrative, category-level enhancement that minimizes encoding interference in novel situations. These observations align the present findings with the CLS framework's logic (Norman & O'Reilly, 2003; O'Reilly et al., 2014), whereby rapid hippocampal binding (supporting item-specific recall) operates alongside slower, distributed cortical representations that embody semantic structure. The central integrative claim, which links the results across different methodological levels, is that successful paired-associate learning arises from the dynamic neural interplay between the following: (i) pre-activated associative networks (cue-driven spreading activation of related target representations) that modulate hippocampal autoassociative pattern-completion dynamics reflected in enhanced CA3 activity and parietal LPC response consistent with recollection-like cortical reinstatement during encoding, while novel episodic input elicits DG-mediated pattern separation processes; (ii) semantic feature overlap driven facilitation, which recruits distributed neocortical semantic circuits together with CA3/CA1; and (iii) trial-by-trial encoding depth, as indicated by SMEs.

In Study A strong associative relations enhanced recall success beyond simple lexical processing advantages, which is consistent with the idea that associative long-term knowledge facilitates cue-dependent binding by lowering the retrieval threshold for related target

representations (Collins & Loftus, 1975; Nelson et al., 2004). Semantic feature overlap also yielded a modest recall benefit, consistent with the idea that broader semantic relatedness facilitates memory integration processes during encoding (Hutchison, 2003). The effect was not moderated by direct association, but exploratory contrasts suggested that the SEM benefit may be more pronounced when direct association was strong. This is compatible with schema-based facilitation models in which semantic congruency can support memory integration, albeit in a less cue-specific way than direct associative relations (Gilboa & Marlatte, 2017; Höltje et al., 2019; Van Kesteren et al., 2012). The selective response time benefits observed for directly associated word pairs suggest that target access is facilitated due to established associative pathways (Collins & Loftus, 1975; Hutchison, 2003), whereas semantic effects may be attenuated by broader co-activation and feature-based competition, leading to less target-specific support at test (Neely, 1977; Plaut & Booth, 2000). The absence of interactive effects between associative-semantic facilitation and SOA challenges the assumption that there is an optimal timing for presenting words during encoding to support the learning process. Instead, the results indicate that the associative and semantic influences on successful memory formation operate partially overlapping and context-dependent. Rather than reflecting a rigid phase of optimal integration, associative and semantic priming processes may flexibly bias hippocampal-cortical processing toward retrieval- or encoding-like states depending on stimulus configuration.

Study B examined the corresponding temporal dynamics of associative-semantic priming and determined whether successful memory formation is facilitated by preceding or concurrent processes associated with encoding depth. The lack of semantic effects, which was attributed to interference when multiple representations are activated simultaneously within overlapping neural populations (cf. Hutchison, 2007; Plaut & Booth, 2000), supports the idea that associative and semantic influences on word processing are logically and functionally separable (Rölke et al., 2018; Rölke & Hofmann, 2020). The co-occurrence of enhanced parietal LPC amplitudes, associated with recollection-like reinstatement processes (Rugg & Curran, 2007), for associatively related items and robust priming-independent SMEs, associated with attentional allocation (Paller & Wagner, 2002; Polich, 2007), indicates that associative facilitation and encoding depth act in parallel rather than sequentially. The temporal

overlap suggests that the effects of direct association lower the encoding threshold via early cortical reinstatement (Staresina et al., 2012), thereby enabling the hippocampus to bind reactivated representations into durable episodic traces (Davachi, 2006; Eichenbaum, 2017). Thus, a dynamic view of encoding, in which retrieval-like and encoding-like neural states coexist and jointly determine the likelihood of later recall, is most likely.

Providing the anatomical counterpart to the behavioral and electrophysiological findings, Study C mapped the effects of direct association, semantic feature overlap, and purely episodic encoding onto the hippocampal trisynaptic loop (DG → CA3 → CA1; Lee, GoodSmith, et al., 2020). This transferred mechanisms from the hippocampal attractor model (Rolls, 2007; Rolls & Treves, 2024) to the human domain, grounding this translation in the anatomical-empirical bridge described in translational reviews of pattern separation and pattern completion (Yassa & Stark, 2011). Consistent with these predictions, the DG responded most strongly to conditions requiring the formation of novel conjunctive traces, supporting its role in pattern separation and the orthogonalization of overlapping inputs (Aimone et al., 2011; Bakker et al., 2008; Leutgeb et al., 2007; Yassa & Stark, 2011). In turn, CA3 activity increased with semantic feature overlap, reflecting attractor-based (autoassociative) matching and pattern completion dynamics that leverage pre-existing knowledge (Grande et al., 2019; Lee et al., 2015; Rolls & Treves, 2024; Yassa & Stark, 2011). This spatial partitioning links directly to the earlier findings, as CA3-biased completion provides a mechanistic basis for the LPC and behavioral facilitation observed for associatively primed items, whereas DG-mediated separation preserves representational fidelity for novel input, mirroring the temporal overlap between reinstatement and encoding-depth processes identified in Study B. By contrast, CA1/SUB exhibited greater activation during trials requiring integrative encoding for both non-associated and highly associated word pairs, consistent with their proposed role as a comparator, mediating the convergence and transfer of information from hippocampal subfields to the neocortex (Duncan et al., 2012; Schlichting & Preston, 2015; Vinogradova, 2001). This suggests that CA1/SUB integration mechanisms are engaged whenever disparate or already-linked representations must be reconciled into a coherent memory trace, thereby providing a neural bridge between associative and novel encoding pathways. Thus, the findings of Study C refine CLS accounts (Norman & O'Reilly, 2003; O'Reilly et al., 2014) by

delineating how associative, semantic, and episodic effects map onto distinct but interacting hippocampal computations: rapid, item-specific binding and pattern separation within the DG-CA3 circuit work together with slower, schema-based integration processes that link CA1/SUB to neocortical networks. These mechanisms jointly constitute an interactive hippocampal motif in which feature-based completion and novelty-driven separation together mediate the transition from distinct representations toward more generalized memory structures.

Taken together, combining spatial and temporal modalities leads to a coherent model-level synthesis: direct associative relations bias the encoding process through recollection-like states that are behaviorally advantageous and are reflected in parietal LPC effects. Semantic feature overlap, by contrast, modulates hippocampal CA3 activity and facilitates the encoding process primarily when direct associations are absent. The DG is engaged when genuinely novel episodic traces must be formed because it orthogonalizes incoming inputs (pattern separation) to reduce interference with existing representations. SMEs, which predict memory performance independently of the priming condition, capture additional trial-by-trial variance (likely reflecting attentional engagement or depth of elaborative encoding) that coexists with the contributions of pre-existing lexical structure. This hybrid perspective suggests that successful memory formation is shaped by both long-term lexical structure and rapid hippocampal encoding via partly distinct but interacting mechanisms during the initial stages of associative and semantic priming.

Despite convergent multilevel evidence, several methodological limitations constrain strong mechanistic claims. Spatial and temporal inference remains imperfect, as high-resolution BOLD signals cannot fully resolve fast, recurrent dynamics and remain susceptible to vascular contributions and layer-/subfield-specific biases (Huber, Finn, et al., 2021; Pfaffenrot et al., 2025). Conversely, EEG provides millisecond precision but offers only limited access to subcortical localization (Buzsáki et al., 2012; Michel & Brunet, 2019). In addition, the imaging datasets are comparatively small and have modest signal-to-noise ratios. This limits statistical power, particularly when it comes to detecting small effects and higher-order interactions (Button et al., 2013). Moreover, the experimental setup lacks causal manipulations (e.g., targeted interference) that could be used to test the directionality between reinstatement and binding. Finally, although corpus-derived co-occurrence statistics provide an objective

operationalization of associative and semantic relations, they remain sensitive to stimulus-set properties. One such property is associative/semantic cohesion, defined as the number of direct associates or semantically related items linked to a single target word within the stimulus set (Rölke-Wellmann, 2021, p. 3). Both types of cohesion can covary with association strength and semantic feature overlap in lexical processing (Rölke-Wellmann, 2021, p. 69) and thereby bias effect estimates. As the present work did not explicitly control for associative/semantic cohesion, the results should be interpreted with caution.

6.3 Implications, Methodological Refinements, and Future Directions

6.3.1 Theoretical and Practical Implications of Utilizing Word Co-occurrences

This doctoral thesis contributes to a growing field of research highlighting the utility of corpus-derived word co-occurrence statistics for elucidating cognitive and neural mechanisms underlying memory formation and language processing. The present approach bypasses the limitations of subjective measures (e.g., free-association norms), which suffer from sampling biases and may conflate associative and semantic similarity (Hutchison, 2003). Thus, using co-occurrence statistics to distinguish direct associations from semantic similarity can help to refine models of lexical access, semantic memory, and neural interactions.

From a theoretical perspective, integrating co-occurrence-based statistics into models of memory formation is congruent with spreading activation accounts (Collins & Loftus, 1975) and the CLS framework (O'Reilly et al., 2014). Within CLS, neocortical networks gradually encode structured, semantic knowledge, while the hippocampus supports rapid episodic binding. Co-occurrence-derived associative measures can be read as proxies for pre-existing neocortical schemata that facilitate integration of new information when lexical or conceptual overlap is high. Conversely, low co-occurrence items will more strongly tax hippocampal encoding. This interpretation is supported by computational models showing that gist-based intrusions can arise from learned word co-occurrence statistics (Spens & Burgess, 2024) and is consistent with behavioral findings from cross-situational statistical learning, where co-occurrence alone can produce robust word-referent memory effects (Warren et al., 2020). The

co-occurrence-based approach also aligns with connectionist and interactive models such as the AROM (Hofmann & Jacobs, 2014). Embedding computationally derived co-occurrence statistics in the model's semantic layer allows simulation of the dynamic interplay of semantic processes during word remembering (Hofmann et al., 2011) or association ratings (Hofmann et al., 2018). Independent manipulation of direct association and semantic feature overlap therefore enables systematic tests of model predictions across different temporal regimes (e.g., automatic vs. strategic priming; Rölke et al., 2018).

Recent empirical work further strengthens the theoretical link between distributional statistics and staged/graded activation in lexical memory. Semantic feature overlap appears to unfold dynamically during reading (Hofmann et al., 2011), and longer SOAs can alter the temporal profile of semantic activation (Hofmann, Kleemann, et al., 2022). In addition, language models and count-based co-occurrence representations seem to capture different aspects of lexical predictability and processing dynamics (Hofmann, Remus, et al., 2022). Finally, co-occurrence-based statistics offer methodological advantages in the field of neuroimaging. Parametric modeling of trial-level corpus-derived association strength and semantic feature overlap can replace coarse categorical contrasts and provide graded tests of how these statistics modulate activity in the MTL and adjacent cortical regions. Given empirical evidence that the hippocampus preferentially supports associative binding while the PRC is more involved in item-specific encoding (Duff & Brown-Schmidt, 2012; Staresina & Davachi, 2008), such parametric regressors can sharpen the interpretability of activation patterns and better constrain neural models.

From a practical perspective, the use of co-occurrence-based statistics has applications that extend into clinical, educational, and computational domains. In clinical neuropsychology, stimulus sets organized according to associative versus semantic word relations could help to differentiate impairments of the associative (hippocampal) and semantic (neocortical) memory systems. Converging evidence suggests that memory processes rely on two partially distinct cortical systems: a posterior medial system supporting relational and contextual binding, and an anterior temporal system more closely linked to item- and feature-based representations (Ranganath & Ritchey, 2012; Staresina & Davachi, 2008). This functional dissociation supports the diagnostic logic of systematically varying associative and semantic cohesion in

test materials. Manipulating either direct association or semantic feature overlap could be used to probe distinct representational operations and thus enhance the diagnostic specificity of assessments for conditions such as hippocampal amnesia or semantic dementia. In educational or rehabilitative contexts, word co-occurrence statistics can inform the design of learning and therapy materials to optimize retention. Word pairs with high co-occurrence can be more easily integrated into existing knowledge structures (Hofmann et al., 2018), thereby reducing cognitive load and improving immediate recall. Consequently, therapy materials that emphasize high-association items may be useful for immediate relearning in populations with impaired encoding efficiency (e.g., those with amnesia or post-stroke aphasia), as they link targets to existing semantic networks. By contrast, introducing low co-occurrence word pairs in interleaved and spaced sequences can promote the formation of novel episodic links by recruiting hippocampal relational-binding mechanisms and minimizing proactive semantic interference (Cepeda et al., 2006; Staresina & Davachi, 2008). Evidence from cross-situational statistical learning demonstrates that even infants track co-occurrences across contexts to form robust word-referent mappings (Smith & Yu, 2008). Such findings underscore the practical value of manipulating the statistical structure of the input data when designing targeted learning programs.

In other words, an optimized timing strategy for targeted learning should pair new vocabulary with associative and semantically related contexts to leverage high-co-occurrence links for rapid anchoring, while systematically spacing and interleaving exposures to low co-occurrence word pairs should encourage the consolidation of novel lexical representations. Co-occurrence statistics may also be relevant to artificial intelligence and natural language processing. While current models often rely on high-dimensional predictive embeddings to capture semantics (Mikolov et al., 2013), incorporating corpus-derived direct association and semantic feature overlap from word corpora can enhance interpretability and facilitate the integration of cognitive theory with machine learning representations. Previous studies have demonstrated that meaningful semantic structures can be extracted from co-occurrence statistics, but that the performance of this process is directly affected by choices such as window size, weighting and dimensionality reduction (Bullinaria & Levy, 2012). This suggests a direct route for aligning model features with human lexical organization. In hybrid

approaches, co-occurrence statistics can serve as transparent, theory-based predictors alongside more opaque dimensions of embeddings, thereby enhancing both predictive accuracy and the mapping of computational mechanisms onto hypothesized memory processes.

However, the reliability of the corpus-derived statistics depends on the quality, size, and representativeness of the underlying text data (Evert, 2005). Co-occurrence alone does not distinguish between thematic co-use and deeper taxonomic similarity. Although the operational dissociation of direct association and semantic feature overlap is feasible, this remains an approximation. Methodological approaches that use topic modeling techniques (e.g., latent semantic analysis, LSA; Deerwester et al., 1990) could, in principle, help distinguish surface-level co-occurrence from deeper semantic similarity. LSA uses dimensionality reduction to transform complex, high-dimensional data into a more manageable form, facilitating the identification of latent structures and patterns in the text. At the same time, domain-specific corpora may capture idiosyncratic associations that cannot be generalized, whereas very large, heterogeneous corpora may dilute context-specific relations that are relevant to specific cognitive processes. A promising approach to address this issue is to derive co-occurrence statistics from individual text corpora, which will be discussed in the following chapter.

6.3.2 Advantages of Using Individualized Text Corpora

To understand how previous language experience shapes the neural and cognitive mechanisms of memory formation, it is necessary to model an individual's actual linguistic exposure. Population-level text corpora provide useful baseline estimates of co-occurrence and semantic structure, but they inherently average over substantial inter-individual variation. As a result, they can obscure individual-specific distributional regularities that determine which lexical associations are most accessible to a person.

Individual text corpora (ICs), derived from a person's actual reading materials, web search history, or other personal text data, address this issue by providing the basis for statistical models of language experience that can be aligned with the memory system of the individual they are meant to approximate. By doing so, ICs strengthen the relationship between the input experienced and the rapid retrieval processes that facilitate encoding and initial lexical access

(Hofmann et al., 2020). This alignment is important because many memory-related cognitive processes depend on precise, context-relevant predictability rather than stable, broad semantic taxonomies. Hofmann et al. (2020), for instance, collected extended samples of everyday reading from participants, trained distributional models on this personal text data, and demonstrated that individualized word-probability estimates predicted first-fixation and first-pass gaze durations during sentence reading. In contrast, predictions derived from norm-based corpora were ineffective. These findings suggest that immediate lexical activation during the initial stages of encoding is influenced by the specific contexts in which learners have previously encountered words. ICs thus increase sensitivity to the distributional cues that accelerate retrieval and consolidation.

In addition to online processing, ICs may provide a more reliable empirical source for disentangling corpus-derived association strength from taxonomic semantic similarity. As ICs capture which words co-occurred for an individual and in which contexts, they permit the derivation of context-dependent co-occurrence statistics alongside broader, embedding-based similarity estimates. Future research might therefore compare the predictive power of these statistics at the individual level to determine whether a behavioral effect is primarily driven by recent, context-specific associations or by more generalized semantic relations. This would reduce the interpretative ambiguity that arises when association estimates are computed from norm-based corpora that do not reflect an individual’s linguistic experience. ICs are also highly valuable for studying individual differences. Using web scraping, Hofmann et al. (2024) generated individual word corpora from participants' Google search histories. Afterward, they trained participant-level skip-gram word2vec models to compute the average cosine similarity between each IC's frequent tokens and a set of label words derived from a lexical approach to personality. These IC-label similarities were then used as predictive features in neural predictive models, explaining a substantial amount of variance in psychometric outcomes such as openness, interests, and domain knowledge. Further variable-importance analyses and model inspections revealed transparent and interpretable relations between topic language exposure and predicted trait constructs. IC-derived similarity measures therefore offer predictive power and mechanistic interpretability in the context of relating experiential language input to individual differences. Furthermore, as IC-derived features can be traced

back to specific texts and topical domains, they might offer a degree of interpretability that often lacks in norm-based corpora. Researchers might therefore not only predict an outcome but also identify the experiential inputs that contributed most to it.

Nevertheless, ICs should be viewed as a valuable methodological complement rather than as universally superior. Their main strength lies in aligning modeled language input with individual experience, which is relevant for studying exposure-dependent retrieval or inter-individual differences. At the same time, the person-specific nature of ICs limits their generalizability to other participants and populations, and their predictions are sensitive to corpus size and preprocessing decisions (Hofmann et al., 2024). Constructing ICs from personal digital traces also raises important ethical constraints. Web search histories and other identifiable text sources require rigorous anonymization, secure handling, and transparent consent procedures, since the risk of re-identification may persist even after de-identification (Deußer et al., 2020; Hofmann et al., 2024). In sum, the advantages of ICs must be weighed against the increased analytical complexity of training numerous subject-level models, and it is important to note that ICs do not render norm-based corpora obsolete, as population-level resources are still necessary for making general claims and ensuring comparability.

6.3.3 Lemmatization of the Stimulus Material

When deriving association strength and semantic feature overlap from large text corpora, a key decision is whether to work with surface word forms (tokens) or canonical dictionary forms (lemmata; e.g., *run* for *runs* or *running*). With regard to the corpus-related representativeness issue discussed in section 6.3.2, lemmatization offers a straightforward methodological approach to mitigate this problem. By collapsing inflectional and derivational variants onto canonical base forms, lemmatization measurably reduces data sparsity and increases the token counts that underlie count-based distributional measures (e.g., *LMI* or χ^2; Biemann et al., 2013; Mandera et al., 2017), thereby enhancing relationship estimates. To evaluate whether this preprocessing choice significantly affects the validity of the corpus-derived statistics, semantic feature overlap measures computed on lemmatized versus surface word forms were compared. The resulting alternative predictor sets were then used to model

behavioral indices of word processing. This comparison, based on a dataset originally collected for the author's Bachelor thesis (Klein, 2016) and reanalyzed for the present thesis, provided a critical test of whether lemmatizing word forms improves both the stability and the predictive validity of semantic predictors.

Specifically, a lexical decision task was employed. Initially, 32 participants were tested, but six were excluded because their overall error rate exceeded 15% (i.e., accuracy < 85%). This was implemented to ensure reliable task engagement. The final sample comprised $N = 26$ participants (13 women), with a mean age of $M = 31.92$ years ($SD = 13.79$). Stimuli were derived from the BAWL-R word corpus (Võ et al., 2009), with CELEX (Baayen et al., 1996) and the Leipzig Corpora Collection (Goldhahn et al., 2012) used as supplements. The experimental stimulus set comprised 150 German prime-target word pairs (i.e., the meaningful trials analyzed here), as well as 75 noun-pseudoword pairs and 75 noun-nonword (random string) pairs. Appendix D1 provides the full stimulus list for the noun-noun prime-target pairs. Items were presented in uppercase Times New Roman font. Prime-target relations were classified into three conditions: (1) Unrelated (1stC=0), defined by an association strength of zero as determined from the $\log_{10}$-transformed log-likelihood ratio between prime and target; (2) semantic feature overlap based on surface word forms (2ndC-S), calculated by extracting the top 1,000 χ^2-ranked contextual features for each surface form and counting the common associates between prime and target; and (3) semantic feature overlap based on lemmatized word forms (2ndC-L), calculated using the same procedure but applied to a lemmatized word corpus processed with the JoBimText UIMA pipeline (tokenization → lemmatization → collapsed dependency parsing → JoBim extraction; Biemann et al., 2013). Across experimental conditions, items did not significantly differ in word length, frequency, or orthographic neighborhood size (all Fs(2,147) ≤ 1, all ps > .05; see Appendix D2). The experiment commenced with 20 practice trials and proceeded in three main blocks with two short breaks. Within each block, the stimuli were pseudo-randomized per participant, and two counterbalanced lists ensured no item repetition confounds. Each trial followed a fixed timing structure (jittered fixation cross 500–1,000 ms, prime 250 ms, blank screen 1,000 ms, target 200 ms, mask 1,300 ms), and participants indicated word/nonword by button press. Table 15 shows the descriptive means across experimental conditions.

Table 15
Means (± SEs) of Error Rates and Response Times (Klein, 2016)

	1stC=0	2ndC-S	2ndC-L
Error Rate	6.7 (1.2)	5.9 (1.1)	4.8 (1.0)
Response Time	654 (12)	639 (12)	621 (13)

Note. N = 26 participants. Error rate (%) = 100 × incorrect trials/total trials. Response times are reported in ms. 1stC=0 = unrelated (association strength equals zero); 2ndC-S = semantic feature overlap based on surface word forms; 2ndC-L = semantic feature overlap based on lemmatized word forms.

Lexical decision accuracy was modeled using binomial GLMMs (logit link), whereas natural-log-transformed RTs were modeled using Gaussian LMMs. The order in which the stimuli were presented to each participant (TrialNumber) was included as a fixed effect to account for time-on-task effects that could otherwise be absorbed by the semantic predictors. To reduce correlations among fixed and random effects, TrialNumber was centered (TrialNumber − 150.5). All models included random intercepts for both participants and items. Random slopes for TrialNumber within participants (participant × TrialNumber) were specified, as participants may differ substantially in the magnitude and direction of learning or fatigue effects across the session. Including these subject-specific trajectories reduces anti-conservative inference on the fixed effects. Surface-based and lemma-based semantic feature overlap were moderately negatively correlated (r = -0.42). To avoid instability caused by multicollinearity, the surface and the lemma predictors were primarily evaluated in separate nested models (TrialNumber + 2ndC-S vs. TrialNumber + 2ndC-L) and only secondarily in a joint model for robustness checks. Before conducting likelihood ratio tests (LRTs) for the RT model, any trial whose standardized residual exceeded ± 2.5 *SD* was excluded as a predefined outlier rule (n = 72 trials excluded). In addition, Q–Q plots were inspected and residual normality was assessed (see Appendix D3). The fitted mixed-effects models and the corresponding LRTs are provided in Tables 16 and 17. A global LRT for response time, which evaluated the joint addition of 2ndC-S and 2ndC-L against a model with TrialNumber alone (M2 → M5), was significant (LR $\chi^2(2) = 6.74$, $p = .034$). However, nested likelihood-ratio tests showed that adding the lemma-based predictor improved model fit relative to the TrialNumber-only model (M2 → M4: LR $\chi^2(1) = 6.16$, $p = .013$), whereas adding the surface-based predictor did not reach significance (M2 → M3: LR $\chi^2(1) = 2.97$, $p = .085$). Furthermore, adding 2ndC-

S to the model already containing 2ndC-L did not significantly improve model fit (M4 → M5: LR $\chi^2(1) = 0.58$, $p = .448$). These findings suggest that 2ndC-L provides greater incremental explanatory value for response times than 2ndC-S in this dataset. Appendix D4 provides robustness checks with AS as an additional fixed effect. For lexical decision accuracy, neither 2ndC-S nor 2ndC-L significantly improved model fit beyond TrialNumber. Given the low error rates (Table 15), this measure may have exhibited restricted variance due to ceiling effects.

Table 16
Model Comparison for Natural-Log-Transformed Response Times (Klein, 2016)

Name	Model	AICc	BIC	R^2_m	R^2_c	ΔAICc	LR χ^2	*df*	*p*	LRT vs.
M1	Baseline	-3,065	-3,035	.000	.366	17.729				
M2	M1 + TrialN	-3,079	-3,042	.016	.365	4.153	15.583	1	<.001	M1
M3	M2 + S	-3,080	-3,037	.017	.366	3.187	2.974	1	.085	M2
M4	M2 + L	-3,083	-3,040	.020	.365	0.000	6.161	1	.013	M2
M5	M2 + S + L	-3,082	-3,032	.020	.365	1.433	0.576	1	.448	M4

Note. $N = 26$ participants; $k = 150$ items; $n = 3{,}607$ trials. Linear mixed-effects models were fitted using maximum likelihood estimation. ΔAICc values are relative to the best-fitting model (M4). The baseline model included random intercepts for participants and items. AICc = corrected Akaike information criterion; BIC = Bayesian information criterion; L = 2ndC-L; LR = likelihood ratio; LRT = likelihood ratio test; S = 2ndC-S; TrialN = centered trial number.

Table 17
Model Comparison for Lexical Decision Accuracy (Klein, 2016)

Name	Model	-2LL	AIC	BIC	LR χ^2	*df*	*p*	LRT vs.
M1	Baseline	22,833	22,839	22,858				
M2	M1 + TrialN	22,819	22,829	22,860	13.898	1	<.001	M1
M3	M2 + S	22,851	22,863	22,901	0.000	1	1.000	M2
M4	M2 + L	22,836	22,848	22,886	0.000	1	1.000	M2
M5	M2 + S + L	22,864	22,878	22,922	0.000	2	1.000	M4

Note. $N = 26$ participants; $k = 150$ items; $n = 3{,}900$ trials. Binomial generalized linear mixed-effects models (logit link). Negative likelihood-ratio statistics were truncated at zero, resulting in $p = 1.000$. Fit indices were computed from the -2 residual log pseudo-likelihood. The baseline model included random intercepts for participants and items. AIC = Akaike information criterion; BIC = Bayesian information criterion; L = 2ndC-L (lemma); LR = likelihood ratio; LRT = likelihood ratio test; S = 2ndC-S (surface); TrialN = centered trial number; -2LL = -2 log-likelihood.

These results support the view that lemmatization can improve the stability and predictive performance of corpus-derived measures, particularly for continuous latency measures. Across Studies A–C, the behavioral effects of semantic feature overlap were smaller and less reliable than those of direct association. Accordingly, the present lexical decision analysis provides targeted validation of the corpus-derived predictors prior to their use in the

paired-associate learning account that form the core of this doctoral thesis. Future work within this framework may therefore preferentially compute semantic feature overlap on lemmatized word corpora or implement parallel surface/lemma pipelines. This would reduce attenuation caused by sparsity and increase the power of detecting small, yet theoretically meaningful, semantic effects. Several mechanisms likely contribute to this gain in sensitivity. First, by consolidating inflectional variants under a shared base form, the frequency counts of low-frequency items are aggregated. This stabilizes count-based statistics and reduces sampling noise (Mandera et al., 2017). Second, by reducing mismatches between experimental stimuli and corpus entries, lemmatization improves the alignment of stimuli with the distributional features used to compute association statistics. This lowers measurement error and the effective out-of-vocabulary rate. Third, when embedded into graph-based pipelines such as JoBimText, lemmatization creates denser and more coherent paradigmatic neighborhoods, as well as cleaner sense clusters (Biemann et al., 2013). This, in turn, strengthens the interpretability of derived statistics and JoBim extractions. However, the effects of lemmatization are not always positive. They depend on the specific task, the model type and the corpus characteristics (Mandera et al., 2017). Tasks based on morphological distinctions, such as differences in tense or derivation differences, can be affected by the consolidation of surface word forms (Boleda, 2020). Furthermore, count-based models typically perform better with lower sparsity, whereas predictive embedding models tend to show inconsistent improvements (Mandera et al., 2017). In morphologically rich languages, such as German, lemmatizers may thus conflate homonymous categories or eliminate behaviorally significant inflectional information, which can distort estimates (Müller et al., 2015). In sum, lemmatization should be considered as an explicit methodological decision whose effects must be empirically validated rather than being assumed. Therefore, it is advisable to use a hybrid strategy: lemmatize to reduce sparsity but retain morphological features that can be used as regressors when necessary. Following the above-described protocol (parallel surface/lemmatized pipelines and predictive evaluations), empirical tests will reveal whether the explanatory power can be significantly improved. More broadly, improving the stability of semantic feature overlap estimates may help to clarify when feature-based similarity contributes to word processing over and above direct association, and how such distinctions align with the neurophysiological correlates of successful encoding.

6.3.4 Extension to Other Types of Priming

The present thesis investigated the neurophysiological correlates of associative and semantic priming during memory encoding in paired-associate learning paradigms. Across studies, reduced error rates were observed in subsequent cued recall, with direct association showing the greater benefit and semantic feature overlap offering a more variable advantage. This suggests that priming effects are not merely by-products of lexical processing but may functionally contribute to successful memory formation. A key question is whether these principles can be generalized to other forms of priming, and if so, through which mechanisms. Crucially, priming types should not be treated as isolated phenomena when addressing this issue, but rather as part of a continuum of processes that differentially influence encoding.

A reasonable starting point is conceptual priming, which captures semantic similarity that extends beyond mere word associations to embed a target in a higher-level context. Conceptual primes are typically comprised of meaningful words that activate broader, related categories or schemas, thereby influencing word processing via context-driven facilitation in a subsequent task (Tulving et al., 1982). ERP studies have shown that conceptual priming is associated with N400 attenuation during encoding, which is indicative of facilitated semantic access (Federmeier, 2022; Kutas & Federmeier, 2011). Furthermore, the magnitude of this attenuation is linked to subsequent familiarity-based recognition (Li et al., 2020). Neuroimaging research extends this picture by showing that conceptual priming engages MTL regions associated with familiarity, such as the PRC, which suggests that conceptual facilitation not only operates at the level of semantic hubs but also relies on brain areas that overlap with recognition memory (Dew & Cabeza, 2013). Taylor et al. (2013) showed that masked conceptual primes increase ‘remember’ responses in recognition paradigms, suggesting that conceptual activation can even support the integration of contextual detail into episodic traces. A logical next step is therefore to manipulate corpus-derived association strength and higher-level conceptual relatedness to examine N400 effects using EEG or test the functional link between PRC activity and hippocampal subfield modulations during encoding, as measured with fMRI. Such a design could clarify whether meaning-based facilitation primarily enhances neocortical semantic integration or instead supports conjunctive hippocampal encoding.

In contrast, perceptual or repetition priming offers a critical counterpoint by facilitating processing at the sensory rather than the conceptual level. While conceptual primes evoke semantic integration, perceptual priming raises the question of whether repeated exposure to a stimulus enhances encoding processes alone or, alternatively, bypasses hippocampal binding altogether. Chauncey et al. (2008) have shown that ERP components sensitive to visual word processing (e.g., N150, N250) exhibit reduced amplitudes during word repetition, an effect also known as repetition suppression. At the same time, fMRI studies have reported repetition suppression in occipitotemporal regions such as the fusiform gyrus and inferior frontal areas, accompanied by reduced hippocampal engagement with repeated items (Lee, Henson, et al., 2020). This pattern suggests a functional divergence, as conceptual primes appear to promote semantic integration and support the consolidation of information into long-term memory, whereas perceptual priming primarily streamlines sensory processing and provides limited benefit for durable memory formation. Therefore, future research could systematically manipulate lag and modality to determine whether repetition suppression in occipitotemporal regions predicts reduced hippocampal subfield engagement or attenuated SMEs. This would help delineate the boundary conditions of priming and clarify whether implicit processing efficiency and explicit encoding processes operate synergistically or in competition for neural resources.

The question of boundary conditions is particularly relevant in the context of cross-modal and contextual priming, as these paradigms require the integration of perceptual and conceptual dimensions within a single encoding episode. Unlike simple conceptual overlap, cross-modal congruence (e.g., sound-image pairs or narrative context preceding a word) requires the merging of various information across sensory and semantic streams to form a coherent episodic representation. This process is thought to critically engage the hippocampus (Mayes et al., 2007), and consistent with this view, multimodal context encoding (e.g., the combination of objects, locations, or voices) has been shown to involve posterior hippocampal SMEs, reflecting the successful binding of contextual details into episodic memory (Staresina et al., 2012). From an electrophysiological perspective, aligning modality-specific components with SMEs could illuminate early sensory-episodic integration, whereas high-resolution fMRI, in combination with laminar or connectivity analyses, offers an additional way to investigate

the flow of information between the sensory cortex, the EC, and the subfields of the hippocampus. In a broader sense, cross-modal priming can be viewed as a case in which perceptual and conceptual facilitation converge and, when highly congruent, can lead to particularly robust encoding effects. Consequently, such paradigms can be used to empirically test theories that propose hippocampal binding as a fundamental mechanism through which memory formation is enhanced by priming.

Finally, a subliminal or masked priming approach would extend these considerations into the realm of unconscious processing. This direction aligns with the SOA manipulations employed in Study A and could clarify the extent to which preconscious activation affects encoding in the absence of awareness. Previous research has shown that masked prime words can activate semantic categories even when participants cannot consciously identify them (Van den Bussche et al., 2009) and that masked semantic primes modulate the N400 response, suggesting that semantic processing even occurs at an unconscious level (Kutas & Federmeier, 2011). Furthermore, Ulrich et al. (2013) demonstrated that both masked and unmasked semantic word primes engage the left fusiform and inferior frontal gyrus, whereas additional activity in bilateral superior temporal and parietal regions only emerged in unmasked conditions. This suggests that there are partially dissociable neural mechanisms involved. Future research could thus manipulate the duration of prime-target exposure to test whether the same EEG signatures and brain areas involved in conscious priming are also engaged by unconscious facilitation.

Taken together, the various types of priming discussed in this section demonstrate that the consolidation of target words is not only driven by associative-semantic relations but may also depend on factors such as perceptual efficiency, conceptual integration, cross-modal binding, or unconscious activation. When these effects are considered as part of a continuum of processes, it becomes clear how prior activation can influence memory formation at different levels, which range from sensory facilitation to contextual integration in the hippocampus. However, within the framework of this thesis such a multimodal perspective underscores that the neurophysiological correlates observed for direct association and semantic feature overlap represent just one component of a broader set of mechanisms through which priming contributes to successful memory formation.

6.3.5 Advancing Toward a Mechanistic Understanding of Memory Formation

The results of Study C indicate a computational division of labor in which the DG subfield is implicated in novelty-driven episodic encoding mechanisms and the CA3 subfield facilitates informational binding when input similarity promotes semantic integration. This is consistent with CLS models (e.g., Norman & O'Reilly, 2003; O'Reilly et al., 2014) and with the pathway-oriented attractor perspective proposed by Rolls and Treves (2024). However, translating these perspectives to human subfield functions requires integrative evidence (Yassa & Stark, 2011) whereby cortical inputs are routed through the DG for pattern separation, engage CA3 for pattern completion, and are relayed via CA1/SUB to the neocortex which acts as a distributed system that integrates across episodic to derive latent semantic structure. To advance the present findings, future work should move beyond descriptive convergence toward explicit tests of directionality and information flow. Simultaneous EEG and fMRI acquisition (Huster et al., 2012) with single-trial EEG-informed regressors could link parietal LPC dynamics to subfield-specific BOLD activity, thereby enabling empirical tests of causal chains such as whether LPC modulations mediate associative effects in the hippocampal subfields, which were absent in the current data. Representational similarity analysis (RSA; see Kriegeskorte et al., 2008), which uses dissimilarity matrices to quantify the informational structure of neural or model-based representations, could be applied within anatomically defined DG/CA3 ROIs to test whether CA3 representational geometry scales with semantic feature overlap, while DG patterns increase for non-associated word pairs. Dynamic causal modeling (DCM; see Friston et al., 2003), which estimates directed effective connectivity by modeling how experimental inputs modulate intrinsic coupling among neural populations within a Bayesian state-space framework, could further test hypotheses about top-down control from the neocortex to the hippocampus. Parametric (continuous or gradual) manipulations of direct association and semantic feature overlap, combined with integrated RSA/DCM pipelines, would allow for the quantification of both correspondence and directed information flow. In addition, future research should examine interindividual variability in the use of associative and semantic encoding strategies, as such differences may systematically modulate hippocampal subfield recruitment and refine mechanistic validation of the proposed model.

7. Conclusion

This doctoral thesis used a computational, corpus-based approach to investigate how associative and semantic priming effects differentially influence paired-associate learning. Co-occurrence statistics enabled this dissociation and were incorporated into three consecutive studies to disentangle the specific contributions of direct association and semantic feature overlap to the successful formation of lasting memory traces. Evidence for this dissociation emerged across behavioral facilitation, parietal electrophysiological encoding signatures, and subfield-specific BOLD responses, suggesting a multilevel encoding architecture. Strong direct associations facilitated cue-dependent retrieval and were linked to increased parietal LPC amplitudes, which are indicative of recollection-oriented or reinstatement states. By contrast, semantic feature overlap enhanced category-level facilitation that proved particularly beneficial when direct associations were absent. This was linked to increased activity in the CA3 region, indicating feature-based completion processes and cortical scaffolding when direct associative routes are weak. Word pairs without an associative or semantic relation preferentially triggered DG activity, indicating pattern separation processes and reduced interference with existing representations during episodic encoding. Thus, it can be concluded that both forms of priming initiate dissociable neural computational operations and are implicated in partially distinct types of processing within memory formation. This conclusion aligns with the spreading-activation theory (Collins & Loftus, 1975), which posits that activation propagates from a concept node along associative links so that directly connected nodes receive faster and stronger activation than more distant (indirect) nodes. From a mechanistic perspective, this work presents an integrative approach in which long-term lexical structure and rapid hippocampal computations jointly determine the success of encoding new information. The findings support certain predictions of attractor-based models (Rolls, 2007; Rolls & Treves, 2024) in the human system while also refining CLS accounts (Norman & O'Reilly, 2003; O'Reilly et al., 2014) by specifying the interaction between cortical representations and hippocampal subfield mechanisms during the initial stages of encoding. Crucially, this inference is strengthened by convergent empirical work on hippocampal pattern separation/completion (Yassa & Stark, 2011), which supports this mechanistic interpretation.

8. References

Abdel Rahman, R., & Melinger, A. (2009). Semantic context effects in language production: A swinging lexical network proposal and a review. *Language and Cognitive Processes*, *24*(5), 713–734. https://doi.org/10.1080/01690960802597250

Adesope, O. O., Trevisan, D. A., & Sundararajan, N. (2017). Rethinking the use of tests: A meta-analysis of practice testing. *Review of Educational Research*, *87*(3), 659–701. https://doi.org/10.3102/0034654316689306

Aimone, J. B., Deng, W., & Gage, F. H. (2011). Resolving new memories: A critical look at the dentate gyrus, adult neurogenesis, and pattern separation. *Neuron*, *70*(4), 589–596. https://doi.org/10.1016/j.neuron.2011.05.010

Alday, P. M., & Kretzschmar, F. (2019). Speed-accuracy tradeoffs in brain and behavior: Testing the independence of P300 and N400 related processes in behavioral responses to sentence categorization. *Frontiers in Human Neuroscience*, *13*, Article 285. https://doi.org/10.3389/fnhum.2019.00285

Amaral, D. G., & Lavenex, P. (2007). Hippocampal neuroanatomy. In P. Andersen, R. Morris, D. G. Amaral, T. Bliss, & J. O'Keefe (Eds.), *The hippocampus book* (pp. 37–114). Oxford University Press.

Amunts, K., Mohlberg, H., Bludau, S., & Zilles, K. (2020). Julich-Brain: A 3D probabilistic atlas of the human brain's cytoarchitecture. *Science*, *369*(6506), 988–992. https://doi.org/10.1126/science.abb4588

Ances, B. M., Leontiev, O., Perthen, J. E., Liang, C., Lansing, A. E., & Buxton, R. B. (2008). Regional differences in the coupling of cerebral blood flow and oxygen metabolism changes in response to activation: Implications for BOLD-fMRI. *NeuroImage*, *39*(4), 1510–1521. https://doi.org/10.1016/j.neuroimage.2007.11.015

Anderson, J. R. (1983). A spreading activation theory of memory. *Journal of Verbal Learning and Verbal Behavior*, *22*(3), 261–295. https://doi.org/10.1016/S0022-5371(83)90201-3

Ashburner, J., & Friston, K. J. (2000). Voxel-based morphometry — The methods. *NeuroImage*, *11*(6), 805–821. https://doi.org/10.1006/nimg.2000.0582

Atkinson, R. C., & Shiffrin, R. M. (1968). Human memory: A proposed system and its control processes. In K. W. Spence & J. T. Spence (Eds.), *The psychology of learning and motivation: Advances in research and theory* (Vol. 2, pp. 89–195). Academic Press. https://doi.org/10.1016/S0079-7421(08)60422-3

Baayen, R. H., Piepenbrock, R., & Gulikers, L. (1996). *The CELEX lexical database* [CD-ROM]. Linguistic Data Consortium.

Baddeley, A. D. (2000). The episodic buffer: A new component of working memory? *Trends in Cognitive Sciences*, *4*(11), 417–423. https://doi.org/10.1016/S1364-6613(00)01538-2

Baddeley, A. D. (2003). Working memory: Looking back and looking forward. *Nature Reviews Neuroscience*, *4*(10), 829–839. https://doi.org/10.1038/nrn1201

Baddeley, A. D. (2012). Working memory: Theories, models, and controversies. *Annual Review of Psychology*, *63*, 1–29. https://doi.org/10.1146/annurev-psych-120710-100422

Bakker, A., Kirwan, C. B., Miller, M., & Stark, C. E. L. (2008). Pattern separation in the human hippocampal CA3 and dentate gyrus. *Science*, *319*(5870), 1640–1642. https://doi.org/10.1126/science.1152882

Balota, D. A., Cortese, M. J., Sergent-Marshall, S. D., Spieler, D. H., & Yap, M. J. (2004). Visual word recognition of single-syllable words. *Journal of Experimental Psychology: General*, *133*(2), 283–316. https://doi.org/10.1037/0096-3445.133.2.283

Besson, M., & Kutas, M. (1993). The many facets of repetition: A cued-recall and event-related potential analysis of repeating words in same versus different sentence contexts. *Journal of Experimental Psychology: Learning, Memory, and Cognition*, *19*(5), 1115–1133. https://doi.org/10.1037/0278-7393.19.5.1115

Biemann, C., Coppola, B., Glass, M. R., Gliozzo, A., Hatem, M., & Riedl, M. (2013). JoBimText visualizer: A graph-based approach to contextualizing distributional similarity. In Z. Kozareva, I. Matveeva, G. Melli, & V. Nastase (Eds.), *Proceedings of TextGraphs-8: Graph-based methods for natural language processing* (pp. 6–10). Association for Computational Linguistics. https://aclanthology.org/W13-5002/

Binder, J. R., Desai, R. H., Graves, W. W., & Conant, L. L. (2009). Where is the semantic system? A critical review and meta-analysis of 120 functional neuroimaging studies. *Cerebral Cortex*, *19*(12), 2767–2796. https://doi.org/10.1093/cercor/bhp055

Bloch, F. (1946). Nuclear induction. *Physical Review*, *70*(7–8), 460–474. https://doi.org/10.1103/PhysRev.70.460

Boleda, G. (2020). Distributional semantics and linguistic theory. *Annual Review of Linguistics*, *6*, 213–234. https://doi.org/10.1146/annurev-linguistics-011619-030303

Bordag, S. (2007). *Elements of knowledge-free and unsupervised lexical acquisition* [Doctoral dissertation, Universität Leipzig].

Brain Products GmbH. (2021). *BrainVision Analyzer* (Version 2.2.2) [Computer software]. https://www.brainproducts.com/downloads/analyzer/

Brown, T. B., Mann, B., Ryder, N., Subbiah, M., Kaplan, J. D., Dhariwal, P., Neelakantan, A., Shyam, P., Sastry, G., Askell, A., Agarwal, S., Herbert-Voss, A., Krueger, G., Henighan, T., Child, R., Ramesh, A., Ziegler, D. M., Wu, J., Winter, C., … Amodei, D. (2020). Language models are few-shot learners. In H. Larochelle, M. Ranzato, R. Hadsell, M. F. Balcan, & H. Lin (Eds.), *Advances in neural information processing systems* (Vol. 33, pp. 1877–1901). Curran Associates, Inc.

Brunel, N., & Wang, X.-J. (2001). Effects of neuromodulation in a cortical network model of object working memory dominated by recurrent inhibition. *Journal of Computational Neuroscience*, *11*(1), 63–85. https://doi.org/10.1023/A:1011204814320

Bullinaria, J. A., & Levy, J. P. (2012). Extracting semantic representations from word co-occurrence statistics: Stop-lists, stemming, and SVD. *Behavior Research Methods*, *44*(3), 890–907. https://doi.org/10.3758/s13428-011-0183-8

Button, K. S., Ioannidis, J. P. A., Mokrysz, C., Nosek, B. A., Flint, J., Robinson, E. S. J., & Munafò, M. R. (2013). Power failure: Why small sample size undermines the reliability of neuroscience. *Nature Reviews Neuroscience*, *14*(5), 365–376. https://doi.org/10.1038/nrn3475

Buzsáki, G., Anastassiou, C. A., & Koch, C. (2012). The origin of extracellular fields and currents — EEG, ECoG, LFP and spikes. *Nature Reviews Neuroscience*, *13*(6), 407–420. https://doi.org/10.1038/nrn3241

Buzsáki, G., & Draguhn, A. (2004). Neuronal oscillations in cortical networks. *Science*, *304*(5679), 1926–1929. https://doi.org/10.1126/science.1099745

Cepeda, N. J., Pashler, H., Vul, E., Wixted, J. T., & Rohrer, D. (2006). Distributed practice in verbal recall tasks: A review and quantitative synthesis. *Psychological Bulletin*, *132*(3), 354–380. https://doi.org/10.1037/0033-2909.132.3.354

Chauncey, K., Holcomb, P. J., & Grainger, J. (2008). Effects of stimulus font and size on masked repetition priming: An event-related potentials (ERP) investigation. *Language and Cognitive Processes*, *23*(1), 183–200. https://doi.org/10.1080/01690960701579839

Collins, A. M., & Loftus, E. F. (1975). A spreading-activation theory of semantic processing. *Psychological Review*, *82*(6), 407–428. https://doi.org/10.1037/0033-295X.82.6.407

Cousineau, D. (2005). Confidence intervals in within-subject designs: A simpler solution to Loftus and Masson's method. *Tutorials in Quantitative Methods for Psychology*, *1*(1), 42–45. https://doi.org/10.20982/tqmp.01.1.p042

Coutanche, M. N., & Thompson-Schill, S. L. (2014). Fast mapping rapidly integrates information into existing memory networks. *Journal of Experimental Psychology: General*, *143*(6), 2296–2303. https://doi.org/10.1037/xge0000020

Cowan, N. (2008). What are the differences between long-term, short-term, and working memory? *Progress in Brain Research*, *169*, 323–338. https://doi.org/10.1016/S0079-6123(07)00020-9

Cox, R. W. (1996). AFNI: Software for analysis and visualization of functional magnetic resonance neuroimages. *Computers and Biomedical Research*, *29*(3), 162–173. https://doi.org/10.1006/cbmr.1996.0014

Curtis, A. T., Hutchison, R. M., & Menon, R. S. (2014). Phase based venous suppression in resting-state BOLD GE-fMRI. *NeuroImage*, *100*, 51–59. https://doi.org/10.1016/j.neuroimage.2014.05.079

Dalton, M. A., D'Souza, A., Lv, J., & Calamante, F. (2022). New insights into anatomical connectivity along the anterior-posterior axis of the human hippocampus using in vivo quantitative fibre tracking. *eLife*, *11*, Article e76143. https://doi.org/10.7554/eLife.76143

Dambacher, M., Dimigen, O., Braun, M., Wille, K., Jacobs, A. M., & Kliegl, R. (2012). Stimulus onset asynchrony and the timeline of word recognition: Event-related potentials during sentence reading. *Neuropsychologia*, *50*(8), 1852–1870. https://doi.org/10.1016/j.neuropsychologia.2012.04.011

Dambacher, M., Kliegl, R., Hofmann, M., & Jacobs, A. M. (2006). Frequency and predictability effects on event-related potentials during reading. *Brain Research*, *1084*(1), 89–103. https://doi.org/10.1016/j.brainres.2006.02.010

Davachi, L. (2006). Item, context and relational episodic encoding in humans. *Current Opinion in Neurobiology*, *16*(6), 693–700. https://doi.org/10.1016/j.conb.2006.10.012

De Deyne, S., Navarro, D. J., & Storms, G. (2013). Better explanations of lexical and semantic cognition using networks derived from continued rather than single-word associations. *Behavior Research Methods*, *45*(2), 480–498. https://doi.org/10.3758/s13428-012-0260-7

Deerwester, S., Dumais, S. T., Furnas, G. W., Landauer, T. K., & Harshman, R. (1990). Indexing by latent semantic analysis. *Journal of the American Society for Information Science*, *41*(6), 391–407. https://doi.org/10.1002/(SICI)1097-4571(199009)41:6<391::AID-ASI1>3.0.CO;2-9

Delorme, A., & Makeig, S. (2004). EEGLAB: An open-source toolbox for analysis of single-trial EEG dynamics including independent component analysis. *Journal of Neuroscience Methods*, *134*(1), 9–21. https://doi.org/10.1016/j.jneumeth.2003.10.009

de Saussure, F. (1959). *Course in general linguistics* (W. Baskin, Trans.). Philosophical Library. (Original work published 1916)

Destrieux, C., Fischl, B., Dale, A., & Halgren, E. (2010). Automatic parcellation of human cortical gyri and sulci using standard anatomical nomenclature. *NeuroImage*, *53*(1), 1–15. https://doi.org/10.1016/j.neuroimage.2010.06.010

Deußer, C., Passmann, S., & Strufe, T. (2020). Browsing unicity: On the limits of anonymizing web tracking data. In *2020 IEEE Symposium on Security and Privacy (SP)* (pp. 777–790). IEEE. https://doi.org/10.1109/SP40000.2020.00018

Devlin, J., Chang, M.-W., Lee, K., & Toutanova, K. (2019). BERT: Pre-training of deep bidirectional transformers for language understanding. In *Proceedings of the 2019 Conference of the North American Chapter of the Association for Computational Linguistics: Human Language Technologies* (Vol. 1, pp. 4171–4186). Association for Computational Linguistics. https://doi.org/10.18653/v1/N19-1423

Dew, I. T. Z., & Cabeza, R. (2013). A broader view of perirhinal function: From recognition memory to fluency-based decisions. *Journal of Neuroscience*, *33*(36), 14466–14474. https://doi.org/10.1523/JNEUROSCI.1413-13.2013

Donchin, E., & Coles, M. G. H. (1988). Is the P300 component a manifestation of context updating? *Behavioral and Brain Sciences*, *11*(3), 357–374. https://doi.org/10.1017/S0140525X00058027

Duff, M. C., & Brown-Schmidt, S. (2012). The hippocampus and the flexible use and processing of language. *Frontiers in Human Neuroscience*, *6*, Article 69. https://doi.org/10.3389/fnhum.2012.00069

Duncan, K., Ketz, N., Inati, S. J., & Davachi, L. (2012). Evidence for area CA1 as a match/mismatch detector: A high-resolution fMRI study of the human hippocampus. *Hippocampus*, *22*(3), 389–398. https://doi.org/10.1002/hipo.20933

Dunning, T. E. (1993). Accurate methods for the statistics of surprise and coincidence. *Computational Linguistics*, *19*(1), 61–74. https://aclanthology.org/J93-1003/

Duvernoy, H. M., Cattin, F., & Risold, P.-Y. (2013). *The human hippocampus: Functional anatomy, vascularization and serial sections with MRI* (4th ed.). Springer. https://doi.org/10.1007/978-3-642-33603-4

Eichenbaum, H. (2017). Memory: Organization and control. *Annual Review of Psychology*, *68*, 19–45. https://doi.org/10.1146/annurev-psych-010416-044131

Eichenbaum, H., Yonelinas, A. P., & Ranganath, C. (2007). The medial temporal lobe and recognition memory. *Annual Review of Neuroscience*, *30*, 123–152. https://doi.org/10.1146/annurev.neuro.30.051606.094328

Eickhoff, S. B., Stephan, K. E., Mohlberg, H., Grefkes, C., Fink, G. R., Amunts, K., & Zilles, K. (2005). A new SPM toolbox for combining probabilistic cytoarchitectonic maps and functional imaging data. *NeuroImage*, *25*(4), 1325–1335. https://doi.org/10.1016/j.neuroimage.2004.12.034

Eldridge, L. L., Engel, S. A., Zeineh, M. M., Bookheimer, S. Y., & Knowlton, B. J. (2005). A dissociation of encoding and retrieval processes in the human hippocampus. *Journal of Neuroscience*, *25*(13), 3280–3286. https://doi.org/10.1523/JNEUROSCI.3420-04.2005

Eriksson, P. S., Perfilieva, E., Björk-Eriksson, T., Alborn, A.-M., Nordborg, C., Peterson, D., & Gage, F. H. (1998). Neurogenesis in the adult human hippocampus. *Nature Medicine*, *4*(11), 1313–1317. https://doi.org/10.1038/3305

Estes, Z., & Jones, L. L. (2009). Integrative priming occurs rapidly and uncontrollably during lexical processing. *Journal of Experimental Psychology: General*, *138*(1), 112–130. https://doi.org/10.1037/a0014677

Evert, S. (2005). *The statistics of word cooccurrences: Word pairs and collocations* [Doctoral dissertation, University of Stuttgart]. https://doi.org/10.18419/opus-2556

Federmeier, K. D. (2022). Connecting and considering: Electrophysiology provides insights into comprehension. *Psychophysiology*, *59*(1), e13940. https://doi.org/10.1111/psyp.13940

Feinberg, D. A., Beckett, A. J. S., Vu, A. T., Stockmann, J., Huber, L., Ma, S., Ahn, S., Setsompop, K., Cao, X., Park, S., Liu, C., Wald, L. L., Polimeni, J. R., Mareyam, A., Gruber, B., Stirnberg, R., Liao, C., Yacoub, E., Davids, M., … Dietz, P. (2023). Next-generation MRI scanner designed for ultra-high-resolution human brain imaging at 7 Tesla. *Nature Methods*, *20*(12), 2048–2057. https://doi.org/10.1038/s41592-023-02068-7

Fernández, G., Weyerts, H., Tendolkar, I., Smid, H. G., Scholz, M., & Heinze, H.-J. (1998). Event-related potentials of verbal encoding into episodic memory: Dissociation between the effects of subsequent memory performance and distinctiveness. *Psychophysiology*, *35*(6), 709–720. https://doi.org/10.1111/1469-8986.3560709

Ferrand, L., & New, B. (2003). Semantic and associative priming in the mental lexicon. In P. Bonin (Ed.), *Mental lexicon: Some words to talk about words* (pp. 25–43). Nova Science.

Finn, E. S., Huber, L., Jangraw, D. C., Molfese, P. J., & Bandettini, P. A. (2019). Layer-dependent activity in human prefrontal cortex during working memory. *Nature Neuroscience*, *22*(10), 1687–1695. https://doi.org/10.1038/s41593-019-0487-z

Fischl, B. (2012). FreeSurfer. *NeuroImage*, *62*(2), 774–781. https://doi.org/10.1016/j.neuroimage.2012.01.021

Förster, E., Zhao, S., & Frotscher, M. (2006). Laminating the hippocampus. *Nature Reviews Neuroscience*, *7*(4), 259–267. https://doi.org/10.1038/nrn1882

Frank, S. L., & Willems, R. M. (2017). Word predictability and semantic similarity show distinct patterns of brain activity during language comprehension. *Language, Cognition and Neuroscience*, *32*(9), 1192–1203. https://doi.org/10.1080/23273798.2017.1323109

Friedman, D., & Johnson, R. (2000). Event-related potential (ERP) studies of memory encoding and retrieval: A selective review. *Microscopy Research and Technique*, *51*(1), 6–28. https://doi.org/10.1002/1097-0029(20001001)51:1<6::AID-JEMT2>3.0.CO;2-R

Friston, K. J., Harrison, L., & Penny, W. (2003). Dynamic causal modelling. *NeuroImage*, *19*(4), 1273–1302. https://doi.org/10.1016/S1053-8119(03)00202-7

Gilboa, A., & Marlatte, H. (2017). Neurobiology of schemas and schema-mediated memory. *Trends in Cognitive Sciences*, *21*(8), 618–631. https://doi.org/10.1016/j.tics.2017.04.013

Glanzer, M., Kim, K., Hilford, A., & Adams, J. K. (1999). Slope of the receiver-operating characteristic in recognition memory. *Journal of Experimental Psychology: Learning, Memory, and Cognition*, *25*(2), 500–513. https://doi.org/10.1037/0278-7393.25.2.500

Glover, G. H., Li, T. Q., & Ress, D. (2000). Image-based method for retrospective correction of physiological motion effects in fMRI: RETROICOR. *Magnetic Resonance in Medicine*, *44*(1), 162–167. https://doi.org/10.1002/1522-2594(200007)44:1<162::aid-mrm23>3.0.co;2-e

Glueck, D. H., Li, Q., Macleod, A. J., Litkowski, E. M., Yang, X., Bian, J., Ritzhaupt, A. D., Sommer, M., Valle, N., Shaw, J. R., & Muller, K. E. (2025). Power and sample size for reversible linear mixed models with clustering and longitudinality: GLIMMPSE Version 3. *PLOS ONE*, *20*(9), Article e0329712. https://doi.org/10.1371/journal.pone.0329712

Goldhahn, D., Eckart, T., & Quasthoff, U. (2012). Building large monolingual dictionaries at the Leipzig Corpora Collection: From 100 to 200 languages. In *Proceedings of the Eighth International Conference on Language Resources and Evaluation (LREC'12)* (pp. 759–765). European Language Resources Association (ELRA). https://aclanthology.org/L12-1154/

Grainger, J., & Jacobs, A. M. (1996). Orthographic processing in visual word recognition: A multiple read-out model. *Psychological Review*, *103*(3), 518–565. https://doi.org/10.1037/0033-295x.103.3.518

Grande, X., Berron, D., Horner, A. J., Bisby, J. A., Düzel, E., & Burgess, N. (2019). Holistic recollection via pattern completion involves hippocampal subfield CA3. *Journal of Neuroscience*, *39*(41), 8100–8111. https://doi.org/10.1523/JNEUROSCI.0722-19.2019

Greenberg, D. L., & Verfaellie, M. (2010). Interdependence of episodic and semantic memory: Evidence from neuropsychology. *Journal of the International Neuropsychological Society*, *16*(5), 748–753. https://doi.org/10.1017/S1355617710000676

Groot, J. M., Miletic, S., Isherwood, S. J. S., Tse, D. H. Y., Habli, S., Håberg, A. K., Bazin, P. L., Mittner, M., & Forstmann, B. U. (2024). A high-resolution 7 Tesla resting-state fMRI dataset optimized for studying the subcortex. *Data in Brief*, *55*, Article 110668. https://doi.org/10.1016/j.dib.2024.110668

Hafting, T., Fyhn, M., Molden, S., Moser, M.-B., & Moser, E. I. (2005). Microstructure of a spatial map in the entorhinal cortex. *Nature*, *436*(7052), 801–806. https://doi.org/10.1038/nature03721

Hainmüller, T., & Bartos, M. (2020). Dentate gyrus circuits for encoding, retrieval and discrimination of episodic memories. *Nature Reviews Neuroscience*, *21*(3), 153–168. https://doi.org/10.1038/s41583-019-0260-z

Hauk, O., & Pulvermüller, F. (2004). Effects of word length and frequency on the human event-related potential. *Clinical Neurophysiology*, *115*(5), 1090–1103. https://doi.org/10.1016/j.clinph.2003.12.020

Hebb, D. O. (1949). *The organization of behavior: A neuropsychological theory*. Wiley.

Heyman, T., Hutchison, K. A., & Storms, G. (2016). Uncovering underlying processes of semantic priming by correlating item-level effects. *Psychonomic Bulletin & Review*, *23*(2), 540–547. https://doi.org/10.3758/s13423-015-0932-2

Hillman, E. M. (2014). Coupling mechanism and significance of the BOLD signal: A status report. *Annual Review of Neuroscience*, *37*, 161–181. https://doi.org/10.1146/annurev-neuro-071013-014111

Hintzman, D. (1984). MINERVA 2: A simulation model of human memory. *Behavior Research Methods*, *16*(2), 96–101. https://doi.org/10.3758/BF03202365

Hofmann, M. J., Biemann, C., Westbury, C., Murusidze, M., Conrad, M., & Jacobs, A. M. (2018). Simple co-occurrence statistics reproducibly predict association ratings. *Cognitive Science*, *42*(7), 2287–2312. https://doi.org/10.1111/cogs.12662

Hofmann, M. J., & Jacobs, A. M. (2014). Interactive activation and competition models and semantic context: From behavioral to brain data. *Neuroscience & Biobehavioral Reviews*, *46*, 85–104. https://doi.org/10.1016/j.neubiorev.2014.06.011

Hofmann, M. J., Jansen, M. T., Wigbels, C., Briesemeister, B., & Jacobs, A. M. (2024). Individual text corpora predict openness, interests, knowledge and level of education. In *Proceedings of the Workshop on Cognitive Aspects of the Lexicon @ LREC-COLING 2024* (pp. 14–25). https://aclanthology.org/2024.cogalex-1.2/

Hofmann, M. J., Kleemann, M. A., Rölke-Wellmann, A., Vorstius, C., & Radach, R. (2022). Semantic feature activation takes time: Longer SOA elicits earlier priming effects during reading. *Cognitive Processing*, *23*, 309–318. https://doi.org/10.1007/s10339-022-01084-3

Hofmann, M. J., Kuchinke, L., Biemann, C., Tamm, S., & Jacobs, A. M. (2011). Remembering words in context as predicted by an associative read-out model. *Frontiers in Psychology*, *2*, Article 252. https://doi.org/10.3389/fpsyg.2011.00252

Hofmann, M. J., Müller, L., Rölke, A., Radach, R., & Biemann, C. (2020). Individual corpora predict fast memory retrieval during reading. In *Proceedings of the Workshop on the Cognitive Aspects of the Lexicon* (pp. 1–11). Association for Computational Linguistics. https://aclanthology.org/2020.cogalex-1.1/

Hofmann, M. J., Remus, S., Biemann, C., Radach, R., & Kuchinke, L. (2022). Language models explain word reading times better than empirical predictability. *Frontiers in Artificial Intelligence, 4,* Article 730570. https://doi.org/10.3389/frai.2021.730570

Holm, S. (1979). A simple sequentially rejective multiple test procedure. *Scandinavian Journal of Statistics*, *6*(2), 65–70. https://doi.org/10.2307/4615733

Höltje, G., Lubahn, B., & Mecklinger, A. (2019). The congruent, the incongruent, and the unexpected: Event-related potentials unveil the processes involved in schematic encoding. *Neuropsychologia*, *131,* 285–293. https://doi.org/10.1016/j.neuropsychologia.2019.05.013

Huber, L., Finn, E. S., Chai, Y., Goebel, R., Stirnberg, R., Stöcker, T., Marrett, S., Uludağ, K., Kim, S.-G., Han, S., Bandettini, P. A., & Poser, B. A. (2021). Layer-dependent functional connectivity methods. *Progress in Neurobiology*, *207,* Article 101835. https://doi.org/10.1016/j.pneurobio.2020.101835

Huber, L. R., Poser, B. A., Bandettini, P. A., Arora, K., Wagstyl, K., Cho, S., Goense, J., Nothnagel, N., Morgan, A. T., van den Hurk, J., Müller, A. K., Reynolds, R. C., Glen, D. R., Goebel, R., & Gulban, O. F. (2021). LayNii: A software suite for layer-fMRI. *NeuroImage, 237,* Article 118091. https://doi.org/10.1016/j.neuroimage.2021.118091

Huettel, S. A., Song, A. W., & McCarthy, G. (2014). *Functional magnetic resonance imaging* (3rd ed.). Sinauer Associates.

Huster, R. J., Debener, S., Eichele, T., & Herrmann, C. S. (2012). Methods for simultaneous EEG-fMRI: An updated review. *Journal of Neuroscience*, *32*(18), 6053–6060. https://doi.org/10.1523/JNEUROSCI.0447-12.2012

Hutchison, K. A. (2003). Is semantic priming due to association strength or feature overlap? A microanalytic review. *Psychonomic Bulletin & Review*, *10*(4), 785–813. https://doi.org/10.3758/BF03196544

Hutchison, K. A. (2007). Attentional control and the relatedness proportion effect in semantic priming. *Journal of Experimental Psychology: Learning, Memory, and Cognition*, *33*(4), 645–662. https://doi.org/10.1037/0278-7393.33.4.645

Hutchison, K. A., Balota, D. A., Neely, J. H., Cortese, M. J., Cohen-Shikora, E. R., Tse, C.-S., Yap, M. J., Bengson, J. J., Niemeyer, D., & Buchanan, E. (2013). The Semantic Priming Project. *Behavior Research Methods*, *45*(4), 1099–1114. https://doi.org/10.3758/s13428-012-0304-z

IBM Corp. (2020). *IBM SPSS Statistics for Windows* (Version 27.0) [Computer software]. https://www.ibm.com/analytics/spss-statistics-software

Iglesias, J. E., Augustinack, J. C., Nguyen, K., Player, C. M., Player, A., Wright, M., Roy, N., Frosch, M. P., McKee, A. C., Wald, L. L., Fischl, B., Van Leemput, K., & Alzheimer's Disease Neuroimaging Initiative. (2015). A computational atlas of the hippocampal formation using ex vivo, ultra-high resolution MRI: Application to adaptive segmentation of in vivo MRI. *NeuroImage*, *115*, 117–137. https://doi.org/10.1016/j.neuroimage.2015.04.042

Jackson, R. L. (2021). The neural correlates of semantic control revisited. *NeuroImage*, *224,* Article 117444. https://doi.org/10.1016/j.neuroimage.2020.117444

Jasper, H. H. (1958). Report of the committee on methods of clinical examination in electroencephalography: 1957. *Electroencephalography and Clinical Neurophysiology*, *10*(2), 370–375. https://doi.org/10.1016/0013-4694(58)90053-1

JMP Statistical Discovery LLC. (2025). *JMP* (Version 19.0.3) [Computer software]. https://www.jmp.com/en/software/predictive-analytics-software

Jones, M. N., Willits, J. A., & Dennis, S. (2015). Models of semantic memory. In J. R. Busemeyer, Z. Wang, J. T. Townsend, & A. Eidels (Eds.), *The Oxford handbook of mathematical and computational psychology* (pp. 232–254). Oxford University Press. https://doi.org/10.1093/oxfordhb/9780199957996.013.11

Kahana, M. J. (2020). Computational models of memory search. *Annual Review of Psychology*, *71*, 107–138. https://doi.org/10.1146/annurev-psych-010418-103358

Kamp, S. M., Bader, R., & Mecklinger, A. (2017). ERP subsequent memory effects differ between inter-item and unitization encoding tasks. *Frontiers in Human Neuroscience*, *11*, Article 30. https://doi.org/10.3389/fnhum.2017.00030

Kandel, E. R., Dudai, Y., & Mayford, M. R. (2014). The molecular and systems biology of memory. *Cell*, *157*(1), 163–186. https://doi.org/10.1016/j.cell.2014.03.001

Kappenman, E. S., & Luck, S. J. (2010). The effects of electrode impedance on data quality and statistical significance in ERP recordings. *Psychophysiology*, *47*(5), 888–904. https://doi.org/10.1111/j.1469-8986.2010.01009.x

Keil, A., Debener, S., Gratton, G., Junghöfer, M., Kappenman, E. S., Luck, S. J., Luu, P., Miller, G. A., & Yee, C. M. (2014). Committee report: Publication guidelines and recommendations for studies using electroencephalography and magnetoencephalography. *Psychophysiology*, *51*(1), 1–21. https://doi.org/10.1111/psyp.12147

Kenward, M. G., & Roger, J. H. (1997). Small sample inference for fixed effects from restricted maximum likelihood. *Biometrika*, *84*(4), 983–997. https://doi.org/10.2307/2533558

Kiesel, A., Miller, J., Jolicoeur, P., & Brisson, B. (2008). Measurement of ERP latency differences: A comparison of single-participant and jackknife-based scoring methods. *Psychophysiology*, *45*(2), 250–274. https://doi.org/10.1111/j.1469-8986.2007.00618.x

Kimball, D. R., Smith, T. A., & Kahana, M. J. (2007). The fSAM model of false recall. *Psychological Review*, *114*(4), 954–993. https://doi.org/10.1037/0033-295X.114.4.954

Klein, A., Andersson, J., Ardekani, B. A., Ashburner, J., Avants, B., Chiang, M. C., Christensen, G. E., Collins, D. L., Gee, J., Hellier, P., Song, J. H., Jenkinson, M., Lepage, C., Rueckert, D., Thompson, P., Vercauteren, T., Woods, R. P., Mann, J. J., & Parsey, R. V. (2009). Evaluation of 14 nonlinear deformation algorithms applied to human brain MRI registration. *NeuroImage*, *46*(3), 786–802. https://doi.org/10.1016/j.neuroimage.2008.12.037

Klein, C. (2016). *Was erklärt semantisches Priming besser? Eine Gegenüberstellung differenzieller Kookkurrenzmaße zweiter Ordnung* [Unpublished bachelor's thesis]. Bergische Universität Wuppertal.

Klein, C. (2018). *Hippocampale Plastizität bei der Konsolidierung neuartiger Gedächtnisengramme: Eine fMRT-Studie* [Unpublished master's thesis]. Bergische Universität Wuppertal.

Klein, C., & Hofmann, M. J. (2026). ERP correlates of associative priming and subsequent memory effects: Evidence from sentence-embedded paired-associate learning. *International Journal of Psychophysiology*, *228*, Article 113458. https://doi.org/10.1016/j.ijpsycho.2026.113458

Kliegl, O., & Bäuml, K.-H. T. (2021). Buildup and release from proactive interference – Cognitive and neural mechanisms. *Neuroscience & Biobehavioral Reviews*, *120*, 264–278. https://doi.org/10.1016/j.neubiorev.2020.10.028

Klimesch, W. (1999). EEG alpha and theta oscillations reflect cognitive and memory performance: A review and analysis. *Brain Research Reviews*, *29*(2–3), 169–195. https://doi.org/10.1016/s0165-0173(98)00056-3

Kounios, J., Smith, R. W., Yang, W., Bachman, P., & D'Esposito, M. (2001). Cognitive association formation in human memory revealed by spatiotemporal brain imaging. *Neuron*, *29*(1), 297–306. https://doi.org/10.1016/s0896-6273(01)00199-4

Kreidler, S. M., Muller, K. E., Grunwald, G. K., Ringham, B. M., Coker-Dukowitz, Z. T., Sakhadeo, U. R., Barón, A. E., & Glueck, D. H. (2013). GLIMMPSE: Online power computation for linear models with and without a baseline covariate. *Journal of Statistical Software*, *54*(10), 1–26. https://doi.org/10.18637/jss.v054.i10

Kreitz, S., Mennecke, A., Konerth, L., Rösch, J., Nagel, A. M., Laun, F. B., Uder, M., Dörfler, A., & Hess, A. (2023). 3T vs. 7T fMRI: Capturing early human memory consolidation after motor task utilizing the observed higher functional specificity of 7T. *Frontiers in Neuroscience*, *17*, Article 1215400. https://doi.org/10.3389/fnins.2023.1215400

Kriegeskorte, N., & Douglas, P. K. (2018). Cognitive computational neuroscience. *Nature Neuroscience*, *21*(9), 1148–1160. https://doi.org/10.1038/s41593-018-0210-5

Kriegeskorte, N., Mur, M., & Bandettini, P. (2008). Representational similarity analysis: Connecting the branches of systems neuroscience. *Frontiers in Systems Neuroscience*, *2*, Article 4. https://doi.org/10.3389/neuro.06.004.2008

Kumar, A. A., Balota, D. A., & Steyvers, M. (2020). Distant connectivity and multiple-step priming in large-scale semantic networks. *Journal of Experimental Psychology: Learning, Memory, and Cognition, 46*(12), 2261–2276. https://doi.org/10.1037/xlm0000793

Kumaran, D., Hassabis, D., & McClelland, J. L. (2016). What learning systems do intelligent agents need? Complementary learning systems theory updated. *Trends in Cognitive Sciences*, *20*(7), 512–534. https://doi.org/10.1016/j.tics.2016.05.004

Kumaran, D., & McClelland, J. L. (2012). Generalization through the recurrent interaction of episodic memories: A model of the hippocampal system. *Psychological Review*, *119*(3), 573–616. https://doi.org/10.1037/a0028681

Kutas, M., & Federmeier, K. D. (2000). Electrophysiology reveals semantic memory use in language comprehension. *Trends in Cognitive Sciences*, *4*(12), 463–470. https://doi.org/10.1016/s1364-6613(00)01560-6

Kutas, M., & Federmeier, K. D. (2011). Thirty years and counting: Finding meaning in the N400 component of the event-related brain potential (ERP). *Annual Review of Psychology*, *62*, 621–647. https://doi.org/10.1146/annurev.psych.093008.131123

Lambon Ralph, M. A., Jefferies, E., Patterson, K., & Rogers, T. T. (2017). The neural and computational bases of semantic cognition. *Nature Reviews Neuroscience*, *18*(1), 42–55. https://doi.org/10.1038/nrn.2016.150

Lau, E. F., Phillips, C., & Poeppel, D. (2008). A cortical network for semantics: (de)constructing the N400. *Nature Reviews Neuroscience*, *9*, 920–933. https://doi.org/10.1038/nrn2532

Lauritzen, M. (2005). Reading vascular changes in brain imaging: Is dendritic calcium the key? *Nature Reviews Neuroscience*, *6*(1), 77–85. https://doi.org/10.1038/nrn1589

Lawrence, S. J. D., van Mourik, T., Kok, P., Koopmans, P. J., Norris, D. G., & de Lange, F. P. (2018). Laminar organization of working memory signals in human visual cortex. *Current Biology*, *28*(21), 3435–3440.e4. https://doi.org/10.1016/j.cub.2018.08.043

Leckey, M., & Federmeier, K. D. (2020). The P3b and P600(s): Positive contributions to language comprehension. *Psychophysiology*, *57*(7), e13351. https://doi.org/10.1111/psyp.13351

Lee, H., GoodSmith, D., & Knierim, J. J. (2020). Parallel processing streams in the hippocampus. *Current Opinion in Neurobiology*, *64*, 127–134. https://doi.org/10.1016/j.conb.2020.03.004

Lee, H., Wang, C., Deshmukh, S. S., & Knierim, J. J. (2015). Neural population evidence of functional heterogeneity along the CA3 transverse axis: Pattern completion versus pattern separation. *Neuron*, *87*(5), 1093–1105. https://doi.org/10.1016/j.neuron.2015.07.012

Lee, S.-M., Henson, R. N., & Lin, C.-Y. (2020). Neural correlates of repetition priming: A coordinate-based meta-analysis of fMRI studies. *Frontiers in Human Neuroscience*, *14*, Article 565114. https://doi.org/10.3389/fnhum.2020.565114

Leutgeb, J. K., Leutgeb, S., Moser, M. B., & Moser, E. I. (2007). Pattern separation in the dentate gyrus and CA3 of the hippocampus. *Science*, *315*(5814), 961–966. https://doi.org/10.1126/science.1135801

Li, B., Gao, C., Wang, W., & Guo, C. (2020). The effect of conceptual priming on subsequent familiarity: Behavioral and electrophysiological evidence. *Biological Psychology*, *149*, Article 107783. https://doi.org/10.1016/j.biopsycho.2019.107783

Libby, L. A., Ekstrom, A. D., Ragland, J. D., & Ranganath, C. (2012). Differential connectivity of perirhinal and parahippocampal cortices within human hippocampal subregions revealed by high-resolution functional imaging. *Journal of Neuroscience*, *32*(19), 6550–6560. https://doi.org/10.1523/JNEUROSCI.3711-11.2012

Loaiza, V. M., & McCabe, D. P. (2012). Temporal-contextual processing in working memory: Evidence from delayed cued recall and delayed free recall tests. *Memory & Cognition*, *40*(2), 191–203. https://doi.org/10.3758/s13421-011-0148-2

Lucas, M. (2000). Semantic priming without association: A meta-analytic review. *Psychonomic Bulletin & Review*, *7*(4), 618–630. https://doi.org/10.3758/BF03212999

Luck, S. J., & Gaspelin, N. (2017). How to get statistically significant effects in any ERP experiment (and why you shouldn't). *Psychophysiology*, *54*(1), 146–157. https://doi.org/10.1111/psyp.12639

Luck, S. J., Stewart, A. X., Simmons, A. M., & Rhemtulla, M. (2021). Standardized measurement error: A universal metric of data quality for averaged event-related potentials. *Psychophysiology*, *58*(6), e13793. https://doi.org/10.1111/psyp.13793

Ma, W. J., Husain, M., & Bays, P. M. (2014). Changing concepts of working memory. *Nature Neuroscience*, *17*(3), 347–356. https://doi.org/10.1038/nn.3655

Maass, A., Schütze, H., Speck, O., Yonelinas, A., Tempelmann, C., Heinze, H. J., Berron, D., Cardenas-Blanco, A., Brodersen, K. H., Stephan, K. E., & Düzel, E. (2014). Laminar activity in the hippocampus and entorhinal cortex related to novelty and episodic encoding. *Nature Communications*, *5*, Article 5547. https://doi.org/10.1038/ncomms6547

Magistretti, P. J., & Allaman, I. (2015). A cellular perspective on brain energy metabolism and functional imaging. *Neuron*, *86*(4), 883–901. https://doi.org/10.1016/j.neuron.2015.03.035

Mandera, P., Keuleers, E., & Brysbaert, M. (2017). Explaining human performance in psycholinguistic tasks with models of semantic similarity based on prediction and counting: A review and empirical validation. *Journal of Memory and Language*, *92*, 57–78. https://doi.org/10.1016/j.jml.2016.04.001

Marr, D. (1970). A theory for cerebral neocortex. *Proceedings of the Royal Society B: Biological Sciences*, *176*(1043), 161–234. https://doi.org/10.1098/rspb.1970.0040

Mayes, A., Montaldi, D., & Migo, E. (2007). Associative memory and the medial temporal lobes. *Trends in Cognitive Sciences*, *11*(3), 126–135. https://doi.org/10.1016/j.tics.2006.12.003

McClelland, J. L., & Goddard, N. H. (1996). Considerations arising from a complementary learning systems perspective on hippocampus and neocortex. *Hippocampus*, *6*(6), 654–665. https://doi.org/10.1002/(SICI)1098-1063(1996)6:6<654::AID-HIPO8>3.0.CO;2-G

McClelland, J. L., McNaughton, B. L., & O'Reilly, R. C. (1995). Why there are complementary learning systems in the hippocampus and neocortex: Insights from the successes and failures of connectionist models of learning and memory. *Psychological Review*, *102*(3), 419–457. https://doi.org/10.1037/0033-295X.102.3.419

McClelland, J. L., & Rumelhart, D. E. (1981). An interactive activation model of context effects in letter perception: I. An account of basic findings. *Psychological Review*, *88*(5), 375–407. https://doi.org/10.1037/0033-295X.88.5.375

McCurdy, R. A., & Duff, M. C. (2025). Semantic memory, traumatic brain injury, and the iceberg effect: What deficits may lie below the surface? *American Journal of Speech-Language Pathology*, *34*(3S), 1878–1895. https://doi.org/10.1044/2024_AJSLP-24-00145

McNamara, D. S. (2011). Computational methods to extract meaning from text and advance theories of human cognition. *Topics in Cognitive Science*, *3*(1), 3–17. https://doi.org/10.1111/j.1756-8765.2010.01117.x

McNamara, T. P. (2005). *Semantic priming: Perspectives from memory and word recognition*. Psychology Press. https://doi.org/10.4324/9780203338001

McRae, K., & Jones, M. (2013). Semantic memory. In D. Reisberg (Ed.), *The Oxford handbook of cognitive psychology* (pp. 206–219). Oxford University Press. https://doi.org/10.1093/oxfordhb/9780195376746.013.0014

Mecklinger, A., & Kamp, S.-M. (2023). Observing memory encoding while it unfolds: Functional interpretation and current debates regarding ERP subsequent memory effects. *Neuroscience & Biobehavioral Reviews*, *153*, Article 105347. https://doi.org/10.1016/j.neubiorev.2023.105347

Mecklinger, A., & Müller, N. (1996). Dissociations in the processing of "what" and "where" information in working memory: An event-related potential analysis. *Journal of Cognitive Neuroscience*, *8*(5), 453–473. https://doi.org/10.1162/jocn.1996.8.5.453

Meltzer, J. A., & Constable, R. T. (2005). Activation of human hippocampal formation reflects success in both encoding and cued recall of paired associates. *NeuroImage*, *24*(2), 384–397. https://doi.org/10.1016/j.neuroimage.2004.09.001

Meng, Y., Ye, X., & Gonsalves, B. D. (2014). Neural processing of recollection, familiarity and priming at encoding: Evidence from a forced-choice recognition paradigm. *Brain Research*, *1585*, 72–82. https://doi.org/10.1016/j.brainres.2014.08.024

Menon, R. S. (2002). Postacquisition suppression of large-vessel BOLD signals in high-resolution fMRI. *Magnetic Resonance in Medicine*, *47*(1), 1–9. https://doi.org/10.1002/mrm.10041

Menon, R. S., & Kim, S. G. (1999). Spatial and temporal limits in cognitive neuroimaging with fMRI. *Trends in Cognitive Sciences*, *3*(6), 207–216. https://doi.org/10.1016/s1364-6613(99)01329-7

Merhav, M., Karni, A., & Gilboa, A. (2014). Neocortical catastrophic interference in healthy and amnesic adults: A paradoxical matter of time. *Hippocampus*, *24*(12), 1653–1662. https://doi.org/10.1002/hipo.22353

Meyer, D. E., & Schvaneveldt, R. W. (1971). Facilitation in recognizing pairs of words: Evidence of a dependence between retrieval operations. *Journal of Experimental Psychology*, *90*(2), 227–234. https://doi.org/10.1037/h0031564

Michel, C. M., & Brunet, D. (2019). EEG source imaging: A practical review of the analysis steps. *Frontiers in Neurology*, *10*, Article 325. https://doi.org/10.3389/fneur.2019.00325

Mikolov, T., Chen, K., Corrado, G. S., & Dean, J. (2013). *Efficient estimation of word representations in vector space* [Preprint]. arXiv. https://doi.org/10.48550/arXiv.1301.3781

Morey, R. D. (2008). Confidence intervals from normalized data: A correction to Cousineau (2005). *Tutorials in Quantitative Methods for Psychology*, *4*(2), 61–64. https://doi.org/10.20982/tqmp.04.2.p061

Moser, M. B., & Moser, E. I. (1998). Functional differentiation in the hippocampus. *Hippocampus*, *8*(6), 608–619. https://doi.org/10.1002/(SICI)1098-1063(1998)8:6<608::AID-HIPO3>3.0.CO;2-7

Müller, T., Cotterell, R., Fraser, A., & Schütze, H. (2015). Joint lemmatization and morphological tagging with Lemming. In *Proceedings of the 2015 Conference on Empirical Methods in Natural Language Processing (EMNLP)* (pp. 2268–2274). Association for Computational Linguistics. https://doi.org/10.18653/v1/D15-1272

Münte, T. F., Urbach, T. P., Düzel, E., & Kutas, M. (2000). Event-related brain potentials in the study of human cognition and neuropsychology. In F. Boller, J. Grafman, & G. Rizzolatti (Eds.), *Handbook of neuropsychology* (2nd ed., Vol. 1, pp. 139–235). Elsevier.

Nairne, J. S. (2002). The myth of the encoding-retrieval match. *Memory*, *10*(5–6), 389–395. https://doi.org/10.1080/09658210244000216

Nakagawa, S., Johnson, P. C. D., & Schielzeth, H. (2017). The coefficient of determination R^2 and intra-class correlation coefficient from generalized linear mixed-effects models revisited and expanded. *Journal of the Royal Society Interface*, *14*(134), Article 20170213. https://doi.org/10.1098/rsif.2017.0213

Neely, J. H. (1977). Semantic priming and retrieval from lexical memory: Roles of inhibitionless spreading activation and limited-capacity attention. *Journal of Experimental Psychology: General*, *106*(3), 226–254. https://doi.org/10.1037/0096-3445.106.3.226

Neely, J. H. (1991). Semantic priming effects in visual word recognition: A selective review of current findings and theories. In D. Besner & G. W. Humphreys (Eds.), *Basic processes in reading: Visual word recognition* (pp. 264–336). Erlbaum.

Nelson, D. L., McEvoy, C. L., & Schreiber, T. A. (2004). The University of South Florida free association, rhyme, and word fragment norms. *Behavior Research Methods, Instruments, & Computers*, *36*(3), 402–407. https://doi.org/10.3758/BF03195588

Neurobehavioral Systems, Inc. (2015). *Presentation* (Version 18.1) [Computer software]. https://www.neurobs.com/

Neville, H. J., Kutas, M., Chesney, G., & Schmidt, A. L. (1986). Event-related brain potentials during initial encoding and recognition memory of congruous and incongruous words. *Journal of Memory and Language*, *25*(1), 75–92. https://doi.org/10.1016/0749-596X(86)90022-7

Norman, K. A., & O'Reilly, R. C. (2003). Modeling hippocampal and neocortical contributions to recognition memory: A complementary-learning-systems approach. *Psychological Review*, *110*(4), 611–646. https://doi.org/10.1037/0033-295X.110.4.611

Ogawa, S., Lee, T. M., Kay, A. R., & Tank, D. W. (1990). Brain magnetic resonance imaging with contrast dependent on blood oxygenation. *Proceedings of the National Academy of Sciences of the United States of America*, *87*(24), 9868–9872. https://doi.org/10.1073/pnas.87.24.9868

Okada, K., Vilberg, K. L., & Rugg, M. D. (2012). Comparison of the neural correlates of retrieval success in tests of cued recall and recognition memory. *Human Brain Mapping*, *33*(3), 523–533. https://doi.org/10.1002/hbm.21229

Olejniczak, P. (2006). Neurophysiologic basis of EEG. *Journal of Clinical Neurophysiology*, *23*(3), 186–189. https://doi.org/10.1097/01.wnp.0000220079.61973.6c

O'Reilly, R. C., Bhattacharyya, R., Howard, M. D., & Ketz, N. (2014). Complementary learning systems. *Cognitive Science*, *38*(6), 1229–1248. https://doi.org/10.1111/j.1551-6709.2011.01214.x

Otten, L. J., & Rugg, M. D. (2001). Electrophysiological correlates of memory encoding are task-dependent. *Cognitive Brain Research*, *12*(1), 11–18. https://doi.org/10.1016/S0926-6410(01)00015-5

Packard, P. A., Rodríguez-Fornells, A., Bunzeck, N., Nicolás, B., de Diego-Balaguer, R., & Fuentemilla, L. (2017). Semantic congruence accelerates the onset of the neural signals of successful memory encoding. *Journal of Neuroscience*, *37*(2), 291–301. https://doi.org/10.1523/JNEUROSCI.1622-16.2017

Pais-Roldán, P., Yun, S. D., & Shah, N. J. (2022). Pre-processing of sub-millimeter GE-BOLD fMRI data for laminar applications. *Frontiers in Neuroimaging*, *1*, Article 869454. https://doi.org/10.3389/fnimg.2022.869454

Paller, K. A. (1990). Recall and stem-completion priming have different electrophysiological correlates and are modified differentially by directed forgetting. *Journal of Experimental Psychology: Learning, Memory, and Cognition*, *16*(6), 1021–1032. https://doi.org/10.1037/0278-7393.16.6.1021

Paller, K. A., & Kutas, M. (1992). Brain potentials during memory retrieval provide neurophysiological support for the distinction between conscious recollection and priming. *Journal of Cognitive Neuroscience*, *4*(4), 375–392. https://doi.org/10.1162/jocn.1992.4.4.375

Paller, K. A., Kutas, M., & Mayes, A. R. (1987). Neural correlates of encoding in an incidental learning paradigm. *Electroencephalography and Clinical Neurophysiology*, *67*(4), 360–371. https://doi.org/10.1016/0013-4694(87)90124-6

Paller, K. A., & Wagner, A. D. (2002). Observing the transformation of experience into memory. *Trends in Cognitive Sciences*, *6*(2), 93–102. https://doi.org/10.1016/S1364-6613(00)01845-3

Pennington, J., Socher, R., & Manning, C. D. (2014). GloVe: Global vectors for word representation. In *Proceedings of the 2014 Conference on Empirical Methods in Natural Language Processing (EMNLP)* (pp. 1532–1543). Association for Computational Linguistics. https://doi.org/10.3115/v1/D14-1162

Peirce, J. W., Gray, J. R., Simpson, S., MacAskill, M. R., Höchenberger, R., Sogo, H., Kastman, E., & Lindeløv, J. (2019). PsychoPy2: Experiments in behavior made easy. *Behavior Research Methods*, *51*(1), 195–203. https://doi.org/10.3758/s13428-018-01193-y

Perconti, P., & Plebe, A. (2020). Deep learning and cognitive science. *Cognition*, *203*, Article 104365. https://doi.org/10.1016/j.cognition.2020.104365

Petzold, G. C., & Murthy, V. N. (2011). Role of astrocytes in neurovascular coupling. *Neuron*, *71*(5), 782–797. https://doi.org/10.1016/j.neuron.2011.08.009

Pfaffenrot, V., Bouyeure, A., Gomes, C. A., Kashyap, S., Axmacher, N., & Norris, D. G. (2025). Characterizing BOLD activation patterns in the human hippocampus with laminar fMRI. *Imaging Neuroscience*, *3*, Article imag_a_00532. https://doi.org/10.1162/imag_a_00532

Picton, T. W., Bentin, S., Berg, P., Donchin, E., Hillyard, S. A., Johnson, R., Jr., Miller, G. A., Ritter, W., Ruchkin, D. S., Rugg, M. D., & Taylor, M. J. (2000). Guidelines for using human event-related potentials to study cognition: Recording standards and publication criteria. *Psychophysiology*, *37*(2), 127–152. https://doi.org/10.1111/1469-8986.3720127

Plaut, D. C., & Booth, J. R. (2000). Individual and developmental differences in semantic priming: Empirical and computational support for a single-mechanism account of lexical processing. *Psychological Review*, *107*(4), 786–823. https://doi.org/10.1037/0033-295X.107.4.786

Plaut, D. C., & McClelland, J. L. (2010). Locating object knowledge in the brain: Comment on Bowers's (2009) attempt to revive the grandmother cell hypothesis. *Psychological Review*, *117*(1), 284–290. https://doi.org/10.1037/a0017101

Polich, J. (2007). Updating P300: An integrative theory of P3a and P3b. *Clinical Neurophysiology*, *118*(10), 2128–2148. https://doi.org/10.1016/j.clinph.2007.04.019

Polich, J. (2020). 50+ years of P300: Where are we now*? Psychophysiology*, *57*(7), e13616. https://doi.org/10.1111/psyp.13616

Polich, J., & Kok, A. (1995). Cognitive and biological determinants of P300: An integrative review. *Biological Psychology*, *41*(2), 103–146. https://doi.org/10.1016/0301-0511(95)05130-9

Polimeni, J. R., Fischl, B., Greve, D. N., & Wald, L. L. (2010). Laminar analysis of 7T BOLD using an imposed spatial activation pattern in human V1. *NeuroImage*, *52*(4), 1334–1346. https://doi.org/10.1016/j.neuroimage.2010.05.005

Pooley, R. A. (2005). Fundamental physics of MR imaging. *RadioGraphics*, *25*(4), 1087–1099. https://doi.org/10.1148/rg.254055027

Poppenk, J., Evensmoen, H. R., Moscovitch, M., & Nadel, L. (2013). Long-axis specialization of the human hippocampus. *Trends in Cognitive Sciences*, *17*(5), 230–240. https://doi.org/10.1016/j.tics.2013.03.005

Poppenk, J., & Moscovitch, M. (2011). A hippocampal marker of recollection memory ability among healthy young adults: Contributions of posterior and anterior segments. *Neuron*, *72*(6), 931–937. https://doi.org/10.1016/j.neuron.2011.10.014

Preston, A. R., & Eichenbaum, H. (2013). Interplay of hippocampus and prefrontal cortex in memory. *Current Biology*, *23*(17), R764–R773. https://doi.org/10.1016/j.cub.2013.05.041

Price, C. J., & Devlin, J. T. (2011). The interactive account of ventral occipitotemporal contributions to reading. *Trends in Cognitive Sciences*, *15*(6), 246–253. https://doi.org/10.1016/j.tics.2011.04.001

Prudent, V., Kumar, A., Liu, S., Wiggins, G., Malaspina, D., & Gonen, O. (2010). Human hippocampal subfields in young adults at 7.0 T: Feasibility of imaging. *Radiology*, *254*(3), 900–906. https://doi.org/10.1148/radiol.09090897

Pykett, I. L., Newhouse, J. H., Buonanno, F. S., Brady, T. J., Goldman, M. R., Kistler, J. P., & Pohost, G. M. (1982). Principles of nuclear magnetic resonance imaging. *Radiology*, *143*(1), 157–168. https://doi.org/10.1148/radiology.143.1.7038763

Quasthoff, U., Richter, M., & Biemann, C. (2006). Corpus portal for search in monolingual corpora. In *Proceedings of LREC-06* (pp. 10–13). European Language Resources Association (ELRA). http://www.lrec-conf.org/proceedings/lrec2006/pdf/641_pdf.pdf

Quian Quiroga, R., Kreiman, G., Koch, C., & Fried, I. (2008). Sparse but not "Grandmother-cell" coding in the medial temporal lobe. *Trends in Cognitive Sciences*, *12*(3), 87–91. https://doi.org/10.1016/j.tics.2007.12.003

Quillian, M. R. (1967). Word concepts: A theory and simulation of some basic semantic capabilities. *Behavioral Science*, *12*(5), 410–430. https://doi.org/10.1002/bs.3830120511

Radach, R., & Hofmann, M. (2016). Graphematische Verarbeitung beim Lesen von Wörtern. In U. Domahs & B. Primus (Eds.), *Handbuch Laut, Gebärde, Buchstabe* (pp. 455–473). De Gruyter. https://doi.org/10.1515/9783110295993-025

Ramirez, S., Liu, X., Lin, P. A., Suh, J., Pignatelli, M., Redondo, R. L., Ryan, T. J., & Tonegawa, S. (2013). Creating a false memory in the hippocampus. *Science*, *341*(6144), 387–391. https://doi.org/10.1126/science.1239073

Ranganath, C., & Ritchey, M. (2012). Two cortical systems for memory-guided behavior. *Nature Reviews Neuroscience*, *13*(10), 713–726. https://doi.org/10.1038/nrn3338

Rapp, D. N., & Samuel, A. G. (2002). A reason to rhyme: Phonological and semantic influences on lexical access. *Journal of Experimental Psychology: Learning, Memory, and Cognition*, *28*(3), 564–571. https://doi.org/10.1037/0278-7393.28.3.564

Roediger, H. L., & Butler, A. C. (2011). The critical role of retrieval practice in long-term retention. *Trends in Cognitive Sciences*, *15*(1), 20–27. https://doi.org/10.1016/j.tics.2010.09.003

Roediger, H. L., & McDermott, K. B. (1995). Creating false memories: Remembering words not presented in lists. *Journal of Experimental Psychology: Learning, Memory, and Cognition*, *21*(4), 803–814. https://doi.org/10.1037/0278-7393.21.4.803

Rölke, A., Franke, N., Biemann, C., Radach, R., Jacobs, A. M., & Hofmann, M. J. (2018). A novel co-occurrence-based approach to predict pure associative and semantic priming. *Psychonomic Bulletin & Review*, *25*(4), 1488–1493. https://doi.org/10.3758/s13423-018-1453-6

Rölke, A., & Hofmann, M. J. (2020). Functional connectivity of the left inferior frontal gyrus during semantic priming. *Neuroscience Letters*, *735*, Article 135236. https://doi.org/10.1016/j.neulet.2020.135236

Rölke-Wellmann, A. (2021). *The interplay of simulation models and neuroimaging: Associative and semantic effects on lexical processing* [Doctoral dissertation, Bergische Universität Wuppertal]. https://doi.org/10.25926/BUW/0-17

Rolls, E. T. (2007). An attractor network in the hippocampus: Theory and neurophysiology. *Learning & Memory*, *14*(11), 714–731. https://doi.org/10.1101/lm.631207

Rolls, E. T., & Treves, A. (2024). A theory of hippocampal function: New developments. *Progress in Neurobiology*, *238*, Article 102636. https://doi.org/10.1016/j.pneurobio.2024.102636

Rugg, M. D., & Curran, T. (2007). Event-related potentials and recognition memory. *Trends in Cognitive Sciences*, *11*(6), 251–257. https://doi.org/10.1016/j.tics.2007.04.004

Rugg, M. D., Fletcher, P. C., Allan, K., Frith, C. D., Frackowiak, R. S., & Dolan, R. J. (1998). Neural correlates of memory retrieval during recognition memory and cued recall. *NeuroImage*, *8*(3), 262–273. https://doi.org/10.1006/nimg.1998.0363

Rugg, M. D., Mark, R. E., Walla, P., Schloerscheidt, A. M., Birch, C. S., & Allan, K. (1998). Dissociation of the neural correlates of implicit and explicit memory. *Nature*, *392*(6676), 595–598. https://doi.org/10.1038/33396

Rumelhart, D. E., & McClelland, J. L. (Eds.). (1986). *Parallel distributed processing: Explorations in the microstructure of cognition: Vol. 1. Foundations*. MIT Press. https://doi.org/10.7551/mitpress/5236.001.0001

Sahay, A., Scobie, K. N., Hill, A. S., O'Carroll, C. M., Kheirbek, M. A., Burghardt, N. S., Fenton, A. A., Dranovsky, A., & Hen, R. (2011). Increasing adult hippocampal neurogenesis is sufficient to improve pattern separation. *Nature*, *472*(7344), 466–470. https://doi.org/10.1038/nature09817

Sahlgren, M. (2006). *The word-space model: Using distributional analysis to represent syntagmatic and paradigmatic relations between words in high-dimensional vector spaces* [Doctoral dissertation, Stockholm University].

Sanquist, T. F., Rohrbaugh, J. W., Syndulko, K., & Lindsley, D. B. (1980). Electrocortical signs of levels of processing: Perceptual analysis and recognition memory. *Psychophysiology*, *17*(6), 568–576. https://doi.org/10.1111/j.1469-8986.1980.tb02299.x

Savic, O., Unger, L., & Sloutsky, V. (2020). Becoming organized: How simple learning mechanisms may shape the development of rich semantic knowledge. In S. Denison, M. Mack, Y. Xu, & B. C. Armstrong (Eds.), *Proceedings of the 42nd Annual Conference of the Cognitive Science Society* (pp. 137–143). Cognitive Science Society. https://escholarship.org/uc/item/92g4141z

Schapiro, A. C., Turk-Browne, N. B., Botvinick, M. M., & Norman, K. A. (2017). Complementary learning systems within the hippocampus: A neural network modelling approach to reconciling episodic memory with statistical learning. *Philosophical Transactions of the Royal Society B: Biological Sciences*, *372*(1711), Article 20160049. https://doi.org/10.1098/rstb.2016.0049

Schlichting, M. L., & Preston, A. R. (2015). Memory integration: Neural mechanisms and implications for behavior. *Current Opinion in Behavioral Sciences*, *1*, 1–8. https://doi.org/10.1016/j.cobeha.2014.07.005

Schott, B., Richardson-Klavehn, A., Heinze, H. J., & Düzel, E. (2002). Perceptual priming versus explicit memory: Dissociable neural correlates at encoding. *Journal of Cognitive Neuroscience*, *14*(4), 578–592. https://doi.org/10.1162/08989290260045828

Skinner, B. F. (1948). 'Superstition' in the pigeon. *Journal of Experimental Psychology*, *38*(2), 168–172. https://doi.org/10.1037/h0055873

Smith, L., & Yu, C. (2008). Infants rapidly learn word-referent mappings via cross-situational statistics. *Cognition*, *106*(3), 1558–1568. https://doi.org/10.1016/j.cognition.2007.06.010

Smolek, A., & Kapatsinski, V. (2023). Syntagmatic paradigms: Learning correspondence from contiguity. *Morphology*, *33*(3), 287–334. https://doi.org/10.1007/s11525-023-09411-w

Snyder, J. S. (2019). Recalibrating the relevance of adult neurogenesis. *Trends in Neurosciences*, *42*(3), 164–178. https://doi.org/10.1016/j.tins.2018.12.001

Sokolovič, L., & Hofmann, M. J. (2024). Mnemonic vs. executive contributions to the N400: A connectionist approach to false memories. *Computational Brain & Behavior*, *7*(3), 357–377. https://doi.org/10.1007/s42113-024-00210-y

Sokolovič, L., Kukolja, J., & Hofmann, M. (2026). A neurocognitive interactive activation model of semantic priming in lexical decisions. Scientific Reports, 16, Article 19183. https://doi.org/10.1038/s41598-026-58866-4

Spens, E., & Burgess, N. (2024). A generative model of memory construction and consolidation. *Nature Human Behaviour*, *8*(3), 526–543. https://doi.org/10.1038/s41562-023-01799-z

Squire, L. R. (1992). Memory and the hippocampus: A synthesis from findings with rats, monkeys and humans. *Psychological Review*, *99*(2), 195–231. https://doi.org/10.1037/0033-295x.99.2.195

Squire, L. R. (2004). Memory systems of the brain: A brief history and current perspective. *Neurobiology of Learning and Memory*, *82*(3), 171–177. https://doi.org/10.1016/j.nlm.2004.06.005

Squire, L. R., & Dede, A. J. O. (2015). Conscious and unconscious memory systems. *Cold Spring Harbor Perspectives in Biology*, *7*(3), e021667. https://doi.org/10.1101/cshperspect.a021667

Squire, L. R., & Wixted, J. T. (2011). The cognitive neuroscience of human memory since H.M. *Annual Review of Neuroscience*, *34*, 259–288. https://doi.org/10.1146/annurev-neuro-061010-113720

Staresina, B. P., & Davachi, L. (2008). Selective and shared contributions of the hippocampus and perirhinal cortex to episodic item and associative encoding. *Journal of Cognitive Neuroscience*, *20*(8), 1478–1489. https://doi.org/10.1162/jocn.2008.20104

Staresina, B. P., Henson, R. N. A., Kriegeskorte, N., & Alink, A. (2012). Episodic reinstatement in the medial temporal lobe. *Journal of Neuroscience*, *32*(50), 18150–18156. https://doi.org/10.1523/JNEUROSCI.4156-12.2012

Steyvers, M., & Tenenbaum, J. B. (2005). The large-scale structure of semantic networks: Statistical analyses and a model of semantic growth. *Cognitive Science*, *29*(1), 41–78. https://doi.org/10.1207/s15516709cog2901_3

Stuellein, N., Radach, R. R., Jacobs, A. M., & Hofmann, M. J. (2016). No one way ticket from orthography to semantics in recognition memory: N400 and P200 effects of associations. *Brain Research*, *1639*, 88–98. https://doi.org/10.1016/j.brainres.2016.02.029

Sun, J., Osth, A. F., & Feuerriegel, D. (2024). The late positive event-related potential component is time locked to the decision in recognition memory tasks. *Cortex*, *176*, 194–208. https://doi.org/10.1016/j.cortex.2024.04.017

Sun, W., Advani, M., Spruston, N., Saxe, A., & Fitzgerald, J. E. (2023). Organizing memories for generalization in complementary learning systems. *Nature Neuroscience*, *26*(10), 1438–1448. https://doi.org/10.1038/s41593-023-01382-9

Suthana, N., Ekstrom, A., Moshirvaziri, S., Knowlton, B., & Bookheimer, S. (2011). Dissociations within human hippocampal subregions during encoding and retrieval of spatial information. *Hippocampus*, *21*(7), 694–701. https://doi.org/10.1002/hipo.20833

Takehara, K., Kawahara, S., & Kirino, Y. (2003). Time-dependent reorganization of the brain components underlying memory retention in trace eyeblink conditioning. *Journal of Neuroscience*, *23*(30), 9897–9905. https://doi.org/10.1523/JNEUROSCI.23-30-09897.2003

Taylor, J. R., Buratto, L. G., & Henson, R. N. (2013). Behavioral and neural evidence for masked conceptual priming of recollection. *Cortex*, *49*(6), 1511–1525. https://doi.org/10.1016/j.cortex.2012.08.008

The MathWorks, Inc. (2017). *MATLAB* (R2017b) [Computer software]. https://www.mathworks.com/products/matlab.html

The MathWorks, Inc. (2022). *MATLAB* (R2022b) [Computer software]. https://www.mathworks.com/products/matlab.html

Tse, D., Langston, R. F., Kakeyama, M., Bethus, I., Spooner, P. A., Wood, E. R., Witter, M. P., & Morris, R. G. (2007). Schemas and memory consolidation. *Science*, *316*(5821), 76–82. https://doi.org/10.1126/science.1135935

Tulving, E. (2002). Episodic memory: From mind to brain. *Annual Review of Psychology*, *53*(1), 1–25. https://doi.org/10.1146/annurev.psych.53.100901.135114

Tulving, E., & Pearlstone, Z. (1966). Availability versus accessibility of information in memory for words. *Journal of Verbal Learning and Verbal Behavior*, *5*(4), 381–391. https://doi.org/10.1016/S0022-5371(66)80048-8

Tulving, E., Schacter, D. L., & Stark, H. A. (1982). Priming effects in word fragment completion are independent of recognition memory. *Journal of Experimental Psychology: Learning, Memory, and Cognition*, *8*(4), 336–342. https://doi.org/10.1037/0278-7393.8.4.336

Ullman, M. T. (2004). Contributions of memory circuits to language: The declarative/procedural model. *Cognition*, *92*(2), 231–270. https://doi.org/10.1016/j.cognition.2003.10.008

Ulrich, M., Hoenig, K., Grön, G., & Kiefer, M. (2013). Brain activation during masked and unmasked semantic priming: Commonalities and differences. *Journal of Cognitive Neuroscience*, *25*(12), 2216–2229. https://doi.org/10.1162/jocn_a_00449

Unger, L., Savic, O., & Sloutsky, V. M. (2020). Statistical regularities shape semantic organization throughout development. *Cognition*, *198*, Article 104190. https://doi.org/10.1016/j.cognition.2020.104190

Van den Bussche, E., Van den Noortgate, W., & Reynvoet, B. (2009). Mechanisms of masked priming: A meta-analysis. *Psychological Bulletin*, *135*(3), 452–477. https://doi.org/10.1037/a0015329

Van Kesteren, M. T., Ruiter, D. J., Fernández, G., & Henson, R. N. (2012). How schema and novelty augment memory formation. *Trends in Neurosciences*, *35*(4), 211–219. https://doi.org/10.1016/j.tins.2012.02.001

Van Petten, C., & Luka, B. (2012). Prediction during language comprehension: Benefits, costs and ERP components. *International Journal of Psychophysiology*, *83*(2), 176–190. https://doi.org/10.1016/j.ijpsycho.2011.09.015

Van Strien, N. M., Cappaert, N. L. M., & Witter, M. P. (2009). The anatomy of memory: An interactive overview of the parahippocampal-hippocampal network. *Nature Reviews Neuroscience*, *10*(4), 272–282. https://doi.org/10.1038/nrn2614

Vaswani, A., Shazeer, N., Parmar, N., Uszkoreit, J., Jones, L., Gomez, A. N., Kaiser, L., & Polosukhin, I. (2017). Attention is all you need. In I. Guyon, U. von Luxburg, S. Bengio, H. Wallach, R. Fergus, S. Vishwanathan, & R. Garnett (Eds.), *Advances in neural information processing systems* (Vol. 30, pp. 5998–6008). Curran Associates, Inc.

Vinogradova, O. S. (2001). Hippocampus as comparator: Role of the two input and two output systems of the hippocampus in selection and registration of information. *Hippocampus*, *11*(5), 578–598. https://doi.org/10.1002/hipo.1073

Võ, M. L.-H., Conrad, M., Kuchinke, L., Urton, K., Hofmann, M. J., & Jacobs, A. M. (2009). The Berlin Affective Word List reloaded (BAWL-R). *Behavior Research Methods*, *41*(2), 534–538. https://doi.org/10.3758/BRM.41.2.534

Vu, A. T., Jamison, K., Glasser, M. F., Smith, S. M., Coalson, T., Moeller, S., Auerbach, E. J., Uğurbil, K., & Yacoub, E. (2017). Tradeoffs in pushing the spatial resolution of fMRI for the 7T Human Connectome Project. *NeuroImage*, *154*, 23–32. https://doi.org/10.1016/j.neuroimage.2016.11.049

Wagner, A. D., Koutstaal, W., Maril, A., Schacter, D. L., & Buckner, R. L. (2000). Task-specific repetition priming in left inferior prefrontal cortex. *Cerebral Cortex*, *10*(12), 1176–1184. https://doi.org/10.1093/cercor/10.12.1176

Warren, D. E., Roembke, T. C., Covington, N. V., McMurray, B., & Duff, M. C. (2020). Cross-situational statistical learning of new words despite bilateral hippocampal damage and severe amnesia. *Frontiers in Human Neuroscience*, *13*, Article 448. https://doi.org/10.3389/fnhum.2019.00448

Watkins, M. J., & Watkins, O. C. (1976). Cue-overload theory and the method of interpolated attributes. *Bulletin of the Psychonomic Society*, *7*(3), 289–291. https://doi.org/10.3758/BF03337192

Weyerts, H., Tendolkar, I., Smid, H. G., & Heinze, H. J. (1997). ERPs to encoding and recognition in two different inter-item association tasks. *NeuroReport*, *8*(7), 1583–1588. https://doi.org/10.1097/00001756-199705060-00007

Wible, C. G., Han, S. D., Spencer, M. H., Kubicki, M., Niznikiewicz, M. H., Jolesz, F. A., McCarley, R. W., & Nestor, P. (2006). Connectivity among semantic associates: An fMRI study of semantic priming. *Brain and Language*, *97*(3), 294–305. https://doi.org/10.1016/j.bandl.2005.11.006

Wiggs, C. L., & Martin, A. (1998). Properties and mechanisms of perceptual priming. *Current Opinion in Neurobiology*, *8*(2), 227–233. https://doi.org/10.1016/s0959-4388(98)80144-x

Wiltgen, B. J., Brown, R. A., Talton, L. E., & Silva, A. J. (2004). New circuits for old memories: The role of the neocortex in consolidation. *Neuron*, *44*(1), 101–108. https://doi.org/10.1016/j.neuron.2004.09.015

Wixted, J. T. (2004). The psychology and neuroscience of forgetting. *Annual Review of Psychology*, *55*, 235–269. https://doi.org/10.1146/annurev.psych.55.090902.141555

Yassa, M. A., & Stark, C. E. L. (2011). Pattern separation in the hippocampus. *Trends in Neurosciences*, *34*(10), 515–525. https://doi.org/10.1016/j.tins.2011.06.006

Yonelinas, A. P. (1994). Receiver-operating characteristics in recognition memory: Evidence for a dual-process model. *Journal of Experimental Psychology: Learning, Memory, and Cognition*, *20*(6), 1341–1354. https://doi.org/10.1037/0278-7393.20.6.1341

Yonelinas, A. P. (2002). The nature of recollection and familiarity: A review of 30 years of research. *Journal of Memory and Language*, *46*(3), 441–517. https://doi.org/10.1006/jmla.2002.2864

Yonelinas, A. P., Hawkins, C., Abovian, A., & Aly, M. (2024). The role of recollection, familiarity, and the hippocampus in episodic and working memory. *Neuropsychologia*, *193*, Article 108777. https://doi.org/10.1016/j.neuropsychologia.2023.108777

Yonelinas, A. P., Ranganath, C., Ekstrom, A. D., & Wiltgen, B. J. (2019). A contextual binding theory of episodic memory: Systems consolidation reconsidered. *Nature Reviews Neuroscience*, *20*(6), 364–375. https://doi.org/10.1038/s41583-019-0150-4

Yu, S. Y., & Rugg, M. D. (2010). Dissociation of the electrophysiological correlates of familiarity strength and item repetition. *Brain Research*, *1320*, 74–84. https://doi.org/10.1016/j.brainres.2009.12.071

Yuen, N. H., Osachoff, N., & Chen, J. J. (2019). Intrinsic frequencies of the resting-state fMRI signal: The frequency dependence of functional connectivity and the effect of mode mixing. *Frontiers in Neuroscience*, *13*, Article 900. https://doi.org/10.3389/fnins.2019.00900

Yun, S. D., Pais-Roldán, P., Palomero-Gallagher, N., & Shah, N. J. (2022). Mapping of whole-cerebrum resting-state networks using ultra-high-resolution acquisition protocols. *Human Brain Mapping*, *43*(11), 3386–3403. https://doi.org/10.1002/hbm.25855

Yun, S. D., & Shah, N. J. (2017). Whole-brain high in-plane resolution fMRI using accelerated EPIK for enhanced characterisation of functional areas at 3T. *PLOS ONE*, *12*(9), Article e0184759. https://doi.org/10.1371/journal.pone.0184759

Yun, S. D., & Shah, N. J. (2020). Analysis of EPI phase correction with low flip-angle excitation to reduce the required minimum TE: Application to whole-brain, submillimeter-resolution fMRI at 3 T. *Magnetic Resonance in Medicine*, *84*(3), 1416–1429. https://doi.org/10.1002/mrm.28218

Yun, S. D., Weidner, R., Weiss, P. H., & Shah, N. J. (2019). Evaluating the utility of EPIK in a finger tapping fMRI experiment using BOLD detection and effective connectivity. *Scientific Reports*, *9*, Article 10978. https://doi.org/10.1038/s41598-019-47341-y

Zhao, Y., Yin, J., Zhang, J., & Wu, L. (2023). Identifying the driving factors of word co-occurrence: A perspective of semantic relations. *Scientometrics*, *128*(12), 6471–6494. https://doi.org/10.1007/s11192-023-04851-x

9. Appendix

Appendix A. Supplementary Materials for Study A

A1. Full Stimulus List (Studies A-B)

Item-Level Overview of the Sentences by Experimental Condition - List A

Condition	Word 1	Word 2	Word 3	Word 4	Word 5	AS	CA
SA-HS	Das	Boot	ist	im	Wasser.	3.50	13
SA-HS	Das	Darlehen	ist	ein	Kredit.	2.77	40
SA-HS	Das	Foto	ist	ein	Porträt.	2.16	31
SA-HS	Das	Heroin	ist	eine	Droge.	2.98	28
SA-HS	Das	Pferd	hat	einen	Reiter.	3.85	14
SA-HS	Das	Schiff	hat	eine	Flagge.	3.49	15
SA-HS	Das	Schloss	wird	ein	Museum.	3.42	12
SA-HS	Das	Theater	hat	eine	Bühne.	3.83	20
SA-HS	Der	Applaus	wird	zu	Jubel.	3.05	26
SA-HS	Der	Bäcker	hat	das	Brötchen.	3.62	31
SA-HS	Der	Beamte	ist	im	Dienst.	3.54	12
SA-HS	Der	Bischof	hat	die	Predigt.	3.29	23
SA-HS	Der	Garten	ist	im	Innenhof.	2.33	26
SA-HS	Der	Helfer	ist	im	Einsatz.	3.75	11
SA-HS	Der	Hörsaal	ist	am	Campus.	2.83	23
SA-HS	Der	Lügner	ist	ein	Verräter.	2.42	23
SA-HS	Der	Patient	hat	einen	Arzt.	4.04	36
SA-HS	Der	Pianist	ist	am	Klavier.	2.98	26
SA-HS	Der	Räuber	hat	die	Beute.	3.78	33
SA-HS	Der	Regen	wird	zu	Schnee.	4.12	27
SA-HS	Der	Zeuge	ist	im	Prozess.	3.43	26
SA-LS	Das	Brot	ist	der	Lohn.	3.94	0
SA-LS	Das	Herz	ist	die	Seele.	3.85	0
SA-LS	Der	Bürger	hat	ein	Anliegen.	3.11	0
SA-LS	Der	Club	hat	den	Computer.	3.59	0
SA-LS	Der	Jäger	wird	zum	Sammler.	3.67	0
SA-LS	Der	Kläger	hat	den	Anspruch.	3.15	0
SA-LS	Der	Kopfball	ist	eine	Chance.	3.27	0
SA-LS	Der	Polizist	hat	eine	Pistole.	2.51	0
SA-LS	Der	Puck	ist	im	Netz.	3.19	0
SA-LS	Der	Richter	hat	den	Vorsitz.	3.36	0
SA-LS	Die	Akademie	hat	ein	Archiv.	3.05	0
SA-LS	Die	Apotheke	hat	das	Rezept.	2.95	0
SA-LS	Die	Getriebe	haben	ein	Rädchen.	3.27	0
SA-LS	Die	Kamera	hat	ein	Mikrofon.	3.27	0
SA-LS	Die	Kirche	hat	eine	Orgel.	3.39	0
SA-LS	Die	Leiche	ist	im	Sarg.	2.99	0
SA-LS	Die	Luft	ist	im	Ballon.	3.03	0
SA-LS	Die	Nutzung	hat	eine	Gebühr.	2.54	0
SA-LS	Die	Stimme	hat	einen	Klang.	3.19	0
SA-LS	Die	Untreue	ist	ein	Verdacht.	3.53	0
SA-LS	Die	Ursache	ist	ein	Brand.	3.89	0
NA-HS	Das	Bärtchen	wird	zum	Vollbart.	0.00	27
NA-HS	Das	Dilemma	ist	eine	Krise.	0.00	19

NA-HS	Das	Element	hat	das	Merkmal.	0.00	28
NA-HS	Das	Gedicht	hat	ein	Vorwort.	0.00	30
NA-HS	Das	Gelände	ist	im	Umbau.	0.00	18
NA-HS	Das	Heft	ist	das	Jahrbuch.	0.00	27
NA-HS	Das	Modell	wird	zum	Produkt.	0.00	25
NA-HS	Das	Plakat	ist	ein	Zettel.	0.00	28
NA-HS	Das	System	hat	das	Konzept.	0.00	22
NA-HS	Das	Werkzeug	ist	im	Vehikel.	0.00	26
NA-HS	Das	Wunder	ist	ein	Zufall.	0.00	18
NA-HS	Der	Anruf	ist	ein	Unfall.	0.00	17
NA-HS	Der	Aspekt	ist	der	Vorteil.	0.00	23
NA-HS	Der	Käse	wird	ein	Gelee.	0.00	24
NA-HS	Der	Konzern	hat	das	Defizit.	0.00	22
NA-HS	Der	Kunde	ist	der	Mensch.	0.00	19
NA-HS	Der	Sekt	ist	mit	Sprudel.	0.00	24
NA-HS	Der	Zuwachs	wird	zum	Verlust.	0.00	36
NA-HS	Die	Geburt	ist	der	Beginn.	0.00	20
NA-HS	Die	Kommune	ist	ein	Bezirk.	0.00	19
NA-HS	Die	Studie	ist	im	Bericht.	0.00	24
NA-LS	Das	Fleisch	ist	vom	Schäfer.	0.00	0
NA-LS	Der	Abflug	wird	ein	Horror.	0.00	0
NA-LS	Der	Angler	hat	eine	Affäre.	0.00	0
NA-LS	Der	Fürst	ist	ein	Raucher.	0.00	0
NA-LS	Der	General	ist	am	Eingang.	0.00	0
NA-LS	Der	Pastor	hat	das	Gerät.	0.00	0
NA-LS	Der	Premier	hat	die	Pflanze.	0.00	0
NA-LS	Der	Prinz	ist	in	Therapie.	0.00	0
NA-LS	Der	Sänger	hat	die	Prüfung.	0.00	0
NA-LS	Der	Sprecher	hat	ein	Beispiel.	0.00	0
NA-LS	Der	Wolf	ist	in	Bewegung.	0.00	0
NA-LS	Der	Zirkus	hat	einen	Hirsch.	0.00	0
NA-LS	Die	Auskunft	ist	ein	Anfang.	0.00	0
NA-LS	Die	Brille	ist	im	Gepäck.	0.00	0
NA-LS	Die	Etappe	ist	ein	Aufwand.	0.00	0
NA-LS	Die	Fliege	ist	im	Becher.	0.00	0
NA-LS	Die	Gräfin	hat	den	Fisch.	0.00	0
NA-LS	Die	Kritiker	haben	einen	Schock.	0.00	0
NA-LS	Die	Oper	ist	ein	Import.	0.00	0
NA-LS	Die	Presse	ist	am	Strand.	0.00	0
NA-LS	Die	Regie	hat	eine	Frist.	0.00	0

Note. AS = Association strength; CA = Number of common associates; HS = high semantic feature overlap; LS = low semantic feature overlap; NA = no direct association; SA = strong direct association.

Item-Level Overview of the Sentences by Experimental Condition - List B

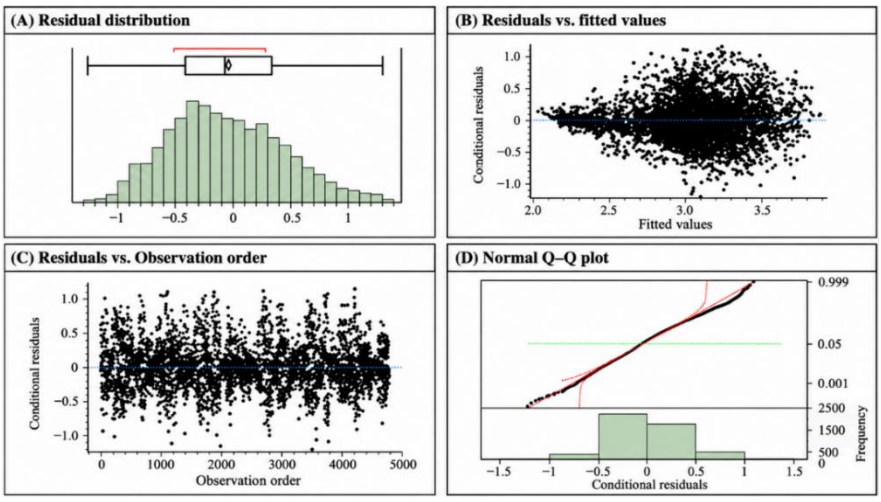
Condition	Word 1	Word 2	Word 3	Word 4	Word 5	AS	CA
SA-HS	Das	Auto	hat	einen	Motor.	3.72	10
SA-HS	Das	Erbgut	ist	im	Zellkern.	2.66	35
SA-HS	Das	Gemälde	ist	im	Atelier.	2.46	27
SA-HS	Das	Gemüse	ist	im	Salat.	3.52	37
SA-HS	Das	Pech	wird	zu	Glück.	3.67	23
SA-HS	Das	Publikum	ist	im	Saal.	3.38	14

SA-HS	Der	Anwalt	ist	bei	Gericht.	3.77	23
SA-HS	Der	Komplex	ist	ein	Gebäude.	2.31	36
SA-HS	Der	Läufer	ist	beim	Marathon.	3.41	29
SA-HS	Der	Neubau	ist	ein	Hochhaus.	2.05	26
SA-HS	Der	Soldat	wird	zum	Offizier.	2.56	37
SA-HS	Der	Täter	hat	ein	Messer.	3.71	15
SA-HS	Die	Armee	hat	den	Panzer.	3.19	29
SA-HS	Die	Beratung	ist	der	Service.	3.40	14
SA-HS	Die	Firma	hat	den	Auftrag.	3.65	15
SA-HS	Die	Flasche	ist	aus	Glas.	3.05	26
SA-HS	Die	Klinik	hat	einen	Direktor.	3.75	13
SA-HS	Die	Theorie	wird	zur	Praxis.	4.36	21
SA-HS	Die	Utopie	ist	die	Illusion.	2.04	31
SA-HS	Die	Wärme	wird	zu	Strom.	4.15	27
SA-HS	Die	Zeitung	ist	im	Gespräch.	4.18	13
SA-LS	Das	Ansehen	hat	einen	Schaden.	3.41	0
SA-LS	Das	Volk	hat	die	Freiheit.	3.38	0
SA-LS	Der	Abstieg	ist	ein	Kampf.	3.79	0
SA-LS	Der	Alkohol	ist	ein	Genuss.	2.86	0
SA-LS	Der	Besucher	hat	den	Kaffee.	3.03	0
SA-LS	Der	Dorn	ist	im	Auge.	4.70	0
SA-LS	Der	Glaube	ist	die	Hoffnung.	3.36	0
SA-LS	Der	Kiosk	hat	eine	Ausgabe.	3.33	0
SA-LS	Der	König	ist	im	Exil.	2.64	0
SA-LS	Der	Manager	ist	im	Magazin.	3.47	0
SA-LS	Der	Papa	hat	eine	Tochter.	3.19	0
SA-LS	Der	Phönix	wird	zu	Asche.	3.77	0
SA-LS	Der	Streit	ist	ein	Auslöser.	3.24	0
SA-LS	Der	Versuch	ist	ein	Irrtum.	2.97	0
SA-LS	Der	Zuhörer	ist	im	Vortrag.	3.05	0
SA-LS	Die	Bombe	ist	im	Flugzeug.	2.66	0
SA-LS	Die	Insel	ist	ein	Paradies.	2.61	0
SA-LS	Die	Kanzlei	hat	einen	Partner.	3.53	0
SA-LS	Die	Serie	wird	ein	Erfolg.	3.30	0
SA-LS	Die	Show	ist	ein	Musical.	2.89	0
SA-LS	Die	Suppe	hat	ein	Haar.	3.51	0
NA-HS	Das	Attentat	ist	das	Unglück.	0.00	30
NA-HS	Das	Bassin	ist	ein	Aquarium.	0.00	26
NA-HS	Das	Büchlein	hat	ein	Bändchen.	0.00	41
NA-HS	Das	Erlebnis	ist	das	Geschenk.	0.00	27
NA-HS	Das	Motto	hat	das	Fazit.	0.00	19
NA-HS	Das	Problem	ist	das	Rätsel.	0.00	20
NA-HS	Das	Signal	ist	der	Hinweis.	0.00	20
NA-HS	Das	Turnier	ist	das	Rennen.	0.00	22
NA-HS	Der	Angriff	ist	ein	Aufstand.	0.00	26
NA-HS	Der	Betrug	wird	zur	Tötung.	0.00	25
NA-HS	Der	Bruder	ist	ein	Kollege.	0.00	24
NA-HS	Der	Einbruch	ist	ein	Anschlag.	0.00	19
NA-HS	Der	Junge	wird	ein	Student.	0.00	18
NA-HS	Der	Makel	ist	der	Nachteil.	0.00	24
NA-HS	Der	Mann	ist	ein	Profi.	0.00	20
NA-HS	Der	Monat	wird	ein	Gewinn.	0.00	21
NA-HS	Der	Text	wird	ein	Krimi.	0.00	27
NA-HS	Der	Vorgang	ist	ein	Ansatz.	0.00	19
NA-HS	Die	Bleibe	ist	eine	Zuflucht.	0.00	27

NA-HS	Die	Empörung	wird	zu	Skepsis.	0.00	21
NA-HS	Die	Vision	wird	zur	These.	0.00	24
NA-LS	Das	Abbild	ist	ein	Engel.	0.00	0
NA-LS	Das	Konzert	ist	in	Ordnung.	0.00	0
NA-LS	Das	Ventil	ist	aus	Metall.	0.00	0
NA-LS	Das	Zimmer	ist	in	Gebrauch.	0.00	0
NA-LS	Der	Abbau	ist	ein	Geschäft.	0.00	0
NA-LS	Der	Abend	ist	eine	Blamage.	0.00	0
NA-LS	Der	Absturz	ist	die	Ausnahme.	0.00	0
NA-LS	Der	Brief	ist	vom	Sportler.	0.00	0
NA-LS	Der	Butler	hat	den	Husten.	0.00	0
NA-LS	Der	Deckel	hat	einen	Umfang.	0.00	0
NA-LS	Der	Farmer	hat	den	Wecker.	0.00	0
NA-LS	Der	Flügel	ist	aus	Papier.	0.00	0
NA-LS	Der	Jurist	hat	eine	Rakete.	0.00	0
NA-LS	Der	Meister	hat	das	Material.	0.00	0
NA-LS	Der	Ordner	ist	beim	Dozent.	0.00	0
NA-LS	Der	Protest	ist	im	Zentrum.	0.00	0
NA-LS	Die	Basis	wird	der	Tempel.	0.00	0
NA-LS	Die	Grafik	ist	ein	Ersatz.	0.00	0
NA-LS	Die	Party	wird	ein	Skandal.	0.00	0
NA-LS	Die	Rettung	wird	ein	Chaos.	0.00	0
NA-LS	Die	Tour	ist	ein	Risiko.	0.00	0

Note. AS = Association strength; CA = Number of common associates; HS = high semantic feature overlap; LS = low semantic feature overlap; NA = no direct association; SA = strong direct association.

A2. Residual Diagnostics for the LMM Fitted to ln(RTs)



Note. Residual diagnostics for the Gaussian linear mixed-effects model (LMM) fitted to natural-log-transformed response times (ln(RTs)). (A) Histogram and boxplot of conditional residuals. (B) Conditional residuals plotted against fitted values. (C) Conditional residuals plotted against observation order. (D) Normal quantile–quantile (Q–Q) plot of conditional residuals with the corresponding frequency distribution. The Anderson–Darling test was statistically significant, $A^2 = 11.175$, $p < .001$.

A3. Type III Wald *F*-Tests for Trial-Level Recall Success

Source	Number of parameters	*df* counter	*df* denominator	*F* value	Prob. > *F*
DA	1	1	157	71.95	< .001
SEM	1	1	156	4.12	.044
SOA	1	1	65	2.14	.148
DA × SEM	1	1	156	1.20	.274
DA × SOA	1	1	11,416	1.01	.314
SEM × SOA	1	1	11,416	2.08	.149
DA × SEM × SOA	1	1	11,416	0.08	.784

Note. Binomial generalized linear mixed-effects model (GLMM) with logit link, including random intercepts for participants and items (N = 68 participants; k = 168 items; n = 11,424 trials). *F*-tests are reported with denominator degrees of freedom approximated using the Kenward–Roger method. DA = direct association; SEM = semantic feature overlap; SOA = stimulus-onset asynchrony.

A4. Type III Wald *F*-Tests for Trial-Level Response Times

Source	Number of parameters	*df* counter	*df* denominator	*F* value	Prob. > *F*
DA	1	1	160	11.02	.001
SEM	1	1	158	0.16	.690
SOA	1	1	66	0.23	.631
DA × SEM	1	1	158	1.44	.232
DA × SOA	1	1	4,363	0.12	.729
SEM × SOA	1	1	4,361	0.09	.767
DA × SEM × SOA	1	1	4,361	1.40	.236

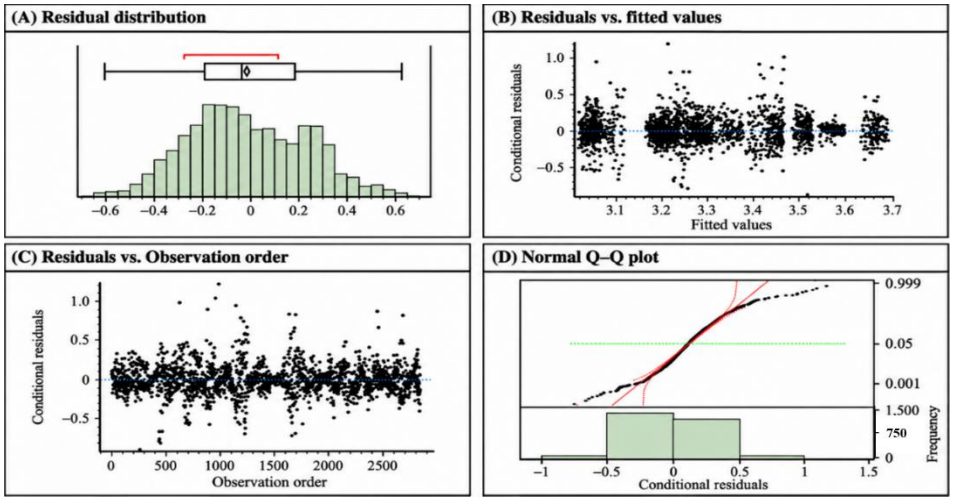
Note. Gaussian linear mixed-effects model (LMM) fitted to natural-log-transformed response times for correctly recalled trials, including random intercepts for participants and items (N = 68 participants; k = 168 items; n = 4,514 trials). *F*-tests are reported with denominator degrees of freedom approximated using the Kenward–Roger method. DA = direct association; SEM = semantic feature overlap; SOA = stimulus-onset asynchrony.

A5. Model Comparison: SOA Effects

Using maximum-likelihood estimation, a full Gaussian linear mixed-effects model including stimulus-onset asynchrony (SOA) and all SOA interactions (direct association [DA] × semantic feature overlap [SEM] × SOA) was compared with a reduced model excluding all SOA terms (DA, SEM, DA × SEM). Model fit indices favored the reduced model (corrected Akaike information criterion [AICc] = 3,575; Bayesian information criterion [BIC] = 3,620) relative to the full model (AICc = 3,581; BIC = 3,652; ΔBIC = 31.95). Consistently, a likelihood-ratio test indicated no improvement in fit for the full model, $\chi^2(4) = 1.71$, $p = .789$.

Appendix B. Supplementary Materials for Study B

B1. Residual Diagnostics for the LMM Fitted to ln(RTs)



Note. Residual diagnostics for the Gaussian linear mixed-effects model (LMM) fitted to natural-log-transformed response times (ln(RTs)). (A) Histogram and boxplot of conditional residuals. (B) Conditional residuals plotted against fitted values. (C) Conditional residuals plotted against observation order. (D) Normal quantile–quantile (Q–Q) plot of conditional residuals with the corresponding frequency distribution. The Anderson–Darling test was statistically significant, $A^2 = 10.272$, $p < .001$.

B2. Type III Wald *F*-Tests for Trial-Level Recall Success

Source	Number of parameters	*df* counter	*df* denominator	*F* value	Prob. > *F*
DA	1	1	149	51.39	< .001
SEM	1	1	148	2.30	.131
DA × SEM	1	1	148	0.48	.488

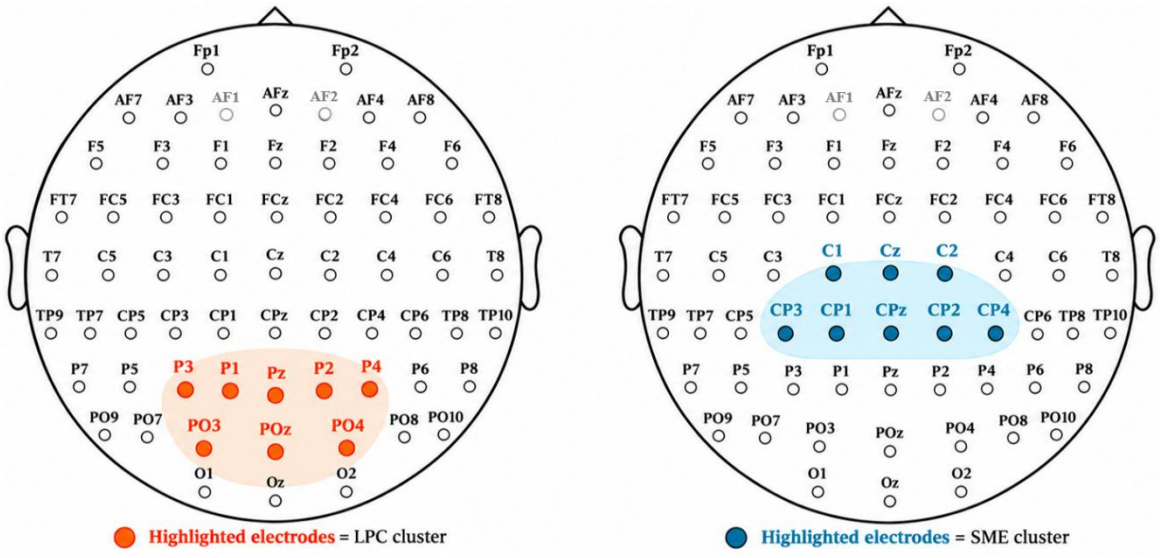
Note. Binomial generalized linear mixed-effects model (GLMM) with logit link, including random intercepts for participants and items (N = 31 participants; k = 168 items; n = 5,208 trials). *F*-tests are reported with denominator degrees of freedom approximated using the Kenward–Roger method. DA = direct association; SEM = semantic feature overlap.

B3. Type III Wald *F*-*T*ests for Trial-Level Response Times

Source	Number of parameters	*df* counter	*df* denominator	*F* value	Prob. > *F*
DA	1	1	162	6.29	.013
SEM	1	1	160	0.86	.356
DA × SEM	1	1	161	0.70	.401

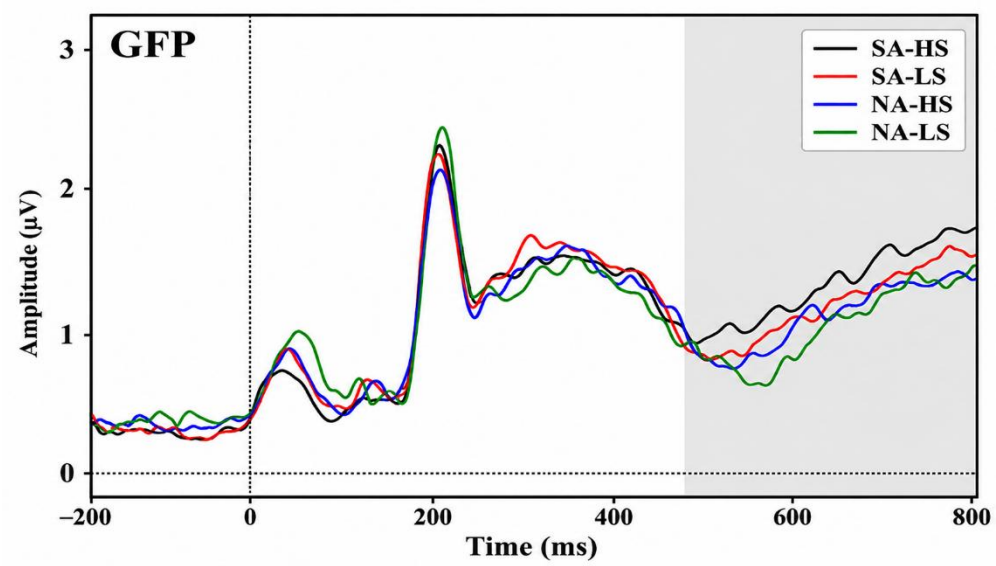
Note. Gaussian linear mixed-effects model fitted to natural-log-transformed response times for correctly recalled trials, including random intercepts for participants and items (N = 31 participants; k = 168 items; n = 2,676 trials). *F*-tests are reported with denominator degrees of freedom approximated using the Kenward–Roger method. DA = direct association; SEM = semantic feature overlap.

B4. Electrode Clusters Used for LPC and SME Analyses



Note. Top view of the electrode setup (nasion at the top). Electrodes AF1 and AF2 were used for electrooculographic recordings (HEOG and VEOG, respectively) and were therefore excluded from EEG analyses. LPC = late positive component; SME = subsequent memory effect.

B5. Global Field Power Used for Late Positive Component Time Window Selection



Note. *N* = 31 participants. Grand-average global field power (GFP) waveforms for subsequently correctly recalled targets. Time zero indicates target onset. The shaded region marks the 460–800 ms late positive component analysis window. SA = strong direct association; NA = no direct association; HS = high semantic feature overlap; LS = low semantic feature overlap.

B6. Analytical Standardized Measurement Error for Participant-Level ERP Estimates

Analysis window	Condition	Recall	aSME *M* (*SD*), µV	Range, µV
LPC (460–800 ms)	SA-HS	Correct	0.71 (0.20)	0.33–1.09
	SA-LS	Correct	0.74 (0.20)	0.41–1.17
	NA-HS	Correct	0.84 (0.25)	0.49–1.42
	NA-LS	Correct	1.02 (0.50)	0.34–2.61
N400 SME (250–500 ms)	SA-HS	Correct	0.52 (0.15)	0.26–0.90
	SA-HS	False	0.93 (0.44)	0.27–2.34
	SA-LS	Correct	0.58 (0.16)	0.29–0.95
	SA-LS	False	0.83 (0.47)	0.37–2.67
	NA-HS	Correct	0.67 (0.22)	0.35–1.25
	NA-HS	False	0.70 (0.48)	0.28–3.07
	NA-LS	Correct	0.72 (0.38)	0.34–1.88
	NA-LS	False	0.59 (0.28)	0.31–1.48
P600 SME (500–800 ms)	SA-HS	Correct	0.66 (0.19)	0.39–1.12
	SA-HS	False	1.12 (0.57)	0.33–2.98
	SA-LS	Correct	0.71 (0.21)	0.42–1.14
	SA-LS	False	0.94 (0.40)	0.48–1.91
	NA-HS	Correct	0.85 (0.30)	0.43–1.70
	NA-HS	False	0.90 (0.75)	0.37–4.59
	NA-LS	Correct	0.88 (0.45)	0.35–2.21
	NA-LS	False	0.74 (0.37)	0.38–2.24

Note. Analytical standardized measurement error (aSME) was calculated separately for each participant and experimental condition using virtual channels representing the equally weighted averages of the predefined late positive component (LPC) and subsequent memory effect (SME) electrode clusters. Lower aSME values indicate greater precision of the participant-level event-related potential (ERP) estimate. HS = high semantic feature overlap; LS = low semantic feature overlap; NA = no direct association; SA = strong direct association.

B7. 2 × 2 × 2 rmANOVA Results for SMEs in the N400 Time Window (250–500 ms)

Source	*F*(1, 30)	*p* value	η_p^2
DA	0.69	.413	.02
SEM	0.08	.776	.00
RS	10.69	.003	.26
DA × SEM	0.02	.894	.00
DA × RS	0.01	.962	.00
SEM × RS	0.19	.663	.01
DA × SEM × RS	3.32	.078	.10

Note. Repeated-measures analysis of variance (rmANOVA) with the within-subject factors direct association (DA: none vs. strong), semantic feature overlap (SEM: low vs. high), and recall success (RS: correct vs. incorrect). SMEs = subsequent-memory effects.

B8. 2 × 2 × 2 rmANOVA Results for SMEs in the P600 Time Window (500–800 ms)

Source	*F*(1, 30)	*p* value	η_p^2
DA	0.65	.426	.02
SEM	3.36	.077	.10
RS	35.08	< .001	.54
DA × SEM	0.02	.895	.00
DA × RS	1.70	.202	.05
SEM × RS	1.41	.245	.05
DA × SEM × RS	3.15	.060	.11

Note. Repeated-measures analysis of variance (rmANOVA) with the within-subject factors direct association (DA: none vs. strong), semantic feature overlap (SEM: low vs. high), and recall success (RS: correct vs. incorrect). SMEs = subsequent-memory effects.

Appendix C. Supplementary Materials for Study C

C1. Full Stimulus List (Study C)

Item-level overview of the word pairs by experimental condition

Word (Left)	Word (Right)	Condition	AS	CA	FixCrossDur
BERATUNG	SCHULUNG	SA-HS	2.90	26	1,000
KAMERA	OBJEKTIV	SA-HS	2.82	17	2,000
MALZ	HOPFEN	SA-HS	3.67	33	2,500
GEN	FORSCHER	SA-HS	3.38	19	1,000
MANTEL	HUT	SA-HS	3.13	23	1,500
BERUF	HOBBY	SA-HS	3.63	20	1,000
LÄRM	ANWOHNER	SA-HS	3.66	23	3,500
TISCH	STUHL	SA-HS	3.38	19	4,000
HAAR	GEL	SA-HS	3.01	19	3,500
HÜFTE	KNIE	SA-HS	2.95	25	3,500
HIMMEL	SONNE	SA-HS	3.85	20	2,000
SCHLAGER	JAZZ	SA-HS	2.76	25	5,500
BEUTE	TÄTER	SA-HS	3.69	33	4,000
TEICH	GARTEN	SA-HS	2.83	23	1,000
ABBAU	SENKUNG	SA-HS	2.91	16	5,000
RIND	SCHWEIN	SA-HS	3.35	26	5,000
PFLEGE	WARTUNG	SA-HS	2.97	20	5,500
FRANZOSE	SPANIER	SA-HS	2.71	18	1,000
GLIED	KETTE	SA-HS	3.74	20	2,500
SKI	SCHNEE	SA-HS	2.85	11	2,000
STUDIUM	LEHRE	SA-HS	3.46	28	2,500
URTEIL	REVISION	SA-HS	3.96	29	1,500
DONNER	BLITZ	SA-HS	3.84	14	4,000
KILO	GEWICHT	SA-HS	3.56	20	4,500
FAHRER	AUTO	SA-HS	3.88	32	2,500
VERLEGER	AUTOR	SA-HS	3.06	19	4,500
SCHWÄCHE	STÄRKE	SA-HS	3.91	26	4,500
ELEND	NOT	SA-HS	3.35	17	3,500

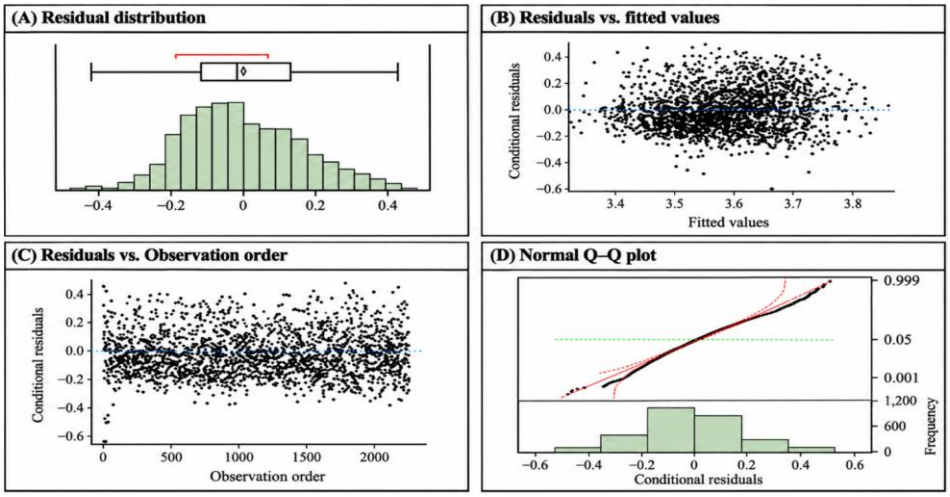
URANUS	NEPTUN	SA-HS	3.47	37	1,000
STROH	HEU	SA-HS	3.17	27	3,000
SPURT	TEMPO	SA-HS	3.32	17	5,500
KINN	GESICHT	SA-HS	2.74	24	4,000
MENSCH	AFFE	SA-HS	2.96	19	3,500
ZUG	GLEIS	SA-HS	3.29	33	4,000
SCHWEIF	KOMET	SA-HS	2.49	23	5,000
WRACK	TAUCHER	SA-HS	2.97	31	5,500
WUT	TRAUER	SA-HS	3.66	31	2,000
ZINN	KUPFER	SA-HS	3.15	31	3,000
PAPST	KIRCHE	SA-HS	3.82	20	4,000
KERAMIK	GLAS	SA-HS	3.27	17	5,500
STOCK	STEIN	SA-LS	3.00	0	4,500
GUNST	STUNDE	SA-LS	4.04	0	2,000
OMEGA	ALPHA	SA-LS	3.05	0	5,500
WÄHLER	STIMME	SA-LS	3.49	0	4,000
SEELE	HERZ	SA-LS	3.67	0	1,500
KABALE	LIEBE	SA-LS	3.41	0	2,000
ARTIKEL	ABSATZ	SA-LS	3.49	0	4,000
TYP	DIABETES	SA-LS	3.19	0	4,500
SIEGER	JURY	SA-LS	3.05	0	5,500
SPRECHER	FRAKTION	SA-LS	3.61	0	4,000
AUSDAUER	KRAFT	SA-LS	3.18	0	2,000
TAFEL	KREIDE	SA-LS	3.05	0	1,000
SCHAUER	RÜCKEN	SA-LS	3.54	0	3,500
STURM	DRANG	SA-LS	3.44	0	3,000
KLIMA	UMWELT	SA-LS	3.19	0	1,000
OHR	KNOPF	SA-LS	3.36	0	1,500
HAMMER	SICHEL	SA-LS	3.71	0	3,000
PRAXIS	ARZT	SA-LS	3.00	0	2,000
ERFOLG	AUSSICHT	SA-LS	3.78	0	4,500
LOHN	BROT	SA-LS	3.86	0	1,500
BÄCKER	METZGER	SA-LS	3.43	0	4,000
METALL	HOLZ	SA-LS	3.41	0	3,500
EHE	SCHUTZ	SA-LS	3.09	0	4,500
KOPF	SCHLINGE	SA-LS	3.40	0	1,500
LOB	KRITIK	SA-LS	3.25	0	3,000
BAHRE	WIEGE	SA-LS	3.38	0	1,000
GERICHT	RECHT	SA-LS	3.40	0	3,500
MESSER	GABEL	SA-LS	3.66	0	5,000
EXEMPEL	PROBE	SA-LS	3.80	0	2,500
TUGEND	PFAD	SA-LS	3.34	0	2,000
DOPING	KAMPF	SA-LS	3.61	0	5,500
DICHTUNG	WAHRHEIT	SA-LS	3.47	0	3,500
BAD	KÜCHE	SA-LS	3.56	0	3,500
KUH	EIS	SA-LS	3.23	0	4,500
PHÖNIX	ASCHE	SA-LS	3.66	0	2,500
SCHWEFEL	PECH	SA-LS	3.11	0	5,500
KÄLTE	HUNGER	SA-LS	3.25	0	1,000
GLORIA	GLANZ	SA-LS	3.55	0	2,000
FLUT	EBBE	SA-LS	3.62	0	1,500
STRICH	FADEN	SA-LS	3.10	0	4,000
KNABE	JUNGE	NA-HS	0.00	20	5,500
ANSATZ	SCHRITT	NA-HS	0.00	23	3,000
FETE	GALA	NA-HS	0.00	22	1,000

EIMER	KOFFER	NA-HS	0.00	21	2,500
OMEN	ZEICHEN	NA-HS	0.00	21	1,000
DEICH	ZAUN	NA-HS	0.00	20	5,000
INDIZ	SIGNAL	NA-HS	0.00	31	4,500
SKALA	SPANNE	NA-HS	0.00	21	2,500
EILE	VORSICHT	NA-HS	0.00	26	5,000
NEUGIER	HINGABE	NA-HS	0.00	20	4,000
STOLZ	IRONIE	NA-HS	0.00	20	4,500
FREUND	NAZI	NA-HS	0.00	23	4,000
ZOO	ANHALTER	NA-HS	0.00	18	3,500
BELEG	GRUND	NA-HS	0.00	29	5,500
ZETTEL	SCHILD	NA-HS	0.00	29	1,500
ZIEL	ANLIEGEN	NA-HS	0.00	29	5,000
GELIEBTE	VEREHRER	NA-HS	0.00	28	2,500
GESCHENK	ERLEBNIS	NA-HS	0.00	27	1,000
ASPEKT	FAKTOR	NA-HS	0.00	26	3,500
METAPHER	VISION	NA-HS	0.00	25	2,000
IDOL	VATER	NA-HS	0.00	22	2,500
HOSE	ROBE	NA-HS	0.00	25	2,500
ZEUG	GEFÜHL	NA-HS	0.00	27	3,000
TEXT	KRIMI	NA-HS	0.00	27	4,500
SATZ	UMSTAND	NA-HS	0.00	20	1,500
TROST	AUSWEG	NA-HS	0.00	28	2,500
SCHADEN	KOSTEN	NA-HS	0.00	19	5,000
KONZEPT	BILD	NA-HS	0.00	22	3,000
ERBE	EGO	NA-HS	0.00	21	5,500
SKRIPT	BUCH	NA-HS	0.00	22	5,000
GELEE	KÄSE	NA-HS	0.00	24	2,000
CHEF	ANWALT	NA-HS	0.00	18	3,000
ANLEIHEN	AKTIE	NA-HS	0.00	18	5,000
KLO	SOFA	NA-HS	0.00	22	1,000
REIS	SCHINKEN	NA-HS	0.00	20	3,500
SCHAL	KRAGEN	NA-HS	0.00	25	2,000
SEKT	WHISKEY	NA-HS	0.00	24	1,500
GESTALT	STATUR	NA-HS	0.00	23	3,500
PODEST	PODIUM	NA-HS	0.00	34	4,500
SUMPF	STRUDEL	NA-HS	0.00	26	1,500
KEKS	TIEFE	NA-LS	0.00	0	2,500
KANNE	FINGER	NA-LS	0.00	0	3,000
SEIFE	KRAUT	NA-LS	0.00	0	4,000
RICHTUNG	SPIELER	NA-LS	0.00	0	2,500
VORLAGE	STIEL	NA-LS	0.00	0	1,500
STADION	FLINTE	NA-LS	0.00	0	2,000
SIEGEL	GATTUNG	NA-LS	0.00	0	5,000
DRAHT	HINSICHT	NA-LS	0.00	0	5,000
GLÜCK	ESSEN	NA-LS	0.00	0	3,500
SCHALTER	MAGAZIN	NA-LS	0.00	0	5,500
SCHLUCK	LEGENDE	NA-LS	0.00	0	1,500
URKUNDE	KLAGE	NA-LS	0.00	0	3,000
PUTZ	SCHNABEL	NA-LS	0.00	0	3,000
SPEICHER	WISCHER	NA-LS	0.00	0	1,500
QUARTAL	SCHLANGE	NA-LS	0.00	0	4,500
ÄRGER	MAGNET	NA-LS	0.00	0	1,000
NUTZEN	ENTWURF	NA-LS	0.00	0	4,000
RADAR	VERLAUF	NA-LS	0.00	0	3,000

ZIMMER	SCHWANZ	NA-LS	0.00	0	5,000
DATUM	ELCH	NA-LS	0.00	0	4,500
KOLBEN	LABOR	NA-LS	0.00	0	5,000
REIFE	KANZLER	NA-LS	0.00	0	5,500
VIRUS	LAWINE	NA-LS	0.00	0	3,500
RECHNUNG	INTRIGE	NA-LS	0.00	0	2,000
LEID	WITZ	NA-LS	0.00	0	2,000
DRUCK	SACHE	NA-LS	0.00	0	3,000
RISIKO	HÖHE	NA-LS	0.00	0	1,500
IRIS	TAKT	NA-LS	0.00	0	5,500
ORT	PFOSTEN	NA-LS	0.00	0	4,000
PUDEL	KREIS	NA-LS	0.00	0	2,500
TICKET	SITZ	NA-LS	0.00	0	5,000
TREPPE	OZON	NA-LS	0.00	0	4,500
FIGUR	KARTON	NA-LS	0.00	0	1,000
KANTE	DELIKT	NA-LS	0.00	0	1,500
ERZ	VERBAND	NA-LS	0.00	0	4,500
ALIBI	HOF	NA-LS	0.00	0	5,500
EIGENTUM	RAUSCH	NA-LS	0.00	0	5,000
BALL	RACHE	NA-LS	0.00	0	3,000
MANGEL	BÄR	NA-LS	0.00	0	3,000
ECKE	WILLE	NA-LS	0.00	0	2,500

Note. AS = association strength; CA = number of common associates; FixCrossDur = fixation cross duration (in ms); HS = high semantic feature overlap; LS = low semantic feature overlap; NA = no direct association; SA = strong direct association.

C2. Residual Diagnostics for the LMM Fitted to ln(RTs)



Note. Residual diagnostics for the Gaussian linear mixed-effects model (LMM) fitted to natural-log-transformed response times (ln(RTs)). (A) Histogram and boxplot of conditional residuals. (B) Conditional residuals plotted against fitted values. (C) Conditional residuals plotted against observation order. (D) Normal quantile–quantile (Q–Q) plot of conditional residuals with the corresponding frequency distribution. The Anderson–Darling test was statistically significant, $A^2 = 10.486$, $p < .001$.

C3. Type III Wald *F*-Tests for Trial-Level Recall Success

Source	Number of parameters	*df* counter	*df* denominator	*F* value	Prob. > *F*
DA	1	1	137	52.62	< .001
SEM	1	1	136	11.81	< .001
DA × SEM	1	1	136	1.12	.293

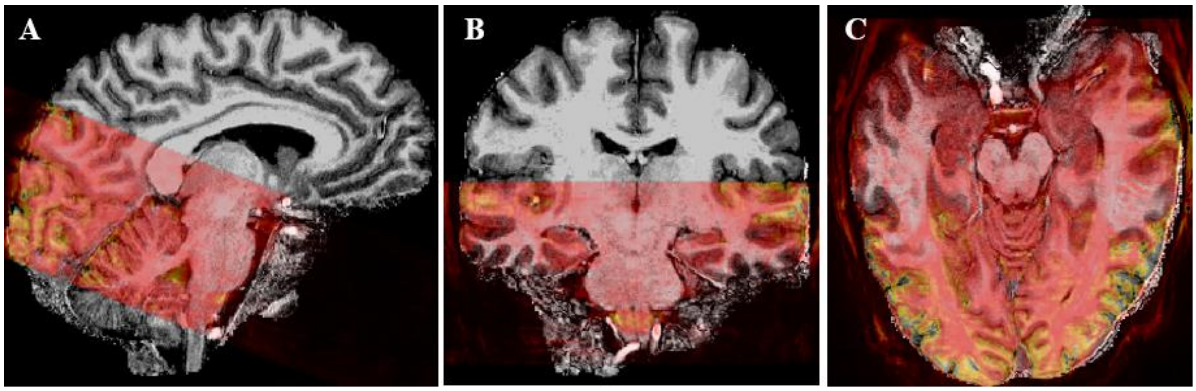
Note. Binomial generalized linear mixed-effects model (GLMM) with logit link, including random intercepts for participants and items (N = 26 participants; k = 160 items; n = 4,160 trials). *F*-tests are reported with denominator degrees of freedom approximated using the Kenward–Roger method. DA = direct association; SEM = semantic feature overlap.

C4. Type III Wald *F*-tests for Trial-Level Response Times

Source	Number of parameters	*df* counter	*df* denominator	*F* value	Prob. > *F*
DA	1	1	154	53.47	< .001
SEM	1	1	153	0.84	.359
DA × SEM	1	1	153	1.12	.292

Note. Gaussian linear mixed-effects model (LMM) fitted to natural-log-transformed response times for correctly recalled trials, including random intercepts for participants and items (N = 31 participants; k = 168 items; n = 2,129 trials). *F*-tests are reported with denominator degrees of freedom approximated using the Kenward–Roger method. DA = direct association; SEM = semantic feature overlap.

C5. Coregistration Quality Control



Note. Representative overlay illustrating the final rigid-body alignment between the mean echo-planar reference image and the structural image. Alignment was visually inspected in FreeView (Version 7.4.1; FreeSurfer Software Suite; Fischl, 2012) and, where necessary, manually refined (translation/rotation) to ensure accurate ROI-to-EPI correspondence in the medial temporal lobe. (A) sagittal, (B) coronal, and (C) axial orientation.

C6. Extracted FreeSurfer Labels and Aggregation to Final Regions of Interest

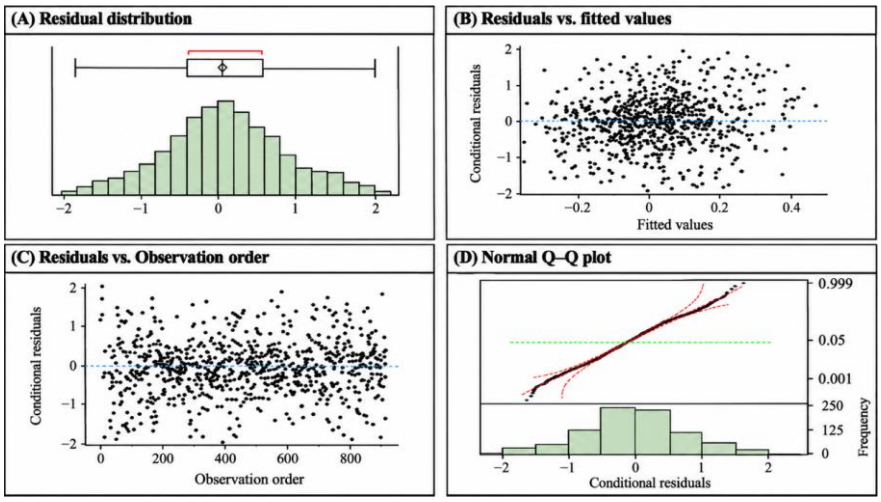
ID	Label	ROI	ID	Label	ROI
1	parasubiculum	–	15	CA4-body	–
2	HATA	–	16	GC-ML-DG-head	DG
3	fimbria	–	17	GC-ML-DG-body	DG
4	hippocampal fissure	–	18	molecular layer HP-head	–
5	HP tail	–	19	molecular layer HP-body	–
6	presubiculum-head	–	20	lateral nucleus	–
7	presubiculum-body	–	21	basal nucleus	–
8	Subiculum-head	SUB	22	central nucleus	–
9	Subiculum-body	SUB	23	medial nucleus	–
10	CA1-head	CA1	24	cortical nucleus	–
11	CA1-body	CA1	25	accessory basal nucleus	–
12	CA3-head	CA3	26	corticoamygdaloid transition	–
13	CA3-body	CA3	27	anterior amygdaloid area	–
14	CA4-head	–	28	paralaminar nucleus	–

Note. Labels were extracted separately for each hemisphere. For the analyses, head and body values were aggregated to form CA1, CA3, DG, and SUB. A dash (–) indicates labels excluded from the analyses but reported for completeness. CA1 = cornu ammonis field 1; CA3 = cornu ammonis field 3; DG = dentate gyrus; GC-ML-DG = granule cell and molecular layer of the dentate gyrus; HATA = hippocampal-amygdala transition area; HP = hippocampus; ROI = region of interest; SUB = subiculum.

C7. Outlier Exclusion and Residual Diagnostics for the Hippocampal Subfield Analysis

	CA1	CA3	DG	SUB
n excluded	7 (3.02%)	11 (4.74%)	29 (12.50%)	20 (8.62%)
n retained	225	221	203	212

Note. Percentages in parentheses refer to the initial number of observations per ROI (n = 232). CA1 = cornu ammonis field 1; CA3 = cornu ammonis field 3; DG = dentate gyrus; SUB = subiculum.



The Anderson–Darling test was statistically significant, $A^2 = 11.215$, $p < .001$.

C8. Type III Wald *F*-Tests for the Hippocampal Subfield Analysis

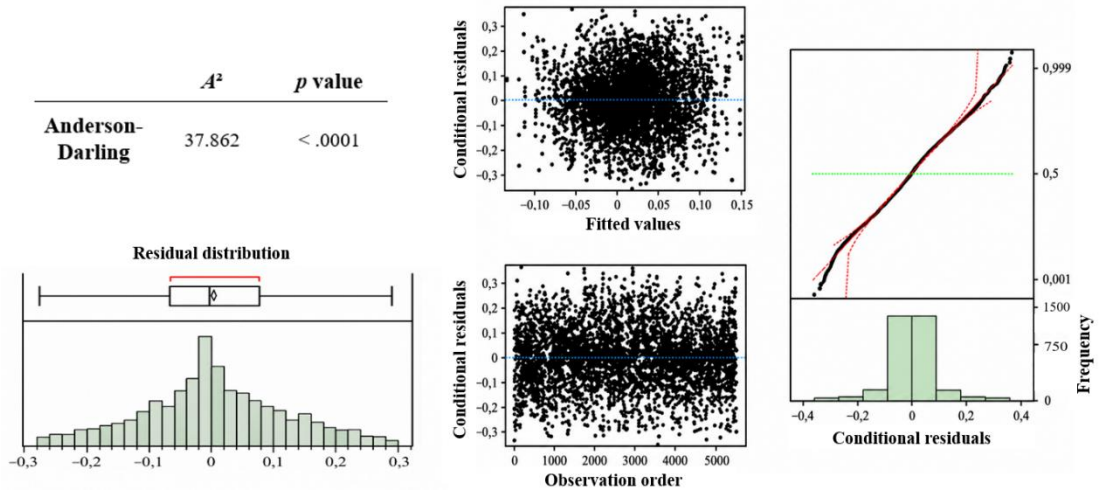
Source	Number of parameters	*df* counter	*df* denominator	*F* value	Prob. > *F*
ROI	3	3	74	0.73	0,537
DA	1	1	650	1.21	0,272
ROI × DA	3	3	650	0.30	0,822
SEM	1	1	645	1.16	0,282
ROI × SEM	3	3	645	1.42	0,235
DA × SEM	1	1	646	0.30	0,586
ROI × DA × SEM	3	3	646	0.23	0,994
HEMI	1	1	646	0.69	0,407
ROI × HEMI	3	3	646	0.96	0,409
DA × HEMI	1	1	646	0.48	0,491
ROI × DA × HEMI	3	3	646	0.42	0,738
SEM × HEMI	1	1	645	0.00	0,998
ROI × SEM × HEMI	3	3	645	0.72	0,543
DA × SEM × HEMI	1	1	646	1.53	0,216
ROI × DA × SEM × HEMI	3	3	646	0.75	0,522

Note. Gaussian linear mixed-effects model including hippocampal subfield (ROI), hemisphere (HEMI), direct association (DA), semantic feature overlap (SEM), and their interactions (N = 26 participants; k = 4 hippocampal subfields; n = 861 ROI-level observations. *F*-tests are reported with denominator degrees of freedom approximated using the Kenward–Roger method.

C9. Outlier Exclusion and Residual Diagnostics for the Cortical ROI Analysis

	IFG	MTG	PCC	OTG	STG	TP	STS	EC	PRC
n excluded	36 (5.77%)	30 (4.81%)	79 (12.66%)	48 (7.69%)	25 (4.01%)	96 (15.38%)	21 (3.37%)	19 (3.04%)	62 (9.94%)
n retained	588	594	545	576	599	528	603	605	562

Note. Percentages in parentheses refer to the initial number of observations per ROI (n = 624). EC = entorhinal cortex; IFG = inferior frontal gyrus; MTG = middle temporal gyrus; OTG = occipitotemporal gyrus; PCC = posterior cingulate cortex; PRC = perirhinal cortex; ROI = region of interest; STG = superior temporal gyrus; STS = superior temporal sulcus; TP = temporal pole.



C10. Type III Wald *F*-Tests for the Cortical ROI Analysis (Depth Terms Excluded)

Source	Number of parameters	*df* counter	*df* denominator	*F* value	Prob. > *F*
DA	1	1	5131	14.93	< .001
SEM	1	1	5131	10.15	.002
HEMI	1	1	5131	24.76	< .001
ROI	8	8	5131	26.71	< .001
DA × SEM	1	1	5131	0.028	.868
ROI × DA	8	8	5131	7.712	< .001
ROI × SEM	8	8	5131	6.86	< .001
ROI × DA × SEM	8	8	5131	1.54	.139
ROI × HEMI	8	8	5131	8.44	< .001

Note. Gaussian linear mixed-effects model including cortical region of interest (ROI), hemisphere (HEMI), direct association (DA), semantic feature overlap (SEM), and their interactions (N = 26 participants; k = 9 cortical regions; n = 5200 ROI-level observations). *F*-tests are reported with denominator degrees of freedom approximated using the Kenward–Roger method.

C11. Cortical ROI Contrasts

ROI	contrast	Difference	*SE*	*t*	*p*	95% CI
EC	DA: none - strong	-0.002	0.012	-0.13	.897	[-0.02, 0.02]
EC	SEM: low - high	-0.024	0.012	-1.97	.184	[-0.03, 0.02]
IFG	DA: none - strong	0.032	0.012	2.66	.008	[0.01, 0.06]
IFG	SEM: low - high	0.066	0.012	4.95	< .001	[0.04, 0.09]
MTG	DA: none - strong	0.052	0.012	4.31	< .001	[0.03, 0.08]
MTG	SEM: low - high	0.061	0.012	5.46	< .001	[0.04, 0.08]
OTG	DA: none - strong	0.006	0.012	0.47	.636	[-0.02, 0.03]
OTG	SEM: low - high	0.027	0.012	1.01	.175	[-0.01, 0.04]
PCC	DA: none - strong	-0.005	0.012	-0.40	.692	[-0.03, 0.02]
PCC	SEM: low - high	-0.002	0.012	-0.15	.882	[-0.03, 0.02]
PRC	DA: none - strong	0.019	0.012	1.53	.126	[-0.01, 0.04]
PRC	SEM: low - high	-0.009	0.012	-0.78	.436	[-0.03, 0.01]
STG	DA: none - strong	-0.042	0.012	-3.48	.001	[-0.07, -0.02]
STG	SEM: low - high	-0.002	0.012	-0.18	.857	[-0.05, 0.00]
STS	DA: none - strong	0.002	0.012	0.13	.898	[-0.02, 0.03]
STS	SEM: low - high	-0.012	0.014	-0.85	.394	[-0.04, 0.02]
TP	DA: none - strong	0.080	0.014	5.69	< .001	[0.05, 0.11]
TP	SEM: low - high	0.013	0.012	1.01	.313	[0.00, 0.05]

Note. Pairwise contrasts are derived from the estimated marginal means of the reduced Gaussian linear mixed-effects model for the cortical ROI analysis (N = 26 participants; k = 9 cortical regions; n = 5200 ROI-level observations), averaged across hemispheres and levels of the other experimental factor. p values are Holm-adjusted. CI = confidence interval; DA = direct association; EC = entorhinal cortex; IFG = inferior frontal gyrus; MTG = middle temporal gyrus; OTG = occipitotemporal gyrus; PCC = posterior cingulate cortex; PRC = perirhinal cortex; ROI = region of interest; SEM = semantic feature overlap; STG = superior temporal gyrus; STS = superior temporal sulcus; TP = temporal pole.

C12. Type III Wald *F*-Tests for Depth-Related Terms from the Full Cortical LMM

Source	Number of parameters	*df* counter	*df* denominator	*F* value	Prob. > *F*
DEPTH	2	2	5106	0.36	.696
DEPTH × DA	2	2	5106	0.01	.989
DEPTH ×SEM	2	2	5106	0.35	.705
DEPTH × DA × SEM	2	2	5106	0.30	.739
DEPTH × ROI	16	16	5106	0.20	.999

Note. Full Gaussian linear mixed-effects model including cortical depth (DEPTH), region of interest (ROI), hemisphere (HEMI), direct association (DA), semantic feature overlap (SEM), and their interactions (N = 26 participants; k = 9 cortical regions; three cortical depth levels). F-tests are reported with denominator degrees of freedom approximated using the Kenward–Roger method.

Appendix D. Supplementary Materials for Klein (2016)

D1. Full Stimulus List (Klein, 2016)

Item-Level Overview of the Prime-Target Pairs by Experimental Condition

Prime	Target	Condition	AS	CA-surface	CA-lemma
EIS	GEBIRGE	2ndC	1.48	17	0
TUCH	HALS	2ndC	2.58	20	0
VERB	PLURAL	2ndC	0.94	20	0
DING	SCHEIßE	2ndC	1.08	30	0
LIED	ZITAT	2ndC	1.09	21	0
SÄGE	SKALPELL	2ndC	1.43	18	0
ORBIT	MARS	2ndC	2.09	25	0
HÜTTE	NÄHE	2ndC	1.40	16	0
KÜBEL	GARTEN	2ndC	0.92	13	0
BÜHNE	TÄNZER	2ndC	3.41	23	0
DURST	WODKA	2ndC	0.87	21	0
HOBBY	HANDICAP	2ndC	1.28	18	0
JUROR	VERLEGER	2ndC	1.02	12	0
MINZE	MAJORAN	2ndC	1.63	29	0
TEMPO	GEFÄHRT	2ndC	1.58	22	0
KATER	SCHWANZ	2ndC	1.77	14	0
SIEGEL	SONG	2ndC	1.93	12	0
ÖKONOM	JURIST	2ndC	2.27	17	0
PROFIL	PARTEI	2ndC	1.34	16	0
TERROR	FEIND	2ndC	1.94	20	0
VORBAU	GESCHOß	2ndC	3.65	16	0
BECHER	LIMONADE	2ndC	1.08	18	0
EROTIK	SEELE	2ndC	0.91	18	0
JUSTIZ	TÖTUNG	2ndC	2.21	21	0
NEURON	JOURNAL	2ndC	1.19	18	0
UNRUHE	AUFSEHEN	2ndC	0.86	17	0
BUCKEL	KILO	2ndC	1.18	16	0

HEIMWEG	MORGEN	2ndC	1.31	22	0
RENTNER	LOHN	2ndC	0.87	16	0
SCHWUNG	GLANZ	2ndC	0.90	19	0
AUFTRAG	OKTOBER	2ndC	0.85	16	0
DIAGNOSE	ARZT	2ndC	3.01	18	0
ABKOMMEN	KONFLIKT	2ndC	1.72	17	0
UNWETTER	SEEBEBEN	2ndC	1.29	14	0
BUCH	EPOS	2ndC	1.61	21	0
ABLEGER	SITZ	2ndC	1.28	21	0
HEILUNG	SKLEROSE	2ndC	1.21	23	0
FLASCHE	GIN	2ndC	2.10	20	0
ZECKE	DARM	2ndC	1.69	12	0
MUSTER	STICH	2ndC	2.55	17	0
SCHEUNE	SCHUPPEN	2ndC	1.36	27	0
SALDO	VORJAHR	2ndC	1.95	33	0
RETINA	GEHIRN	2ndC	1.69	20	0
KOMPOTT	JOGHURT	2ndC	0.98	31	0
BÜRO	BALKON	2ndC	1.19	24	0
NAZI	MENSCH	2ndC	1.06	22	0
MANTEL	SCHLIPS	2ndC	0.83	29	0
SPARTE	VOLUMEN	2ndC	0.99	26	0
KÖRPER	DASEIN	2ndC	0.97	20	0
DORF	HEIM	2ndC	0.90	24	0
ODE	VERS	2ndC-L	1.39	0	26
KUH	PFERD	2ndC-L	2.43	0	92
KNIE	SCHÄDEL	2ndC-L	1.08	0	41
HARZ	HEIDE	2ndC-L	2.34	0	17
LAMM	HIRSCH	2ndC-L	1.84	0	21
ZIMT	APFEL	2ndC-L	1.59	0	25
BASIS	ERFOLG	2ndC-L	2.11	0	39
JACHT	VILLA	2ndC-L	0.92	0	17
DROGE	PULVER	2ndC-L	1.24	0	26
HECKE	WIESE	2ndC-L	1.05	0	63
DOSIS	PRISE	2ndC-L	1.64	0	48
VOGEL	FROSCH	2ndC-L	1.32	0	44
WITWE	OMA	2ndC-L	1.02	0	24
PILLE	MITTEL	2ndC-L	1.51	0	40
LÄRM	STAU	2ndC-L	2.20	0	54
HAKEN	TRICK	2ndC-L	0.89	0	27
FLORA	PFLANZE	2ndC-L	0.96	0	30
EIFER	GEDULD	2ndC-L	1.35	0	34
FÜHLER	SENSOR	2ndC-L	1.14	0	13
KIEFER	EICHE	2ndC-L	2.47	0	82
LACHEN	HUMOR	2ndC-L	2.68	0	44
BARREN	SPRUNG	2ndC-L	2.68	0	15
PUTSCH	AUFSTAND	2ndC-L	1.67	0	45
RÜCKEN	OHR	2ndC-L	1.75	0	43
TENNIS	KANU	2ndC-L	1.36	0	19
DENKER	PROPHET	2ndC-L	0.85	0	32
GRAUEN	LEERE	2ndC-L	0.88	0	34
SCHAUM	WASSER	2ndC-L	2.27	0	43
UMWELT	HANDEL	2ndC-L	1.88	0	43
VERRAT	VERGEHEN	2ndC-L	1.77	0	33
ZIRKUS	RUMMEL	2ndC-L	1.34	0	15
GLAUBEN	JUDE	2ndC-L	1.78	0	24

BERICHT	GERÜCHT	2ndC-L	0.98	0	55
COLLAGE	BILD	2ndC-L	1.97	0	65
EINFALL	METAPHER	2ndC-L	0.84	0	49
FORELLE	FLEISCH	2ndC-L	1.08	0	33
TOASTER	LAMPE	2ndC-L	1.12	0	16
WÄHRUNG	DEVISE	2ndC-L	1.16	0	53
PASSAGE	GEDICHT	2ndC-L	1.08	0	37
BEMÜHUNG	AMBITION	2ndC-L	0.90	0	45
DOM	TEMPEL	2ndC-L	0.99	0	44
TEE	TOMATE	2ndC-L	0.90	0	74
BEDENKEN	ANSICHT	2ndC-L	1.43	0	73
NIVEAU	HÖHE	2ndC-L	0.87	0	52
HÖHLE	SCHLUCHT	2ndC-L	1.19	0	51
BAKTERIE	ZELLE	2ndC-L	1.18	0	72
SPEISE	KUCHEN	2ndC-L	0.96	0	61
AUTO	MODELL	2ndC-L	1.74	0	73
CHEF	FÜHRUNG	2ndC-L	0.88	0	58
PUNKT	LINIE	2ndC-L	0.90	0	52
HOF	ÖKONOMIE	1stC=0	0.00	0	0
SEX	ASIEN	1stC=0	0.00	0	0
WAL	WACHSTUM	1stC=0	0.00	0	0
BURG	MESSER	1stC=0	0.00	0	0
FILM	NATUR	1stC=0	0.00	0	0
IRIS	TROMPETE	1stC=0	0.00	0	0
LÜGE	URIN	1stC=0	0.00	0	0
NEON	FAMILIE	1stC=0	0.00	0	0
RUIN	PUMA	1stC=0	0.00	0	0
VOLK	DICHTUNG	1stC=0	0.00	0	0
ZINS	GERICHT	1stC=0	0.00	0	0
ÄRGER	NICKEL	1stC=0	0.00	0	0
GEBOT	DIÄT	1stC=0	0.00	0	0
IMAGE	INVASION	1stC=0	0.00	0	0
KANTE	STALL	1stC=0	0.00	0	0
NOTIZ	TRAGÖDIE	1stC=0	0.00	0	0
OPFER	POSE	1stC=0	0.00	0	0
RAUCH	GEWICHT	1stC=0	0.00	0	0
SÄURE	SATIRE	1stC=0	0.00	0	0
WAFFE	ZYKLUS	1stC=0	0.00	0	0
ZWECK	ETUI	1stC=0	0.00	0	0
MIETE	KLO	1stC=0	0.00	0	0
CREME	LUXUS	1stC=0	0.00	0	0
ANGABE	EINKAUF	1stC=0	0.00	0	0
DACKEL	GOTT	1stC=0	0.00	0	0
FINGER	BAUWERK	1stC=0	0.00	0	0
GEGNER	VATIKAN	1stC=0	0.00	0	0
JAGUAR	LÄNGE	1stC=0	0.00	0	0
KUMMER	ERZ	1stC=0	0.00	0	0
RASTER	TAPETE	1stC=0	0.00	0	0
STIMME	FERKEL	1stC=0	0.00	0	0
UMKEHR	WAHRHEIT	1stC=0	0.00	0	0
WANDEL	RUNDGANG	1stC=0	0.00	0	0
ZETTEL	LIGA	1stC=0	0.00	0	0
LEKTOR	PARTY	1stC=0	0.00	0	0
NENNER	AKT	1stC=0	0.00	0	0
DREIECK	TREPPE	1stC=0	0.00	0	0

GARDINE	PINSEL	1stC=0	0.00	0	0
KLASSIK	SCHATTEN	1stC=0	0.00	0	0
MAGAZIN	PROFI	1stC=0	0.00	0	0
PFENNIG	GRÜNDER	1stC=0	0.00	0	0
URSACHE	JOD	1stC=0	0.00	0	0
WOHNUNG	HEXE	1stC=0	0.00	0	0
ANTILOPE	TEXT	1stC=0	0.00	0	0
FRÜHLING	PASSION	1stC=0	0.00	0	0
STELLUNG	LEID	1stC=0	0.00	0	0
LICHTUNG	FICHTE	1stC=0	0.00	0	0
GEL	AFTER	1stC=0	0.00	0	0
LEKTION	REIZUNG	1stC=0	0.00	0	0
FELS	CLUB	1stC=0	0.00	0	0

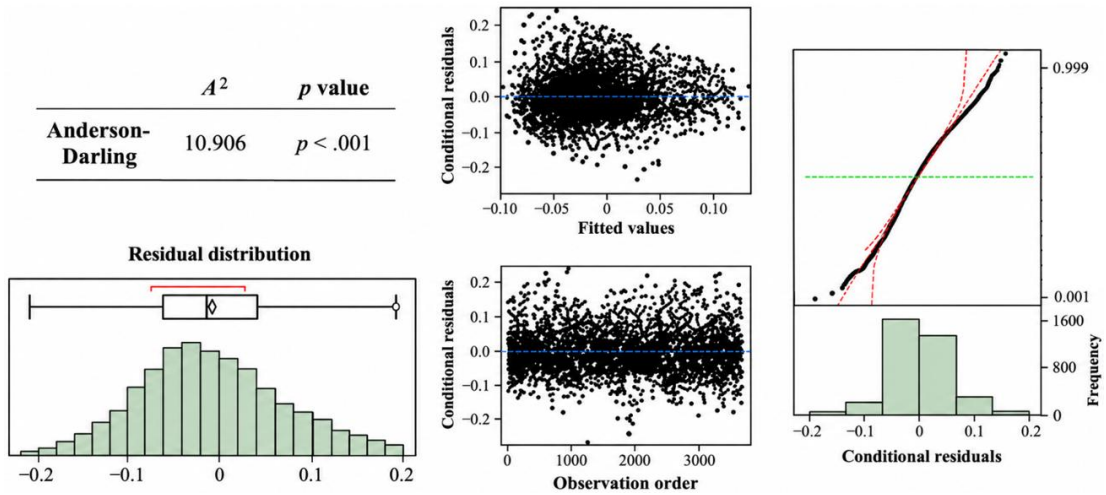
Note. AS = Association strength; CA-surface = Number of common associates from surface word forms; CA-lemma = Number of common associates from lemmatized word forms.

D2. Means (*SD*s) and *F* Statistics for Controlled Variables (Study D)

	Prime			
	1stC=0	**2ndC**	**2ndC-L**	***F* Value**
Length	5.48 (1.39)	5.64 (1.21)	5.50 (1.31)	0.22
Frequency	11.62 (2.26)	12.14 (2.51)	11.90 (2.24)	0.62
Orthographic Neighbors	1.60 (1.46)	1.64 (1.70)	1.94 (2.15)	0.54
	Target			
	1stC=0	**2ndC**	**2ndC-L**	***F* Value**
Length	5.70 (1.62)	5.98 (1.48)	5.74 (1.27)	0.53
Frequency	11.58 (2.18)	11.50 (2.18)	11.16 (2.14)	0.51
Orthographic Neighbors	1.52 (1.76)	1.40 (1.52)	1.82 (1.67)	0.80

Note. F statistics for the lexical control variables were obtained from separate one-way between-item analyses of variance across the three experimental word pair conditions, $F(2, 147)$. Analyses were conducted separately for primes and targets. Length is reported in letters. 1stC=0 = unrelated (association strength equals zero); 2ndC-S = semantic feature overlap based on surface word forms; 2ndC-L = semantic feature overlap based on lemmatized word forms.

D3. Residual Diagnostics for the Gaussian Linear Mixed-Effets Model Fitted to Natural-Log-Transformed Response Times (Baseline Model)



D4. Robust Model Comparison for Response Times

Name	Model	AICc	ΔAICc	-2LL	LR χ^2	*df*	*p*	LRT vs.
M1	TrialN	-3079	2.138	-3091				
M2	M1 + U	-3077	3.541	-3091	0.605	1	.436	M1
M3	M2 + S	-3081	0.461	-3097	5.089	1	.024	M2
M4	M2 + L	-3081	0.000	-3097	5.550	1	.018	M2
M5	M2 + S + L	-3080	1.131	-3098	0.879	1	.348	M4

Note. Gaussian linear mixed-effects models fitted to natural-log-transformed response times, including random intercepts for participants and items, as well as participant-specific random slopes for centered trial number (N = 26 participants; k = 150 items; n = 3,607 trials). Models were fitted using maximum likelihood estimation. ΔAICc values are relative to the best-fitting model (M4). AICc = corrected Akaike information criterion; L = 2ndC-L (semantic feature overlap based on lemmatized word forms); LR = likelihood ratio; LRT = likelihood ratio test; S = 2ndC-S (semantic feature overlap based on surface word forms); TrialN = centered trial number; U = Unrelated (association strength = 0); -2LL = -2 log-likelihood.

Association strength did not explain any additional variance in response time (M1 → M2: LR $\chi^2(1) = 0.61$, $p = .436$). Adding 2ndC-S to the model (M2 → M3) significantly improved the model fit (LR $\chi^2(1) = 5.09$, $p = .024$). Including 2ndC-L also led to a significant improvement in the model (M2 → M4: LR $\chi^2(1) = 5.55$, $p = .018$). However, a direct comparison shows that surface does not contribute anything additional if the model already includes 2ndC-L (M4 → M5: LR $\chi^2(1) = 0.88$, $p = .348$). A global test, adding 2ndC-S and 2ndC-L to a model with trial number and association strength was significant (LR $\chi^2(2) = 6.43$, $p = .040$), with comparisons indicating that this effect is primarily driven by 2ndC-L.

Appendix E. Open Science Repository for Experimental Materials

To facilitate transparency and reuse, the experimental materials associated with this doctoral thesis (scripts, instructions, and complete item-level stimulus lists, including controlled stimulus-variable values) are available in the following repository:

Repository: Zenodo.

DOI: https://doi.org/10.5281/zenodo.18325024

License: Creative Commons Attribution 4.0 International (CC BY 4.0)

Project title: Successful Memory Formation in Paired-Associate Learning:
Associative and Semantic Effects on Episodic Encoding (Stimulus Lists and Experiment Files)

Appendix F. Administrative Information

Funding

Parts of this work were conducted while the author was employed in a position funded by the German Research Foundation (DFG; grants HO 5139/2-1 and HO 5139/2-2, awarded to PD Dr. Markus J. Hofmann).

Data Availability

The raw data underlying the studies were collected at the institutions listed below. Processed data (including derived variables/outputs) supporting the findings of this thesis are available from the author upon reasonable request. Due to data protection regulations, access to raw data may be limited and granted only under specific conditions.

Study A: Bergische Universität Wuppertal, Germany
Study B: Bergische Universität Wuppertal, Germany
Study C: Freie Universität Berlin and Forschungszentrum Jülich, Germany

Ethics Approval and Preregistration

The study protocol for Study C was approved by the Ethics Committee of the Medical Faculty of RWTH Aachen University (internal reference no. EK 318/19), and all participants provided written informed consent. Study C was pre-registered prior to data collection on OSF Registries (title: The impact of associative vs. semantic long-term knowledge on hippocampal subfield processing; OSF project: krb4p; registration draft ID: 60ec78ff04e38b035c3d8106).

Language Editing Statement

To improve readability, DeepL was used to refine linguistic clarity and fluency, while LanguageTool was used to check grammar and spelling. No large language models were used to generate scientific content or interpret results. All suggested edits were reviewed by the author, who retains full responsibility for the content of the dissertation.

10. Declaration of Authorship

I, Carsten Klein (born on March 7th, 1994, in Düsseldorf), hereby declare that this dissertation, which is titled *Successful Memory Formation in Paired-Associate Learning: Associative and Semantic Effects on Episodic Encoding*, is my own work. In accordance with § 10 of the Doctoral Regulations dated May 21, 2015, the submitted dissertation has been written independently, with only the specified sources and aids being used. All quotations and derivations from other works have been clearly marked. This dissertation has not been submitted, either in its present form or in any other version, to any other department or academic institution.